Lead sulfide quantum dots and their application for solar cells

Aabhash Shrestha

B.E., M.S.

Thesis submitted for the degree of

Doctor of Philosophy

School of Chemical Engineering

Faculty of Engineering, Computer and Mathematical Sciences

The University of Adelaide, Australia

July 2016

Dedication

This thesis is dedicated to my loving mom and dad Uma and Arun Shrestha, my sister Agya Shrestha

Declaration

I certify that this work contains no material which has been accepted for the award of any other degree or diploma in my name, in any university or other tertiary institution and, to the best of my knowledge and belief, contains no material previously published or written by another person, except where due reference has been made in the text. In addition, I certify that no part of this work will, in the future, be used in a submission in my name, for any other degree or diploma in any university or other tertiary institution without the prior approval of the University of Adelaide and where applicable, any partner institution responsible for the joint-award of this degree.

I give consent to this copy of my thesis when deposited in the University Library, being made available for loan and photocopying, subject to the provisions of the Copyright Act 1968.

The author acknowledges that copyright of published works contained within this thesis resides with the copyright holder(s) of those works. I also give permission for the digital version of my thesis to be made available on the web, via the University's digital research repository, the Library Search and also through web search engines, unless permission has been granted by the University to restrict access for a period of time.

Aabhash Shrestha Date: 20 July 2016

Abstract

Quantum dot sensitized solar cells (QDSSCs) are interesting third generation solar cells that have potential to address the current energy related issues due to their low manufacturing cost, ease of fabrication as well as good performance. Quantum dots (QDs) offer several advantages such as size tunable band gaps across a wide range of energy levels, high molar extinction coefficients and enhanced stability. Among them, colloidal near infrared (NIR) QDs of lead sulfide (PbS) are attractive due to their narrow bulk bandgap, large exciton Bohr radii and the possibility of multiple exciton generation. Utilizing these QDs in solar cells with extendable IR absorption is promising. However, the progress of PbS QDSSCs is lacking due to the limited understanding regarding the synthesis and surface chemistry of QDs. The development of QDSSCs is also hindered by lack of proper counter electrode materials for the reduction of electrolytes. Hence, further developments in the synthesis and application of new materials for QDSSCs are necessary.

This PhD project focuses on the materials development for PbS QDSSCs such as PbS QD synthesis, surface ligand exchange of PbS QDs, and the development of new counter electrode materials. The following researches are included in this thesis:

1) A robust method to synthesize monodisperse lead sulfide (PbS) QDs is presented. PbS QDs with different sizes is produced by stepwise heating of the preformed seed QDs in the presence of excess oleic acid. A combination of "living" monomer addition and Ostwald ripening is identified as the mechanism for such QD growth processes.
2) The detailed synthesis mechanism of PbS QDs is investigated. Here, the various synthesis parameters influencing the nucleation and growth of PbS QDs are elucidated.

In addition, the detailed understanding of the synthesis mechanism is used to guide the synthesis of PbS QDs at ultra-small regime.

3) A versatile solution phase ligand exchange of PbS QDs in the presence of Pb-thiolate as the exchanging ligands is presented. The ligand exchange procedure better preserves the optical properties of PbS QDs and is applicable to a number of ligand/solvent systems.
4) The implementation of PbS QDs in QDSSCs is presented. The treatment of PbS QD photoelectrodes with cadmium salts is necessary to maintain the stability of PbS QDs in polysulfide based electrolytes. In addition, the number of cycles of CdS and ZnS treatment is optimized to achieve a photoconversion efficiency of 1.77 %.
5) Finally, N-doped CN_x/CNT hetero-electrocatalyst materials using polydopamine is synthesized, which are explored as counter electrode materials for dye-sensitized solar cell (DSSC). These CN_x/CNTs material show excellent electrocatalytic activities towards the reduction of tri-iodide electrolytes with the optimized solar devices using CN_x/CNTs showing comparable performance (7.3 %) to reference Pt based devices (7.1 %).

List of publications

This doctoral thesis is prepared in "Publication" format according to the "specifications for Thesis (2016)" of the University of Adelaide. The thesis includes the following publications that have been published, submitted for publication, or ready for submission:

1) Aabhash Shrestha, Shizhang Qiao, Sheng Dai, "Near infrared (NIR) lead chalcogenide QDs- recent progress in their synthesis, post-synthesis ligand exchange and applications in solar cells" (To be submitted)
2) Aabhash Shrestha, Bo Jin, Tak Kee, Shizhang Qiao, and Sheng Dai, "A Robust Strategy for Living Growth of Lead Sulphide Quantum Dots", Published in Journal ChemNanoMat (DOI: 10.1002/cnma.201500110)
3) Aabhash Shrestha, Nigel A. Spooner, Shizhang Qiao, and Sheng Dai, "Mechanistic insight into the nucleation and growth of oleic acid capped lead sulfide quantum dots", Submitted to Journal Physical Chemistry Chemical Physics (Submission ID: CP-ART-03-2016-002119)
4) Aabhash Shrestha, Nigel A. Spooner, Shizhang Qiao, and Sheng Dai, "Versatile PbS quantum dot ligand exchange systems in the presence of Pb-thiolates", Submitted to Journal Small (Submission ID: smll.201601046)
5) Aabhash Shrestha, Munkhbayar Batmunkh, , Cameron J. Shearer, Yanting Yu, Gunther Andersson, Joseph G. Shapter, Shizhang Qiao, Sheng Dai, "Nitrogen-doped CN_x/CNTs hetero-electrocatalysts for highly efficient dye sensitized solar cells", (To be submitted in Journal Advanced Energy Materials)

6) Aabhash Shrestha, Munkhbayar Batmunkh, Joseph G. Shizhang Qiao, Shapter, Sheng Dai, “Enhancing the stability of pre-synthesized PbS quantum dot sensitized solar cells in polysulfide electrolyte by treating with cadmium salts”, (To be submitted)

Some relevant components of the work have also been presented in the following conferences:

1) Aabhash Shrestha, Munkhbayar Batmunkh, Joe Shapter, Shizhang Qiao, Sheng Dai “Hybrid carbon nanomaterials for highly efficient dye sensitized solar cells (DSSCs)” MRS 2015, Fall Meeting, Boston, USA, 2015

2) Aabhash Shrestha, Shizhang Qiao, Sheng Dai “ Understanding the nucleation and growth mechanism towards synthesis of Lead Sulphide Quantum Dots” ICONN 2014, International Conference on Nanoscience and Nanotechnology, Adelaide Conventional Center, Adelaide, Australia, 2014

3) Aabhash Shrestha, Shizhang Qiao, Sheng Dai, “Precursor and ligand influenced growth mechanism and living chain polymerization of post focused Lead Sulfide Quantum dots” SA Polymer and Biotechnology Symposium, Flinders University City Campus, Adelaide, Australia, 2013

Acknowledgements

First and foremost, I would like to express my deepest gratitude to Associate Professor Sheng Dai for being a truely unique and wonderful supervisor. I'm grateful for his excellent guidance, patience and providing an excellent research environement. He has been supportive from my early days of candidature and his guidance helped me complete this thesis. I would also like to thank my co-supervisor Professor Shizhang Qiao for his guidance and motivation.

I would like to express my deepest gratitude for all our lab members and colleagues who have made my PhD studies fruitful and enjoyable. Especially I would like to thank Associate Professor Bo Jin, Dr. Hu Zhang and Associate Professor Jingxiu Bi for their motivation and encouragement. I would also like to thank my colleagues Munkhbayar Batmunkh, Umar Azhar, Yusak Haranto, Steven Cui, Amir Mellati, Leiyuan Guo, Bingyang Zhang, Masoumeh Zagar, Mailin mission and others for being wonderful friends and helping me succeed. In addition, I would like to thank Accociate Professor Tak Kee, Professor Nigel Spooner and Professor Joe Shapter for allowing me to use their lab facilities and incorporating me in their research teams.

My grateful thank also goes to the staff of Chemical Engineering and colleagues in the department. Especially, I would like to thank Associate Professor Zeyad Alawahabi for being a wonderful postgraduate coordinator and my teaching mentor. I would also like to thank Dr. Quihong Hu, Dr. Sanaz Orandi and Jason Peak for their technical support. I have thoroughly enjoyed knowing these wonderful people and have cherished their company during my PhD studies.

Last but not the least; I would like to thank all my family and friends for their wonderful support in my life. Especially, I would like to thank my mom and dad for being wonderful parents and their unconditional love. I’m truly blessed to have such wonderful and caring parents. I would also like to thank my lovely sister for supporting my every step in life.

Table of Contents

List of Tables

List of Figures

Chapter 1

Introduction

1.1 Background

Current energy crisis and associated climate change present a major challenge for sustainable future. Solar cells are photovoltaic devices that can directly convert the light energy from sun to electricity without adverse impact to climate. The energy conversion process of solar cells consists of the generation of electron-hole pairs in semiconductor and their separation through charge carriers. Currently, the third generation solar cells utilizing organic dyes, conducting polymers, quantum dot (QDs) and perovskites have great potential owing to their low manufacturing cost, ease of fabrication as well as good performance. Amongst these third generation solar cells, QDs based solar cells are emerging with promising photovoltaic efficiencies.

QDs in solar cells offer several advantages such as size tunable band gaps across a wide range of energy levels, high extinction coefficients and enhanced stability. QDs with its size tunable band gaps offer new opportunities to harvest light energy from the entire region of solar spectrum.[1-3, 4] In addition, QDs possesses other desirable properties such as efficient charge separation and transport,[5, 6] their quantum confinement effects including impact ionization,[6, 7] hot electron-hole generation[1, 4] and high extinction coefficients. Hence, the photovoltaic systems utilizing QDs as light harvesters have the potential to exceed the theoretical efficiency limit of 33 % for a single junction cell, also known as Shockley–Queisser limit.[8]

Till date, various architectures for QD based solar cells have been developed[9] which includes photo-electrochemical cells based on QD sensitized wide bandgap semiconductor nanostructures, QD films immersed in electrolytes, solid state cells based on QD/polymer blends as well as QD/inorganic heterojuctions with the QD layers sandwiched between

electron and hole conductors.[9] Recently, the QD/inorganic heterojunction as well as the QDs sensitized solar cells (QDSSCs) have shown promising photovoltaic efficiencies approaching up to 10 %.[10, 11]

The QDs of lead chalcogenide (PbS, PbTe and PbSe) are interesting for solar cells due to their narrow bulk bandgap, large exciton Bohr radii and the possibility of multiple exciton generation.[1, 12] Utilizing these QDs in solar cells with extendable IR absorption is promising. Although the QD/inorganic heterojunction solar cells utilizing lead chalcogenide QDs have shown efficiencies up to 10 %,[11] the efficiency of QDSSCs is still low. Recently, visible to NIR emitting cadmium based QDSSCs have shown efficiencies close to 10 %.[10] Since the lead chalcogenide based QDs can potentially harvest the light energy extendable to IR region, the efficiency of QDSSCs can further be improved by utilizing them as light harvesters.[2, 13] Although efforts have been made for the utilization of lead chalcogenide QDs in sensitized solar cells,[14] their efficiencies are typically limited by the lack of fundamental understanding regarding the synthesis and surface chemistry of these QDs. Further development in their synthesis and the efficient modulation of their surface properties is highly desirable. On the other hand, the development of QDs based sensitized solar cells is also hindered by the lack of suitable catalyst materials at the counter electrode for the reduction of electrolytes.[15] Cheaper and efficient catalyst materials are highly desirable. Therefore, this PhD research aims to solve the current material relevant issues associated with the development of high performance lead chalcogenide based QDs solar cells.

1.2 Aims and objectives

The aim of this thesis is to explore the utilization of lead chalcogenide QDs for solar cell application. This thesis is focused on the development of NIR lead sulfide (PbS) QDs and CNTs based carbon materials for potential use in solar cells. As such, following objectives were set for the PhD thesis:

a) Understanding the mechanism of PbS QD formation and the various synthesis parameters influencing PbS QD synthesis.
b) Exploring the efficient method for the ligand exchange of PbS QDs.
c) Application of the ligand exchanged QDs as a potential light harvester in sensitized solar cells
d) Development of efficient electro-catalyst materials for use as counter electrodes in sensitized solar cells.

1.3 Outline of the thesis

The outline of the thesis is described below:

Chapter 1 provides an overview of the research topics together with a brief outline of the thesis.

Chapter 2 reviews the recent progress in the synthesis of near infrared (NIR) lead chalcogenide QDs, their solution phase ligand exchange and their prospects as a high efficiency light harvesters in QDs based solar devices.

Chapter 3 presents a novel and robust approach for the synthesis of monodisperse lead sulfide (PbS) QDs through a "living" growth process, where a series of differently sized QDs can be easily produced upon steply heating the preformed seed QDs in the presence

of excess oleic acid. The mechanism of such QD growth is dominated by the combination of "living" monomer addition and Ostwald ripening.

Chapter 4 presents a detailed investigation on the synthesis mechanism of PbS QDs. A better understanding on the nucleation and growth of PbS QDs synthesis under various reaction conditions has been documented. The outcome can be used for the synthesis of PbS QDs at ultra-small regime.

Chapter 5 presents a versatile solution phase ligand exchange strategy for PbS QDs in the presence of Pb-thiolate ligands that can better address the challenges pertaining to the ligand exchange of PbS QDs. The presence of Pb-thiolate ligands can better preserve the excitonic absorption features as well as its emission intensities during the ligand exchange. Such a ligand exchange approach of utilizing Pb-thiolate can be expanded to a number of hydrophobic ligands, hydrophilic ligands and different solvent systems.

Chapter 6 presents the application of ligand exchanged PbS QDs as light harvesters to replace organic dyes in sensitized solar cells. We also explored the methods to enhance the stability of PbS QDs in liquid electrolytes and find that the treatment with cadmium ions enhances the stability of PbS QDs in polysulfide based electrolytes.

Chapter 7 applies polydopamine as the nitrogen source to generate electrocatalytically active N-doped CNTs. The resulting hybrids materials can be explored as an alternative to platinum counter electrode for the reduction of tri-iodide electrolytes in dye-sensitized solar cells. The optimized device fabricated with the CN_x/CNTs hybrid catalyst delivers a power conversion efficiency (PCE) of 7.3 %, which is comparable to Pt CE based DSSC (7.1 %).

Chapter 8 summarizes the research work and recommends potential future work in relevant research fields.

References

[1] A. J. Nozik, *Physica E: Low-dimensional Systems and Nanostructures* 2002, 14, 115.

[2] M. A. Hines, G. D. Scholes, *Adv. Mater*. 2003, 15, 1844.

[3] (a) P. V. Kamat, *J. Phys. Chem. C* 2008, 112, 18737; (b) I. Moreels, K. Lambert, D. De Muynck, F. Vanhaecke, D. Poelman, J. C. Martins, G. Allan, Z. Hens, *Chem. Mater*. 2007, 19, 6101; (c) I. Robel, M. Kuno, P. V. Kamat, *J. Am. Chem. Soc*. 2007, 129, 4136.

[4] A. J. Nozik, M. C. Beard, J. M. Luther, M. Law, R. J. Ellingson, J. C. Johnson, *Chem. Rev*. 2010, 110, 6873.

[5] (a) M. Gratzel, *Nature* 2001, 414, 338; (b) H. Wang, Y. Bai, H. Zhang, Z. Zhang, J. Li, L. Guo, *J. Phys. Chem. C* 2010, 114, 16451.

[6] L. Li, X. Yang, J. Gao, H. Tian, J. Zhao, A. Hagfeldt, L. Sun, *J. Am. Chem. Soc*. 2011, 133, 8458.

[7] Y. Tian, T. Tatsuma, *J. Am. Chem. Soc*. 2005, 127, 7632.

[8] W. Shockley, H. J. Queisser, *J. Appl. Phys.* 1961, 32, 510.

[9] S. Rühle, M. Shalom, A. Zaban, *ChemPhysChem* 2010, 11, 2290.

[10] J. Yang, J. Wang, K. Zhao, T. Izuishi, Y. Li, Q. Shen, X. Zhong, *J. Phys. Chem. C* 2015, 119, 28800.

[11] G.-H. Kim, F. P. García de Arquer, Y. J. Yoon, X. Lan, M. Liu, O. Voznyy, Z. Yang, F. Fan, A. H. Ip, P. Kanjanaboos, S. Hoogland, J. Y. Kim, E. H. Sargent, *Nano Lett.* 2015, 15, 7691.

[12] (a) R. J. Ellingson, M. C. Beard, J. C. Johnson, P. Yu, O. I. Micic, A. J. Nozik, A. Shabaev, A. L. Efros, *Nano Lett.* 2005, 5, 865; (b) J. E. Murphy, M. C. Beard, A. G. Norman, S. P. Ahrenkiel, J. C. Johnson, P. Yu, O. I. Mićić, R. J. Ellingson, A. J. Nozik, *J. Am. Chem. Soc*. 2006, 128, 3241.

[13] F. W. Wise, *Acc. Chem. Res*. 2000, 33, 773.

[14] (a) S. D. Sung, I. Lim, P. Kang, C. Lee, W. I. Lee, *Chem. Commun*. 2013, 49, 6054; (b) J.-W. Lee, D.-Y. Son, T. K. Ahn, H.-W. Shin, I. Y. Kim, S.-J. Hwang, M. J. Ko, S. Sul, H. Han, N.-G. Park, *Sci. Reports* 2013, 3, 1050; (c) X. Li, W. Lu, Y. Wang, Y. Fang, L. Wang, Q. Ai, X. Zhou, Y. Lin, *Electrochimica Acta* 2014, 144, 71.

[15] I. Hwang, K. Yong, *ChemElectroChem* 2015, 2, 634.

Chapter 2

Near infrared (NIR) lead chalcogenide QDs- recent progress in their synthesis, post-synthesis ligand exchange and applications in solar cells

Aabhash Shrestha, Shizhang Qiao, Sheng Dai*

The School of Chemical Engineering, University of Adelaide, Adelaide, SA 5005, Australia

*Corresponding author

Email: s.dai@adelaide.edu.au

To be submitted for publication

Statement of Authorship

Title of Paper	Near infrared (NIR) lead chalcogenide QDs- recent progress in their synthesis, post-synthesis ligand exchange and applications in solar cells
Publication Status	☐ Published ☐ Accepted for Publication ☐ Submitted for Publication ☑ Unpublished and Unsubmitted work written in manuscript style
Publication Details	Aabhash Shrestha, Shi Zhang Qiao, and Sheng Dai*, **Near infrared (NIR) lead chalcogenide QDs- recent progress in their synthesis, post-synthesis ligand exchange and applications in solar cells**

Principal Author

Name of Principal Author (Candidate)	Aabhash Shrestha
Contribution to the Paper	Writing of the manuscript, review and analysis of the literature
Certification:	This paper reports on original research I conducted during the period of my Higher Degree by Research candidature and is not subject to any obligations or contractual agreements with a third party that would constrain its inclusion in this thesis. I am the primary author of this paper.
Signature	Date: 04/April/2016

Co-Author Contributions

By signing the Statement of Authorship, each author certifies that:

the candidate's stated contribution to the publication is accurate (as detailed above);

permission is granted for the candidate in include the publication in the thesis; and

the sum of all co-author contributions is equal to 100% less the candidate's stated contribution.

Name of Co-Author	Shizhang Qiao
Contribution to the Paper	Assisting in the manuscript review
Signature	Date: 08/April/2016

Name of Co-Author	Sheng Dai
Contribution to the Paper	Supervising, manuscript review and assessment.
Signature	Date: 04/04/2016

Please cut and paste additional co-author panels here as required.

Abstract

Quantum dots (QDs) of lead chacogenides (PbS, PbSe and PbTe) are exciting NIR active materials with potential applications in photovoltaics, optoelectronics, sensors, bio-electronics and many others. The successful utilization of these functional materials for end user application requires proper understanding of their synthesis and material processing methodologies. Surface ligands play an essential role in QD synthesis, their post-synthesis processing and their integration to applications. As such, understanding the influence of surface ligands on QDs synthesis, modulation of surface properties and the impact on optoelectronic properties is essential. Our review elaborates the application of colloidal synthesis techniques for the synthesis of lead chalcogenide based QDs. We specifically focus on the influence of surface ligands on QD synthesis and their solution phase ligand exchange. Given the importance of lead chalcogenide QDs as potential light harvesters, we also review current progress of these QDs in solar photovoltaic applications.

TOC Figure:

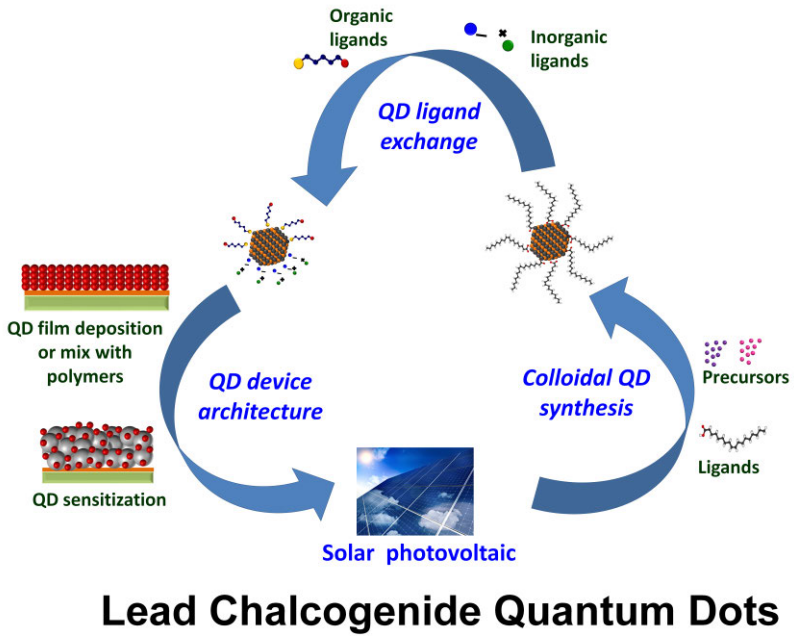

Table of Content

2.1 Introduction

Semiconducting quantum dots (QDs) have received much attention due to their size tunable band gaps, efficient charge separation and transport,[1-3] their quantum confinement effects including impact ionization,[3, 4] hot electron-hole generation[5, 6] and high molar extinction coefficients.[5, 6] In addition, QDs with its size tunable band gaps offer new opportunities to harvest light energy covering the entire region of solar spectrum.[5-8, 9] Hence, utilizing QDs as electron donors have potential applications in solar cells,[3, 8, 10, 11, 12] nanostructured electronic arrays[12, 13] and optoelectronic displays.[14]

Recently, narrow bandgap near infrared (NIR) active materials are receiving much interest due to their potential in solar cells with extendable IR absorption, biolabels for deep tissue imaging and other optoelectronic applications. Lead chalcogenide (PbS, PbSe and PbTe) QDs are promising NIR active materials due to their narrow bulk band gaps, large excitonic Bohr radii and the possibility of multiple exciton generation.[5, 15, 16] The large excitonic Bohr radii along with their narrow band gaps allow these materials to have a broadband absorption tunable from 0.3 to >1.5 eV.[7, 17] The broadband absorption of lead chalcogenide QDs make them attractive for solar photovoltaic devices as light harvesters. It is predicted that these QDs have the possibility of surpassing the theoretical photo conversion efficiency (PCE) limit of 30 %, which is also known as Shockley–Queisser limit.[18]

One of the key criteria for the practical application of QDs is their controlled synthesis with desired size, shape and optoelectronic properties. The colloidal synthesis offers an effective route for the production of nanocrystals (NCs) with the desired size and narrow size distribution. Better control over the QD synthesis is achieved by understanding the

fundamental processes inherent in colloidal synthesis such as precursor reactivity, QD nucleation and growth, their stability and the parameters modulating the QD morphology. Most colloidal synthesis techniques for lead chalcogenide QDs have been adopted from the cadmium based QDs. Recent progresses in colloidal synthesis techniques have enabled the fabrication of high quality lead chalcogenide QDs scalable for commercial production.[19, 20] Also, morphology of these QDs can be controlled by varying the synthesis conditions to yield asymmetric structures with unique properties.[21] A proper account of recent progress for the synthesis of lead chalcogenide QDs is essential for their future development.

Ligands also play an essential role for the utilization of lead chalcogenide QDs. Ligands, which are generally introduced during the synthesis of QDs, provide the stabilization of QDs in solution, provide the passivation for trap states and maintain the charge balance on QDs surface.[22] The nature of ligands such as hydophilicity or hydrophobicity and their sizes becomes crucial for their usability. The majority of successful colloidal lead chalcogenide QD synthesis relies on the use of long chain hydrophobic ligands to provide colloidal stabilization in solution.[7, 19, 23] These bulky ligands are usually insulative and non-functional. Efficient replacement of these bulky ligands becomes essential for many end user applications. The solution phase ligand exchange of QDs offer potential benefits in future optoelectronic application such a low cost solution processable deposition techniques, a better control over the thin film morphologies and possibly better electronic transportation. In addition, it also enables a better understanding of QD surface chemistry which provides potential benefits in various applications.

Recent advances in the synthesis of lead chalcogenide QDs and their material processing have enabled their application in solar photovoltaics, light emitting diodes, sensors,

fluorescent bio-markers and many more. Especially, the developments in lead chalcogenide QDs based solar photovoltaic application are promising. The key reasons for the improved efficiencies of lead chalcogenide QD based solar photovoltaic are the progress in QD synthesis technique, better understanding of surface ligand chemistries and the ligand based modulation of various optoelectronic properties. As a result, the photovoltaic efficiencies over 10 % have been recently reported and further gains in efficiency are expected with the new developments in the ligand chemistry and their utilizations to various QDs solar device architectures.

In this review, we first highlight the recent progresses in the synthesis of colloidal lead chalcogenide (PbS, PbSe and PbTe) QDs and the influence of surface ligands on controlling their growth, morphology and stability. Next, we provide a comprehensive analysis on the current state of solution phase ligand exchange of these QDs. Finally, we will conclude by highlighting the current progress in ligand chemistry in the utilization of lead chalcogenide QDs as light harvesters in solar photovoltaic devices.

2.2 Recent advances in lead chalcogenide QDs synthesis

2.2.1 Overview of colloidal QD synthesis

A typical colloidal QD synthesis system consists of precursor, ligands (or surfactants) and solvents. In some cases the solvent also acts as the ligand for QDs. Usually, heating of the reaction system to high temperature chemically transforms the precursors into active species or monomer. As the monomer starts to builds up in solution, it becomes supersaturated and initiates nucleation. Nucleation is the spontaneous formation of small nano-crystals (NCs) from a saturated solution that may grow larger or dissolve back into the solution depending on their surface energies.[24] The nucleation is controlled by

temperature, interfacial/surface tension and the level of supersaturation in solution.[25] The nucleation event is followed by the particle growth, where the nuclei grow larger to form the final QD particles. The growth of nuclei occurs either by the addition of monomeric species remaining in the solution or by the consumption of a fraction previously formed particles.

Separating the QD nucleation from growth is believed to achieve high quality and mono-dispersed QDs.[26] The separation between the QD nucleation and growth stage is achieved by controlling the precursor conversion kinetics. Since the precursor conversion kinetics is mostly influenced by the temperature in reaction system, their control is usually achieved by a hot precursor injection method or a heat-up synthesis method as shown in **Figure 2-1**. In hot injection method, the precursors are quickly injected at high temperature which allows spontaneous reaction between the precursors to initiate nucleation. The term 'quick' and 'spontaneous reaction' are not elusive in most reaction system as the precursor conversion kinetics determines the spontaneity of reaction. Nevertheless, the choice of injection temperature is critical as the temperature can regulate the decomposition of precursors. Typically one of the precursors is maintained at room temperature so that the overall temperature of reaction is reduced and can terminate the nucleation to commence QD growth. In the non-injection based heat-up method, the control over nucleation and growth is achieved by the steady heating of precursors. All the precursors are mixed at room temperature and heated at the same time. Both these methods are seen to produce high quality and mono-dispersed particles; however the exact mechanism of how the particle synthesis is controlled is not elucidated.

Besides the synthesis methods, the choice of stabilizing ligands also significantly influences QD synthesis. Ligands are introduced during QD synthesis and act as the

surface passivating agents to compensate the high surface to volume ratios of colloidal QDs. The choice of ligand is determined by their coordination chemistry with colloidal QD surface atoms and influences the size, morphology and optoelectronic properties of QDs.[27] Ligands can also alter the reactivity of precursors during the synthesis and provide better control over the nucleation and growth rates.[28]

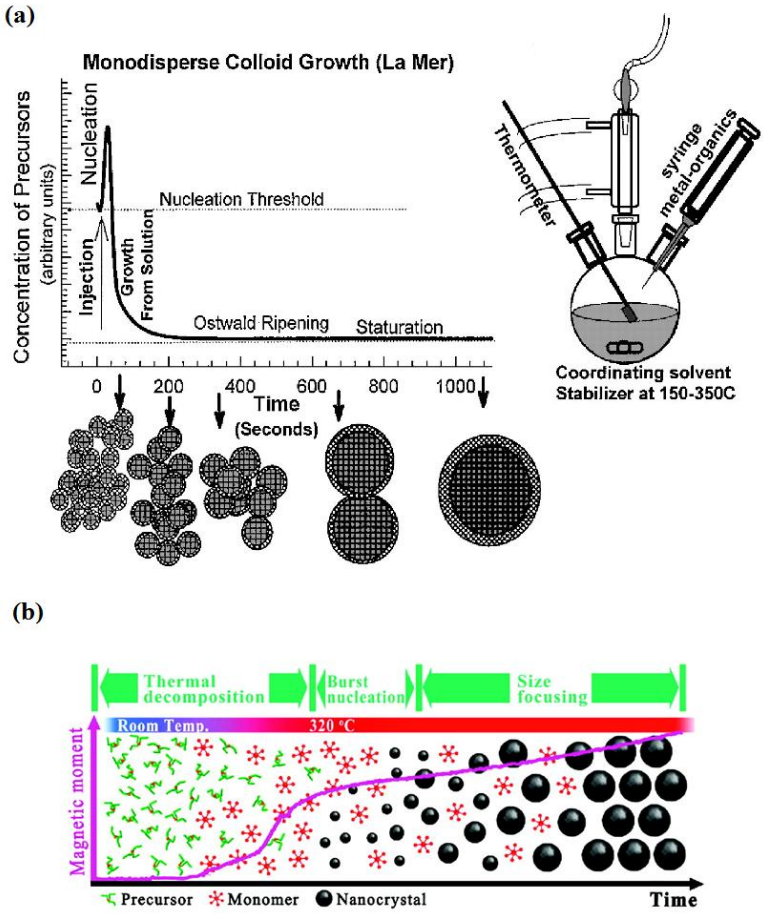

Figure 2-1. Schematic diagram depicting the nucleation and growth stages for the synthesis of NCs using (a) hot-injection method[29] (b) heat-up method.[30] Reprinted with permission from ref [29] © Annual review of material science 2000 and ref [30] © Journal of the American Chemical Society, ACS publications 2007

2.2.2 Lead Selenide (PbSe) Quantum dots

Murray et al[31] first reported the synthesis of PbSe QDs using wet chemistry method. In their hot injection approach, lead oleate and n-tri-octylphosphine selenide (TOPSe) precursors in n-tri-octylphosphine (TOP) were injected into a solution of diphenylether at 150 ^{o}C. As shown in **Figure 2-2**, PbSe QDs synthesized using this approach showed clear excitonic absorption features from 1200 to 2200 nm. The high resolution transmission electron microscopy (HRTEM) images and wide angle x-ray scattering (WAXS) patterns showed that highly crystalline PbSe QDs can be formed using this method. Increasing the reaction temperatures was found to enhance the QD growth and the modulation of reaction temperatures were used to control the particle size. The reaction temperatures of 90 to 220 ^{o}C were used to tune the particle size from 3.5 nm to 15 nm.

Following Murray's approach, many others have proposed different variants for the synthesis of PbSe QDs (**Table 2-1**).[32-36] TOPSe used in Murray's synthesis are toxic and instable in air. As such efforts have been reported to replace TOPSe as a selenium source to improve their air stability and toxicity. The use of less toxic and stable selenium dioxide (SeO_2) as a selenium precursor using the heat up synthesis method was reported by Chen et al.[36] Heating SeO_2 together with a solution of lead myristrate in octadecene (ODE) reduced SeO_2 to its active form Se^0, where ODE acted as both the solvent and the reducing agent for SeO_2 based reaction system. However, the reduction temperature of SeO_2 was relatively high (~240 ^{o}C) and the obtained PbSe QDs were much larger (~15 nm). Elemental Se in ODE has also been used as a selenium source and PbSe QDs from 6 nm to 25 nm have been synthesized by varying the reaction temperatures.[37] Unlike SeO_2, elemental Se reduces at lower reaction temperatures and smaller sized QDs can be synthesized. Additionally, others have used selenourea in N,N dimethylformamide

(DMF),[38] tri(diethylamino)phosphine selenide,[39] tris(diethylamino)phosphine selenide (TDPSe)[23] and OLASe[40] as a selenium source to replace TOPSe for PbSe QDs synthesis. However, TOPSe is still a widely used selenium precursor as it provides better control over PbSe QD synthesis as compared to other sources for selenium.

A commonly used approach for the size tuning of PbSe QDs is the modulation of reaction temperatures. The lower reaction temperature yields smaller sized QDs while increasing the reaction temperature forms larger sized QDs. For example, PbSe QDs from NIR emitting ultra-small QDs (< 2 nm)[33, 34] to mid-IR emitting large QDs (~17 nm)[35] have been synthesized by varying the reaction temperatures from room temperature to 250 ^{o}C. Apart from the reaction temperatures, the type of ligand and their concentration also influence the size of PbSe QDs. The nature of ligand-metal binding influences the reduction kinetics of precursors and the monomers access to QD surface for further QD growth. Increasing the ligand concentration such as oleic acid increased the growth of PbSe QDs.[41, 42] On the other hand, varying the length of trialkylphosphine ligands influenced the reduction of selenium precursor.[41] The shorter tributylphosphine (TBP) was found to slow the reduction of precursors as compared to the longer trioctylphosphine (TOP). The slower reduction of precursors allowed the formation of smaller sized PbSe QDs with better size distribution.[41] The presence of impurities in TOP such as dialkylphosphines also significantly influenced the reduction of precursors and the size of PbSe QDs.[42] Since the QD nucleation and growth is influenced by the monomer formation rate, a clear understanding of the reduction pathways for various precursor systems is essential for the better control over QDs formation. Recently, the non-molecular growth processes such as Ostwald ripening also found to influence the synthesis of various QDs systems such as cadmium selenide (CdSe),[43] indium phosphide (InP)[44] and lead

sulfide (PbS)[45] QDs and can significantly influence the final QD sizes. However, a clear consensus on the various factors influencing the nucleation and growth of PbSe QDs has not been reached.

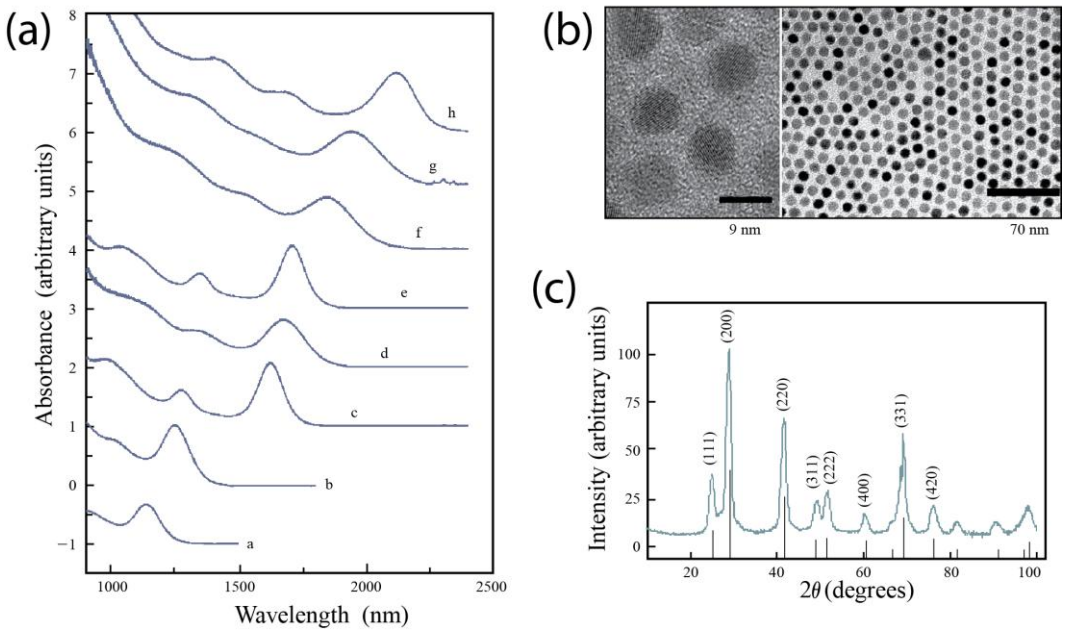

Figure 2-2. (a) Absorption spectra of PbSe QDs synthesized using hot injection of lead oleate and n-tri-octylphosphine selenide (TOPSe) into a mixture of diphenylether and n-tri-octylphosphine (TOP) at 150 ^{o}C (b) Representative transmission electron microscopy (TEM) image of as-synthesized PbSe QDs with diameter 8 nm (c) XRD of as-synthesized PbSe QDs.[31] Reprinted with permission from ref [31] © IBM Journal of Research and Development 2001.

Since the quantum confinement of QDs varies significantly with its geometry, the control over QD morphology during the synthesis is highly desirable. Ligands and QD growth environment have significant influence on the shape control of PbSe QDs. Orientation attachment of PbSe QDs in presence of different ligands such as hexadecylamine (HDA), oleic acid and tetradecylphosphonic acid (TDPA) formed nanowires of various shapes.[46] The orientation attachment of PbSe QDs was induced by utilizing TDPA and oleic acid as

ligands that preferentially bind to <111> crystal surface while leaving <100> surface open for directed attachment. The large dipole moment in PbSe QDs along <100> direction facilitated the directed assembly of QDs into nanowires. The nanowires then grew thicker by eliminating the high energy <111> surface in the presence of excess precursors. The higher reaction temperature (>170 ^{o}C) further facilitated the orientation attachment of PbSe particles. Amines on the other hand suppressed the growth of PbSe nanowires by enhancing the growth along <100> surface and leading to the formation of octahedral shaped PbSe QDs. Recently, Bealing et al[27] applied the density functional theory (DFT) to show that the equilibrium shape of PbSe QDs is a function of ligand coverage on QDs surface and the QD shape could be changed from octahedral to cubic by changing the ligand concentration during synthesis. The oleate ligands, which bind preferentially to <111> surface of the PbSe QDs influenced the surface energy of QDs and the higher concentration of oleate ligands transformed the crystal shape from octahedral to cubic. Such shape evolution of PbSe QDs has also been experimentally observed where the QD shape evolved from the octahedral/spherical to cubic and nanowires in the presence of various ligand systems.[21, 37, 47] These studies show that the interaction of ligands on PbSe QDs have profound effect on the resulting geometry of QDs, where the shape of PbSe QDs can be tuned by changing the concentrations of ligands that preferentially bind on different faces of QDs during the synthesis. In addition, impurities such as water and acetic acid present during the synthesis can also influence the shape of PbSe QDs.[48] The incomplete removal of acetic acid and water while forming the lead precursor i.e. lead oleate resulted in the formation of faceted QDs such as a star and octahedral shaped particles while the spherical shaped PbSe QDs are formed upon using completely dried precursors. The

presence of smaller acetic acid lowered the steric hindrance between different crystals and increased the possibility for orientation attachment to produce faceted particles.

One of the major hindrances for the utilization of PbSe QDs is their instability against oxidation. PbSe QDs degrade even after brief exposure to air due to the formation of oxides with surface Pb and Se atoms.[49] This can induce uncontrollable changes in the bandgap and photocharging of QDs,[50] which leads to a reduction in their photoluminescence quantum efficiencies and generate surface trap states in QDs film. As such, some approaches have been developed to improve the PbSe air stability, including the formation of core-shell structures with the shell of CdS, CdSe[51] or PbS,[52] surface treatment with molecular chlorine to replace surface Se atoms with chloride,[53] insitu passivation using halide precursors such as $PbCl_2$[20, 40] or injecting halide salts such as $PbCl_2$ or PbI_2 during QDs growth.[49] Most of these approaches have focused on coating the PbSe QDs with a robust shell to limit the access of oxygen molecules on QDs surface. The stability of PbSe QDs can also be improved through surface passivation via ligands such as phosphonic acids.[23] TDPSe, which was produced by the reaction of tris(diethylamino)phosphine (TDP) with elemental selenium, was used as a selenium precursor instead of TOPSe. The alteration of ligand structure drastically enhanced the air stability of PbSe QDs through the formation P-O- moieties on QDs surface that passivated the reactive PbSe surface. Direct cation exchange of CdSe QDs to PbSe QDs have also been used to enhance the air stability of PbSe QDs (**Figure 2-3(a)**).[54] The injection of pre-synthesized CdSe QDs into a hot precursor solution containing $PbCl_2$/oleylamine completely transformed CdSe QDs to PbSe QDs with in-situ halide passivation, and improving the air stability. As shown in **Figure 2-3(b) and 2-3(e)**, such direct cation exchange completely transformed the CdSe to PbSe QDs and the final PbSe QDs retains

the shape and size of the original CdSe QDs. The temperature required for complete transformation of CdSe to PbSe QDs depends on the size of initial CdSe QDs, where the larger sizes require higher temperatures for complete transformation. Similar cation exchange of ZnSe QDs to form air stable PbSe QDs upon heating in $PbCl_2$/oleylamine have also been reported.[55] In addition to enhanced QDs stability, the cation exchange of NCs allows the formation of varying morphologies of QDs. However, the complete transformation various NCs to PbSe can be an issue and careful design of reaction condition may be necessary to fully utilize the potential of such cation exchange reactions.

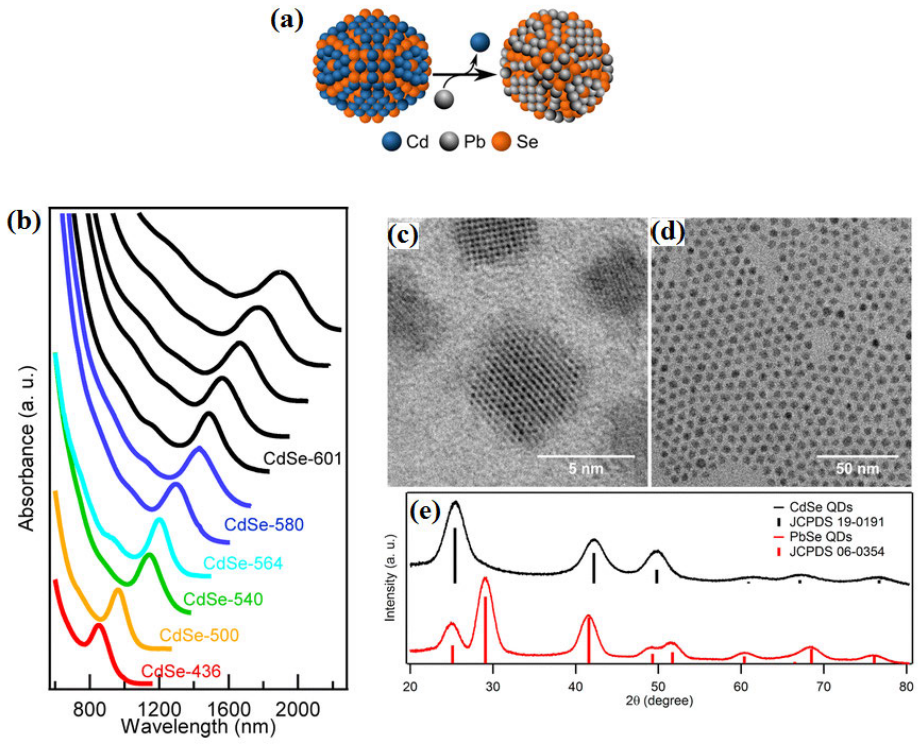

Figure 2-3. (a) Schematic illustration of direct cation exchange of CdSe QDs to PbSe QDs (b) Absorption spectra of PbSe QDs prepared by using various CdSe QDs. First excitonic absorption peaks of CdSe QDs are noted for each PbSe QDs. (c) & (d) Representative TEM images of 4.7 nm PbSe QDs (e) XRD for CdSe and PbSe QDs before and after cation exchance reactions.[54] Reprinted with permission from ref [54] © Nano Letters ACS publications 2014.

In addition to the colloidal synthesis in organic phase, attempts have also been made for the synthesis of PbSe QDs in aqueous phase. The aqueous synthesis of PbSe QDs usually has problems of instability, uncontrollable QD growth and low quantum efficiencies. Most aqueous based synthesis of PbSe QDs utilized water soluble lead salts and sodium selenite (Na_2SeO_3) as precursors. Various ligands such as poly (vinyl alcohol),[56] glutathione reductase,[57] and RNA[58] have been used to control QDs growth and act as a biocompatible ligands to produce water soluble PbSe QDs. However, the control over PbSe QD size and their distributions using aqueous synthesis are relatively poor as compared with that being synthesized in organic solvents.

2.2.3 Lead Sulfide Quantum dots

The synthesis of colloidal NIR emitting PbS QDs with a good size distribution was reported by Hines et al.[7] Their synthesis was based on the hot-injection procedure developed by Murray et al,[59] where the injection of bis(trimethylsilyl)sulfide (TMS sulfide) into a hot lead precursor solution of lead oleate yielded the PbS QDs with a quantum efficiency of 20-30 %. As-synthesized PbS QDs showed pronounced excitonic spectrum and is one of the most cited works for colloidal PbS QDs synthesis. The excitonic absorption peaks can be tuned from 800 nm to 1800 nm (**Figure 2-4**) with a size distribution of 10-15 %. The synthesis temperature and ligand concentrations have been varied to tune particle sizes.

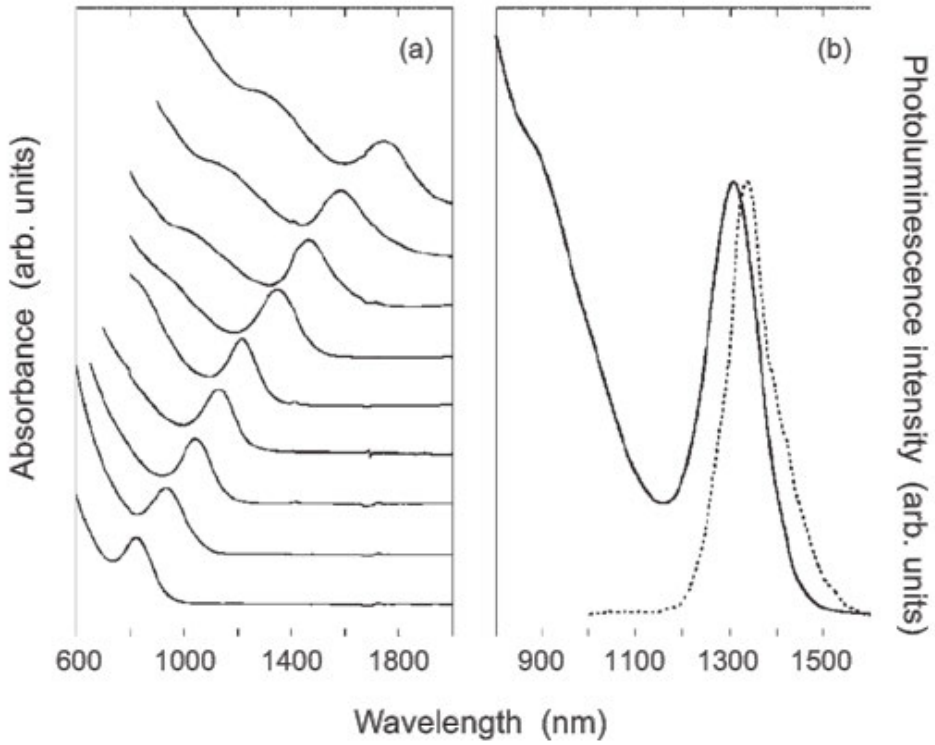

Figure 2-4. Optical characterization of PbS QDs (a) excitonic absorption spectra (b) representative photoluminescence (PL) spectra of QDs with an average diameter ~ 6.5 nm.[7] Reprinted with permission from ref [7] © Advanced Materials, Wiley publishing 2003

Followed the report of Hines et al,[7] many attempts have been made to synthesize the PbS QDs with extended broadband absorption and improved size distributions (**Table 2-1**). Similar to PbSe QDs, temperature and ligand concentration significantly influenced the sizes of PbS QDs. Low temperature promoted the formation of small PbS QDs while the higher temperature formed larger sized QDs. The increase in oleic acid concentration also enhanced QDs growth.[60] As a result, PbS QDs with emission wavelengths from 680 nm[61] to mid-IR[62] have been reported. Introducing a small amount of trioctylphosphine (TOP) into the reaction mixture proposed by Hines et al[7] had beneficial effect on improving the QD size distribution and yielded high luminescence PbS QDs.[63] The

quantum yields (QY) as high as 80 % could be achieved by the introduction of TOP. However, the size of PbS QDs was found to decrease as compared to the growth without TOP. Better passivation of surface traps states and stronger coordination of PbS QDs surface by TOP were identified as reasons for improving QD quality and reducing particle size. Attempts have also been made to synthesize PbS QDs in micro-fluidic devices to automate and enhance the reproducibility of the synthesis.[64] Others attempted to replace air and moisture sensitive TMS sulfide by using elemental sulfur,[19, 37, 65] thioactamide,[65, 66] sodium sulfide,[67, 68] hydrogen sulfide gas[69] and many others.[67] However, TMS sulfide was still widely used for the synthesis of high quality PbS QDs.

Besides the synthesis approach of Hines et al,[7] PbS QDs synthesis as reported by Cademartiri et al[19] is also widely adopted. Their synthesis was based on the heat-up method using a solventless technique. Oleylamine (OLA) acted as both the reacting medium and ligand while lead chloride ($PbCl_2$) and elemental sulfur were used as precursors. The method is able to produce multigram scale (~1.4 g) of PbS QDs with a narrow size distribution, lower Stokes shift (~10 meV) and gave relatively higher photoluminescence QY (~40 %). The calculated price of PbS QDs synthesized using this technique was estimated to be USD 14 per gram demonstrating the industrial scalability of the technique. However, the excitonic absorption tunability for the technique was limited (1245 to 1625 nm). Recently, Weidman et al[70] extended the excitonic absorption tunability range of the synthesis from 1000 nm to 1800 nm by controlling the precursor stiochiometry. $PbCl_2$: sulfur ratio and the synthesis temperatures were modulated to tune QD sizes. Further, the use of highly reactive TMS sulfide as a sulfur precursor allowed the reaction to occur at room temperature and extended the excitonic absorption wavelength to ~700 nm.[20] The synthesis batches up to 47 grams with a clear excitonic absorption peak

and good size distribution were produced using the technique (**Figure 2-5**). However, the requirement of extensive post-synthesis processing steps such as isolation of pure PbS QDs that is free from the residual $PbCl_2$ and the ligand exchange of OLA with OA limit the applicability of the synthesis technique.

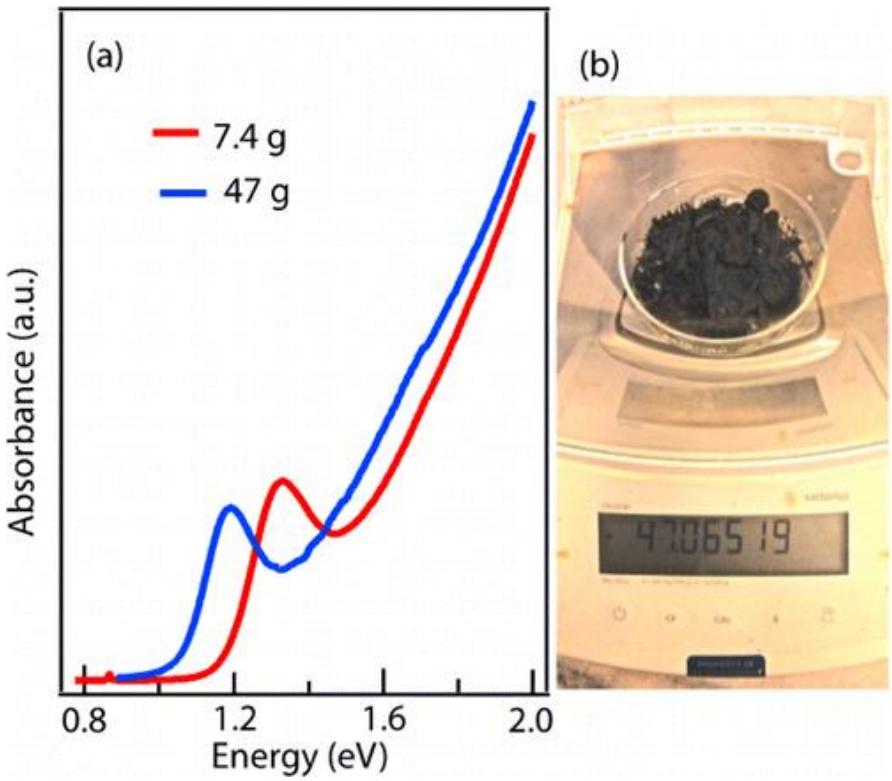

Figure 2-5. Multi-gram synthesis of PbS QDs using $PbCl_2$/OLA as lead precursor and TMS sulfide as sulfur precursor (a) Excitonic absorption spectra of as-synthesized PbS QDs producing 7.9 g and 47 g of product (b) Representative photograph showing 47 g of PbS QDs.[20] Reprinted with permission from ref [20] © ACS Nano ACS publications 2013.

Other notable synthesis approach include the 'top-down' strategy[71] to synthesize mono-dispersed colloidal PbS QDs instead of commonly used 'bottom-up' synthesis. The PbS QDs with controllable sizes (3.5 to 5.5 nm) and narrow dispersions (5.5 to 9.1 %) can be produced using millisecond pulse laser irradiation of initially large and poly-dispersed PbS

QDs solutions. The two step laser ablation and irradiation route was used to synthesize the PbS QDs capped with 1-dodecanethiol. Differently sized PbS QDs could also be formed by stepwise heating the preformed PbS QDs in the presence of excess oleic acid.[45] Oleic acid is able to disintegrate some preformed QDs to generate PbS monomers (i.e. un-crystallized PbS), and these monomers can add to the un-disintegrated QDs to increase particle size resembling to a "living" growth process.

Similar to PbSe QDs, many attempts have been made to control the morphology of PbS QDs. Ultrathin two-dimensional (2D) nanosheets of PbS were synthesized by orientation attachment of spherical PbS nanoparticles along reactive <110> surface.[72] Heating of spherical PbS QDs in the presence of chlorine containing co-solvents such as 1,2-dichloroethane exposed the reactive <110> surface and the ordered monolayer assembly of oleic acid on the flat <100> surface initiated the two dimensional growth. The spectral position of absorption and emission spectra remained at the same position during the two dimensional growth and the only notable difference was the spectral peak intensity. The spectral peak broadened over time during the growth of 2D nanosheets. Similarly, zero-dimensional (0D) nanoparticles, one-dimensional (1D) nano-rods and two-dimensional (2D) nano-sheets can also be produced by the decomposition of lead ethylxanthate or lead hexadecylxanthate in trioctylamine (TOA) at various reaction conditions.[73] The preferential growth along <110> crystal surface initiated the growth of these PbS nanostructures and the injection temperature of precursors were used as the shape tuning parameter. In addition, various shapes of QDs such as star, octahedral, cubo-octahedral and cubic can be synthesized using different ligands such as oleic acid, oleylamine and dodecanethiol during the synthesis.[74] Similar to PbSe QDs, the shape of oleate capped PbS QDs changes from octahedral to cubic upon increasing the QDs size indicating similar

crystalline structures.[75] Sequential cation exchange reactions with full or partial inter-conversions between CdS, Cu_2S and PbS have also been used to synthesize the isotropic and anisotropic shapes of PbS QDs (i.e. nanorods).[76] The ligand that binds preferentially to either monvalent or divalent cations was used to drive the cation exchange reactions. The exchange of cadmium cation (Cd^{2+}) with copper cation (Cu^{+}) can be promoted in presence of methanol (MeOH), which preferentially binds to Cd^{2+} cation to produce Cu_2S nanorods. Similarly, the exchange of Cu^{+} with lead cation (Pb^{2+}) can be promoted in presence of tributylphosphine (TBP) to produce PbS nanorods. Such two step cation exchange reactions should be beneficial to produce anisotropic shapes and sizes of PbS QDs, which are otherwise difficult to synthesize using the traditional colloidal synthesis approach.

In addition to the colloidal synthesis in organic solvents, several attempts have been made to synthesize the PbS QDs in water. In comparison to PbSe QDs, better control over the QDs size can be observed for the aqueous synthesis of PbS QDs. The aqueous synthesis of PbS QDs involves the use of lead salts such as lead acetate as lead precursor and sodium sulfide as sulfur precursor. Various water soluble thiols such as mercaptopropionic acid, thioglycerol, dihydrolipoic acid etc can be used as ligands.[77-79] The PbS QDs with reasonable luminescence (quantum yield, QY up to 10 %) has been synthesized using the mixture of thioglycerol and dithioglycerol as ligands.[80] Although QY close to 10 % can be obtained using the aqueous synthesis, the size tunability of the method is rather limited. PbS QDs with emission wavelengths from 870 nm to 1400 nm can be synthesized by optimizing the ratios of Pb:S and ligands during the synthesis.[77-79] However, it still remains a challenge to synthesize high quality and differently sized PbS QDs using aqueous synthesis approaches.

2.2.4 Lead Telluride Quantum dots

Although the growth of PbTe nanocrystals (NCs) in glasses has been reported since early 1990s,[81] relatively less work have been reported on the synthesis of NIR to mid-IR emitting PbTe QDs (**Table 2-1**). The reason for its limited developments could be its similarity with PbSe QDs synthesis. Murphy et al[82] reported the synthesis of PbTe QDs with average diameter of ~3 nm to 8 nm following the similar hot injection procedure as reported by Murray et al[31] for the synthesis of PbSe QDs. PbTe QDs were synthesized by injecting trioctylphosphine telluride (TOPTe) into the hot lead oleate solution. Octadecene was used as the reacting medium for the synthesis. As shown in **Figure 2-6**, PbTe QDs with narrow size distributions (~7 %) and high photoluminescence quantum efficiencies (~52 %) can be produced using the method. Temperature and ligand concentrations were adjusted to tune particle sizes[16] The shape of PbTe QDs were found to change from spherical to cubic on increasing QD sizes (**Figure 2-6(c)**). Similar shape evolution from spherical/octahedral to cubic has also been observed for PbSe and PbS QDs which shows that similar crystalline structure exists within all lead chalcogenide QDs.[27, 75] Also, the reaction temperature and ligand concentration showed similar trends as in PbSe and PbS QDs. Higher temperature promoted the formation of larger sized particles while the lower temperatures produced smaller sized particles. Increasing the ligand concentration enhanced the particle growth. Adaptations to the multi-gram synthesis of PbS QDs[19] have also been applied for the synthesis of PbTe QDs.[83] The synthesis protocol involved the preparation of $PbCl_2$ solution in OLA followed by the injection of TOPTe instead of sulfur dissolved in OLA. The sizes of PbTe QDs were tuned from 2.4 nm to 14 nm using this synthesis technique.

Ligands play similar role on tuning the shape of PbTe QDs as that in PbSe and PbS QDs. Cubic PbTe QDs can be synthesized using a mixture of oleic acid and oleyamine.[84] Various phosphonic acid or amine based ligands such as tetradecylphosphonic acid (TDPA), octadecylphosphonic acid (ODPA), hexylphosphine acid (HPA), hexadecylamine (HDA) and dodecylamine (DDA) can also be used to control the shape and size of PbTe QDs.[85] The presence of phosphonic acid ligands influenced the particle size while the amine based ligands influenced the shape of PbTe QDs.[85]

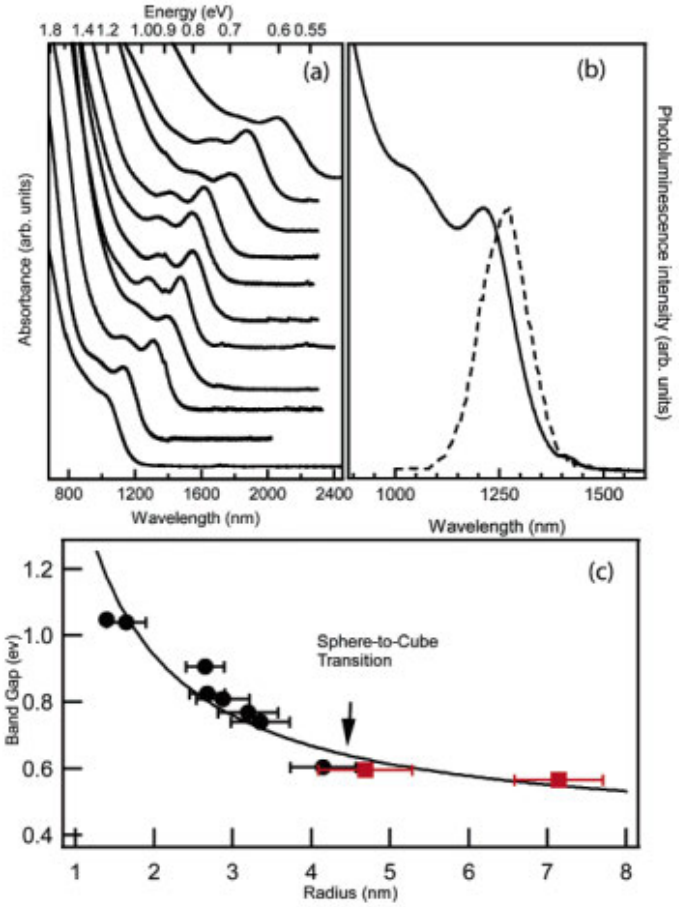

Figure 2-6. (a) Excitonic absorption spectra of PbTe QDs (b) representative PL spectra of PbTe QDs with particle diameter of 2.9 nm (c) shape transition of PbTe QDs with the change in size of QDs.[16] © Reprinted with permission from ref [16] © Journal of the American Chemical Society, ACS publications 2006

Table 2-1. Summary of progress in the synthesis of colloidal lead chalcogenide QDs

QDs Type	Shape	Synthesis Method	Precursors	Ligand	Solvent	Dia. (nm) and Abs. Peaks	SD (%) and Quality	Year	Ref
PbSe QDs	Quasi-Spherical	Hot-Injection	$Pb(OA)_2$ and TOPSe	TOP	DPE	(3.5-11)[a] and (1200-2200)[b]	SD ~10%	2001	[31]
			PbO and TOPSe	OA and TOP	ODE	(3-13)[a] and (1100-2520)[b]	SD 5-7%	2004	[32]
			$Pb(OA)_2$ and TOPSe	TOP	DPE	(8-22)[a]	-	2004	[35]
			Pb(OA)2 and Selenourea	OA	PE and DMF	(3-15)[a]		2011	[38]
			$Pb(OA)_2$ and TDPSe	TDP	ODE	(~1450)[b]	Air-stability, QY ~20%	2015	[23]
			$PbCl_2$-OLA and Se-OLA	OLA	OLA	(4.4-12)[a]	Air-stability, SD 6-8%	2015	[40]
		RT Inj.	$Pb(OA)_2$ and TOPSe	OA and TOP	ODE	(<2)[a] and (900)[b]	QY> 50%	2008	[33]
		Heat-up	Pb-myristate and SeO_2		ODE	(~15.9)[a]	SD 7%	2008	[36]
		Cation exchange	CdSe QDs and $PbCl_2$/OLA	OLA	OLA	(850-1500)[b]	Air-stability, QY ~43%	2014	[54]
			ZnSe QDs and $PbCl_2$/OLA			(2-7)[a]	Air-stability	2015	[55]
		Aqueous	$Pb(CH_3COO)_2$ and Na_2SeO_3	PVA	Water	(920-1450)[b]	-	2011	[56]
	Nanowires	Hot Injection	PbO-TDPASe	OA, TOP, HDA and TDPA	DPE	(3.5-18)[a]	-	2005	[46]
	Multirods		$Pb(Ac)_2$ and TOPSe	OA and	ODE	(4.7)[a]	-	2011	[21]
	Nanostars		$Pb(Ac)_2$ and TOPSe	TOP		-	-	2005	[48]
		Aqueous	$Pb(CH_3COO)_2$ and Na_2SeO_3	GSH	Water	(13-16)[a]		2012	[57]
PbS QDs	Quasi-Spherical	Hot Injection	$Pb(OA)_2$ and TMS sulfide	OA	ODE	(800-1600)[b]	SD 10-15%; QY ~20-30%	2003	[7]
			$Pb(OA)_2$ and TMS sulfide	OA/TOP	ODE	(5.9)[a]	SD~4% and QY ~80%	2008	[63]
		Heat up	$PbCl_2$ and sulfur	OLA	OLA	(1245-1645)[b]	SD 20%	2006	[19]
			$PbCl_2$ and sulfur	OLA	OLA	(1000-1800)[b]	SD <5%	2014	[70]
			$Pb(OA)_2$ and TMS sulfide	OA	ODE	(620-900)[b]	QY ~20%	2009	[65]
			$PbCl_2$ and TMS sulfide	OLA	OLA	(~700-1800)[b]	SD 6-7%	2013	[20]
		Physical	Polydispersed PbS QDs	DDT		(3.5-5.5)[a]	SD 5.5-9.1%	2013	[71]
		Aqueous	$Pb(Ac)_2$ and Na_2S	TG	Water	(1050-1200)[b]	QY ~10%	2005	[80]
			$Pb(Ac)_2$ and Na_2S	TG	Water	(1000-1400)[b]	QY ~10%	2004	[77]
			$Pb(Ac)_2$ and Na_2S	DHLA	Water	(870-1010)[b]	QY ~10%	2009	[78]
	Nanorods	Cation exchange	CdSe QDs	MeOH and TBP	ODE	-	-	2009	[76]
	Nanosheets	Heat up	lead hexadecylxanthate	TOA	TOA	(1.7-2.5)[a]		2011	[73]
			lead ethylxanthate	TOA	TOA	(25)[a]		2011	[73]
			Spherical PbS QDs	DCE	DCM	-	-	2010	[72]
PbTe QDs	Quasi-Spherical and cubic	Hot Injection	$Pb(OA)_2$ and TOPTe	TOP	DPE	(8-14)[a]	-	2004	[82]
			$Pb(OA)_2$ and TOPTe	TOP	DPE	(2.6-8.3)[a]	SD ~7% and QY ~53%	2006	[16]
			$PbCl_2$-OLA and TOPTe	TOP/OLA	OLA	(14)[a]	-	2008	[84]
			$PbCl_2$-OLA and TOPTe	TOP/OLA	OLA	(2.4-14)[a]	SD ~5.6-9.1%	2012	[83]

TOP: Trioctylphosphine; DMF: N,N-dimethylformamide; TBP: Tributylphosphine; TOA: Trioctylamine; PE: phenyl ether; TDP:tris(diethylamino)phosphine PVA: polyvinyl alcohol; DPE: Diphenylethane; ODE: Octadecene; DCE: 1,2 dichloroethane; DCM: dichloromethane; MEOH: methanol; DHLA:dihydrolipoic acid; TG: 1-thioglycerol; DDT:1-dodecanethiol; [a]QD Diameter; [b]QD Exciton Absorption peak

2.3 Ligand Exchange of Lead Chalcogenide QDs

Ligands play an important role on maintaining colloidal solubility, preventing oxidation and controlling the nucleation and growth of lead chalcogenide QDs. Ligands are introduced during the synthesis and are usually composed of bulky hydrocarbons for high quality QD synthesis. However, these bulky ligands are insulating and non-functional for applications in optoelectronic devices and bio-conjugation. Efficient replacement of these bulky ligands with non-insulating and functional ligands is crucial for the applications of these QDs.

The ligand exchange reactions at QDs surface occur on the basis of the HSAB (Hard and Soft Acid and Base) principle as proposed by Pearson.[86] According to the HSAB principle, hard acids form stable complexes with hard bases while soft acids prefer to react with soft bases. The lead chalcogenide QDs are cation rich on surface (i.e. Pb:S >1) and the ligands bind to these cation rich surfaces of QDs.[87] Pb on QD surfaces are categorized as soft acids and prefer to react with soft bases like carboxylate or thiolate.[88] The affinity of incoming ligands to QD surfaces as compared to the existing native ligands determines the efficiency of ligand exchange. In presence of excess new ligands, the steric crowding of new ligands favors desorption of native ligands and the new ligand from solution binds on QDs surface. The type of exchanging ligands such as L-type ligand i.e. two electron donor Lewis bases, X-type ligand i.e. one electron donor anions and Z-type ligand i.e. two electron acceptor Lewis acids also influences ligand exchange.[89] For example, direct replacement of X-type ligands with L-type ligands disturb the charge neutrality on QD surface in non-polar solvents and promotes Z-type displacement i.e. removal of surface metal cation along with X-type ligand as a neutral metal ligand complex to maintain

charge neutrality.[89] However, the use of polar solvent can lift the restrictions on maintaining the charge neutrality on QD surfaces and a proper choice of ligand affinity to QDs surface can enhance the ligand exchange efficiency.

The ligand exchange of QDs can be performed in solid state or in solution phase. The solid state ligand exchange is performed exclusively in QD thin films when the native ligands are required to be replaced with shorter and more conductive ligands. The solid state ligand exchange is performed by immersing the QD thin films into new ligand solutions, where the new ligands replace the native ligands. The solid state exchange allows the easy control over QDs inter-particle distance by using a wide range of ligand chemistries.[90] However, the volume change during the replacement of native ligands leads to the formation of voids and cracks in QD thin films.[91] The cracking of film can potentially reduce film density, create electrical shorts within the film and reduce its conductivity. Layer-by-layer deposition is an alternative for crack free surfaces but it is a time-consuming process for industrial applications.[92] Further, the solid state ligand exchange also leads to the surface trap states due to inefficient ligand exchange which is detrimental to the overall device performance.[91]

The solution phase ligand exchange is performed prior to any device fabrication or when the intended applications require QDs in solution phase such as in bio-related applications. Although the solid state ligand exchange is still the most popular and widely used technique for QD thin film fabrication, the solution phase ligand exchange can lead to better replacement of native ligands and can dramatically improve the film properties in devices.[93] Further, the solution phase ligand exchange is beneficial for attaching the QDs to various substrates using multi-functional ligands. Until now, the solution phase ligand exchange of lead chalcogenide QDs have been typically challenging due to its different

surface chemistry as compared to the well understood cadmium based QDs. Nevertheless, recent developments in understanding the surface chemistry and ligand engineering have enabled tremendous progress in the solution phase ligand exchange of lead chalcogenide QDs. Some of the recent progresses in solution phase exchange are highlighted below.

2.3.1 Organic Ligand

The interaction of organic ligands with QD surface and the surrounding medium is schematically shown in **Figure 2-7**.[94] Organic ligands are composed of an anchoring or head group that interacts with QD surfaces and a pendant moiety or tail group which mediates the QDs interaction with surroundings and maintains their colloidal stability. As shown in **Figure 2-7**, the pendant moiety consists of an organic backbone and a substituent functional group. The pendant moiety maintains colloidal stability either by steric repulsion of non-polar substituent group or by electrostatic repulsion of polar substituent group. The non-polar substituent groups usually require longer organic backbone to prevent the aggregation of QDs. For example, the native organic ligands such as oleic acid consist of a pendant moiety with non-polar substituent group and a long chain aliphatic molecule (octadecene, C18) as backbone. The long chain aliphatic molecule provides the colloidal stability through steric interaction in non-polar organic solvents. Similarly the pendant moiety of small molecules such as mercaptopropionic acid (MPA) has short chain aliphatic molecule (C3) as backbone and a polar carboxylate (COO^-) as the substituent group. The polar substituent group maintains the colloidal stability through electrostatic repulsion in polar solvents.

The organic ligand exchange can be classified on the basis of anchoring groups or on pendant moieties. Since the interaction of anchoring groups on QD surface is the

dominating factor for effective ligand exchange, we would like to classify the organic ligand exchange based on the anchoring groups on QD surface. (**Table 2-2**)

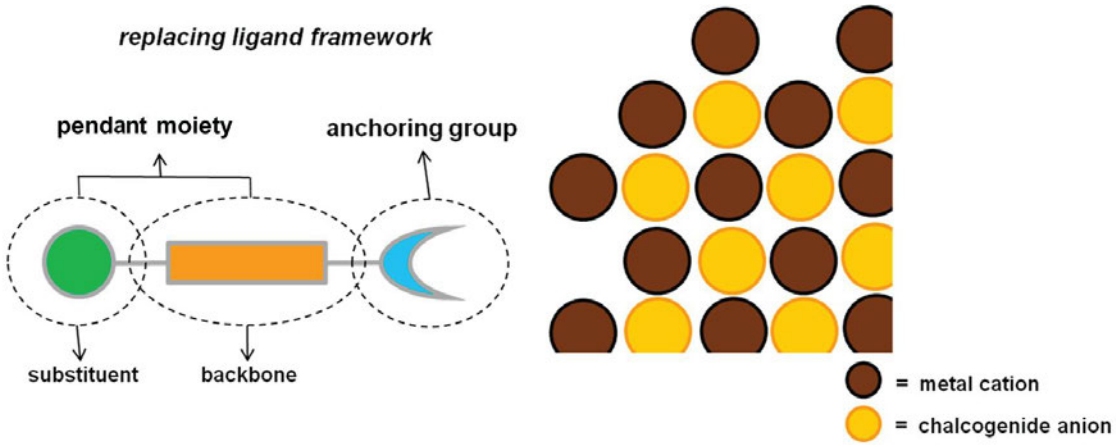

Figure 2-7. Schematic illustration of organic ligands interaction with QD surface.[94] Reprinted with permission from ref [94] © Journal of the American Chemical Society, ACS publications 2015.

2.3.1.1 Thiol based organic ligands

Thiols have relatively stronger binding affinity with heavy metal cations (such as lead, arsenic, cadmium and mercury) and these ligands have been successfully implemented as the exchanging ligand in gold and cadmium based nanoparticles.[95] This leads them to be the replacing ligand in lead based QDs. Most early works on thiol based ligands were targeted towards enhancing the bio-compatibility of QDs as NIR fluorophores. Typically the native oleate ligands were replaced with thiol containing bio-polymers for phase transfer to water. Thiol-based bio-compatible polymers such as (1-mercaptoundec- 11-yl)tetra(ethylene glycol) (MTPEG),[96] 16-mercaptohexadecanoic acid (MHDA, 90%)[97] and 11-mercaptoundecanoic acid (MUA, 95%)[97] could successfully exchange the native oleate ligands of PbS QDs and PbSe QDs and enhance their solubility in water and relevant buffers. One typical observation after thiol ligand exchange was a relatively larger

bathochromic shift (~30-80 nm) in their absorption and emission spectra in comparison to cadmium based QDs (**Figure 2-8**). The larger bathochromic shift of the absorption excitonic peak is attributed to the change in electronic density and confinement due to Pb-thiol bond, which has different binding strength compared to Cd-thiol bond.[97] These thiol-based polymers were found to preserve the photoluminescence from ~70 % - 5 % relative to that of oleate capped QDs.[96, 97] The photoluminescence of ligand exchanged QDs were influenced by the type of exchanging ligands. Longer chain polymers showed higher luminescence in water than shorter ligands due to limited access of water to QD surface. However, the stability of QDs in water and buffers were maintained only up to 5 or few days after the ligand exchange.[96] The oxidation of thiols to disulfides in water at ambient conditions was observed as the reason for the instability of these QDs upon long term storage.

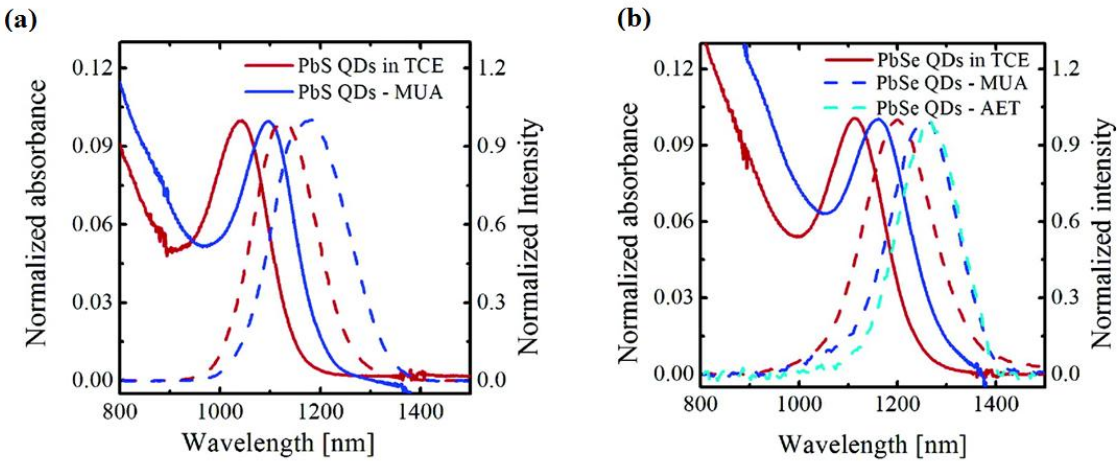

Figure 2-8. Excitonic absorption and emission spectra of (a) PbS QDs before ligand exchange in TCE and after ligand exchange with MUA in water (b) PbSe QDs before ligand exchange in TCE and after ligand exchange with MUA and AET in water.[97] Reprinted with permission from ref [97] © The Journal of Physical Chemistry B, ACS publications 2007.

Moody et al[98] investigated the stability of PbS QDs using a monothiol and dithiol anchoring groups. The chelating dithiol ligands were more stable as compared to their monothiol counterpart under light and dark conditions. The formation of oligodisulfide on the surface of PbS QDs was argued as the reason for the higher stability of dithiol ligands. The influence of multiple chelating short chained amino acids has also been investigated for the phase transfer of oleophilic PbS QDs to water.[99] The ligands with multiple chelating functional groups were more efficient in the phase transfer process (**Figure 2-9**). The emission intensity after the ligand exchange with L-glutathione (GSH) was preserved up to ~70 % of the oleate capped QDs and showed the storage stability of more than 20 days under ambient condition. The multiple chelating sites of GSH along with possible surface passivation through secondary coordination to surface Pb sites contributed to the efficient ligand exchange and long term storage stability of PbS QDs. These studies indicate that the multiple chelation of ligands to QD surface is beneficial for the phase transfer and stability of QDs during the ligand exchange.

The choice of ligand exchange solvent along with ligand exchange conditions also plays an important role in achieving the best quantum efficiency and colloidal stability. The ligand exchange conditions such as solution pH and ligand concentration influenced the emission intensity and stability of QDs during the ligand exchange process.[99, 100] For example, Deng et al[99] found that the optimal ligand exchange pH using GSH to be 5 and the ligand solution concentration to be 0.15 M ([QD]=30 mM) (**Figure 2-9(c)**). GSH has multi-functional groups and the pH of solution influences their co-ordination with Pb. On the other hand, less ligand can lead to inefficient exchange while excess ligands can introduce surface trap states due to extensive surface Pb removal. Thus, an optimal ligand exchange condition needs to be identified for different ligands. Ligand exchanging solvents also play

an important role in enhancing the efficiency of exchange. Ligand exchange using thioglycerol induced dramatic reduction in photoluminescence quantum yield (QY) from ~50 % in organic solvent to only ~10 % in water while only a moderate loss in QY (to ~26 %) was observed in DMSO.[92] Similarly, the phase transfer of PbS QDs using mercaptopropionic acid (MPA) was more facile in DMSO than in water.[100] The luminescence intensity as well as the stability of PbS QDs was improved in DMSO indicating the role of solvent for efficient ligand exchange of lead chalcogenide QDs. Since water and DMSO are both polar solvents, maintaining the charge neutrality on QDs surface should not be an issue. However, the presence of hydroxides (OH) in water can potentially quench the photoluminescence of QDs while DMSO provides polar solvent environment that is free from hydroxide quencher.[92] Shielding of lead chalcogenide QDs from the possible hydroxide quenching through efficient ligand coverage and ligand engineering can potentially lead to an efficient phase transfer of these QDs to aqueous environments.

The nature of pendant moiety also influences the ligand exchange of lead chalcogenide QDs. Arenethiolate ligands in non-polar solvent (dichloromethane) were found to improve the spectral features of PbS QDs during the ligand exchange process.[94, 101] The stronger acidic character of arenethiols allowed their complete deprotonation using organic bases in polar solvents and enhanced the ligand exchange efficiency by preventing the protic attack by thiols. Further, optical absorption enhancement (up to 300 %) was observed at high energies (>3.1 eV) in the presence of electron donating pendant moiety while no such enhancement was observed in the presence of electron accepting pendant moiety.[94] The ground state ligand/QDs mixing in the presence of electron donating pendant moiety contributed to the enhanced optical enhancement. The type of pendant moiety i.e. aromatic

or aliphatic also influences the degree of optical enhancement. Aromatic moiety provided higher degree of optical enhancement possibly through π-resonance of aromatic rings. Further, the aromatic pendant moiety with dithiol anchoring group was found to result in poor colloidal stability as compared to its monothiolate counterpart.[94] This result is in contrast with the stability enhancement using multiple chelating ligands.[98] Large strain induced by the bulky aromatic pendant moiety led to incomplete coverage of arenedithiolate ligands on PbS QD surface and resulted in its poor colloidal stability. These results show that the ligand structure can potentially influence efficient ligand exchange of lead chalcogenide QDs.

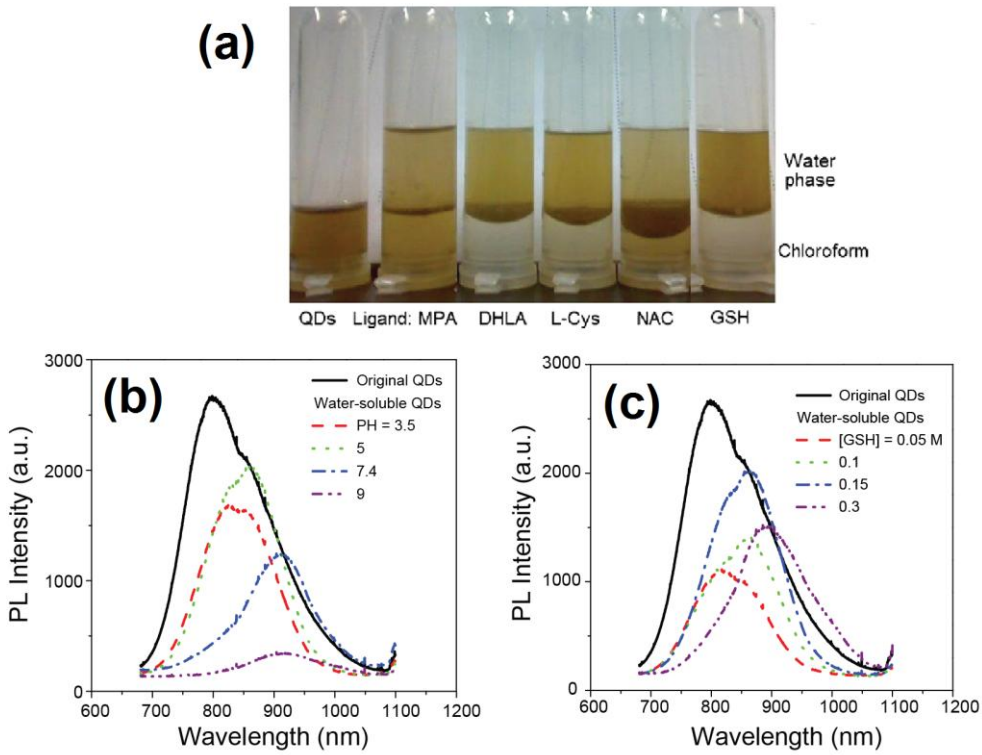

Figure 2-9. (a) Photographs showing ligand exchange using various amino acids. (b) photoluminescence spectra of PbS QDs after ligand exchange using various ligands such as GSH, DHLA, L-Cys, MPA and NAC (c) influence of pH on the ligand exchange using GSH.[99] Reprinted with permission from ref [99] © Journal of Colloid and Interface Science, Elsevier publishing 2012.

2.3.1.2 Selenide based ligands

In comparison to thiol ligands, the ligand exchange using selenide ligands is rare. The possible reason can be associated with their less commercial availability and their similarity to thiol based ligands. Hughes et al[102] attempted to control the PbSe QDs surface chemistry using alkyl selenide based ligands (**Figure 2-10**). The ligand exchange using these ligands (dioctadecyl diselenide, $[CH_3(CH_2)17Se]_2$, and octadecylselenol, $CH_3(CH_2)17SeH$) was found to completely replace the native oleate ligands. Similar to thiol based ligands, treatments with Se ligands induced the red-shift in absorption and emission spectra and the reduction in photoluminescence QY. Ligand exchange with selenide ligands also altered the stiochiometry of PbSe QDs and the ratio of Pb:Se decreased upon ligand exchange. However, the complete reversal of QDs stiochiometry from Pb rich to Se was not possible as Se ligands preferentially bind to the <111> face of QDs surface only.

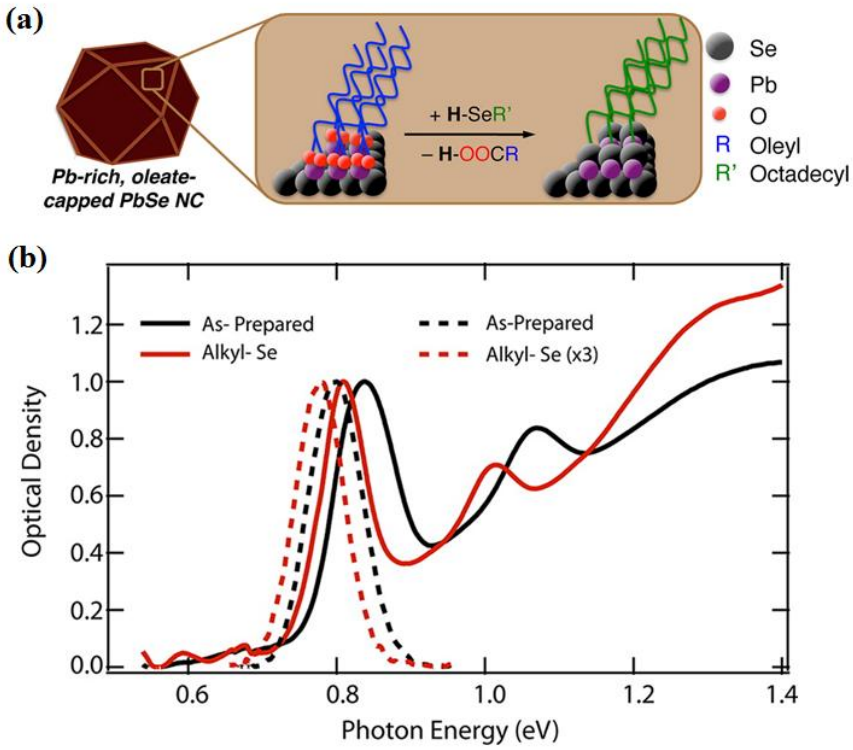

Figure 2-10. (a) Schematic illustration of ligand exchange using alkyl selenide ligands (b) excitonic absorption and photoluminescence spectra before and after ligand exchange using alkyl selenide ligands.[102] Reprinted with permission from ref [102] © ACS Nano, ACS publications 2012.

2.3.1.3 Multidentate carboxylate ligands

Similar to thiol based ligands, multidentate carboxylate ligands are also investigated to enhance the bio-compatibility of lead chalcogenide QDs. The thiol based ligands usually suffer from self-oxidation on QDs surface when being exposed to air and light in aqueous solutions.[95] As a solution, Lin et al[103] proposed using amphiphilic multidentate polyacrylic acid (PAA) as a replacing ligand. The native oleate ligand were replaced with PAA by mixing the oleate capped PbS QDs in excess PAA in THF and stirring at room temperature for overnight reaction. In contrast to thiol based ligands, the absorption and fluorescence spectra blue shift after ligand exchange with PAA. The photoluminescence

(PL) quantum efficiencies also decreased after the exchange (from ~82 % in toluene to ~24 % in water). The formation of defects and oxidative etching on QDs surface were attributed for the observed blue shift and decreased quantum efficiencies. Similary, the amphiphilic poly(maleic anhydride-alt-1-octadecene-co-poly(ethylene glycol)) or PMAO-PEG has also been used for the phase transfer of oleylamine (OLA) capped PbS QDs into water.[104] Ligand exchange using PMAO-PEG led to the formation of double size distribution in water while only mild etching was observed upon transferring to ethanol. Etching of QDs in the co-presence of amphiphilic polymers and water induced the double size distribution. The PL quantum efficiencies also decreased upon phase transfer to water. However, the PL of small PbS QDs in the bimodal distributions recovered when stored in dark for three months while that of larger sized QDs did not recover. The smaller QDs are usually terminated with <111> surface and the oleic acid preferentially binds to the <111> surface.[75] PMAO-PEG consists of carboxylic anchoring group and can provide better coverage for better passivation. Although hydroxide quenching of fluorescence is widely accepted for the PL reduction in water, the recovery of PL in water shows that proper ligand engineering can potentially preserve PL and prevent from hydroxide quenching. The type of the native capping ligand i.e. oleylamine (OLA), oleic acid (OA) or oleic acid/trioctylphosphine (OA/TOP) was found to influence the extent of etching by PMAO-PEG upon ligand exchange.[105] As shown in **Figure 2-11**, OLA capped PbS QDs showed most significant etching while OA capped QDs had least etching. The type ligands could influence different etching behaviors. OLA is considered L-type ligand while OA and PMAO-PEG are X-type ligand. Since the ligand exchange was conducted in non-polar (chloroform), replacement of L-type ligand with X-type can potentially lead to higher degrees of etching. However, during the replacement of OLA capped PbS QDs with OA,

no such etching is observed.[20] Further, etching of oleate capped lead chalcogenide QDs in presence of excess OA i.e. carboxylic acids has been observed in organic solvents.[41, 45, 106] Hence, the different etching behavior of PMAO-PEG suggests various etching mechanism between OA and PMAO-PEG. Upon covering the PbS QDs with CdS shell, the PL intensity of PbS QDs improved (photoluminescence QY ~30 %) and no broadening of QDs size distribution was observed.[107] These studies show that the carboxylate ligands induce the etching of lead chalcogenide QDs and the degree of etching is determined by the type of initial ligands, exchanging ligands and solvents. Further, these studies also highlighted the differences in surface chemistry of lead chalcogenide QDs in comparison to cadmium based QDs.

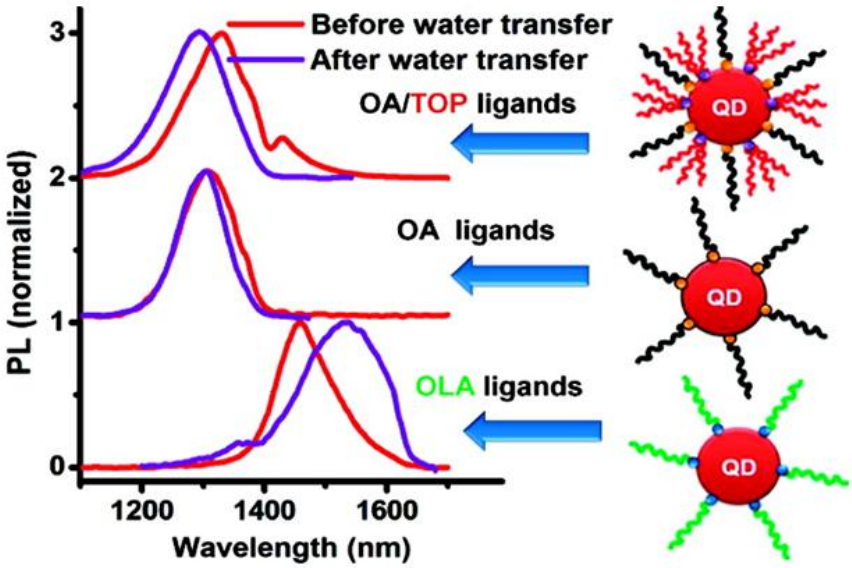

Figure 2-11. Photoluminescence spectra of PbS QDs before and after ligand exchange using PMAO-PEG. The PbS QDs were initially capped with OA/TOP, OA and OLA as ligands before ligand exchange with PMAO-PEG.[105] Reprinted with permission from ref [105] © The Journal of Physical Chemistry C, ACS publications 2011.

2.3.1.4 Metalated organic ligands

In metalated organic ligand exchange, the replacing ligands are bound to metal cations prior to the ligand exchange; and the ligand exchange is performed by replacing the native ligands together with the surface metal cations (**Figure 2-12**). Lingley et al[106] demonstrated the metalated ligand exchange of lead chalcogenide QDs where the surface lead oleate of PbS QDs were exchanged with a shorter lead octanoate or lead dodecanoate ligands. The complete replacement of oleate ligands with metalated ligands was possible upon heating and could also preserve the PL quantum efficiency during the ligand exchange. Such cation to cation exchange was initially demonstrated by Pietryga et al,[51] where the surface lead oleate were exchanged with cadmium oleate to form PbS/CdS core/shell structures. In such core/shell structures, the reaction temperature and Pb:Cd ratio influenced the thickness of shell formation. Complete transformation of PbS QDs to CdS was possible on prolonged heating of small sized QDs. A similar mechanism was proposed for the metalated ligand exchange of PbS QDs[106] where the thermodynamic gradient enhanced the diffusion of surface lead oleate while the mass effect of incoming ligands (either cadmium oleate or lead octanoate) eventually replaced the original lead oleate. In case of lead to cadmium exchange, the surface cadmium cation can further diffuse inside the PbS QDs to form a thicker shell while in case of lead to lead exchange no such phenomenon is observed as the same cation is involved. No changed in crystalline structures were reported for ligand exchange with lead octanote. Temperature plays an important role in diffusion of surface cation, however the applicability of such metalated exchange for phase transfer of lead chalcogenide QDs is not reported till date. In addition, cation to cation exchange has only been demonstrated in non-polar solvents and their applicability in polar solvents is still unclear. In contrast, Liu et al[108] reported a similar

metalated exchange of CdSe/ZnS core/shell QDs using Zn-thiolate ligands. A different mechanism of surface metathesis reaction at QDs surface was proposed as a possible mechanism for ligand exchange. In surface metathesis reaction, the presence of metal cation allows the softer replacement of surface ligands with minimal etching of surface cations rather than cation to cation exchange. The ligand exchange with Zn-thiolate ligands better preserved the PL intensities as compared to the control thiolate ligands. However, such metathesis exchange with metal-thiolate ligands is yet to be reported for lead chalcogenide based QDs.

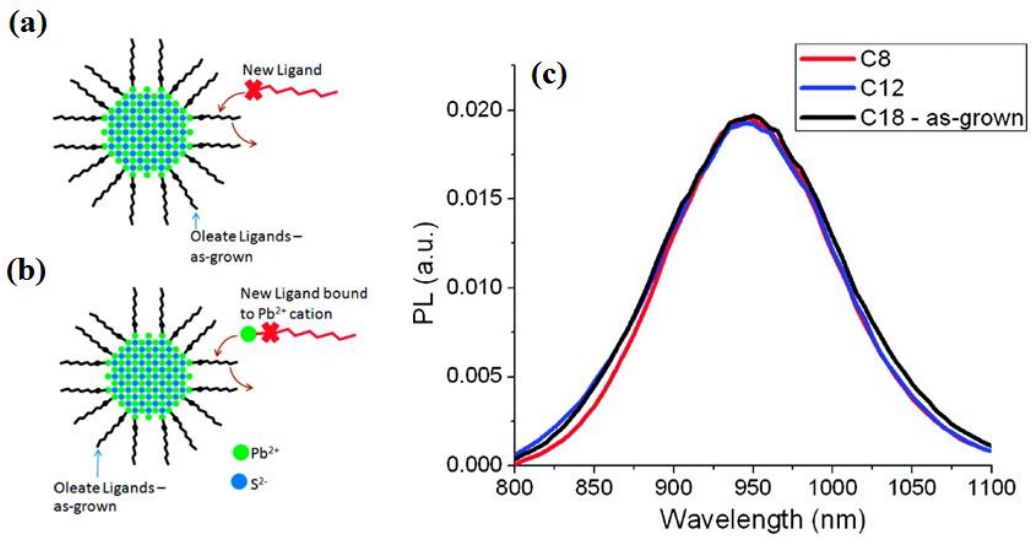

Figure 2-12. (a) and (b) Schematic illustrations of (a) convention ligand exchange (b) metalated ligand exchange (c) photoluminescence spectra before and after ligand exchange using metalated ligands.[106] Reprinted with permission from ref [106] © Nano Letters, ACS publications 2011.

Table 2-2. Summary of solution phase ligand exchange using various organic ligands

Organic Ligand Exchange (LE)							
LE type	**QDs**	**Native Ligands**	**Replacing Ligands**	**Solvent**	**Remarks about LE**	**Year**	**Ref.**
Thiol	PbS	OA	MTPEG	Buffers	QY reduced from 40-50% to 26 % max	2007	[96]
	PbS, PbSe	OA	MHDA, MUA, and AET	Water	PL reduced- For PbS: MUA 30% , MHDA 58% and AET precipitation For PbSe: MUA 57%, MHDA 38% and AET 95%	2007	[97]
	PbS	OA	(MT) and (DT)	Water	Studied the stability of dithiol versus mono thiol ligands. Dithiol more stable and less susceptible to oxidation.	2008	[98]
	PbS	OA	MPA,L-cys, NAC, GSH and DHLA	Water	PL: GSH>L-cys>DHLA, NAC & MPA. GSH PL: pH 5>3.5>7.4>9. Conc. 0.15mM>0.3>0.1>0.05. After 20 days, QY of 30% (org 40%)	2012	[99]
	PbTe	OLA	Py-SH	DCM	Precipitation of QDs	2012	[83]
	PbS	OA	TG, TLA and DMPA	DMSO, Water, DMF, FA	Only DMSO formed stable solution. For TG, QY decrease from 50% to 24% in DMAO. In water much larger decrease	2013	[92]
	PbS	OA	ArS−·H+, AlSH	DCM	Role of tri-ethylamine in arenethiol LE. Presence of arene group and deprotonation caused efficient LE.	2013	[101]
	PbS	OA	ArS−·H+	DCM	Surface chemistry of Ar.thiol exchanged QDs. Found 2 thiol bind per Pb atoms	2014	[109]
	PbS	OA	ArS with pendant moiety NH2, F3C and methyl. Different anchor like thiol, di-thiol, COOH, NH2	DCM	Electron donor moiety increased absorbance. Arene moiety also increase absobance compared to aliphatic. Bidentate anchor increase absorbance but lower stability. COOH anchor partially replaces oleate due to sofer nature while NH2 does not	2015	[94]
	PbS	OA	MPA	DMSO	PL and stability improves. Absorbance peak broadening with excess ligands	2015	[100]
Alkyl selenide	PbSe		$[CH_3(CH_2)_{17}Se]_2$ and $CH_3(CH_2)_{17}SeH$			2012	[102]
Multidentate carboxylate	PbS	OA	PAA	Water, THF	Abs. and PL blue shift. QY decrease from 82% to 24% in water	2008	[103]
	PbS	OLA	PMAO-PEG	Water, EtOH	Significant etching; formed double size distribution	2010	[104]
	PbS	OLA, OA and OA/TOP	PMAO-PEG	Water	Etching OA<OA/TOP<OLA	2011	[105]
	PbS/CdS	OA	PMAO-PEG	Water	Reduced etching and QY in water ~30%	2010	[107]
Metalated	PbS, PbSe	OLA	$Cd(OA)_2$	ODE	Blue-shift in abs. and PL. Formed PbS/CdS core/shell. QY increases with shell thickness.	2008	[51]
	PbS	OA	$Pb(OD)_2$ and $Pb(DD)_2$	ODE	No spectral shift. PLQY preserved after exchange	2011	[106]

MTPEG: (1-mercaptoundec- 11-yl)tetra(ethylene glycol); MHDA:16-mercaptohexadecanoic acid, 90%; MUA: 11-mercaptoundecanoic acid, 95%; GSH: glutathione, 98%; AET:aminoethanethiol-HCl; MT: sodium 3-mercaptopropanesulfonate; DT: sodium 2,3-dimercaptopropanesulfonate; DMPA: dimercaptopropionic acid; MPA: 3-mercaptopropionic acid, 99%; L-cys: L-cysteine, 99%; THF: tetrahydrofuran; DHLA: dihydrolipoic acid TG: 1-thioglycerol; Pb(OT)2 : Lead octanoate; ArS−·H+: 4-methylbenzenethiol; ArSH: benzenethiol; DMF: dimethylformamide; Pb(DD)2: Lead dodecanoate; FA: Formamide; DMSO: Dimethylsulfoxide; EtOH: ethanol; Cd(OA)2: cadmium oleate; Py-SH: 4-mercaptopyridine; PAA: polyacrylic acid; ODE: octadecene

2.3.2 Inorganic ligands

Kovalenko et al[110] introduced a new concept of inorganic ligand exchange, where the native organic ligands were replaced with inorganic species such as molecular metal chalcogenide complexes (MCCs) through a post-synthesis exchange process. These inorganic ligands provide colloidal stability for nanocrystals in polar solvents, passivate the trap states and enhance the electronic coupling and charge transport properties. Following Kovalenko's work,[110] various types of inorganic ligands have been reported till date. We can broadly classify these inorganic ligands as a) metal chalcogenide, metal free chalcogenide and oxoanion ligands and b) halides, pseudo-halides and metal-halide ligands (Table 3).

2.3.2.1 Inorganic metal chalcogenide, chalcogenide, and oxo ligands

2.3.2.1.1 Metal chalcogenide complex (MCC)

Kovalenko et al[110] reported the preparation of metal chalcogenide complex (MCCs) capped nanocrystals (NCs) using a simple two-phase ligand exchange procedure, where the phase transfer of NCs occurs from the original non-polar to polar solvents such as hydrazine or dimethylsulfoxide (DMSO). These MCCs were the first category of inorganic ligands discovered for the solution phase ligand exchange of NCs. The MCCs were synthesized by dissolving the bulk main group or transition metal chalcogenides in hydrazine to form soluble anionic species such as $Sn_2S_6^-$ and hydrazinium ($N_2H_5^+$) cation in polar solvents. Here, S_2^- anion replaces the original ligands and bind to the NCs surface producing electrostatic stabilization (**Figure 2-13(a)**). $N_2H_5^+$ counter-ions do not interact with NCs and forms a diffusive ion layer around the NCs to provide overall charge balance. Several MCC ligands such as Ga_2Se_3, Sb_2Se_3, Sb_2Te_3, $CuInSe_2$, $CuIn_xGa_{1-x}Se_2$,

and HgSe were reported and utilized for the inorganic ligand exchange of various NCs such as gold (Au) NCs, palladium (Pd) NCs, cadmium telluride (CdTe) QDs, cadmium sulfide (CdS) nanorods, cadmium selenide (CdSe) nanowires, bismuth sulfide (Bi_2S_3) nanorods.[110] The QDs after MCC ligand exchange preserved their excitonic absorption features and luminescence intensities upon phase transfer to polar solvents such as DMSO, formamide and ethanolamine. Further development in inorganic exchange technique using the main group metal sulfide MCCs such as Na_4SnS_6, $Na_4Sn_2S_6$, Na_3AsS_3, $(NH_4)_4Sn_2S_6$, and $(NH_4)_3AsS_3$ has also been reported.[111] These main group sulfide MCCs were used as an exchanging ligands for PbS and PbTe QDs. The ligand exchange of PbS QDs using Na_4SnS_6 and Na_3AsS_3 as exchanging ligands in formamide had well resolved excitonic peaks, without any changes in peak width; and it also had pronounced excitonic red-shift (**Figure 2-13(c)**).[111] The larger red-shift in excitonic peaks upon MCC ligand exchange of lead chalcogenide QDs showed resemblance to that of organic thiol ligands. The films as well as suspensions of MCC capped PbS QDs showed the reduction in photoluminescence (PL) intensities in comparison to oleate capped QDs and were much similar to organic thiol based ligands. In a recent study,[112] high IR photoconductivity was achieved in the films of As_2S_3 capped PbS QDs which was associated with the enhanced electronic coupling between the adjacent nanocrystals. Such enhancement in film conductivity was also observed in organic thiol treated QD films. However, the relative advantages of inorganic and organic treatments are unclear for enhancing the QD film conductivity as the electronic coupling depends on QD to QD interaction and the inter-particle distance plays important role for good coupling.

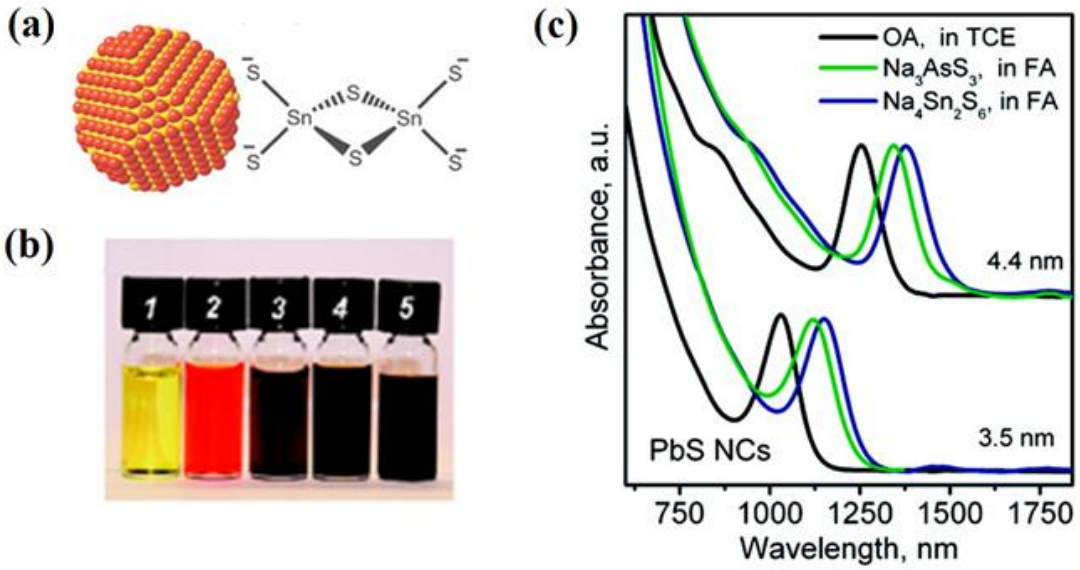

Figure 2-13. (a) Schematic illustration of NCs after inorganic ligand exchange using MCCs[110] (b) photographs of colloidal solutions of carious NCs capped by MCCs 1) CdS nanorods capped by $Na_4Sn_2S_6$ in formamide, 2) CdSe/ZnS core/shells capped by Na_4SnS_4 in H_2O, 3) Au NCs capped by Na_3AsS_3 in formamide, 4) PbS QDs capped by $Na_4Sn_2S_6$ in formamide, 5) PbTe QDs capped by K_4SnTe_4 in DMSO[111] (c) absorption spectra of PbS QDs before and after ligand exchange using MCCs inorganic ligands.[111] Reprinted with permission from ref [110] © Science, American Association for Advancement of Science 2009 and ref [111] © Journal of the American Chemical Society, ACS publications 2010.

The presence of metal ion in MCCs was also shown to influence the PL, charge transport, catalytic and magnetic properties of all inorganic colloidal NCs and their thin films.[113] The cations such as Cd^{2+}, Ca^{2+} or In^{3+} can bind to the NCs surface in solution and inverse the charge of metal free chalcogenides from negative to positive along with an enhancement in PL. As-synthesized NCs are usually cation rich and display n-type properties. The chalcogenide capped NCs on the other hand display p-type characteristics. The presence of metal cations in MCC can modulate the properties of MCC capped NCs from p-type to n-type thus enhancing the PL properties. Further, the surface cations on

NCs can act as a bridge in NCs films to provide the magnetic and catalytic properties to NCs. For example, bridging S^{2-} capped CdSe QDs film with Mn^{2+} provided magnetic properties while bridging with Pt^{2+} provided catalytic properties to the films.[113]

MCCs capped NCs usually requires solvents with high polarity such as formamide to maintain the colloidal stability in solution. Bodnarchuk et al[114] reported a simple methodology to disperse MCCs capped NCs in solvents of any polarity using the host-guest coordination of NCs using macrocycles. As illustrated in **Figure 2-14**, the K_3AsS_4 MCC exchanged PbS QDs can be suspended in a range of solvents with different polarities containing decyl-18-crown-6 macrocycle. The assembled layers of QDs containing macrocycles can form NCs super lattice for improved self-organization and photoconductivity. Such ligand solvent interactions are interesting and further developments can be expected for better utilization of inorganic capped QDs.

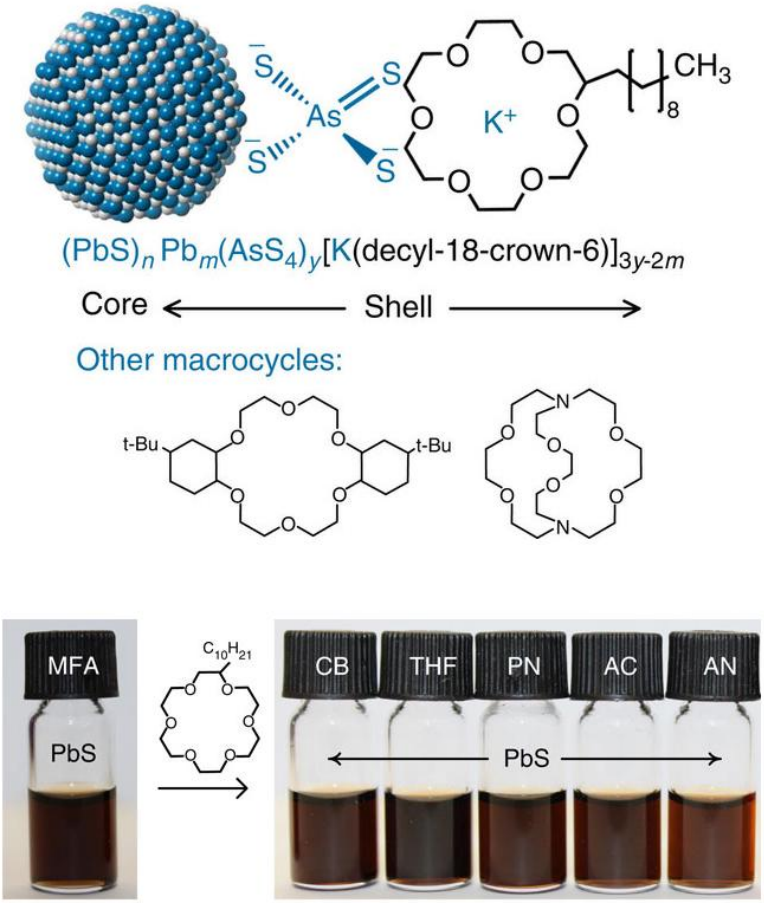

Figure 2-14. Schematic illustrations of host-guest coordination of MCCs capped QDs using macrocycles.[114] The photograph illustrates the versatility of using macrocycles in which the PbS QDs in MFA is readily suspended in many other polar solvents such as THF, acetone, acetonitrile etc. Reprinted with permission from ref [114] © Nature Communications, Nature publishing 2015.

2.3.2.1.2 Metal free chalcogenide complex

Nag et al[88] introduced the metal free chalcogenide ions such as S^{2-}, HS^{-}, Se^{2-}, HSe^{-}, Te^{2-}, HTe^{-}, TeS_3^{2-}, OH^{-} and NH_2^{-} as the inorganic ligands for colloidal NCs. These metal free inorganic chalcogenide ligands were structurally much simpler than MCCs and easily available. The chalcogenide anions adhered to the nanocrystal surfaces similar to the MCCs while the counter ions such as K^{+} or NH_4^{+} provided overall charge neutrality (**Figure 2-15(a)**). The inorganic exchange of CdSe QDs with S^{2-} preserved the excitonic

absorption features while the PL quantum efficiencies were reduced from initial 13 % to 2 %. However, only S^{2-} anions could not provide stable colloidal solutions for PbS QDs while TeS_3^{2-} ligands with two chalcogens in different oxidation states provided stable colloidal solutions. The reaction of TeS_3^{2-} ligands with metal telluride NCs such as PbTe on the other hand led to their complete or partial transformation to PbS QDs. Although the reasoning behind such observations is unclear, it seems the oxidation states of cations as well as their corresponding anions influence the efficiency of ligand exchange. Upon comparing with MCCs ligands, the MCCs and mixed chalcogenides were better for Pb based chalcogenides as compared to single anions (i.e. S^{2-}), while S^{2-} was superior for CdSe/ZnS NCs for which MCCs showed poor affinity. However, Ocier et al[115] reported that the PbSe QDs are difficult to be stabilized using MCCs and was applicable to only PbS and PbTe NCs. These studies show that different interaction of MCCs and metal free chalcogenides are possible with various metal chalcogenide NCs depending on their cationic and anionic species.

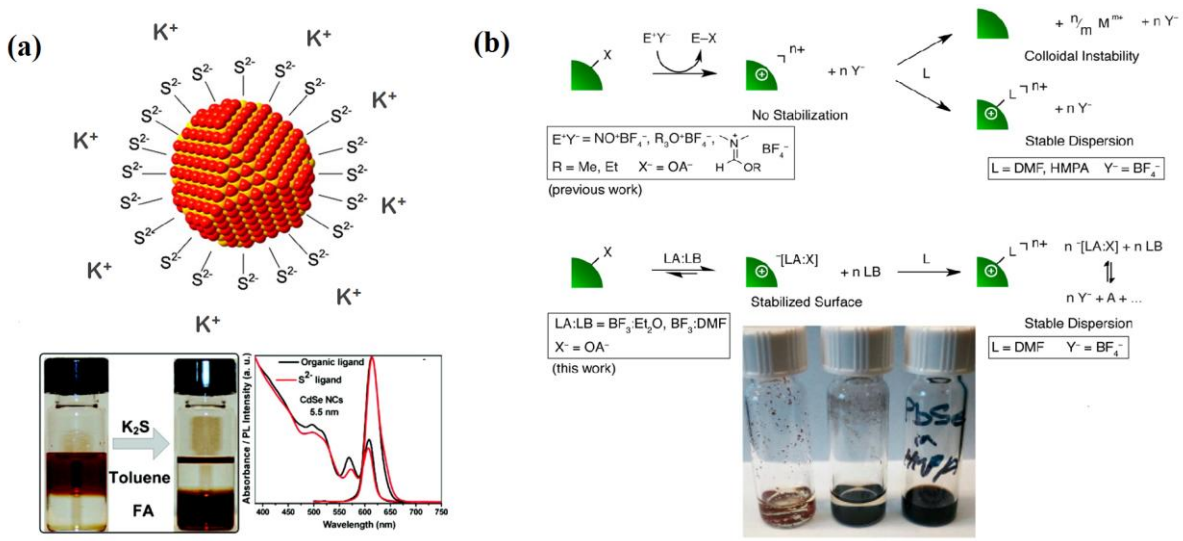

Figure 2-15. Schematic illustrations of (a) inorganic ligand exchange using metal free chalcogenide ligands.[88]The Photographs shows that the CdSe QDs are transferred to the polar solvent (FA) upon exchange with K_2S. The excitonic peak as well as PL intensities are preserved upon ligand exchange (b) mechanism of ligand stripping using BF_3 ligands and the photographs shows that exchange with BF_3 forms a stable PbSe QDs colloids via ion pairing.[116] Reprinted with permission from ref [88] © Journal of the American Chemical Society, ACS publications 2011 and ref [116] © Journal of the American Chemical Society, ACS publications 2014.

2.3.2.1.3 Oxonium ligands

Another class of inorganic ligands i.e. trialkyloxonium salt (or Meerwein's salt) was reported by Rosen et al[117], where the stipping of oleate capped PbSe QDs with trialkyloxonium salt was used to produce naked PbSe QDs thin film. The resulting PbSe films exhibited p-type conductivity without any post processing. The dispersion of ligands stripped NCs such as CdSe/ZnS QDs, CdSe/CdS QDs, upconverting $NaYF_4$:Yb/Tm, Ag, FePt etc. in DMF were demonstrated using the trialkyloxonium salts as inorganic ligands. However, the PbSe QDs were not dispersible after inorganic ligand exchange and naked NCs could only be achieved through solid state exchange. The colloidal dispersions of naked PbSe QDs were achieved by stripping native oleate ligands using lewis base adducts

of BF_3.[116] It was proposed that the colloidal treatment of oleate capped PbSe QDs with the lewis base adducts of BF_3 would strip the native oleate ligands without removal of excess surface Pb atoms. The formation of BF_4^- as the charge compensating species at the cationic NCs surface resulted in colloidal stability (**Figure 2-15(b)**). However, no information was provided on the optical properties of PbSe QDs after post-exchange with these ligands. Other inorganic oxoanions and polyoxometalate ligands have also been reported for various NCs however such ligands are still to be reported for lead chalcogenides QDs.[118] The developments in the chalogenides and oxo-ligands are still in early stage and are yet to be fully explored for lead chalcogenide based QDs.

2.3.2.2 Halide and metal-halides

Halides and metal halides are another class of inorganic ligands where the halide anions replace the native organic ligands on QD surfaces similar to chalcogenide based ligands (**Figure 2-16(a)**). The positive counter ions provide the overall charge balance to NCs for colloidal stability. In comparison to chalcogenide based ligands, halide ligands transform the NCs to n-type rather than making it p-type. Niu et al[119] first reported the solution phase ligand exchange of CdSe and PbS QDs using inorganic methylammonium halides (CH_3NH_3X, where X= Cl^-, Br^- or I^-). Two phase transfer technique using hexane and methanol were utilized for inorganic halide ligand exchange. The inorganic halide exchange using lead halide perovskites (i.e. methylammonium lead iodide, $MAPbI_3$) and other metal halide complexes such as sodium iodide (NaI) and potassium iodide (KI) has also been reported.[120, 121] The inorganic halides completely displaced the native oleate and TOPO ligands from PbS and CdSe QDs. The halide ligands preserved the sharp excitonic features of PbS QDs during the exchange with a red-shift in the absorption and emission

spectrum (**Figure 2-16(b) and (c)**).[121] Interestingly, the ligand exchange of PbS QDs with lead halide perovskite preserved the NIR PL of PbS (i.e. quantum yield of 20-30 % after exchange).[120] The halide capped QDs were re-dispersible in high polarity solvents such as formamide (FA) and N-methylformamide (NMF). The affinity of incoming anions to NCs surface, solvent dielectric constant, and solvation of anion/cation were critical parameters for efficient ligand exchange using inorganic halides. The ligand exchange with inorganic chloride (Cl^-) based halides were relatively unstable as compared to iodide and bromide based halides. Chloride anions have relatively weaker interaction with heavy metal cations and can desorb from the surface resulting in unstable colloidal dispersion.[120] Recently many research groups have reported other inorganic halides such as ammonium iodide (NH_4I) [55, 122], pseudohalides[123] and other metal halides for ligand exchange of lead chalcogenides. Similar to chalcogenides and oxo-ligands, the inorganic halide based ligand exchange is still new. Most studies are focused on the development of solution processable thin film devices. The stability of inorganic capped QDs in commonly used polar solvents and their colloidal stability after purification is still challenging.[120] Further research in understanding the fundamental mechanism of their interaction with QDs surface and surrounding solvent is warranted.

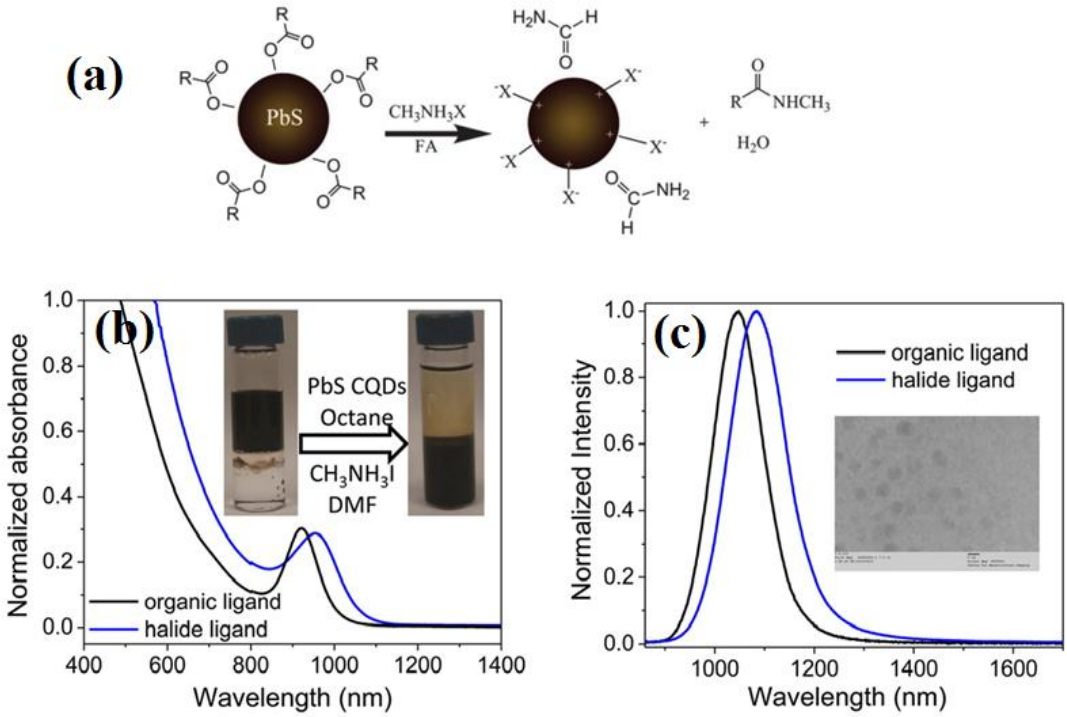

Figure 2-16. (a) Schematic illustration of ligand exchange using halide based inorganic ligands[119] (b) absorption spectrum of PbS QDs before and after ligand exchange using CH_3NH_3I ligands. Photographs show the images of PbS QDs before and after ligand exchange[121] (c) PL spectra of PbS QDs before and after ligand exchange using CH_3NH_3I ligands. Inset image show the TEM of QDs after exchange[121] Reprinted with permission from ref [119] Physical Chemistry Chemical Physics © RSC publishing 2013 and ref [121] © ACS Nano, ACS publications 2014

Table 2-3. Summary of solution phase ligand exchange using various inorganic ligands

Inorganic Ligand Exchange (LE)							
LE type	**QDs**	**Native Ligands**	**Replacing Ligands**	**Solvent**	**Remarks about LE**	**Year**	**Ref**
MCCs	PbS, PbTe	OA	Na_4SnS_6 and Na_3AsS_3	FA	Well resolved abs. peak. PL decreases ~80%	2010	[111]
	PbS	OA	K_3AsS_4, AsS_4	FA, AC, AN,THF	Macrocycles stabilized QDs through host-guest coordination	2015	[114]
Metal free chalco genide	PbS, PbTe	OA	S^{2-},TeS_3^{2-}	FA	For PbS: only TeS_3^{2-} formed stable colloidal solution while S^{2-} could not Fpr PbTe: changed to PbS on LE with TeS_3^{2-}	2011	[88]
	PbSe	OA	S^{2-},TeS_3^{2-}		For PbSe: could not form stable colloid	2014	[115]
Oxo	PbSe	OA	trialkyloxonium salt	FA	For PbSe: could not form stable colloid	2012	[117]
	PbSe	OA	BF^{4-}	FA	Formed stable colloidal solution	2014	[116]
Halide	PbS	OA	CH_3NH_3X, X= Cl, Br, I	MeOH, FA	Cl- did not form stable solution, I- and Br- had stable colloidal solution	2013	[119]
	PbS	OA	$MAPbI_3$	NMF, PC	Stable solution in PC, QY ~20% same as in OA	2014	[120]
	PbTe	OA	$MAPbI_3$	NMF	stable colloidal solution	2014	[123]
	PbS	OA	CH_3NH_3I and $MAPbI_3$	NMF	High efficiency solar cells	2014	[121]
	PbS, PbSe	OA	NH_4I	DMF	stable colloidal solution	2015	[55]

FA: Formamide; MeOH: Methanol; AC: Acetone; PC: Propylene carbonate; $MAPbI_3$: Methylammonium lead iodide
NMF: N, methylformamide; DMF: N,N dimethylformamide; AN: Acetonitrile; THF: Tetrahydrofuran

2.4 Recent advances in lead chalcogenide based solar cells

QDs based solar cells were first reported in 1998 with efficiency of 1 %.[124] Since then, QDs have been actively pursued as a potential for next generation solar cells. The progress in QDs solar cells was relatively slow in early 2000s. However, the photo conversion efficiencies (PCE) of QDs based solar cells has seen rapid increase in the recent years from ~4 % (in 2010)[125] to ~10% (in 2015).[126-128] The surge in PCE of QDs based solar cells is mostly due to the better understanding of lead chalcogenide QDs synthesis and their surface chemistries. In fact, lead chalcogenide based QDs solar cells have shown one of the highest PCEs for QDs based solar cells.[126-128]

Till now, various architectures of QDs based solar cells have been developed which includes QD sensitized solar cells (QDSSCs), QD/polymer heterojunction solar cells,

schottky type QD solar cells and inorganic heterojunction solar cells.[129] These various device architectures are schematically shown in **Figure 2-17**. We would briefly summarize major progresses in lead chalcogenide QDs solar cells utilizing these various QDs solar architectures.(**Table 2-4**)

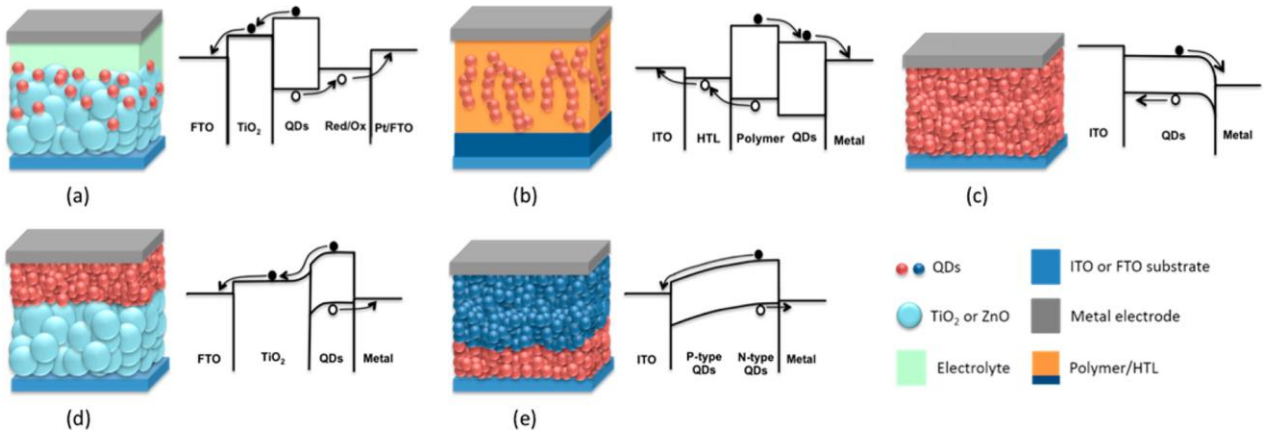

Figure 2-17. Schematic illustration of various QDs based solar cell architectures (a) QDs sensitized solar cells (b) QDs/polymer heterojunction solar cells (c) Schottky QDs solar cells (d) QDs/inorganic heterojunction solar cells with single QDs layer (e) QDs/inorganic heterojunction solar cells with bi-layer QDs film.[130] Reprinted with permission from ref [130] © The Journal of Physical Chemistry Letters, ACS publications 2015.

2.4.1 Quantum dot sensitized solar cells (QDSSCs)

QDSSCs are one of the earliest reported architectures for QD based solar cells. The working principle of QDSSCs is much similar to the dye sensitized solar cells (DSSCs) in which organic dyes are replaced with QDs to generate photons. In QDSSCs, the light absorption, electron transport and hole transport are handled by different materials in the cells.[1, 131] In brief, QDSSCs are composed of a transparent conductive oxide coated glass substrate, a semiconductor film, a sensitizer adsorbed onto the surface of semiconductor,

an electrolyte and a counter electrode capable of regenerating the electrolyte. The schematic diagram of most common QDs sensitized solar cell is shown in **Figure 2-17(a)**.

QD sensitizers can be synthesized either in-situ or ex-situ. Chemical bath deposition (CBD)[132, 133] and successive ionic layer adsorption and reaction (SILAR)[134] are commonly used in-situ methods for the sensitization of QDs on nanostructured wide band gap semiconductors. It usually leads into a polydispersed QD size distribution and has a relatively higher QD coverage. The direct connection between the QDs and wide-bandgap semiconductors also leads to efficient charge injection from the QD onto the wide bandgap semiconductors. In ex-situ approach, the QDs are pre-synthesized and are bound onto wide bandgap semiconductors by molecular linkers[133, 135] or by direct adsorption.[133, 136] The ex-situ approach allows the tuning of absorption onset; however their progress is limited by the chemical nature of bi-functional molecular linkers and have usually led to limited QD coverage in comparison with the in-situ approach.

Although QDSSCs with efficiencies ~9 % have been reported for tertinary CdSeTe QDs,[127] the progress for lead chalcogenide QDSSCs has been slow. The highest reported efficiencies for lead chalcogenide QDSSCs is ~5.73 % based on in-situ growth of PbS QDs using SILAR.[137] The maximum efficiency reported by utilizing pre-synthesized lead chalcogenide QDs is ~2.67 % for PbS QDs.[138] One of the reasons for relatively low efficiencies for lead chalcogenide QDSSCs is their instability in liquid electrolytes used for making these solar cells.[139] Although efforts have been reported on using solid state hole transport layers (HTL) such as spito-OMeTAD, they have resulted in efficiencies of only 1.5 %.[140] The electron-hole recombination at anode-QDs-HTL interface was identified as the reason for low efficiencies using solid hole transport layers in QDSSCs.[141] Recently, Seo et al[142] reported that the performance enhancements of in-situ grown PbS QDSSCs

can be achieved by using $CH_3NH_3PbI_3$ pervoskite as a shell material to enhance the performance of solid state solar cells. The modulation of QDs surface chemistries by inorganic halide shells enhanced the performance of resulting QDSSCs cells. Efficiencies of 3.2 % were achieved by QD passivation using pervoskite shell. Recently, current densities (J_{sc}) as high as 30 $mA.cm^{-2}$ have also been reported for Hg^{+} doped in-situ grown PbS QDs solar cells,[143] and better efficiencies can be further expected through improved understanding of QDs surface chemistries. The low open circuit voltages (V_{oc}) are another major reason resulting in low efficiencies for lead chalcogenide QDSSCs. Another avenue for improvement of lead chalcogenide based QDSSCs is the lower fill factors (*FF*). A proper design of hole transporting layers (or redox electrolytes) and suitable catalysts can improve the open circuit voltages and fill factors.

2.4.2 QD/polymer heterojunction solar cells

In QD/polymer heterojunction solar cells, a single photoactive layer is formed by either blending the QDs together with polymers or arranging the QDs and polymers in separate layers to form a planar heterojunction (**Figure 2-17(b)**). The charge separation takes place at QD-polymer heterojunction. The early QD/polymer based lead chalcogenide QD solar cells reported the efficiency 2.2 % by using a thin film of 1,3-benzenedithiol (1,3-BDT) crosslinked with PbS QDs.[144] PbS QDs were deposited on C60-fullerene (PCBM) layer to form the planar heterojunction solar cells. The introduction of n-type C60 layer reduced the charge recombination leading to enhanced efficiency. Others have reported bulk heterojunctions of lead chalcogenide QDs with various other conducting polymers such as 1,3-BDT PbS QDs with [6,6]-phenyl C61 butyric acid methyl ester (PC61BM) and achieved an efficiency of 3.7 %,[145] PbS QDs with the blend of PC61BM and poly[4,40-

bis(2-ethylhexyl)dithieno[3,2-b:2'3'-d]silole-2,6-diyl-alt-(2,1,3-benzothiadiazole)-4,7-diyl] (PSBTBT) polymer and achieved the efficiency of ~4.1 %[146] and ethanedithiol (EDT) capped PbSe QDs with PEDOT:PSS as active layers and achieved the efficiency of 3.4 %.[147] Although many other works have also been reported on lead chalcogenide QDs/polymer hybrid solar cells, their efficiency still remains low. One of the primary reasons for the low efficiency of these cells is the lack of proper QDs/polymers interface and the phase structure in active layers. A robust interface between the QDs and polymers can form an interpenetrating network of QDs and polymers allowing efficient charge separation. The QD surface ligand engineering and developing efficient methods to adhere QDs in polymer chains is a major challenge for QDs/polymers heterojunction solar cells. Since the surface chemistry of lead chalcogenide QDs is still evolving, future research might lead to higher efficiency devices.

2.4.3 Schottky type solar cells

The schottky type solar cells employ a metal-semiconductor work function to separate the electron-hole pairs generated at photoactive layer (**Figure 2-17(c)**). The photoactive layers are usually composed of thin QDs layers sandwiched between the transparent electrode (FTO, ITO in glass) and a low work function metal contact. The schottky based solar cells are simple and easy to fabricate. However, these solar cells are limited by the lower thickness of QDs layers and low open circuit voltages. Johnson et al[148] reported the first schottky solar cells based on butylamine capped PbS QDs and achieved an efficiency of 1.8 %. However, the reported devices were unstable under ambient atmosphere and required encapsulation in inert atmosphere. The first air stable schottky solar cells were made by treating PbSe QDs with 1,4 benzenedithiol (1,4 BDT) solution.[149] The stronger

cross-linking of QDs via thiols and improved surface passivation led to their enhanced air stability in comparison with weaker coordinating primary amines. These solar cells showed an efficiency of 1.1 % under illumination of AM1.5G, 100 $mW.m^{-2}$ and retained around 80 % of initial PCE even when exposed to air for over 48 hrs. The air stable schottky solar cells with 1,3-EDT treated PbSe QDs thin films sandwitched between ITO and gold metal contact were also reported and achieved an efficiency of 2.1 %.[150] Most of these studies utilized the solid state ligand exchange to replace the native oleate ligands and improved the air stability by surface passivation through thiol ligands. The depth of trap states within the QDs influences the performance of solar devices[125] and various surface treatments have been employed to remove these trap states. Szendrei et al[125] achieved an impressive efficiency of 4 % and a high fill factor of 60 % using 1,4-BDT treated PbS QDs. The size of lead chalcogenide QDs[34] as well as the processing of the QDs has been found to influence the efficiency of the cells.[151] The size of QDs influenced the open circuit voltage (V_{oc}) of the devices and the PbSe QDs with diameter ~2.3 nm showed the highest V_{oc} and high PCE of 4.57 %.[34] The QDs processing such as the number of washing steps also influenced the QDs to ligand ratio and by optimizing the number of washing steps the PCE of 5.2 % was achieved for schottky based solar cells.

2.4.4 Inorganic heterojunction based solar cells

The inorganic heterojunction based solar cells have only been developed since 2009 with the purpose to overcome the limitations of schottky based solar cells. Leschkies et al[152] first reported the solar cells based on planar heterojunction between the PbSe QDs and thin ZnO films. The PCE of 1.6 % was reported using such a device structure. These solar cells typically use a heterojunction between the QDs and n-type electron acceptor such as ZnO,

TiO_2 etc. to split the charge carriers generated in QD layers (**Figure 2-17(d) and (e)**). The working principle of planar heterojunction solar cells is much similar to planar QDs/polymer solar cells. Abraham et al[153] introduced a new depleted heterojunction based solar cells to address the architectural issues of planar and schottky based devices. In this type of solar cells, n-type nanostructures and QDs are assembled in a manner such that the interfacial area is maximized and allowing a certain level of interpenetration (**Figure 2-17(e)**). As such the depletion layers are spread in three dimensions within the active layer. This allowed the active layer to be much thicker and thus harvest more solar energy. These depleted heterojunction between PbS QDs and transparent TiO_2 layer produced a PCE of 5.1 %. Following this research, much effort was invested in generating ideal architecture for most efficient depleted heterojunctions. Some of the advancements include the solution processed depleted heterojunctions of TiO_2 and PbS QDs (PCE = 5.5 %),[154] formation of ordered nanopillars structured electrodes of TiO2 (PCE = 5.6 %)[155] and utilization of ZnO nanowires (PCE = 6.1 %).[156]

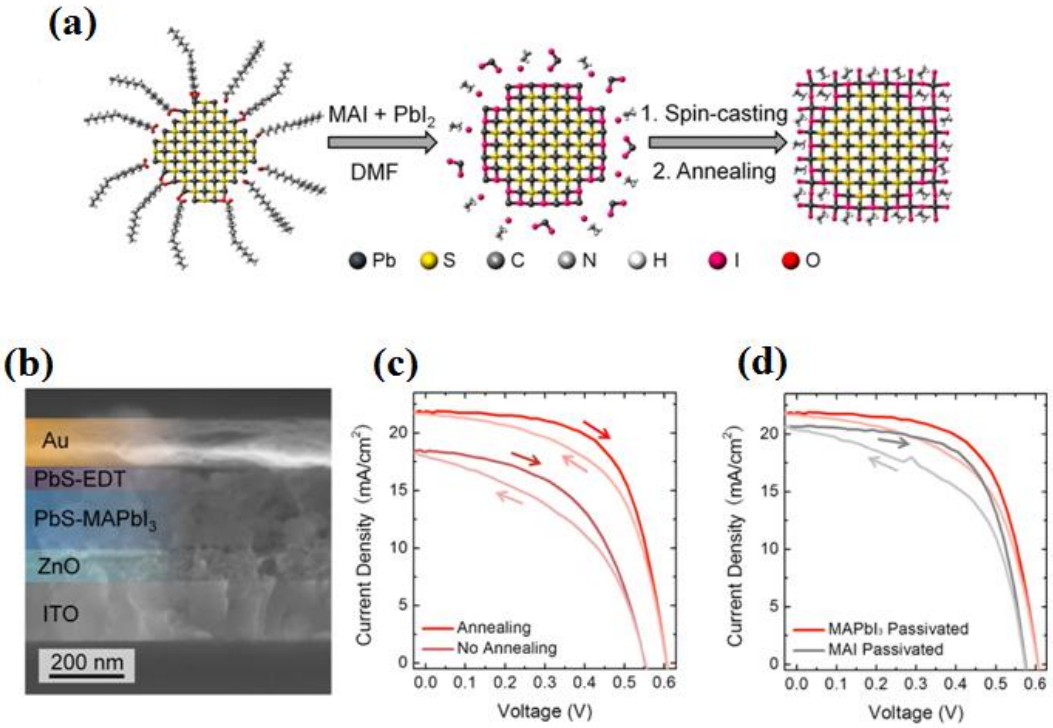

Figure 2-18. (a) Schematic illustration of colloidal inorganic ligand exchange using $MAPbI_3$ and subsequent film formation (b) SEM image of various components of heterojunction based solar cells (c) J-V curve for $MAPbI_3$ exchanged PbS QDs with and without annealing step (d) J-V curve for MAI and $MAPbI_3$ passivated PbS QDs solar cells.[93] Reprinted with permission from ref [93] Nano Letters, ACS publications 2015.

Recently, the depleted heterojunction solar cells of lead chalcogenide QDs have achieved rapid improvement in efficiencies due to the progress in colloidal synthesis and improved understanding of surface chemistry. Surface passivation of the trap states and bandgap engineering using various ligands has contributed to rapid development in PCE of these solar cells. The atomic ligand passivation of colloidal PbS QDs using monovalent halide anions to passivate the defects in QDs surface achieved a PCE of 6 %.[157] Moreover, the density of mid-gap trap states within the QDs film was found to limit the performance of solar cells by acting as electron-hole recombination sites. The removal of these traps states

using hybrid halide anions passivation resulted in 7 % efficient solar cells.[11] Further, inorganic passivation of PbS QD solids improved the efficiencies of solar cells to 8 %.[158] these studies show that the improvements in ligand engineering can enhance the level of passivation of QD solids and enhance the performance of the cells. In addition, the smaller size of halide based ligands is free from steric hinderances on QD surface and provides more robust passivation. Ligand exchange treatments have also found to influence the band gap alignments of QD thin films and showed that the appropriate band alignments of QDs thin films can produce highly efficient depleted heterojunction solar cells.[159] For example, iodide treatment of PbS QD films downshifts the bandgaps towards more negative in comparison to thiol treatment of PbS QDs films. Using appropriate band gap alignments for PbS QD layers, a certified efficiency of 8.55 % was achieved. The solution phase ligand exchange of QDs have also been reported for heterojunction based solar cells.[93] The solution phase ligand exchange of PbS QDs using methyl ammonium lead iodide perovskite improved the PCE to 8.95 % (**Figure 2-18**). A single step deposition of PbS QDs was used to generate the thin films of PbS QDs. The solution phase ligand exchange provides improved surface passivation of QD surface and the better film quality can be achieved through solution processable deposition of QDs. In addition, engineering the interface between the photoelectrode and QDs has also found to enhance the efficiency of the heterojunction solar cells. Self-assembled monolayers of organic molecules to engineer the interface between the ZnO photoelectrode and the solution deposited iodide capped PbS QDs achieved the record efficiency of 10.7 % for QD based solar devices.[128] More developments in QD surface chemistry and QDs device engineering are further expected to enhance the PCE of QD based solar cells.

Table 2-4. Summary of recent progress in lead chalcogenide based QDs solar cells

Device Type	QDs	Ligand Exchange	Device structure	J_{sc}, mA/cm^2	V_{oc}, V	FF	Eff. %	Year	Ref
QDSSCs	PbS	in-situ SILAR	FTO/TiO2/PbS QDs/Spiro-OMeTAD	4.58	0.56	0.57	1.46	2009	[140]
	PbS	in-situ SILAR	FTO/TiO2/PbS QDs/ZnS/polysulfide/Cu_2S/FTO	24.17	0.42	0.56	5.73	2013	[137]
	PbS	solid state LE using MPA	FTO/TiO2/PbS QDs/CdS/polysulfide/Pb:PbS/FTO	15.14	0.36	0.48	2.67	2014	[138]
	Hg-PbS	in-situ SILAR	FTO/TiO2/PbS QDs/ZnS/polysulfide/Cu_2S/FTO	30	0.398	0.47	5.6	2013	[143]
	PbS	in-situ SILAR	FTO/TiO2/PbS QDs/$MAPbI_3$/ZnS/polysulfide/Cu_2S/FTO	20.6	0.343	0.45	3.2	2014	[142]
QDs/ Polymers	PbS	solid state LE using BDT	ITO/PbS-BDT/C60/LiF/Al	10.5	0.4	0.52	2.2	2009	[144]
	PbSe	solid state LE using EDT	Al/ZnO/PbSe-EDT/PEDOT:PSS/ITO	24	0.44	0.32	3.4	2009	[147]
	PbS	solid state LE using BDT	ITO/PbS-BDT/PC_{61}BM/Al	10.1	0.59	0.63	3.8	2010	[145]
	PbS	solid state LE using MPA	ITO/PbS/PSBTBT:PCBM/Al	14.8	0.45	0.63	4.1	2011	[146]
Schottky	PbS	solid state LE using butylamine	ITO/PbS/Al	12.3	0.33	-	1.8	2008	[148]
	PbSe	solid state LE using BDT	ITO/PbS-BDT/Mg-Ag	-	-	-	1.1	2008	[149]
	PbSe	solid state LE using EDT	ITO/PbS-EDT/Ca-Al	24.5	0.239	0.4	2.1	2008	[150]
	PbS	solid state LE using BDT	ITO/PbS-BDT/Ca-Al	11.3	0.46	0.6	4	2010	[125]
	PbSe	solid state LE using BDT	ITO/PEDOT/PbS-BDT/Al	17.2	0.47	0.57	4.57	2011	[34]
	PbS	solid state LE using BDT	ITO/PbS-BDT/LiF-Al	19.3	0.46	0.58	5.2	2013	[151]
Depleted Hetero-junction	PbS	solid state LE using EDT	ITO/ZnO/PbSe-EDT/NPD/Au	15.7	0.39	0.27	1.6	2009	[152]
	PbS	solid state LE using MPA	FTO/TiO2/PbS-MPA/Au	16.2	0.51	0.58	5.1	2010	[153]
	PbS	solid state LE using MPA	FTO/sol processed TiO2/PbS-MPA/Au	20.6	0.48	0.56	5.5	2011	[154]
	PbS	solid state LE using MPA	FTO/ordered TiO2/PbS-MPA/Au/Ag	20.1	0.58	0.49	5.7	2012	[155]
	PbS	$CdCl_2$ passivation and solid state LE using CTAB	ITO/TiO2/PbS-CTAB/Au/Ag	20.2	0.48	0.62	6	2011	[157]
	PbS	solid state LE using CTAB	FTO/ZnO NW/PbS-CTAB/Au	34.47	0.36	0.48	6.07	2013	[156]
	PbS	hybrid passivation and solid state exchange using MPA	FTO/TiO2/ZnO/PbS-MPA/MoOx/Au/Ag	21.8	0.59	0.58	7.4	2012	[11]
	PbS	solution halide treatment and LE using I-, Br- and MPA	FTO/TiO2/PbS-I/PbS-Br/PbS-MPA/MoOx/Au/Ag	26.6	0.51	0.59	8	2014	[158]
	PbS	solid state LE using TBAI and EDT	ITO/ZnO/PbS-TBAI/PbS-EDT/MoOx/Au	24.2	0.55	0.64	8.55	2014	[159]
	PbS	solution phase LE using $MAPbI_3$	ITO/ZnO/PbS-$MAPbI_3$/PbS-EDT/MoOx/Au	21.8	0.61	0.68	8.95	2015	[93]

EDT: Ethanedithiol; NPD: N,N0-bis(1-naphthalenyl)-N,N 0-bis(phenylbenzidine); BDT: Benzenedithiol; MPA: Mercaptopropionic acid; TBAI: Tetrabutylammonium iodide

2.5 Conclusions and Outlook

In this review, we summarized the recent advances in colloidal synthesis of lead chalcogenide (PbSe, PbS and PbTe) QDs and highlighted the major achievements in the field thus far. After that, we provided a comprehensive review of solution phase ligand exchange of these QDs using various organic and inorganic ligands. Finally, we concluded the article by providing a brief overview of recent progress in utilizing these QDs in various solar cells architectures. Based on our critical review we conclude:

a) Over the last decade, tremendous progress has been made to optimize the synthesis of lead chalcogenide QDs. Consequently, high quality and mono-dispersed lead chalcogenide QDs with the broad band absorption from NIR to mid-IR have been synthesized. Most of these synthesis techniques have replicated previously reported cadmium based QDs synthesis. Although these synthesis techniques have been successful in producing good quality lab-scale products, the progress towards commercialization is still hindered by the lack of fundamental understanding on their nucleation and growth, influence of ligand surface chemistry, using of air/moisture sensitive reagents, air instability of QDs and the lack of cost-effective QDs isolation procedures for multi-gram scale synthesis. The progress of PbTe based QDs seems much slower than that of PbS and PbSe QDs. A renewed interest in these QDs can reveal interesting applications. Further, the quantum efficiencies of lead chalcogenide QDs are comparatively lower (~30-40 %)[7] as compared to cadmium based QDs (up to 90 %).[160] Hence, further research in improving their quality might be beneficial for the utilization of these QDs.

b) Although a lot of progress has been made on the synthesis of lead chalcogenide QDs, the utilization of these QDs in various applications is still hindered due to difficulties in understanding their surface chemistry. Especially the issues of colloidal instability and

retaining their luminescence properties after ligand exchange are still a major challenge. Considering the impact of trap states on the overall performance of various optoelectronic devices, the progress towards efficient ligand exchange is essential. Recent progress in inorganic ligand exchange looks promising and more effort in this area might reveal interesting applications. The major challenges of inorganic ligand exchange are the re-dispersion of QDs after ligand exchange to commonly use polar solvents and the lack of surface functional groups for attachment to other substrates.

c) The utilization of lead chalcogenide QDs in various solar cell architectures has produced high performing QD based solar devices. Further improvements in efficiencies can be expected considering a lot of progress is still ongoing in the areas of QD synthesis and ligand exchange. Regarding various device architectures, bulk inorganic heterojunction based solar cells seems most promising however more progress in the areas of QDSSCs and QDs/polymer heterojunction solar cells can be expected in near future.

References

[1] M. Gratzel, *Nature* 2001, 414, 338.

[2] H. Wang, Y. Bai, H. Zhang, Z. Zhang, J. Li, L. Guo, *J. Phys. Chem. C* 2010, 114, 16451.

[3] L. Li, X. Yang, J. Gao, H. Tian, J. Zhao, A. Hagfeldt, L. Sun, *J. Am. Chem. Soc.* 2011, 133, 8458.

[4] Y. Tian, T. Tatsuma, *J. Am. Chem. Soc.* 2005, 127, 7632.

[5] A. J. Nozik, *Physica E: Low-dimensional Systems and Nanostructures* 2002, 14, 115.

[6] A. J. Nozik, M. C. Beard, J. M. Luther, M. Law, R. J. Ellingson, J. C. Johnson, *Chem. Rev.* 2010, 110, 6873.

[7] M. A. Hines, G. D. Scholes, *Adv. Mater.* 2003, 15, 1844.

[8] (a) P. V. Kamat, *J. Phys. Chem. C* 2008, 112, 18737; (b) I. Robel, M. Kuno, P. V. Kamat, *J. Am. Chem. Soc.* 2007, 129, 4136.

[9] I. Moreels, K. Lambert, D. De Muynck, F. Vanhaecke, D. Poelman, J. C. Martins, G. Allan, Z. Hens, *Chem. Mater.* 2007, 19, 6101.

[10] (a) P. V. Kamat, *J. Phys. Chem. C* 2007, 111, 2834; (b) J. Tang, K. W. Kemp, S. Hoogland, K. S. Jeong, H. Liu, L. Levina, M. Furukawa, X. Wang, R. Debnath, D. Cha, K. W. Chou, A. Fischer, A. Amassian, J. B. Asbury, E. H. Sargent, *Nat. Mater.* 2011, 10, 765; (c) H. Liu, J. Tang, I. J. Kramer, R. Debnath, G. I. Koleilat, X. Wang, A. Fisher, R. Li, L. Brzozowski, L. Levina, E. H. Sargent, *Adv. Mater.* 2011, 23, 3832; (d) P. K. Santra, P. V. Kamat, *J. Am. Chem. Soc.* 2012, 134, 2508; (e) Z. Yang, C.-Y. Chen, P. Roy, H.-T. Chang, *Chem. Commun.* 2011, 47, 9561.

[11] A. H. Ip, S. M. Thon, S. Hoogland, O. Voznyy, D. Zhitomirsky, R. Debnath, L. Levina, L. R. Rollny, G. H. Carey, A. Fischer, K. W. Kemp, I. J. Kramer, Z. J. Ning, A. J. Labelle, K. W. Chou, A. Amassian, E. H. Sargent, *Nat. Nanotechnol.* 2012, 7, 577.

[12] D. V. Talapin, J.-S. Lee, M. V. Kovalenko, E. V. Shevchenko, *Chem. Rev.* 2009, 110, 389.

[13] E. V. Shevchenko, D. V. Talapin, N. A. Kotov, S. O'Brien, C. B. Murray, *Nature* 2006, 439, 55.

[14] (a) S. Coe-Sullivan, *Nat. Photon.* 2009, 3, 315; (b) J. M. Caruge, J. E. Halpert, V. Wood, V. Bulovic, M. G. Bawendi, *Nat. Photon.* 2008, 2, 247; (c) P. O. Anikeeva, J. E. Halpert, M. G. Bawendi, V. Bulović, *Nano Lett.* 2009, 9, 2532.

[15] R. J. Ellingson, M. C. Beard, J. C. Johnson, P. Yu, O. I. Micic, A. J. Nozik, A. Shabaev, A. L. Efros, *Nano Lett.* 2005, 5, 865.

[16] J. E. Murphy, M. C. Beard, A. G. Norman, S. P. Ahrenkiel, J. C. Johnson, P. Yu, O. I. Mićić, R. J. Ellingson, A. J. Nozik, *J. Am. Chem. Soc. 2006*, 128, 3241.

[17] F. W. Wise, *Acc. Chem. Res.* 2000, 33, 773.

[18] W. Shockley, H. J. Queisser, *J. Appl. Phys.* 1961, 32, 510.

[19] L. Cademartiri, J. Bertolotti, R. Sapienza, D. S. Wiersma, G. von Freymann, G. A. Ozin, *J. Phys. Chem. B* 2005, 110, 671.

[20] J. Zhang, J. Gao, E. M. Miller, J. M. Luther, M. C. Beard, *ACS Nano* 2013, 8, 614.

[21] D. K. Kim, T. R. Vemulkar, S. J. Oh, W.-K. Koh, C. B. Murray, C. R. Kagan, *ACS Nano* 2011, 5, 3230.

[22] A. H. Ip, S. M. Thon, S. Hoogland, O. Voznyy, D. Zhitomirsky, R. Debnath, L. Levina, L. R. Rollny, G. H. Carey, A. Fischer, K. W. Kemp, I. J. Kramer, Z. Ning, A. J. Labelle, K. W. Chou, A. Amassian, E. H. Sargent, *Nat. Nanotechnol.* 2012, 7, 577.

[23] J. Y. Woo, S. Lee, S. Lee, W. D. Kim, K. Lee, K. Kim, H. J. An, D. C. Lee, S. Jeong, *J. Am. Chem. Soc*. 2015.

[24] J. Baumgartner, A. Dey, P. H. H. Bomans, C. Le Coadou, P. Fratzl, N. A. J. M. Sommerdijk, D. Faivre, *Nat. Mater*. 2013, 12, 310.

[25] S. G. Kwon, T. Hyeon, *Small* 2011, 7, 2685.

[26] D. V. Talapin, A. L. Rogach, M. Haase, H. Weller, *J. Phys. Chem. B* 2001, 105, 12278.

[27] C. R. Bealing, W. J. Baumgardner, J. J. Choi, T. Hanrath, R. G. Hennig, *ACS Nano* 2012, 6, 2118.

[28] (a) D. C. Gary, B. M. Cossairt, *Chem. Mater.* 2013, 25, 2463; (b) S. Abe, R. K. Capek, B. De Geyter, Z. Hens, *ACS Nano* 2013, 7, 943; (c) J. S. Owen, E. M. Chan, H. Liu, A. P. Alivisatos, *J. Am. Chem. Soc.* 2010, 132, 18206.

[29] C. B. Murray, C. R. Kagan, M. G. Bawendi, *Annu. Rev. Mater. Sci*. 2000, 30, 545.

[30] S. G. Kwon, Y. Piao, J. Park, S. Angappane, Y. Jo, N.-M. Hwang, J.-G. Park, T. Hyeon, *J. Am. Chem. Soc.* 2007, 129, 12571.

[31] C. B. Murray, S. Sun, W. Gaschler, H. Doyle, T. A. Betley, C. R. Kagan, *IBM J. Res. Develop.* 2001, 45, 47.

[32] W. W. Yu, J. C. Falkner, B. S. Shih, V. L. Colvin, *Chem. Mater.* 2004, 16, 3318.

[33] C. M. Evans, L. Guo, J. J. Peterson, S. Maccagnano-Zacher, T. D. Krauss, *Nano Lett.* 2008, 8, 2896.

[34] W. Ma, S. L. Swisher, T. Ewers, J. Engel, V. E. Ferry, H. A. Atwater, A. P. Alivisatos, *ACS Nano* 2011, 5, 8140.

[35] J. M. Pietryga, R. D. Schaller, D. Werder, M. H. Stewart, V. I. Klimov, J. A. Hollingsworth, *J. Am. Chem. Soc*. 2004, 126, 11752.

[36] O. Chen, X. Chen, Y. Yang, J. Lynch, H. Wu, J. Zhuang, Y. C. Cao, *Angew. Chem*. 2008, 120, 8766.

[37] H. Li, D. Chen, L. Li, F. Tang, L. Zhang, J. Ren, *CrystEngComm* 2010, 12, 1127.

[38] M. A. Sliem, A. Chemseddine, U. Bloeck, R. A. Fischer, *CrystEngComm* 2011, 13, 483.

[39] W.-k. Koh, A. C. Bartnik, F. W. Wise, C. B. Murray, *J. Am. Chem. Soc.* 2010, 132, 3909.

[40] Y. Pan, M. A. Sohel, L. Pan, Z. Wei, H. Bai, M. C. Tamargo, R. John, *Materials Today: Proceedings* 2015, 2, 281.

[41] Q. Dai, Y. Zhang, Y. Wang, Y. Wang, B. Zou, W. W. Yu, M. Z. Hu, *J. Phys. Chem. C* 2010, 114, 16160.

[42] J. Joo, J. M. Pietryga, J. A. McGuire, S.-H. Jeon, D. J. Williams, H.-L. Wang, V. I. Klimov, *J. Am. Chem. Soc.* 2009, 131, 10620.

[43] C. M. Evans, A. M. Love, E. A. Weiss, *J. Am. Chem. Soc.* 2012, 134, 17298.

[44] P. M. Allen, B. J. Walker, M. G. Bawendi, *Angew. Chem. Int. Ed.* 2010, 49, 760.

[45] A. Shrestha, B. Jin, T. W. Kee, S. Z. Qiao, S. Dai, *ChemNanoMat* 2015.

[46] K.-S. Cho, D. V. Talapin, W. Gaschler, C. B. Murray, *J. Am. Chem. Soc.* 2005, 127, 7140.

[47] W. Lu, J. Fang, Y. Ding, Z. L. Wang, *J. Phys. Chem. B* 2005, 109, 19219.

[48] A. J. Houtepen, R. Koole, D. Vanmaekelbergh, J. Meeldijk, S. G. Hickey, *J. Am. Chem. Soc.* 2006, 128, 6792.

[49] J. Y. Woo, J.-H. Ko, J. H. Song, K. Kim, H. Choi, Y.-H. Kim, D. C. Lee, S. Jeong, *J. Am. Chem. Soc.* 2014, 136, 8883.

[50] (a) J. W. Stouwdam, J. Shan, F. C. J. M. van Veggel, A. G. Pattantyus-Abraham, J. F. Young, M. Raudsepp, *J. Phys. Chem. C* 2007, 111, 1086; (b) S. J. Oh, N. E. Berry, J.-H. Choi, E. A. Gaulding, H. Lin, T. Paik, B. T. Diroll, S. Muramoto, C. B. Murray, C. R. Kagan, *Nano Lett.* 2014, 14, 1559; (c) K. S. Leschkies, M. S. Kang, E. S. Aydil, D. J. Norris, *J. Phys. Chem. C* 2010, 114, 9988.

[51] J. M. Pietryga, D. J. Werder, D. J. Williams, J. L. Casson, R. D. Schaller, V. I. Klimov, J. A. Hollingsworth, *J. Am. Chem. Soc.* 2008, 130, 4879.

[52] E. Lifshitz, M. Brumer, A. Kigel, A. Sashchiuk, M. Bashouti, M. Sirota, E. Galun, Z. Burshtein, A. Q. Le Quang, I. Ledoux-Rak, J. Zyss, *J. Phys. Chem. B* 2006, 110, 25356.

[53] W. K. Bae, J. Joo, L. A. Padilha, J. Won, D. C. Lee, Q. Lin, W.-k. Koh, H. Luo, V. I. Klimov, J. M. Pietryga, *J. Am. Chem. Soc*. 2012, 134, 20160.

[54] J. Zhang, J. Gao, C. P. Church, E. M. Miller, J. M. Luther, V. I. Klimov, M. C. Beard, *Nano Lett*. 2014, 14, 6010.

[55] S. Kim, A. R. Marshall, D. M. Kroupa, E. M. Miller, J. M. Luther, S. Jeong, M. C. Beard, *ACS Nano* 2015, 9, 8157.

[56] W. E. Mahmoud, *Polymers Adv. Technol*. 2011, 22, 2550.

[57] R. Cui, Y.-P. Gu, Z.-L. Zhang, Z.-X. Xie, Z.-Q. Tian, D.-W. Pang, *J. Mater. Chem*. 2012, 22, 3713.

[58] A. Kumar, B. Singh, *Chem. Commun*. 2011, 47, 4144.

[59] C. B. Murray, D. J. Norris, M. G. Bawendi, *J. Am. Chem. Soc*. 1993, 115, 8706.

[60] H. Fu, S.-W. Tsang, Y. Zhang, J. Ouyang, J. Lu, K. Yu, Y. Tao, *Chem. Mater*. 2011, 23, 1805.

[61] H. Choi, J. H. Ko, Y. H. Kim, S. Jeong, *J. Am. Chem. Soc*. 2013, 135, 5278.

[62] A. H. Khan, U. Thupakula, A. Dalui, S. Maji, A. Debangshi, S. Acharya, *J. Phys. Chem. C* 2013, 117, 7934.

[63] K. A. Abel, J. Shan, J.-C. Boyer, F. Harris, F. C. J. M. van Veggel, *Chem. Mater*. 2008, 20, 3794.

[64] (a) J. Pan, A. a. O. El-Ballouli, L. Rollny, O. Voznyy, V. M. Burlakov, A. Goriely, E. H. Sargent, O. M. Bakr, *ACS Nano* 2013, 7, 10158; (b) I. Lignos, L. Protesescu, S. Stavrakis, L. Piveteau, M. J. Speirs, M. A. Loi, M. V. Kovalenko, A. J. deMello, *Chem. Mater*. 2014, 26, 2975.

[65] T.-Y. Liu, M. Li, J. Ouyang, M. B. Zaman, R. Wang, X. Wu, C.-S. Yeh, Q. Lin, B. Yang, K. Yu, *J. Phys. Chem. C* 2009, 113, 2301.

[66] S. Krüger, S. G. Hickey, S. Tscharntke, A. Eychmüller, *J. Phys. Chem. C* 2011, 115, 13047.

[67] D. Deng, J. Cao, J. Xia, Z. Qian, Y. Gu, Z. Gu, W. J. Akers, *Eur. J. Inorg. Chem.* 2011, 2011, 2422.

[68] P. Jiang, D.-L. Zhu, C.-N. Zhu, Z.-L. Zhang, G.-J. Zhang, D.-W. Pang, *Nanoscale* 2015, 7, 19310.

[69] D. Zhang, J. Song, J. Zhang, Y. Wang, S. Zhang, X. Miao, *CrystEngComm* 2013, 15, 2532.

[70] M. C. Weidman, M. E. Beck, R. S. Hoffman, F. Prins, W. A. Tisdale, *ACS Nano* 2014, 8, 6363.

[71] J. Yang, T. Ling, W.-T. Wu, H. Liu, M.-R. Gao, C. Ling, L. Li, X.-W. Du, *Nat Commun* 2013, 4, 1695.

[72] C. Schliehe, B. H. Juarez, M. Pelletier, S. Jander, D. Greshnykh, M. Nagel, A. Meyer, S. Foerster, A. Kornowski, C. Klinke, H. Weller, *Science* 2010, 329, 550.

[73] A. H. Khan, Q. Ji, K. Ariga, U. Thupakula, S. Acharya, *J. Mater. Chem*. 2011, 21, 5671.

[74] Y. Wang, A. Tang, K. Li, C. Yang, M. Wang, H. Ye, Y. Hou, F. Teng, *Langmuir* 2012, 28, 16436.

[75] H. Choi, J.-H. Ko, Y.-H. Kim, S. Jeong, *J. Am. Chem. Soc*. 2013, 135, 5278.

[76] J. M. Luther, H. M. Zheng, B. Sadtler, A. P. Alivisatos, *J. Am. Chem. Soc*. 2009, 131, 16851.

[77] L. Bakueva, I. Gorelikov, S. Musikhin, X. S. Zhao, E. H. Sargent, E. Kumacheva, *Adv. Mater*. 2004, 16, 926.

[78] D. Deng, W. Zhang, X. Chen, F. Liu, J. Zhang, Y. Gu, J. Hong, Eur. *J. Inorg. Chem.* 2009, 2009, 3440.

[79] Y. Yu, K. Zhang, S. Sun, Applied Surface Science 2012, 258, 7181; Y. Yu, K. Zhang, S. Sun, *J. Mol. Struc*. 2013, 1031, 194.

[80] X. Zhao, I. Gorelikov, S. Musikhin, S. Cauchi, V. Sukhovatkin, E. H. Sargent, E. Kumacheva, *Langmuir* 2005, 21, 1086.

[81] (a) K. Wundke, J. Auxier, A. Schülzgen, N. Peyghambarian, N. F. Borelli, *Appl. Phys. Lett.* 1999, 75, 3060; (b) R. Espiau de Lamaestre, J. Majimel, F. Jomard, H. Bernas, *J. Phys. Chem. B* 2005, 109, 19148.

[82] W. Lu, J. Fang, K. L. Stokes, J. Lin, *J. Am. Chem. Soc*. 2004, 126, 11798.

[83] Y. Pan, H. Bai, L. Pan, Y. Li, M. C. Tamargo, M. Sohel, J. R. Lombardi, *J. Mater. Chem.* 2012, 22, 23593.

[84] J. Zhang, A. Kumbhar, J. He, N. C. Das, K. Yang, J.-Q. Wang, H. Wang, K. L. Stokes, J. Fang, *J. Am. Chem. Soc*. 2008, 130, 15203.

[85] T. Mokari, M. Zhang, P. Yang, *J. Am. Chem. Soc*. 2007, 129, 9864.

[86] R. G. Pearson, *J. Am. Chem. Soc*. 1963, 85, 3533.

[87] I. Moreels, B. Fritzinger, J. C. Martins, Z. Hens, *J. Am. Chem. Soc*. 2008, 130, 15081.

[88] A. Nag, M. V. Kovalenko, J.-S. Lee, W. Liu, B. Spokoyny, D. V. Talapin, *J. Am. Chem. Soc*. 2011, 133, 10612.

[89] N. C. Anderson, M. P. Hendricks, J. J. Choi, J. S. Owen, *J. Am. Chem. Soc*. 2013, 135, 18536.

[90] H. Zhang, B. Hu, L. Sun, R. Hovden, F. W. Wise, D. A. Muller, R. D. Robinson, *Nano Lett*. 2011, 11, 5356.

[91] G. H. Carey, K. W. Chou, B. Yan, A. R. Kirmani, A. Amassian, E. H. Sargent, *MRS Commun*. 2013, 3, 83.

[92] A. Fischer, L. Rollny, J. Pan, G. H. Carey, S. M. Thon, S. Hoogland, O. Voznyy, D. Zhitomirsky, J. Y. Kim, O. M. Bakr, E. H. Sargent, *Adv. Mater*. 2013, 25, 5742.

[93] Z. Yang, A. Janmohamed, X. Lan, F. P. García de Arquer, O. Voznyy, E. Yassitepe, G.-H. Kim, Z. Ning, X. Gong, R. Comin, E. H. Sargent, *Nano Lett*. 2015, 15, 7539.

[94] C. Giansante, I. Infante, E. Fabiano, R. Grisorio, G. P. Suranna, G. Gigli, *J. Am. Chem. Soc*. 2015, 137, 1875.

[95] J. Aldana, Y. A. Wang, X. Peng, *J. Am. Chem. Soc*. 2001, 123, 8844.

[96] S. Hinds, S. Myrskog, L. Levina, G. Koleilat, J. Yang, S. O. Kelley, E. H. Sargent, *J. Am. Chem. Soc*. 2007, 129, 7218.

[97] B.-R. Hyun, Chen, D. A. Rey, F. W. Wise, C. A. Batt, *J. Phys. Chem. B* 2007, 111, 5726.

[98] I. S. Moody, A. R. Stonas, M. C. Lonergan, *J. Phys. Chem. C* 2008, 112, 19383.

[99] D. Deng, J. Xia, J. Cao, L. Qu, J. Tian, Z. Qian, Y. Gu, Z. Gu, *J. Colloid Interface Sci.* 2012, 367, 234.

[100] C. C. Reinhart, E. Johansson, *Chem. Mater*. 2015, 27, 7313.

[101] C. Giansante, L. Carbone, C. Giannini, D. Altamura, Z. Ameer, G. Maruccio, A. Loiudice, M. R. Belviso, P. D. Cozzoli, A. Rizzo, G. Gigli, *J. Phys. Chem. C* 2013, 117, 13305.

[102] B. K. Hughes, D. A. Ruddy, J. L. Blackburn, D. K. Smith, M. R. Bergren, A. J. Nozik, J. C. Johnson, M. C. Beard, *ACS Nano* 2012, 6, 5498.

[103] W. Lin, K. Fritz, G. Guerin, G. R. Bardajee, S. Hinds, V. Sukhovatkin, E. H. Sargent, G. D. Scholes, M. A. Winnik, *Langmuir* 2008, 24, 8215.

[104] H. Zhao, M. Chaker, D. Ma, *Phys. Chem. Chem. Phys*. 2010, 12, 14754.

[105] H. Zhao, D. Wang, M. Chaker, D. Ma, *J. Phys. Chem. C* 2011, 115, 1620.

[106] Z. Lingley, S. Lu, A. Madhukar, *Nano Lett*. 2011, 11, 2887.

[107] H. Zhao, D. Wang, T. Zhang, M. Chaker, D. Ma, *Chem. Commun*. 2010, 46, 5301.

[108] D. Liu, P. T. Snee, *ACS Nano* 2011, 5, 546.

[109] C. Giansante, L. Carbone, C. Giannini, D. Altamura, Z. Ameer, G. Maruccio, A. Loiudice, M. R. Belviso, P. D. Cozzoli, A. Rizzo, G. Gigli, *Thin Solid Films* 2014, 560, 2.

[110] M. V. Kovalenko, M. Scheele, D. V. Talapin, *Science* 2009, 324, 1417.

[111] M. V. Kovalenko, M. I. Bodnarchuk, J. Zaumseil, J. S. Lee, D. V. Talapin, *J. Am. Chem. Soc.* 2010, 132, 10085.

[112] S. Yakunin, D. N. Dirin, L. Protesescu, M. Sytnyk, S. Tollabimazraehno, M. Humer, F. Hackl, T. Fromherz, M. I. Bodnarchuk, M. V. Kovalenko, W. Heiss, *ACS Nano* 2014, 8, 12883.

[113] A. Nag, D. S. Chung, D. S. Dolzhnikov, N. M. Dimitrijevic, S. Chattopadhyay, T. Shibata, D. V. Talapin, *J. Am. Chem. Soc.* 2012, 134, 13604.

[114] M. I. Bodnarchuk, S. Yakunin, L. Piveteau, M. V. Kovalenko, *Nat. Commun.* 2015, 6.

[115] C. R. Ocier, K. Whitham, T. Hanrath, R. D. Robinson, *J. Phys. Chem. C* 2014, 118, 3377.

[116] S. E. Doris, J. J. Lynch, C. Li, A. W. Wills, J. J. Urban, B. A. Helms, *J. Am. Chem. Soc*. 2014, 136, 15702.

[117] E. L. Rosen, R. Buonsanti, A. Llordes, A. M. Sawvel, D. J. Milliron, B. A. Helms, *Angew. Chem., Int. Ed*. 2012, 51, 684.

[118] J. Huang, W. Liu, D. S. Dolzhnikov, L. Protesescu, M. V. Kovalenko, B. Koo, S. Chattopadhyay, E. V. Shenchenko, D. V. Talapin, *ACS Nano* 2014, 8, 9388.

[119] G. Niu, L. Wang, R. Gao, W. Li, X. Guo, H. Dong, Y. Qiu, *Phys. Chem. Chem. Phys.* 2013, 15, 19595.

[120] D. N. Dirin, S. Dreyfuss, M. I. Bodnarchuk, G. Nedelcu, P. Papagiorgis, G. Itskos, M. V. Kovalenko, *J. Am. Chem. Soc*. 2014, 136, 6550.

[121] Z. Ning, H. Dong, Q. Zhang, O. Voznyy, E. H. Sargent, *ACS Nano* 2014, 8, 10321.

[122] V. Sayevich, N. Gaponik, M. Plötner, M. Kruszynska, T. Gemming, V. M. Dzhagan, S. Akhavan, D. R. T. Zahn, H. V. Demir, A. Eychmüller, *Chem. Mater*. 2015, 27, 4328.

[123] H. Zhang, J. Jang, W. Liu, D. V. Talapin, *ACS Nano* 2014, 8, 7359.

[124] A. Zaban, O. I. Mićić, B. A. Gregg, A. J. Nozik, *Langmuir* 1998, 14, 3153.

[125] K. Szendrei, W. Gomulya, M. Yarema, W. Heiss, M. A. Loi, *Appl. Phys. Lett*. 2010, 97, 203501.

[126] G. H. Carey, L. Levina, R. Comin, O. Voznyy, E. H. Sargent, *Adv. Mater*. 2015, 27, 3325; J. Yang, J. Wang, K. Zhao, T. Izuishi, Y. Li, Q. Shen, X. Zhong, *J. Phys. Chem. C* 2015, 119, 28800.

[127] J. Yang, J. Wang, K. Zhao, T. Izuishi, Y. Li, Q. Shen, X. Zhong, *J. Phys. Chem. C* 2015, 119, 28800.

[128] G.-H. Kim, F. P. García de Arquer, Y. J. Yoon, X. Lan, M. Liu, O. Voznyy, Z. Yang, F. Fan, A. H. Ip, P. Kanjanaboos, S. Hoogland, J. Y. Kim, E. H. Sargent, *Nano Lett.* 2015, 15, 7691.

[129] S. Rühle, M. Shalom, A. Zaban, *ChemPhysChem* 2010, 11, 2290.

[130] M. R. Kim, D. Ma, *J. Phys. Chem. Lett.* 2015, 6, 85.

[131] (a) A. Hagfeldt, M. Grätzel, *Acc. Chem. Res.* 2000, 33, 269; (b) B. E. Hardin, H. J. Snaith, M. D. McGehee, *Nat. Photon.* 2012, 6, 162.

[132] (a) C.-H. Chang, Y.-L. Lee, *Appl. Phys. Lett*. 2007, 91, 053503; (b) W. Lee, S. K. Min, V. Dhas, S. B. Ogale, S.-H. Han, *Electrochem. Commun*. 2009, 11, 103; (c) O. Niitsoo, S. K. Sarkar, C. Pejoux, S. Rühle, D. Cahen, G. Hodes, *J. Photochem. Photobio. A: Chemistry* 2006, 181, 306; (d) Y.-L. Lee, B.-M. Huang, H.-T. Chien, *Chem. Mater*. 2008, 20, 6903.

[133] N. s. Guijarro, T. Lana-Villarreal, I. n. Mora-Seró, J. Bisquert, R. Gómez, *J. Phys. Chem. C* 2009, 113, 4208.

[134] H. J. Lee, P. Chen, S.-J. Moon, F. d. r. Sauvage, K. Sivula, T. Bessho, D. R. Gamelin, P. Comte, S. M. Zakeeruddin, S. I. Seok, M. Grätzel, M. K. Nazeeruddin, Langmuir 2009, 25, 7602; D. R. Baker, P. V. Kamat, *Adv. Func. Mater*. 2009, 19, 805.

[135] (a) S. Yu-Jen, L. Yuh-Lang, *Nanotechnol.* 2008, 19, 045602; (b) B. Farrow, P. V. Kamat, *J. Am. Chem. Soc*. 2009, 131, 11124; (c) J. R. Mann, D. F. Watson, *Langmuir* 2007, 23, 10924.

[136] G. Sixto, M.-S. Iván, M. Lorena, G. Nestor, L.-V. Teresa, G. Roberto, J. D. Lina, S. Qing, T. Taro, B. Juan, *Nanotechnol*. 2009, 20, 295204.

[137] S. D. Sung, I. Lim, P. Kang, C. Lee, W. I. Lee, *Chem. Commun*. 2013, 49, 6054.

[138] X. Li, W. Lu, Y. Wang, Y. Fang, L. Wang, Q. Ai, X. Zhou, Y. Lin, *Electrochimica Acta* 2014, 144, 71.

[139] G. Niu, L. Wang, R. Gao, B. Ma, H. Dong, Y. Qiu, *J. Mater. Chem*. 2012, 22, 16914.

[140] H. Lee, H. C. Leventis, S.-J. Moon, P. Chen, S. Ito, S. A. Haque, T. Torres, F. Nüesch, T. Geiger, S. M. Zakeeruddin, M. Grätzel, M. K. Nazeeruddin, *Adv. Func. Mater*. 2009, 19, 2735.

[141] K. E. Roelofs, S. M. Herron, S. F. Bent, *ACS Nano* 2015, 9, 8321.

[142] G. Seo, J. Seo, S. Ryu, W. Yin, T. K. Ahn, S. I. Seok, *J. Phys. Chem. Lett*. 2014, 5, 2015.

[143] J.-W. Lee, D.-Y. Son, T. K. Ahn, H.-W. Shin, I. Y. Kim, S.-J. Hwang, M. J. Ko, S. Sul, H. Han, N.-G. Park, *Sci. Reports* 2013, 3, 1050.

[144] S. W. Tsang, H. Fu, R. Wang, J. Lu, K. Yu, Y. Tao, *Appl. Phys. Lett*. 2009, 95, 183505.

[145] S.-W. Tsang, H. Fu, J. Ouyang, Y. Zhang, K. Yu, J. Lu, *Appl. Phys. Lett*. 2010, 96, 243104.

[146] H.-Y. Chen, J. Hou, S. Dayal, L. Huo, N. Kopidakis, M. C. Beard, J. M. Luther, *Adv. Energy Mater*. 2011, 1, 528.

[147] J. J. Choi, Y.-F. Lim, M. E. B. Santiago-Berrios, M. Oh, B.-R. Hyun, L. Sun, A. C. Bartnik, A. Goedhart, G. G. Malliaras, H. D. Abruña, F. W. Wise, T. Hanrath, *Nano Lett*. 2009, 9, 3749.

[148] K. W. Johnston, A. G. Pattantyus-Abraham, J. P. Clifford, S. H. Myrskog, D. D. MacNeil, L. Levina, E. H. Sargent, *Appl. Phys. Lett*. 2008, 92, 151115.

[149] G. I. Koleilat, L. Levina, H. Shukla, S. H. Myrskog, S. Hinds, A. G. Pattantyus-Abraham, E. H. Sargent, *ACS Nano* 2008, 2, 833.

[150] J. M. Luther, M. Law, M. C. Beard, Q. Song, M. O. Reese, R. J. Ellingson, A. J. Nozik, *Nano Lett*. 2008, 8, 3488.

[151] C. Piliego, L. Protesescu, S. Z. Bisri, M. V. Kovalenko, M. A. Loi, *Energy Environ. Sci.* 2013, 6, 3054.

[152] K. S. Leschkies, T. J. Beatty, M. S. Kang, D. J. Norris, E. S. Aydil, *ACS Nano* 2009, 3, 3638.

[153] A. G. Pattantyus-Abraham, I. J. Kramer, A. R. Barkhouse, X. Wang, G. Konstantatos, R. Debnath, L. Levina, I. Raabe, M. K. Nazeeruddin, M. Grätzel, E. H. Sargent, *ACS Nano* 2010, 4, 3374.

[154] D. A. R. Barkhouse, R. Debnath, I. J. Kramer, D. Zhitomirsky, A. G. Pattantyus-Abraham, L. Levina, L. Etgar, M. Grätzel, E. H. Sargent, *Adv. Mater*. 2011, 23, 3134.

[155] I. J. Kramer, D. Zhitomirsky, J. D. Bass, P. M. Rice, T. Topuria, L. Krupp, S. M. Thon, A. H. Ip, R. Debnath, H.-C. Kim, E. H. Sargent, *Adv. Mater*. 2012, 24, 2315.

[156] H. Wang, T. Kubo, J. Nakazaki, T. Kinoshita, H. Segawa, *J. Phys. Chem. Lett*. 2013, 4, 2455.

[157] J. Tang, K. W. Kemp, S. Hoogland, K. S. Jeong, H. Liu, L. Levina, M. Furukawa, X. Wang, R. Debnath, D. Cha, K. W. Chou, A. Fischer, A. Amassian, J. B. Asbury, E. H. Sargent, *Nat Mater* 2011, 10, 765.

[158] Z. Ning, O. Voznyy, J. Pan, S. Hoogland, V. Adinolfi, J. Xu, M. Li, A. R. Kirmani, J. Sun, J. Minor, *Nat. Mater*. 2014, 13, 822.

[159] C.-H. M. Chuang, P. R. Brown, V. Bulović, M. G. Bawendi, *Nat Mater* 2014, 13, 796.

[160] O. Chen, J. Zhao, V. P. Chauhan, J. Cui, C. Wong, D. K. Harris, H. Wei, H.-S. Han, D. Fukumura, R. K. Jain, M. G. Bawendi, *Nat Mater* 2013, 12, 445.

Chapter 3

A Robust Strategy for "Living" Growth of Lead Sulfide Quantum Dots

Aabhash Shrestha[1], Bo Jin[1], Tak W. Kee[2], Shi Zhang Qiao[1]*, and Sheng Dai[1]*

[1] School of Chemical Engineering, The University of Adelaide, Adelaide, SA, 5005, Australia

[2] School of Physical Sciences, Department of Chemistry, The University of Adelaide, Adelaide, SA, 5005, Australia

* Corresponding Authors

Email: s.dai@adelaide.edu.au , s.qiao@adelaide.edu.au

Published in the Journal ChemNanoMat (DOI: 10.1002/cnma.201500110). The published copy of the manuscript is attached in Appendix A.

Statement of Authorship

Title of Paper	A Robust Strategy for "Living" Growth of Lead Sulfide Quantum Dots
Publication Status	☑ Published ☐ Accepted for Publication ☐ Submitted for Publication ☐ Unpublished and Unsubmitted work written in manuscript style
Publication Details	Aabhash Shrestha, Bo Jin, Tak W. Kee, Shi Zhang Qiao*, and Sheng Dai*, **A Robust Strategy for "Living" Growth of Lead Sulfide Quantum Dots**, ChemNanoMat (DOI: 10.1002/cnma.201500110)

Principal Author

Name of Principal Author (Candidate)	Aabhash Shrestha
Contribution to the Paper	Experimental design, performing of the experiments, analysis of the results and writing of the manuscript
Certification:	This paper reports on original research I conducted during the period of my Higher Degree by Research candidature and is not subject to any obligations or contractual agreements with a third party that would constrain its inclusion in this thesis. I am the primary author of this paper.
Signature	Date 06/ April /2016

Co-Author Contributions

By signing the Statement of Authorship, each author certifies that:

the candidate's stated contribution to the publication is accurate (as detailed above);

permission is granted for the candidate in include the publication in the thesis; and

the sum of all co-author contributions is equal to 100% less the candidate's stated contribution.

Name of Co-Author	Bo Jin
Contribution to the Paper	Assisting in manuscript review
Signature	Date 07/04/2016

Name of Co-Author	Tak W. Kee
Contribution to the Paper	Assistance in fluorescence characterization and assessment.
Signature	Date 6/4/2016

Name of Co-Author	Shizhang Qiao		
Contribution to the Paper	Assisting in the manuscript review and assessment.		
Signature		Date	08/April/2016

Name of Co-Author	Sheng Dai		
Contribution to the Paper	Supervising the development of the work, assisting in the data interpretation, manuscript review and assessment.		
Signature		Date	4/04/2016

Please cut and paste additional co-author panels here as required.

Abstract

Colloidal quantum dot (QD) nanocrystals of lead sulfide (PbS) have promising applications in diverse scientific fields due to their size tuned band gaps, but the batch synthesis of differently sized QDs is cumbersome. In this paper, we report a robust method to synthesize monodisperse PbS QDs through a novel "living" growth process, where a series of differently sized QDs can be easily produced upon step-wise heating the preformed seed QDs in the presence of excessive PbS monomers i.e. un-crystallized PbS. The mechanism for such a QD growth is associated with the combination of "living" monomer addition to existing QDs to increase particle sizes and Ostwald ripening to focus particles. The outcome is not only able to produce various high quality QDs without extensive synthetic work, but also provide new insight on the mechanism of synthesizing semiconducting colloidal nanocrystals.

Keywords: Lead Sulfide, Quantum Dots, “Living Growth”, Oleic Acid, Crystal Growth

TOC Figure

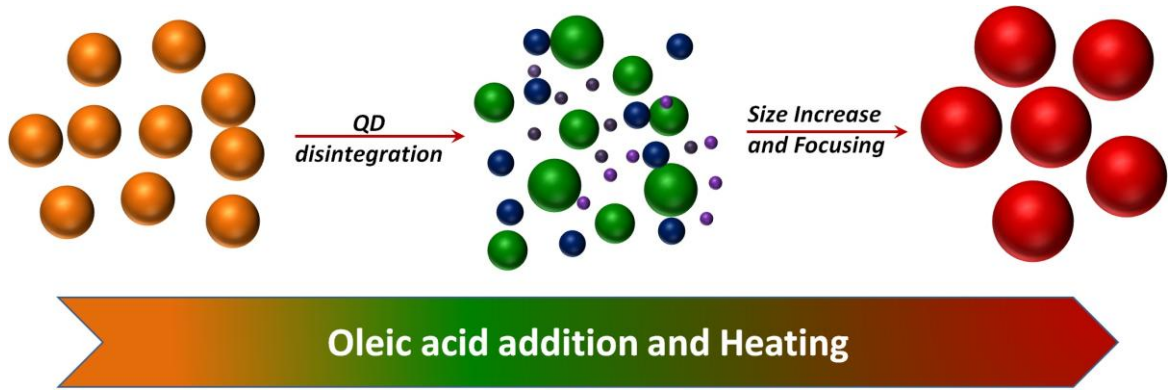

Ever since the recognition that quantum confinement effect determines the optical properties of cadmium sulfide (CdS) nanocrystals,[1] there have been tremendous efforts on the synthesis of various types of semiconducting nanocrystals.[2] Among them, colloidal near-infrared (NIR) quantum dots (QDs) have received growing interest due to their size tunability across the NIR region relevant to the applications in bio-imaging[3] (700 - 1000 nm), telecommunications[2c] (1300 - 1600 nm), photovoltaics,[4] and many others. Among them, lead sulfide (PbS) QDs have attracted great attention associated with their high molar extinction coefficients,[5] large excitonic Bohr radii (~ 18 nm),[3a, 5a, 5c] multiple exciton generation[6] and relatively better air stability than other lead based chalcogenides.[7] To date, many efforts have been reported on optimizing the synthesis of PbS QDs such as using various chemical precursors,[2c, 5a, 8] different stabilizing ligands,[5a, 9] diverse synthesis medium[7-8, 10] and miscellaneous methodologies.[2c, 7, 11] However, it always requires extensive synthetic work to produce differently sized colloidal nanoparticles. Generally, there are two approaches to tune the particle sizes of QDs: manipulating synthetic precursor ratios and controlling synthesis temperatures. The variation in synthetic precursor ratios requires multiple batches to produce differently sized nanoparticles,[2c, 5a] whereas controlling the synthesis temperature is sensitive to small variation in precursor types and ratios.[11a, 12] The shift of excitonic wavelength in the absorption spectrum of PbS QDs during a single batch synthesis can be varied between 100 to 450 nm by changing precursor ratios or synthesis temperatures.[11a, 12] The batch-to-batch variation cannot be avoided. Moreover, these synthesis procedures is complicated due to the lack of fundamental understanding on the precursor conversion kinetics[13] (which varies with different precursors and ligands), nucleation and crystal growth mechanisms.[14] In this study, we report a robust strategy to synthesize differently sized

PbS QDs by step by step heating the preformed (seed) QDs in the presence of excessive oleic acid at different temperatures. Oleic acid is able to partially disintegrate some seed QDs to generate monomers (i.e. un-crystallized PbS) in solution, and these monomers can add to those undisintegrated nanocrystals to increase particle sizes resemble to a "living" growth process. The associated controlled Ostwald ripening facilitates to produce high quality large QDs with narrow size distribution. Moreover, larger QDs can be further obtained by introducing more PbS monomers upon heating. The growth of PbS nanocrystals through such a "living" growth process can be used as a convenient approach to synthesize series of differently sized PbS QDs.

Followed the protocol described by Hines & Scholes,[2c] our seed PbS QDs (~600-650 nm exciton peak) were pre-synthesized. The obtained seed QDs were washed multiple times using acetone to fully remove reaction residuals and redispersed in octadecene. Various amounts of oleic acid (OA) were charged to the washed seed QD solutions at a fixed concentration, and the mixed systems were immediately heated to different temperatures under the protection of argon. **Figure 3-1(a)** shows the evolution of the absorption spectra of seed QDs being heated at 60 ^{o}C in the presence of oleic acid. The absorption spectra can be fitted to a Gaussian distribution and the corresponding wavelengths of the spectra are utilized in the empirical sizing curve to convert into size distributions.[9] From the figure, an obvious red shift (~160 nm) of the excitonic band can be observed over time, indicating the increase in the size of QDs. On the other hand, the continuous red-shift in the normalized steady-state photoluminescence (PL) emission spectra (**Figure S3-1,** Supporting Information) also indicates the elevation in particle size. The average full-width-half-maximum (FWHM) of absorption spectra of ≈119±14 nm (**Figure 3-1(b)**) and

the average PL FWHM of ≈110±20 nm imply the narrow size distribution of QDs. These results are comparable to previously reported PbS QDs batchly synthesized through hot injection approach.[2c] The transmission electron microscopy (TEM) images of the QDs (exciton peak ≈870 nm), synthesized through the heating of seed QDs in the presence of excessive oleic acid, indicate that these nanoparticles are monodisperse and spherical in shape **(Figure 3-1(c))**. The measured particle size from the TEM is ≈2.8±0.1 nm and that agrees well with the size calculated from its absorption spectrum (≈2.7 nm for 870 nm exciton peak).[5c]

In order to elucidate the contribution of oleic acid to the size tuning behaviors of QDs, we heated the seed QDs without addition of oleic acid. **Figure S3-2 (Supporting Information)** compares the spectra of the seed QDs before and after one hour heating at 80 ^{o}C. It is interesting that such a heating process cannot induce any change in QD size, which strongly suggests the significant role of oleic acid in the size tuning of PbS QDs. **Figure 3-2(a) (filled symbols/solid lines)** shows the time dependence of the excitonic peaks for the seed QDs being heated at 80 ^{o}C in the presence of various concentrations of oleic acid. The excitonic wavelength is used rather than particle diameter in our analysis because it is more intuitive and practical to monitor the exciton wavelength. The exciton wavelengths increase rapidly during the initial stage of nanocrystal growth (within 2 h), indicating the fast increase in particle size. With time progressing, the growth rate slows down and the QD size is inclined to reach saturation. It has to be noted that the capability of oleic acid to tune particle size drops at high oleic acid concentrations. Similar observation of particle size increase have also been observed for the batch synthesis of PbS

QDs in the presence of high oleic acid to Pb^{2+} ratios,[2c, 11a] where the size tunability of QDs saturates at high OA:Pb ratios.

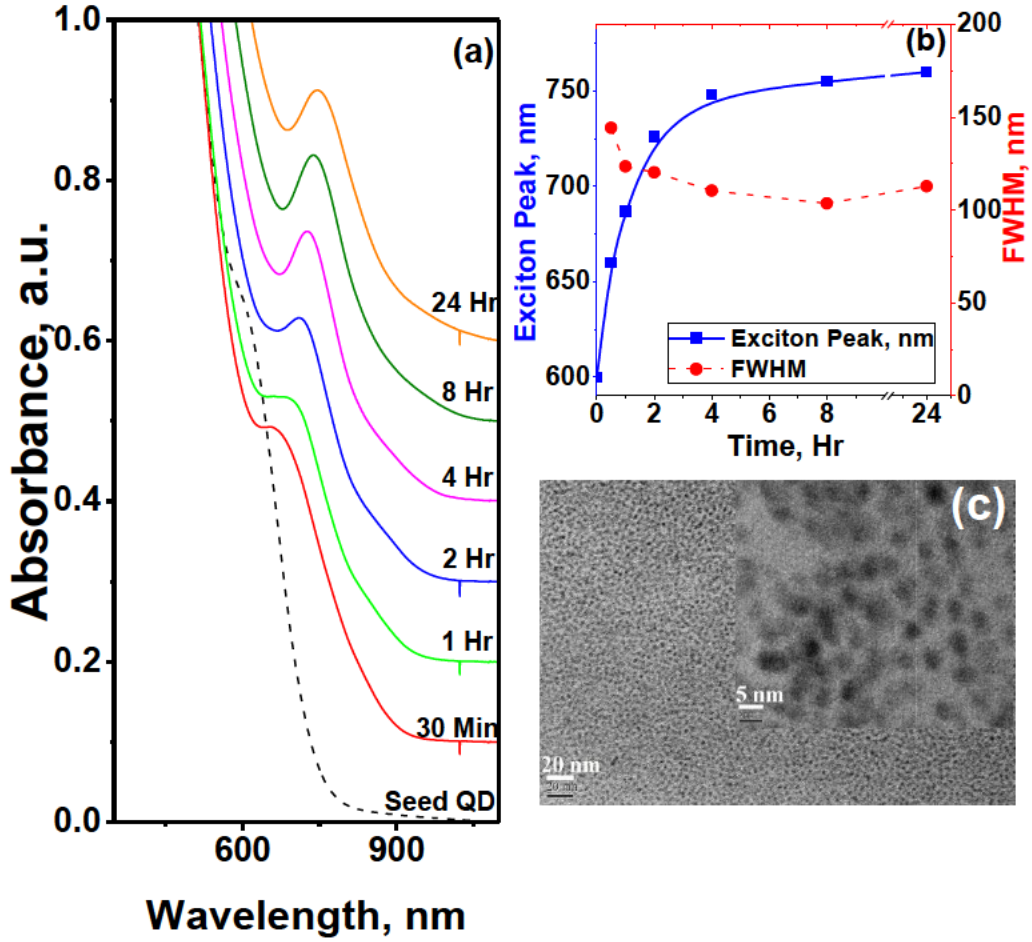

Figure 3-1. (a) Temporal evolution of seed QDs in presence of 0.5 mmol oleic acid and heated at 60 °C. (b) The average FWHM of excitonic peaks in absorbance spectra and position of exciton peak wavelengths for various PbS QDs obtained by heating seed QDs at 60 °C in the presence of excess oleic acid. (c) TEM image of QDs (exciton peak at ~860 nm) synthesized through heating the seed QDs at 90 °C in the presence of extra oleic acid. The scale bar for the TEM image is 20 nm and the inset TEM image is 5 nm.

The formation of large QD nanocrystals (NCs) with increasing oleic acid concentration upon heating indicates that there is a strong but yet reversible interaction between oleic acid and PbS NCs. Previous reports have indicated the existence of dynamic interaction of OA ligands on PbS NC surface through an adsorption and desorption process.[15] There is also the evidence that presence of excessive free oleic acid in PbS QD solutions significantly accelerates the removal of Pb atoms from QD surface i.e. oleic acid is able to etch QD NCs.[15a, 16] Bartl et al[17] evaluated the stability of cadmium selenide (CdSe) QD nanocrystals in the presence of various ligands and a reversible dissolution/regrowth phenomenon was observed. These observations imply towards the disintegration of some QDs in the presence of excessive oleic acid. At room temperature, a continuous blue-shift of the absorption peak for PbS QDs with increasing oleic acid concentrations can be observed, corresponding to the increased disintegration of QD nanocrystals (**Figure S3-3,** Supporting Information), from which small QD particles are easier to be disintegrated. **Figure S3-4** (Supporting Information) shows the evolution of seed QDs over time at room temperature in the presence of excessive oleic acid over a period of 24 hrs. The result clearly suggests that not all QDs can be disintegrated in the presence of excessive oleic acid. The disintegration of seed QD nanocrystals on the other hand results in the increase of monomer (i.e. uncrystallized PbS) concentration in solution (**Scheme 3-1**).

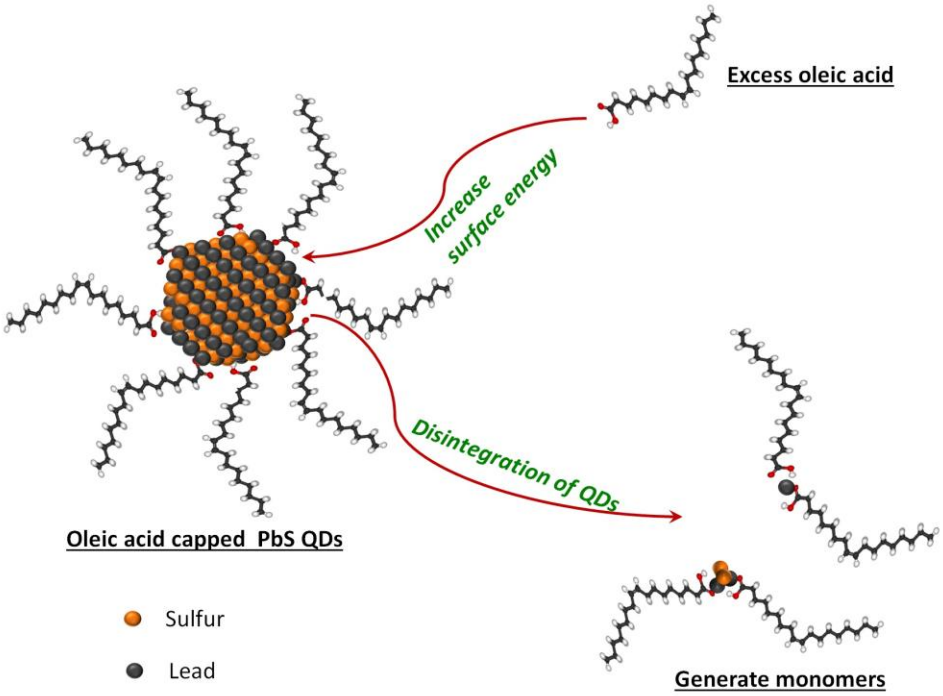

Scheme 3-1. Schematic illustration of the oleic acid interaction with PbS on QD surfaces. The addition of free oleic acid initiates the disintegration of preformed seed QDs via surface etching to generate PbS monomers and lead oleate. In the presence of lead oleate, the disintegration of the QDs is reduced due to the shift of chemical equilibrium.

Upon heating the above QD solutions to a high temperature, large sized QDs can be formed in solution (**Figure S3-5**, Supporting Information) as evident by the red-shift in the absorption spectra. On the other hand, if we directly injected oleic acid at high temperatures, the temporal evolution of absorption spectra and concentrations of PbS QDs are shown in **Figures S3-6 & S3-7** (Supporting Information), where the molar concentration (C) of QDs in solution were calculated from excitonic absorbance through the Lambert-Beer's law.[5c, 18] Due to absorption spectra overlap, the QD disintegration cannot be clearly observed under hot oleic acid addition. However, the increase in QD particle size and the decrease in QD concentrations are evident. That indicates the formation of large QDs in solution is accompanied with the sacrifice of some seed QDs.

Excessive amount of oleic acid can dissolve some QDs to generate QD monomers in solution. At high temperature, these monomers can simultaneously add to these undisintegrated QDs to form large nanoparticles in solution. The mass of each QD is proportional to the cubic of particle size R. The normalized mass ratios of nanocrystallized PbS QDs in solution after oleic acid addition can be expressed using the values of $C_iR_i^3/C_0R_0^3$, where C_0 and R_0 are the concentration and radius of seed QDs and C_i and R_i are the concentration and radius of newly formed QDs after free oleic acid addition and heating (**Figure S3-8**, Supporting Information). The decrease on the total mass of nanocrystallized PbS QDs in solution in the presence of excessive amount of oleic acid and heating also implies that oleic acid is able to disintegrate seeds QDs. However, not all disintegrated seed QDs can be added to the newly formed QDs due to the formation of lead oleate in solution and incomplete incorporation of all generated monomers onto new QDs.

To further understand the mechanism involved in the above size tuning behaviors of the QDs, the seed QDs were heated in the presence of excessive lead oleate and oleic acid. A series of experiments were performed where various concentrations of oleic acid were added to the solutions of seed QDs together with a fixed amount of (0.2 mmol) lead oleate. **Figure 3-2(a) (open symbols/dotted lines)** shows the evolution of QD exciton peaks when being heated in the presence of excessive oleic acid and lead oleate. The growth of seed QDs in the presence of lead oleate and oleic acid is less significant than that without lead oleate. On the other hand, no growth of QDs can be observed when only lead oleate is present. This evidence further verifies the existence of dynamic equilibrium between the oleic acid in solution and the oleate on PbS QD surface. In the presence of excessive oleic acid, oleic acid interacts with the PbS on NC surface and the equilibrium shifts towards the

disintegration of QDs via continuous etching of surface Pb and the formation of lead oleate and un-crystallized/disintegrated PbS units (monomers/oligomers) (**Scheme 3-1**). However, the presence of lead oleate in solution shifts the equilibrium towards less dissolution, which reduces the available PbS monomers/oligomers for nanocrystal growth and thus new QDs with relatively little sizes are obtained. At the same time, the formation of relatively large PbS QDs with increasing oleic acid concentration can be attributed to the increased disintegration of seed QDs to generate more PbS monomers/oligomers and the addition of these monomers onto those undisintegrated QDs to form large particles upon heating.

Obviously, heating provides the thermal energy beneficial for the addition of PbS monomers onto those undisintegrated QDs. Increasing temperature promotes particle growth as evidenced by the significant red-shift of the absorption peaks at high temperatures (**Figure 3-2(b)**). As mentioned previously, heating alone in the absence of oleic acid cannot induce particle growth, which implies the thermal energy is insufficient to overcome the energy barrier imposed by the steric hindrance of surface ligands for the coalescence or reorganization of seed QDs. In the presence of excessive oleic acid, the disintegration of QDs to PbS monomers is more favored.[19] More importantly, high temperature provides additional energy necessary to overcome the barrier for monomers/oligomers addition to these undisintegrated QDs. The growth of the nanocrystal ceases when it is large enough such that the balance of steric repulsion and crystallization adhesion is re-established. The increase in the particle size (absorption peak) at a given concentrations of seed QDs and oleic acid at various temperatures yields the rate constants for the addition of monomers/oligomers onto those undisintegrated QDs and a barrier

energy of ≈27.60 kJ/mol is obtained (**Section S3-1**, Supporting Information). The calculated activation energy for the addition of PbS monomers is comparable to that calculated for ZnS nanoparticles ripening under hydrothermal synthesis.[20] It can be argued that a high temperature facilitates monomer addition to those undisintegrated QDs.

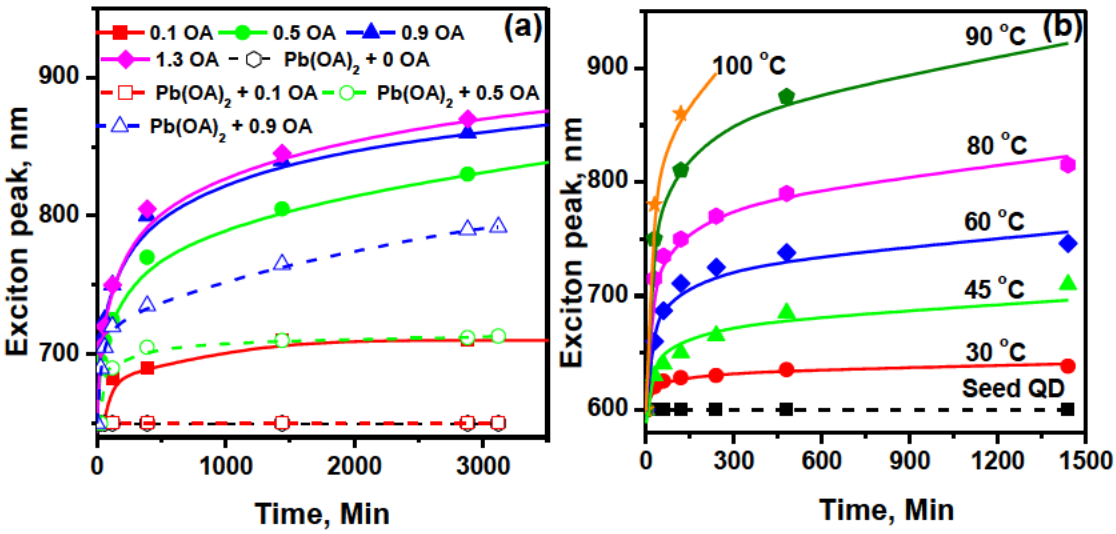

Figure 3-2. (a) Comparison on heating seed QDs in the presence of various amount of oleic acid and lead oleate. Here, filled/solid (symbol/guidelines) represent heating in presence of oleic acid only and open/dashed (symbol/guidelines) represent heating in the presence of oleic acid and lead oleate. The molar concentrations of oleic acid were varied as 0.1 mmol, 0.5 mmol, 0.9 mmol and 1.3 mmol while the molar concentration of lead oleate was fixed at 0.2 mmol. The heating temperature was set at 80 °C. (b) Effect of heating temperature on the size tuning of PbS QDs. Here, equivalent concentrations of seed QDs were heated in the presence of 0.5 mmol oleic acid at various temperatures varied from 30 to 100 °C.

To date, the mechanism for PbS QD growth is still not elusive. Previous studies have indicated the competition between orientation attachment (step growth or QD coalescence in one direction) and controlled Ostwald ripening (chain addition mechanism of QD monomers) for the growth of CdSe nanocrystals.[21] In the presence of extra ligands, the step growth of CdSe QDs is overtaken by chain addition mechanism. However, it cannot

be excluded that the growth can also occur simultaneously via the coalescence of tiny QD oligomers along with Ostwald ripening. Alivisatos et al,[22] study of in-situ transmission electron microscope showed that the platinum nanocrystals can grow either by monomer addition or by tiny particle coalescence. The combination of these two processes was found to be responsible for narrowing the initially broad size distribution. Similar results were also found during the growth of Bi_2S_3 nanowires.[23] The disintegration of PbS seed QDs via the consumption of oleic acid generates lead oleate and PbS monomers or oligomers in solution, and the generated monomers could be added to those undisintegrated QDs to form new QDs with large particle size. The size of the newly formed QDs can be influenced by reaction temperature and oleic acid feed. Normally, high temperature facilitates the formation of large sized new QDs. In order to further elucidate the mechanism associated with the above NC growth, a mixture of small and big seed QD particles upon excessive oleic acid addition was studied (**Figure S3-9**, Supporting Information). After introducing extra oleic acid to the mixed QD system at room temperature, the drop of small particle concentration is evident. However, for the addition of extra oleic acid to the mixed QD system at a high temperature (e.g. 80 ^{o}C), time dependent decrease in small seed QD concentration together with red-shift of the excitonic peaks of big seed QD particles is observed. The drop in the concentration of small seed QDs upon oleic acid addition is attributed to the disintegration of these QDs to form monomers/oligomers in solution. At room temperature, these monomers/oligomers cannot add to big seed QDs due to the existence of an energy barrier, and thus there is no shift on the excitonic peaks of big seed QDs. At a high temperature where the thermal energy is able to overcome the energy barrier, these disintegrated moieties could add to these undisintegrated big seed QDs to produce new large QDs as evident from the red-shift of

the excitonic peaks. With time passing by, depletion of small seed QDs slows down particle growth. The depletion of small seed QDS along with the similar FWHMs of big seed QDs and newly formed large QDs indicate that the new large QDs are formed through the addition of PbS monomers (or oligomers) to these undisintegrated QDs till a new equilibrium is re-established, where controlled Ostwald ripening places an important role to focus nanoparticles but no orientation attachment is observed.

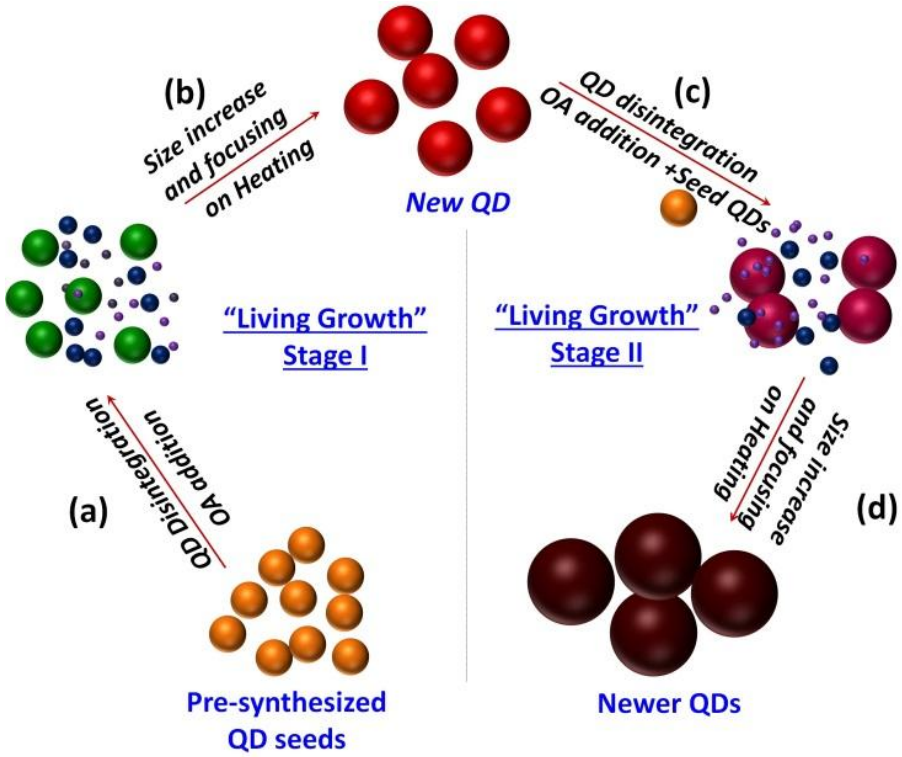

Scheme 3-2. Schematic illustration on the "living" growth mechanism of PbS QDs. Briefly, (a) addition of oleic acid to seed QDs initiates the disintegration of some seed QDs. (b) The generated monomers (or oligomers) can be added to those undisintegrated QDs to form large new QDs upon heating and focusing. (c) The obtained large QDs (after washing) can again be initiated to grow by adding oleic acid and seed QDs followed by heating. (d) The addition of monomers/oligomers QDs to the new QDs to produce newer larger QDs.

The overall growth of QD nanoparticles resembles to the "living" growth mechanism[23] in which particle size increases with monomer feed. The "living" growth mechanism of QD particles is depicted in **Scheme 3-2**. The addition of oleic acid to the seed QDs initiates the disintegration of some seed QDs. This generates PbS monomers/oligomers, which can be added to the undisintegrated QDs to form large particles upon heating (**Figure S3-5**, Supporting Information). Saturation can be reached once all PbS monomers are consumed. The obtained new QDs (after washing) can again be initiated to grow by adding extra oleic acid and heating. The PbS monomer generation occurs by the disintegration of seed QDs, and the rate of QD disintegration decreases with increasing QD size. As such, external QD monomer feed are required to achieve the continuous "living" growth of QD nanocrystals. The QD monomers feed can be introduced by two approaches: (1) addition of the small seed QD particles with excessive oleic acid, where seed QD particles can be dissolved to generate monomers (or oligomers) in solution; (2) addition of the precursors i.e. $PbOA_2$ and $(TMS)_2S$ along with extra oleic acid. A typical “living” growth of PbS QDs is presented in **Figure 3-3**, where the two stage growth is implemented. Briefly, the addition of oleic acid to the seed QDs together with heating induces the particle growth. After reaching growth saturation, the obtained new QDs were thoroughly washed to remove any reaction residual. The further particle growth of new QDs is initiated by adding oleic acid and initial seed QDs (as PbS monomer source) followed by heating. The newer larger sized QDs are synthesized. On the other hand, the sulfur precursor of $(TMS)_2S$ along with the lead precursor of lead oleate in the presence of extra oleic acid can also be used as an alternative approach for the supply of PbS monomers. **Figure S3-10** (Supporting Information) shows the growth of seed QDs when being heated in the presence of sulfur precursor along with lead oleate and extra oleic acid. It should be noted that the sulfur

precursor alone cannot be added to the washed QD suspensions as it can react with ligands on QD surface and induce nanoparticle precipitation.[24] In the presence of lead oleate and extra oleic acid, it would generate new PbS monomers for the addition to the existing QDs.

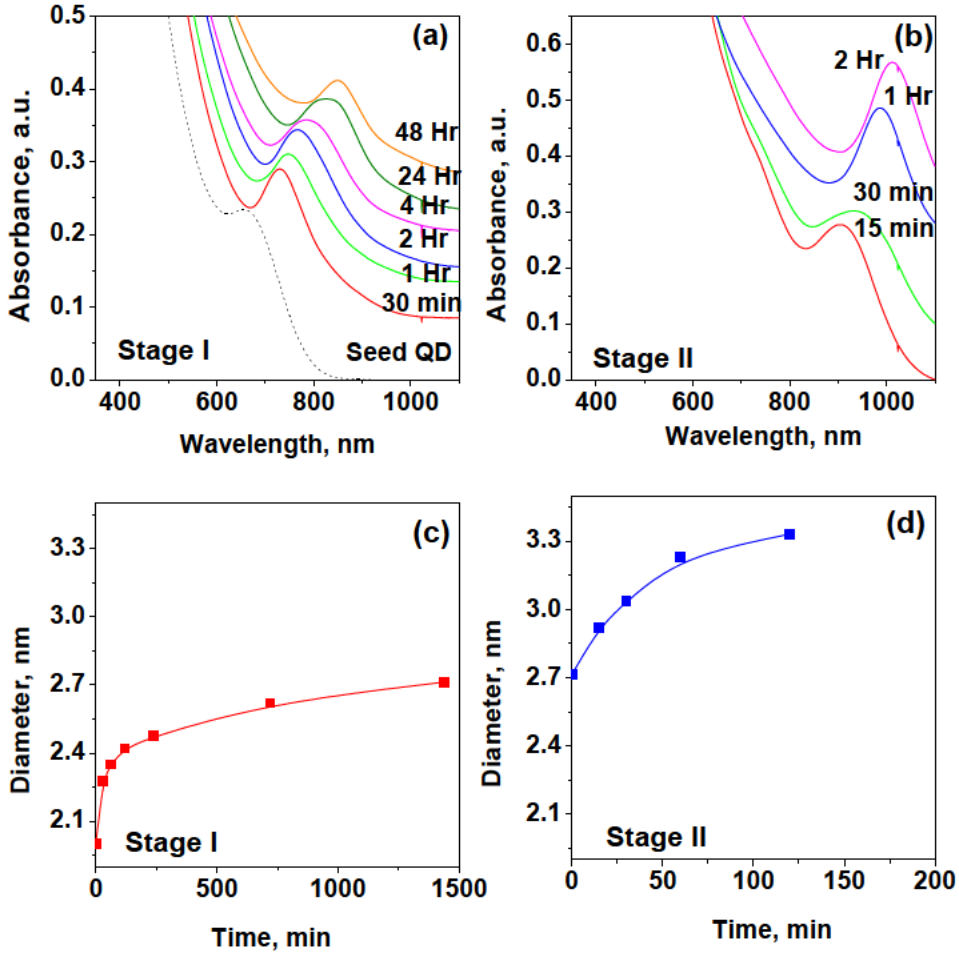

Figure 3-3. "Living" growth of PbS QDs. (a) shows the temporal evolution of stage I living growth where the seed QDs are heated (at 80 °C) in the presence of oleic acid. (b) shows the temporal evolution of stage II living growth where the new QDs obtained after stage I are washed and reheated (at 90 °C for higher growth rates) in the presence of excessive oleic acid and seed QDs (c) and (d) are the plots of particle diameters vs. time for the above two stage PbS QD growth. The particle diameters were calculated using the position of excitonic peaks in the absorption spectra based on the method developed by Moreels et al.[5c]

In conclusion, this work reports a novel strategy for the step "living" growth synthesis of a series of differently sized lead sulfide colloidal quantum dots by heating the preformed PbS QDs in the presence of excessive oleic acid, which provides a simple method for producing high quality QDs. Our observation also elucidates the detailed PbS QD growth mechanism, where QD "living" growth dominates size increases and Ostwald ripening oversees particle focusing.

Acknowledgements

This work was financially supported by the Australian Research Council Discovery Projects DP110102877 and DP140104062.

References

[1] (a) A. P. Alivisatos, *J. Phys. Chem.* 1996, 100, 13226-13239; (b) C. de Mello Donegá, P. Liljeroth, D. Vanmaekelbergh, *Small* 2005, 1, 1152-1162.

[2] (a) C. B. Murray, D. J. Norris, M. G. Bawendi, *J. Am. Chem. Soc.*1993, 115, 8706-8715; (b) D. V. Talapin, A. L. Rogach, A. Kornowski, M. Haase, H. Weller, *Nano Lett.* 2001, 1, 207-211; (c) M. A. Hines, G. D. Scholes, *Adv. Mater.* 2003, 15, 1844-1849; (d) Y. Liang, C. Lu, D. Ding, M. Zhao, D. Wang, C. Hu, J. Qiu, G. Xie, Z. Tang, *Chem. Sci.* 2015, 6, 4103-4108.

[3] (a) E. H. Sargent, *Adv. Mater.* 2005, 17, 515-522; (b) E. B. Voura, J. K. Jaiswal, H. Mattoussi, S. M. Simon, *Nat. Med.* 2004, 10, 993-998; (c) X. Gao, Y. Cui, R. M. Levenson, L. W. K. Chung, S. Nie, *Nat. Biotechnol.* 2004, 22, 969-976; (d) S. Kim, Y. T. Lim, E. G. Soltesz, A. M. De Grand, J. Lee, A. Nakayama, J. A. Parker, T. Mihaljevic, R. G. Laurence, D. M. Dor, L. H. Cohn, M. G. Bawendi, J. V. Frangioni, *Nat. Biotechnol.* 2004, 22, 93-97.

[4] (a) A. H. Ip, S. M. Thon, S. Hoogland, O. Voznyy, D. Zhitomirsky, R. Debnath, L. Levina, L. R. Rollny, G. H. Carey, A. Fischer, K. W. Kemp, I. J. Kramer, Z. Ning, A. J. Labelle, K. W. Chou, A. Amassian, E. H. Sargent, *Nat. Nanotechnol.* 2012, 7, 577-

582; (b) J. Tang, K. W. Kemp, S. Hoogland, K. S. Jeong, H. Liu, L. Levina, M. Furukawa, X. Wang, R. Debnath, D. Cha, K. W. Chou, A. Fischer, A. Amassian, J. B. Asbury, E. H. Sargent, *Nat. Mater.* 2011, 10, 765-771.

[5] (a) L. Cademartiri, J. Bertolotti, R. Sapienza, D. S. Wiersma, G. von Freymann, G. A. Ozin, *J. Phys. Chem. B* 2005, 110, 671-673; (b) L. Cademartiri, E. Montanari, G. Calestani, A. Migliori, A. Guagliardi, G. A. Ozin, *J. Am. Chem. Soc.* 2006, 128, 10337-10346; (c) I. Moreels, K. Lambert, D. Smeets, D. De Muynck, T. Nollet, J. C. Martins, F. Vanhaecke, A. Vantomme, C. Delerue, G. Allan, Z. Hens, *ACS Nano* 2009, 3, 3023-3030.

[6] J. B. Sambur, T. Novet, B. A. Parkinson, *Science* 2010, 330, 63-66.

[7] D. Deng, J. Cao, J. Xia, Z. Qian, Y. Gu, Z. Gu, W. J. Akers, *Eur. J. Inorg. Chem*. 2011, 2011, 2422-2432.

[8] L. Bakueva, I. Gorelikov, S. Musikhin, X. S. Zhao, E. H. Sargent, E. Kumacheva, *Adv. Mater*. 2004, 16, 926-929.

[9] (a) K. A. Abel, J. Shan, J.-C. Boyer, F. Harris, F. C. J. M. van Veggel, *Chem. Mater.* 2008, 20, 3794-3796; (b) I. Moreels, Y. Justo, B. De Geyter, K. Haustraete, J. C. Martins, Z. Hens, *ACS Nano* 2011, 5, 2004-2012.

[10] D. Deng, W. Zhang, X. Chen, F. Liu, J. Zhang, Y. Gu, J. Hong, *Eur. J. Inorg. Chem.* 2009, 2009, 3440-3446.

[11] (a) T.-Y. Liu, M. Li, J. Ouyang, M. B. Zaman, R. Wang, X. Wu, C.-S. Yeh, Q. Lin, B. Yang, K. Yu, *J. Phys. Chem. C* 2009, 113, 2301-2308; (b) J. Yang, T. Ling, W.-T. Wu, H. Liu, M.-R. Gao, C. Ling, L. Li, X.-W. Du, *Nat. Commun.* 2013, 4, 1695; (c) G. Chen, J. Fan, T. Zhao, X. Xu, M. Zhu, Z. Tang, *J. Nanosci. Nanotechnol.* 2011, 11, 7807-7812.

[12] J. Zhang, J. Gao, E. M. Miller, J. M. Luther, M. C. Beard, *ACS Nano* 2013, 8, 614-622.

[13] J. S. Owen, E. M. Chan, H. Liu, A. P. Alivisatos, *J. Am. Chem. Soc.* 2010, 132, 18206-18213.

[14] (a) S. Abe, R. K. Capek, B. De Geyter, Z. Hens, *ACS Nano* 2013, 7, 943-949; (b) S. Abe, R. K. Čapek, B. De Geyter, Z. Hens, *ACS Nano* 2011, 6, 42-53.

[15] (a) Q. Dai, Y. Zhang, Y. Wang, Y. Wang, B. Zou, W. W. Yu, M. Z. Hu, *J. Phys. Chem. C* 2010, 114, 16160-16167; (b) I. Moreels, B. Fritzinger, J. C. Martins, Z. Hens, *J. Am. Chem. Soc.* 2008, 130, 15081-15086; (c) X. Ji, D. Copenhaver, C. Sichmeller, X. Peng, *J. Am. Chem. Soc.* 2008, 130, 5726-5735; (d) C. Bullen, P. Mulvaney, *Langmuir* 2006, 22, 3007-3013.

[16] Z. Lingley, S. Lu, A. Madhukar, *Nano Lett.* 2011, 11, 2887-2891.

[17] J. T. Siy, M. H. Bartl, *Chem. Mater.* 2010, 22, 5973-5982.

[18] J. Thessing, J. Qian, H. Chen, N. Pradhan, X. Peng, *J. Am. Chem. Soc.* 2007, 129, 2736-2737.

[19] C. R. Bealing, W. J. Baumgardner, J. J. Choi, T. Hanrath, R. G. Hennig, *ACS Nano* 2012, 6, 2118-2127.

[20] M. Tiemann, F. Marlow, J. Hartikainen, Ö. Weiss, M. Lindén, *J. Phys. Chem.* C 2008, 112, 1463-1467.

[21] C. M. Evans, A. M. Love, E. A. Weiss, *J. Am. Chem. Soc.* 2012, 134, 17298-17305.

[22] H. Zheng, R. K. Smith, Y.-w. Jun, C. Kisielowski, U. Dahmen, A. P. Alivisatos, *Science* 2009, 324, 1309-1312.

[23] L. Cademartiri, G. Guerin, K. J. M. Bishop, M. A. Winnik, G. A. Ozin, *J. Am. Chem. Soc.* 2012, 134, 9327-9334.

[24] J. S. Owen, J. Park, P.-E. Trudeau, A. P. Alivisatos, *J. Am. Chem. Soc.* 2008, 130, 12279-12281.

Supporting Information

A Robust Strategy for "Living" Growth of Lead Sulfide Quantum Dots

Aabhash Shrestha[1], Bo Jin[1], Tak W. Kee[2], Shi Zhang Qiao[1]*, and Sheng Dai[1]*

[1] School of Chemical Engineering, The University of Adelaide, Adelaide, SA, 5005, Australia

[2] School of Physical Sciences, Department of Chemistry, The University of Adelaide, Adelaide, SA, 5005, Australia

* Corresponding Authors

Email: s.dai@adelaide.edu.au , s.qiao@adelaide.edu.au

Experimental

S3-1. Materials

Lead (II) oxide (PbO, 99.99 %), hexamethyldisilathiane $(TMS)_2S$, oleic acid (OA, 90% technical grade), 1-octadecene (ODE, 99.99%), acetone and hexane were purchased from Sigma- Aldrich. All chemicals were used as received.

S3-2. Synthesis of preformed PbS QDs

The PbS QD seeds were synthesized using a previously described method with modification[1]. Briefly, 89.3 mg (0.4 mmol) of PbO, 0.317 mL (0.8 mmol) oleic acid and 4 mL 1-octadecene were charged to a 25 mL schlenk flask under argon protection and heated to 150 ℃ for 1 hour to obtain a clear yellow lead oleate solution. The obtained lead oleate solution was protected using argon and immersed into a pre-heated oil-bath set at different designated injection temperatures. In another schlenk flask, 42 µl (0.2 mmol) $(TMS)_2S$ were charged to 2 ml of degassed ODE under argon. Once the temperature of the lead oleate solution was stabilized, the $(TMS)_2S$ solution was quickly injected using an argon washed syringe. The QD growth could be saturated in about 10 min. The obtained QDs were washed 3-4 times using acetone to remove unreacted reactants and re-dispersed in ODE. Differently sized PbS seed QDs were synthesized (a) small QDs (~570-650 nm exciton peak) (b) big QDs (~865 nm exciton peak). The small QDs (570-650 nm exciton peak) were synthesized by injecting the precursors at ~90 ^{o}C and then quickly (~ 10-15 s) quenching the reaction for the particles to grow at ~40-50 ^{o}C. For the synthesis of big QDs (~865 nm exciton peak), the precursors were typically injected at high temperatures (~120 ^{o}C) and also grow at relatively higher temperatures (~90 ^{o}C).

S3-3. Living growth of QDs

The washed seed QDs in ODE were transferred to a schlenk flask and degassed for ~15-30 minutes by purging argon and heated to various designated temperatures. Different amounts of oleic acid were added to the preheated seed QD solutions under argon protection and small aliquots were taken at different time intervals for experimental analysis. The aliquots were washed with acetone to remove excess oleic acid and re-dispersed in hexane. Once the nanocrystal growth was saturated, the resulting new QDs were washed, re-dispersed in ODE or hexane and stored in argon. The re-growth of the above new QDs was carried out by adding excess amount of oleic acid and heating or adding extra seed QD particles with excess oleic acid and heating.

S3-4. Absorption and fluorescence emission measurements

The absorption measurements were performed in a Shimadzu 1601 UV-vis. spectrometer. The fluorescence measurements were carried in a Varian Cary Eclipse spectroflurometer. The excitation wavelength during the fluorescence measurements was maintained as 600 nm while the slits of excitation and emission were set to 5 mm.

S3-5. TEM measurements

The TEM measurements were performed using a Phillips CM200 transmission electron microscope under a 200 kV accelerating voltage. Size of PbS QDs was analyzed using the ImageJ© software.

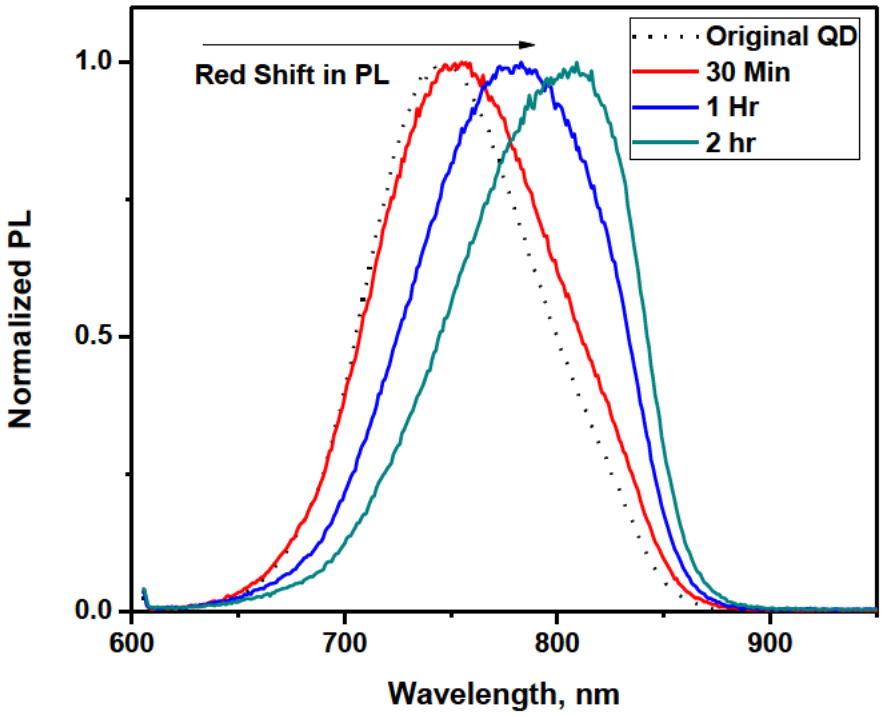

Figure S3-1. Normalized steady state photoluminescence (PL) emission spectra of the PbS seed QDs living growth at 60 °C. The absorption spectra of these QDs are shown in **Figure 3-1(a)**. The red shift of PL emission spectra clearly indicates the increase in particle size.

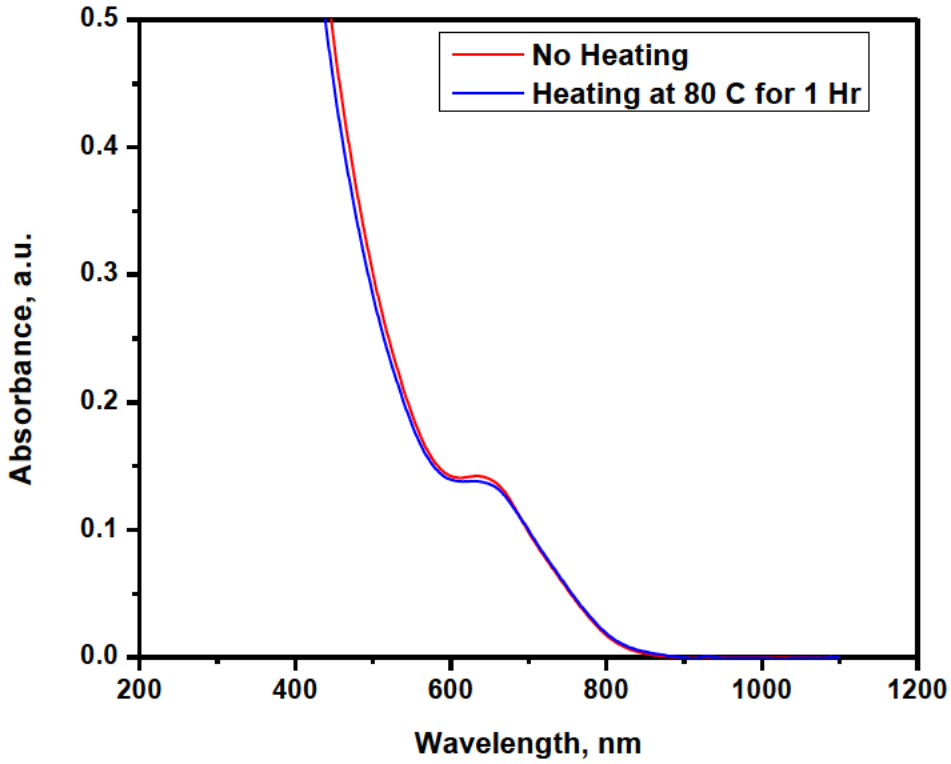

Figure S3-2. Comparison on the absorption spectra of seed QDs and that being heated at 80 °C for 1 hour in octadecene and in the absence of extra oleic acid. Obviously, heating process cannot induce significant change in the absorption and particle size of seed QDs. In addition, the heating of pre-synthesized seed QDs at other temperatures were also carried out and the results are consistent, where no particle size change can be observed.

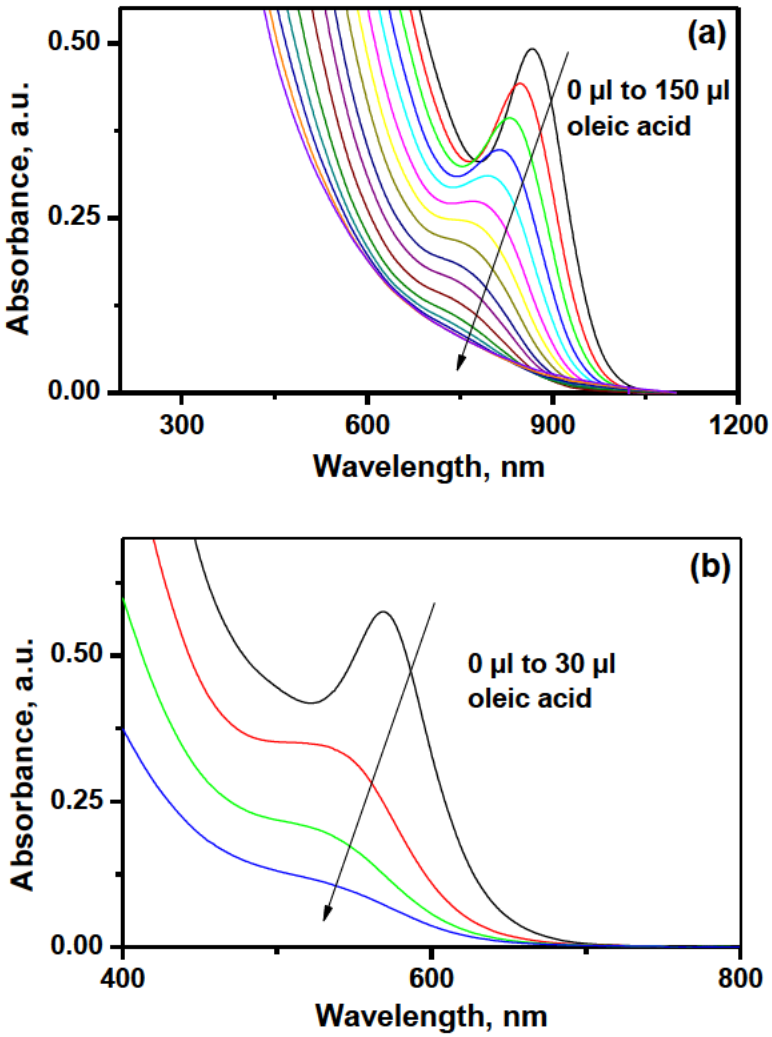

Figure S3-3. Effect of oleic acid on the disintegration of different sized PbS QDs at room temperature. (a) represents the big PbS seed QDs with their initial excitonic peak at ~865 nm, and (b) represents the small PbS seed QDs with their initial excitonic peak at ~570 nm. It can be seen that the absorption blue-shifts with the addition of excess oleic acid and the dissolution of small seed QDs is faster than that of big seed QDs.

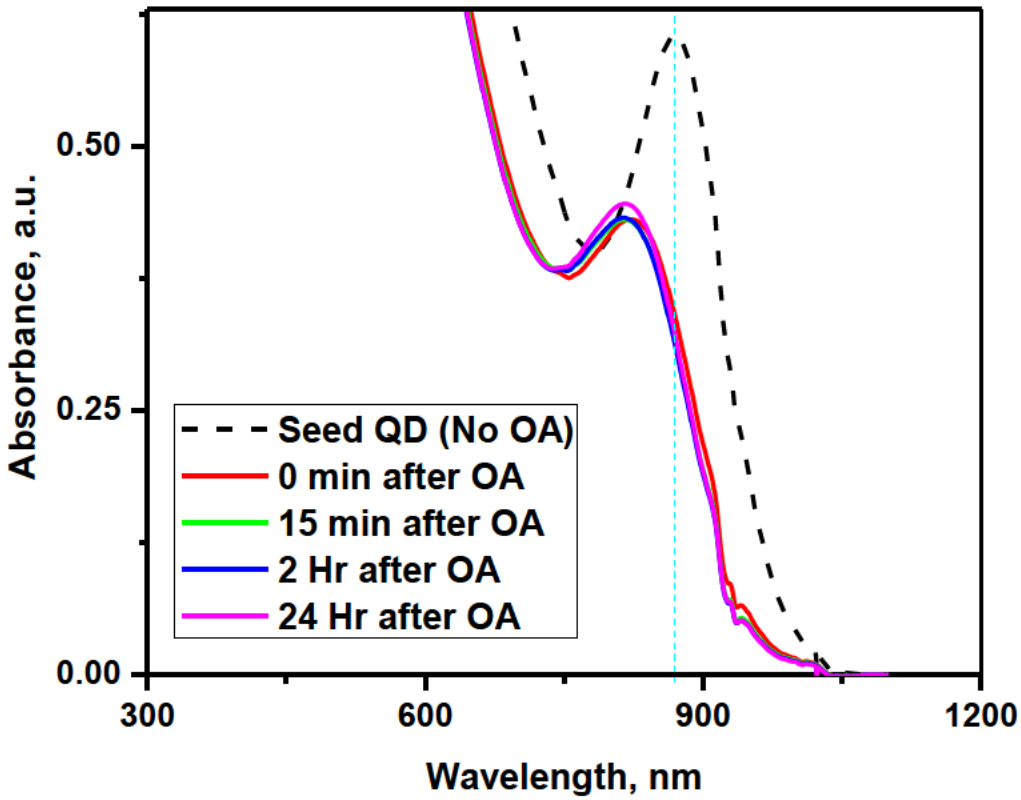

Figure S3-4. Time evolution of seed QDs (excitonic peak at 865 nm) at room temperature in the presence of 30 µL of oleic acid over a period of 24 hours. The results suggest not all QDs can be disintegrated.

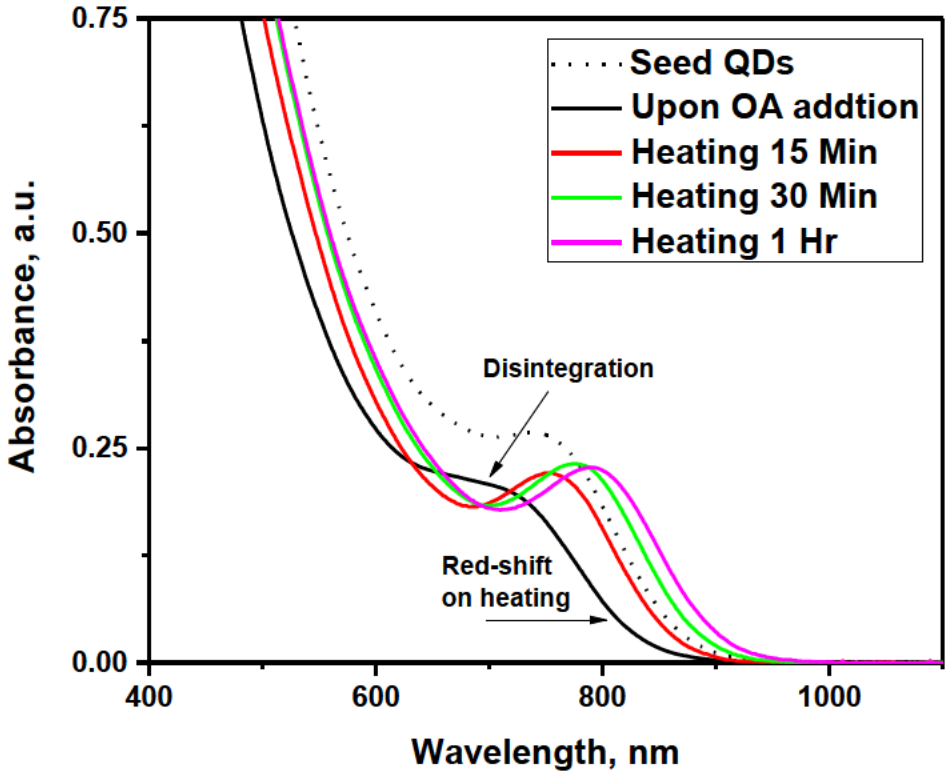

Figure S3-5. Influence of adding oleic acid to a PbS QD solution at room temperature, and then heating to the mixture to 80 °C. Adding oleic acid initiates the disintegration of QDs as shown by the blue-shift in absorption spectrum. Upon heating the mixture solution, the size of newly formed QDs increases as evident by the red-shift in the absorption spectra.

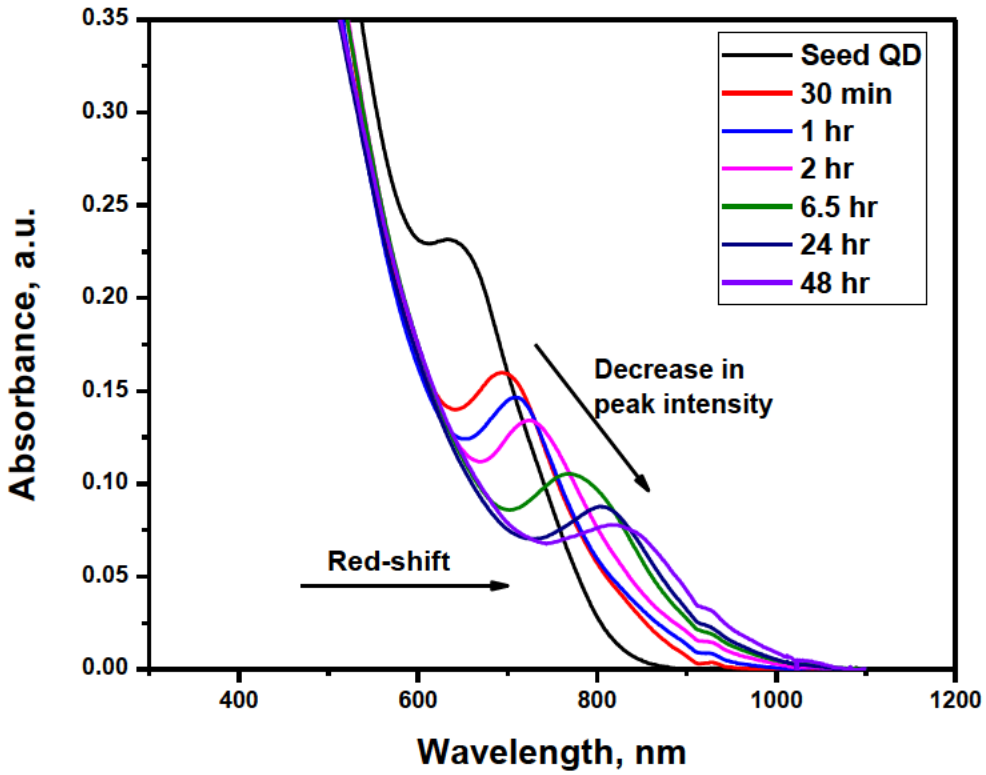

Figure S3-6. Temporal evolution of the absorption spectra of PbS QDs formed after addition of 0.5 mmol oleic acid at 80 °C. It can be seen that the addition of oleic acid and heating gives rise to the increase of QD size as evident by the red-shift of the absorption spectra. The decrease of peak intensity on the other hand indicates the decrease in the concentration of newly formed QDs.

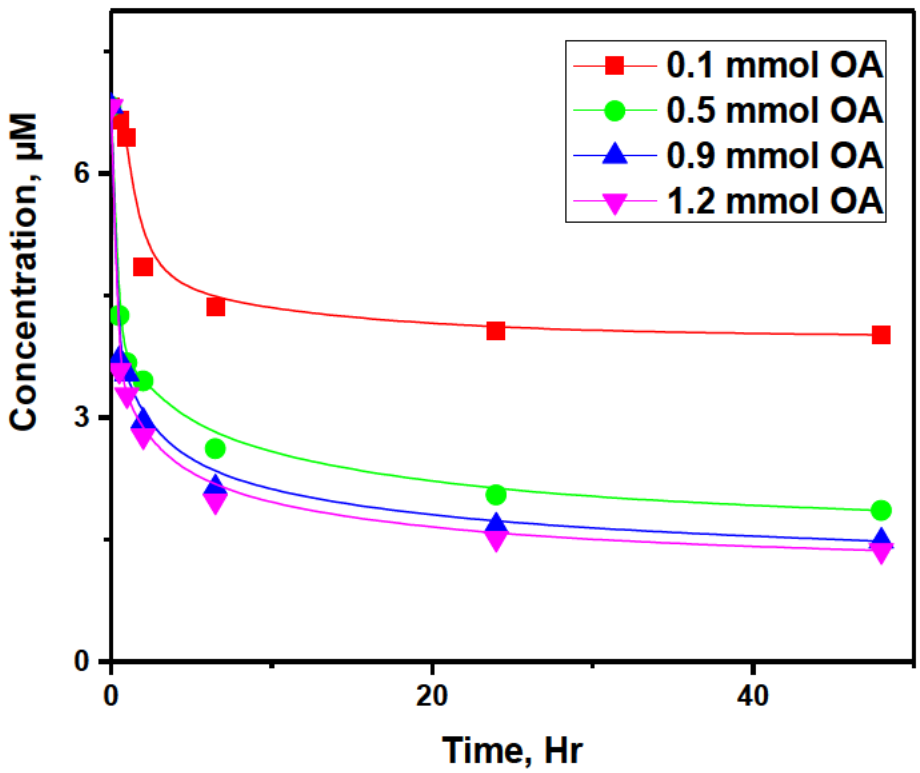

Figure S3-7. Temporal evolution of PbS QD concentrations after adding various amounts of oleic acid to seed QDs at 80 oC. Increasing the amount of oleic acid decreases the concentration of newly formed QDs together with the increase in QD particle size (a sample absorption spectra in 0.5 mmol is shown in **Figure S3-6**).

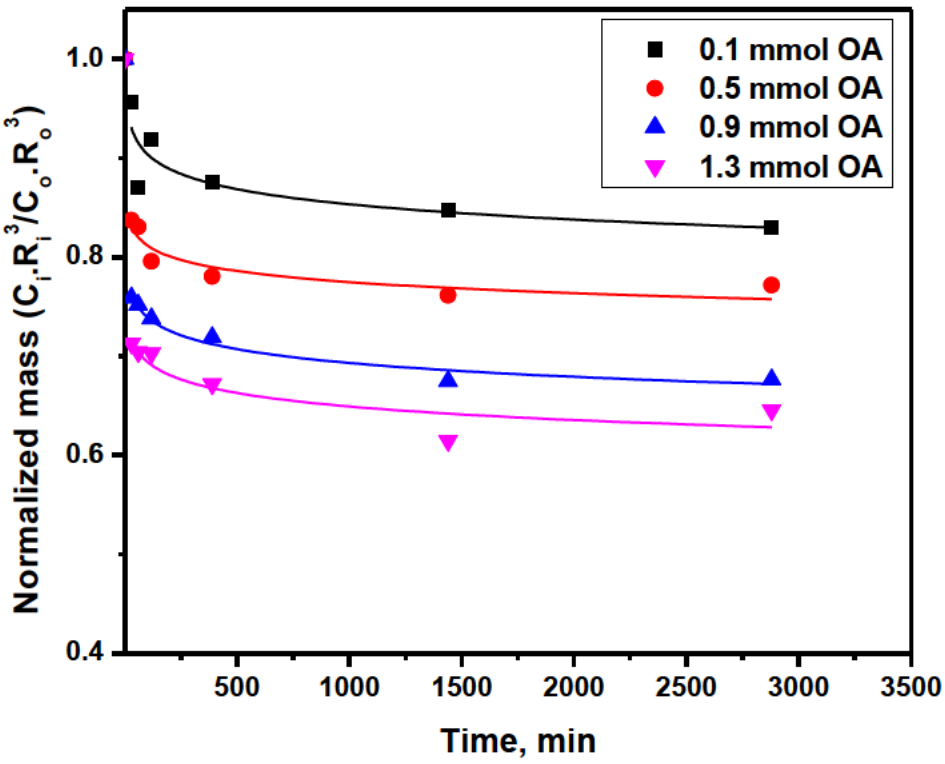

Figure S3-8. The normalized mass ratios ($\frac{C_i R_i^3}{C_o R_o^3}$) of PbS QDs formed during particle "living" growth process. Here, C_o and C_i are the initial concentration of seed QDs and the concentration of grown QDs after time t. R_o and R_i are the initial QD size and the QD size at time t. It can be seen that the total mass of QDs drops with increasing time and oleic acid contents, which indicates the increased disintegration and not all of the disintegrated the QDs can be added to these undisintegrated QDs.

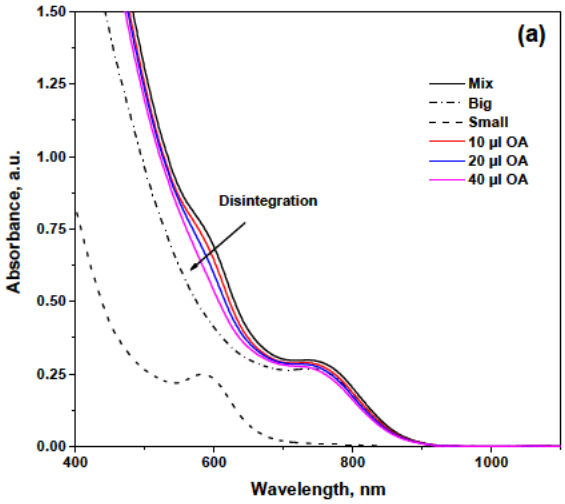
(a)
Absorbance, a.u.
Wavelength, nm
Mix
Big
Small
10 µl OA
20 µl OA
40 µl OA
Disintegration

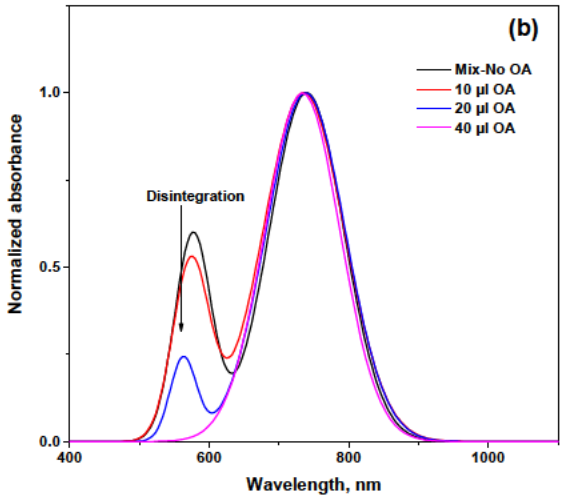
(b)
Normalized absorbance
Wavelength, nm
Mix-No OA
10 µl OA
20 µl OA
40 µl OA
Disintegration

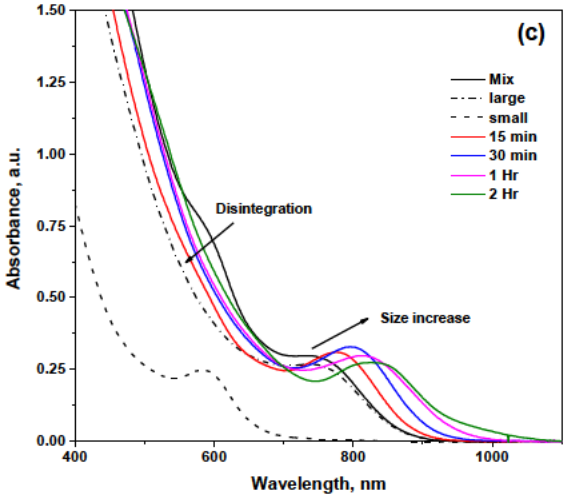
(c)
Absorbance, a.u.
Wavelength, nm
Mix
large
small
15 min
30 min
1 Hr
2 Hr
Disintegration
Size increase

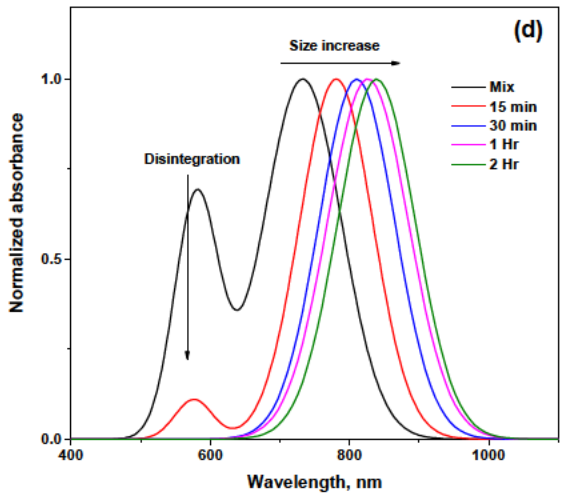
(d)
Normalized absorbance
Wavelength, nm
Size increase
Disintegration
Mix
15 min
30 min
1 Hr
2 Hr

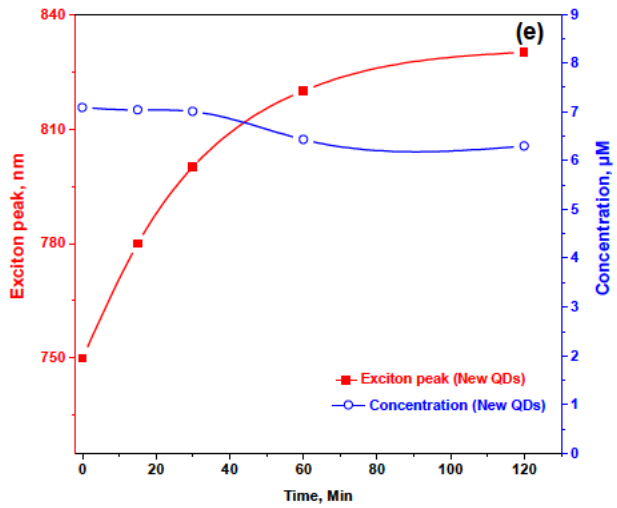
(e)
Exciton peak, nm
Concentration, µM
Time, Min
Exciton peak (New QDs)
Concentration (New QDs)

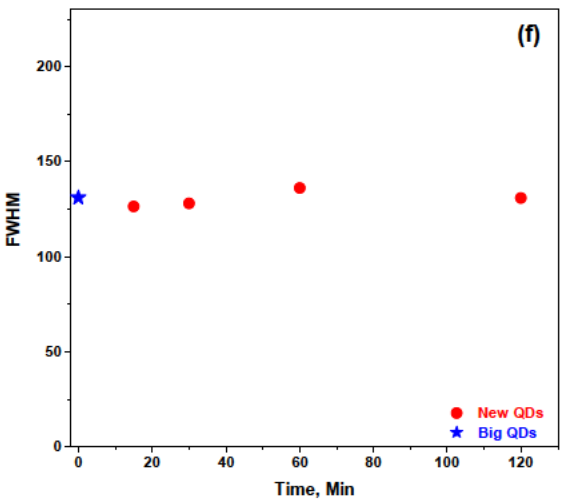
(f)
FWHM
Time, Min
New QDs
Big QDs

Figure S3-9. Addition of oleic acid to a mixture of small and big seed QD particles. (a) Temporal evolution of absorption spectra upon addition of oleic acid at room temperature, (b) Peak splitting by fitting the absorbance spectra in **Figure S3-9a** to standard Gaussian distributions using Origin pro© software.(c) Temporal evolution of absorption spectra upon addition of oleic acid to a mixture of small and big particles at 80 ^{o}C for various times, (d) Peak splitting by fitting the absorbance spectra in **Figure S3-9c** to standard Gaussian distributions using Origin Pro© software.

It can be seen that addition of oleic acid without heating can disintegrate small seed QD particles while no particle size change in big seed QDs can be observed, Addition of oleic acid at high temperature initiates the disintegration of small seed QDs, together with the size increase in big seed QDs, (e) Position of excitonic peaks and concentration of big PbS QDs at various aliquot times upon oleic acid addition at 80 ^{o}C, (f) FWHMs of the absorbance spectra for the big seed QD and the newly formed large QDs upon oleic acid addition at 80 ^{o}C. The similar FWHMs together with the identical large new QD size distributions in Figure S9 (d) indicates the “living” growth mechanism in operation, where no orientation attachment.

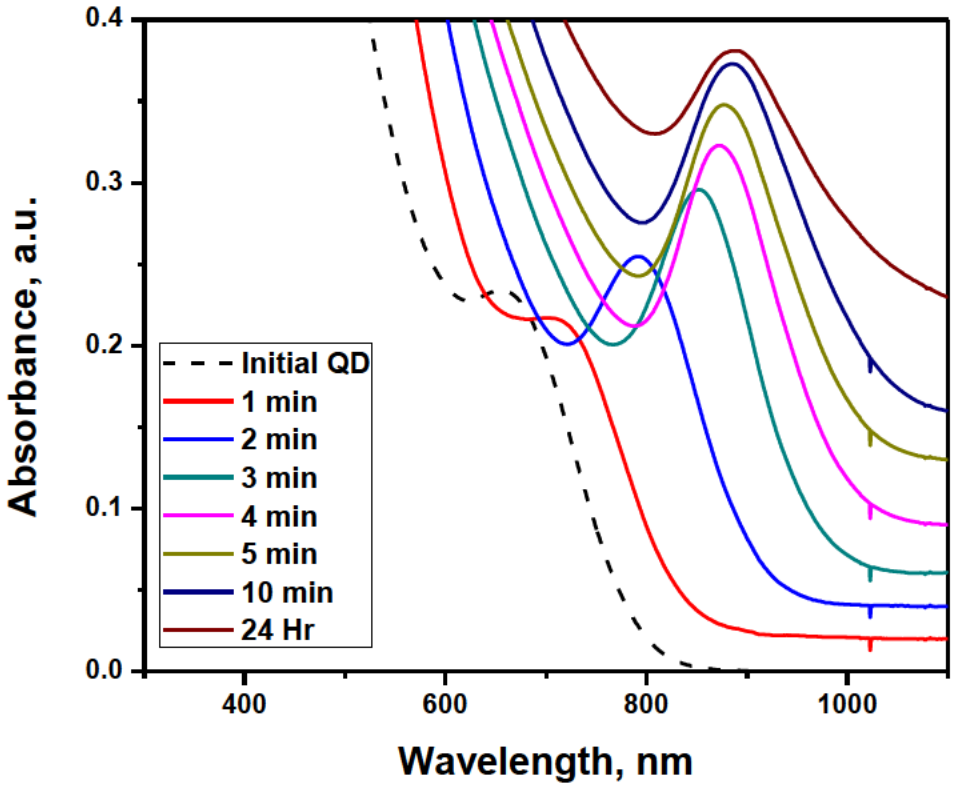

Figure S3-10. "Living" growth of PbS QDs in the presence of extra precursors (lead oleate and $(TMS)_2S$) and OA. In this case, 0.05 mmol of $(TMS)_2S$ was added along with 0.5 mmol of oleic acid and 0.2 mmol of lead oleate into the preformed PbS QD solutions. The temperature was maintained at 80 °C. It should to be noted that the addition of $(TMS)_2S$ only would lead to the precipitation of QDs.

Section S1. **Details on the activation energy calculation for PbS QD living growth**

From the fitted equations in Table S1

$$\lambda = \alpha . ln(time) + \beta \quad \text{(S1)}$$

If we consider the rate of increase in particle size (1st order derivative of the above equation) as a function of PbS monomer addition rate, then

$$f(r) = \alpha . \frac{1}{time} = K(T) \frac{F(Co)}{time} \quad \text{(S2)}$$

Where, f(r) is the rate of increase in particle size, K(T) is the temperature dependent function, and F(C_o) is a monomer concentration dependent term. If initial concentrations of QD particles and generated monomers are identical i.e. same amount of oleic acid added, F (C_o) can be considered as a constant. The plot of α versus inverse of temperature should follow an exponential relation.

Also, the monomer addition rate constant for Ostwald ripening is given as

$$k(t) = A . exp(\frac{-E_a}{RT}) \quad \text{(S3)}$$

k (t) is the rate constant of monomer addition, E_a is the activation energy, R is the universal gas constant and T is absolute temperature. From the fitted curve in Figure S11, the exponential term should be related to the exponential term in Equation 3. Thus, the activation energy for addition of monomers to existing QDs can be calculated to be 27.6 kJ/mol.

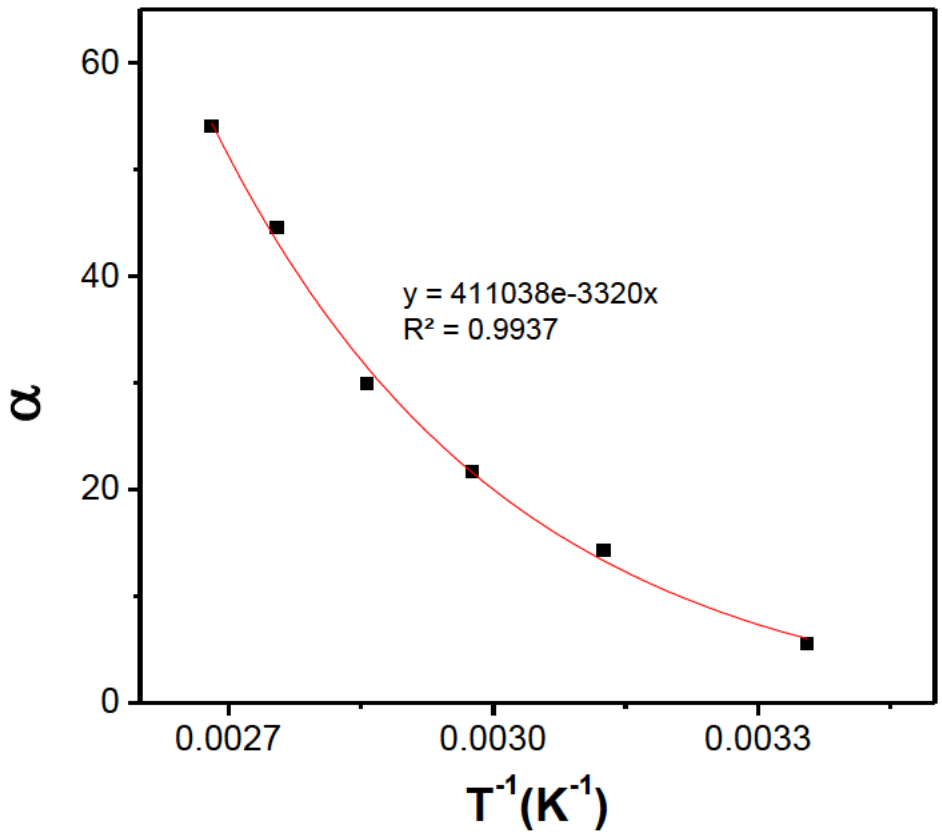

Figure S3-11. A plot of the reciprocal of growth temperature and the slope (α) of fitted logarithmic term in Table S1. α is the fitted natural logarithm term at various heating temperatures, and the solid line represents the exponential fit between α and T^{-1}.

Table S 3-1. Fitted logarithmic equations and R^2 for the time (t) dependent excitonic wavelength (λ) in **Figure 2b**.

Temperature (^oC)	Fitted to the equation: $\lambda=\alpha\ln(t)+\beta$	R^2
30 ^oC	λ =5.328 ln(t)+601.39	0.9874
45 ^oC	λ =14.843 ln(t)+588.11	0.9217
60 ^oC	λ =21.624 ln(t)+598.87	0.9735
80 ^oC	λ =29.666 ln(t)+607.02	0.9931
90 ^oC	λ =44.327 ln(t)+599.43	0.9998
100 ^oC	λ =54.047 ln(t)+599.14	0.9996

[1] M. A. Hines, G. D. Scholes, *Advanced Materials* 2003, 15, 1844-1849.

Chapter 4

Mechanistic insight into the nucleation and growth of oleic acid capped lead sulfide quantum dots

Aabhash Shrestha[1], Nigel A. Spooner[2,3], Shi Zhang Qiao[1]*, and Sheng Dai[1]*

[1] School of Chemical Engineering, The University of Adelaide, Adelaide, SA, 5005, Australia

[2] School of Physical Sciences, Physics, The University of Adelaide, Adelaide, SA, 5005, Australia

[3]DST Group, PO Box 1500, Edinburg, SA 5111, Australia

* Corresponding Authors

Email: s.dai@adelaide.edu.au , s.qiao@adelaide.edu.au

Submitted to the Journal **Physical Chemistry Chemical Physics** (Submission ID: CP-ART-03-2016-002119)

Statement of Authorship

Title of Paper	Mechanistic insight into the nucleation and growth of oleic acid capped lead sulfide quantum dots
Publication Status	☐ Published ☐ Accepted for Publication ☑ Submitted for Publication ☐ Unpublished and Unsubmitted work written in manuscript style
Publication Details	Aabhash Shrestha, Nigel A. Spooner, Shi Zhang Qiao*, and Sheng Dai*, **Mechanistic insight into the nucleation and growth of oleic acid capped lead sulfide quantum dots**, ***Physical Chemistry Chemical Physics*** (Submission ID: CP-ART-03-2016-002119)

Principal Author

Name of Principal Author (Candidate)	Aabhash Shrestha
Contribution to the Paper	Experimental design, performing of the experiments, analysis of the results and writing of the manuscript
Certification:	This paper reports on original research I conducted during the period of my Higher Degree by Research candidature and is not subject to any obligations or contractual agreements with a third party that would constrain its inclusion in this thesis. I am the primary author of this paper.
Signature	Date: 07/April/2016

Co-Author Contributions

By signing the Statement of Authorship, each author certifies that:

the candidate's stated contribution to the publication is accurate (as detailed above);

permission is granted for the candidate in include the publication in the thesis; and

the sum of all co-author contributions is equal to 100% less the candidate's stated contribution.

Name of Co-Author	Nigel A. Spooner
Contribution to the Paper	Assistance in fluorescence characterization and assessment.
Signature	Date: 05/04/2016.

Name of Co-Author	Shizhang Qiao
Contribution to the Paper	Assisting in the manuscript review and assessment.
Signature	Date: 08/April/2016

Name of Co-Author	Sheng Dai		
Contribution to the Paper	Supervising the development of the work, assisting in the data interpretation, manuscript review and assessment.		
Signature		Date	4/04/2016

Please cut and paste additional co-author panels here as required.

Abstract

The quantum dots (QDs) of lead sulfide (PbS) are attractive near-infrared (NIR) active materials and have promising applications in a wide variety of applications. Till date many efforts have been made on optimizing its synthesis; however, current mechanistic understanding involving the nucleation and growth of these QDs has not reached the same level as that for other QDs. In this study, we present a detailed understanding on synthesis mechanism of PbS QDs so as to provide guidance for future QDs synthesis. The synthesis of PbS QDs is largely independent of classical nucleation process and the hot-injection of precursors may not be necessary for the successful synthesis of PbS QDs. The synthesis is basically a growth dominated process and is controlled by the Ostwald ripening of PbS QDs. In addition, reaction temperature and ligand are the key parameters for controlling QD growth. Temperature provides energy for overcoming activation barrier of QD growth while the ligands enhance QD growth via altering the environment for QD growth. Following the mechanism governing the synthesis of PbS QDs, we demonstrate that the size tuning of PbS QDs in ultra-small (< 2 nm) can be achieved, which has been typically challenging following the hot injection synthesis.

Keywords: Lead Sulfide, Quantum Dots, Nucleation, Crystal Growth, Oleic Acid

TOC Figure

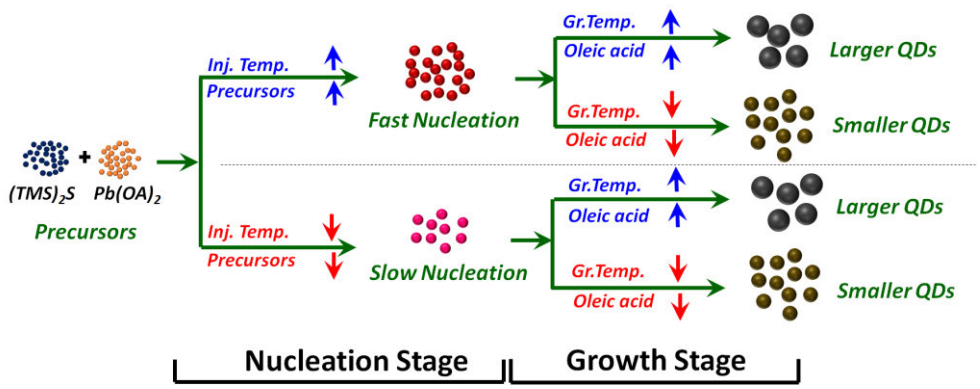

4.1 Introduction

The size dependent optoelectronic properties of semiconducting quantum dots (QDs) have attracted a lot of attention due to their potential applications in solar cells,[1, 2] light emitting diodes (LEDs),[3] Forster resonance energy transfer (FRET),[4] biolabeling,[5] sensors[4] and many others. Over the past decades, much effort has been focused on the QDs with their bandgaps positioned to give emissions in visible region. Recently, narrow bandgap near infrared (NIR) active materials are receiving much interest due to their potential in solar cells with extendable NIR absorption, bio-labels for deep tissue imaging and other optoelectronic applications.[6] Lead sulphide (PbS) QDs are one of the attractive NIR active materials associated with their ability for multiple electron generation,[7] large exciton Bohr radii[8] and constantly providing the highest solar conversion efficiencies (~ 8 %) for its QD based devices.[1, 9]

One of the key criteria for the characterization of material properties and the development of potential applications is the controlled synthesis of QDs with desired sizes and distributions. Until now, numerous approaches have been developed for the synthesis of lead sulphide (PbS) QDs such as using colloidal synthesis in organic[10-14] or aqueous media;[15-17] chemical growth inside polymers[18] or glass;[19] physical methods such as using milli-second pulsed laser[20] and many more.[21] Among them, the colloidal growth in organic solvents based on 'hot injection' so far has been the most successful and reliable approach for producing high quality PbS QDs.

In a typical 'hot injection' synthesis of nano-crystals (NCs), the molecular precursors at the room temperature (e.g. hexamethyldisilathiane in octadecene for PbS QDs) are swiftly injected into a hot precursor solution (e.g. lead oleate in octadecene). The spontaneous

reaction between the precursors rapidly increases the PbS monomer concentration in solution i.e. it becomes supersaturated. This initiates the nucleation of particles. The formation of monodisperse NCs in a solution is generally thought to occur via a nucleation event (commonly referred as 'burst nucleation') followed by the subsequent growth of these nuclei by the addition of more monomers.[22, 23] The control and separation of nucleation and growth stage is thought to be the essential criteria for successful synthesis of NCs using the hot injection approach.[23, 24]

Understanding the mechanism of particle nucleation and growth is crucial for controllable size tuning using this bottom-up synthesis method. To date, many efforts have been reported on optimizing the synthesis of PbS QDs such as varying chemical precursors,[11, 13, 16] different stabilizing ligands,[11, 13, 16, 25] diverse synthesis medium[16, 17, 26] and miscellaneous methodologies.[11, 12, 20, 26] Although the synthesis protocols for the preparation of these quantum dots are well documented, the mechanistic understanding involving the nucleation and growth of PbS QDs has not reached the same level as that for other QDs. Generally, there are two major approaches on tuning the particle sizes of PbS QDs: manipulating synthetic precursor ratios and controlling synthesis temperatures. However, the specific influence of these parameters on the nucleation and growth of PbS QDs is still not elusive.

Herein, we systematically investigated the nucleation and growth of oleic acid capped PbS QDs based on the 'hot injection' synthesis.[11] Our attempt is to elucidate the key parameters (temperature, precursor ratios and ligand) influencing the synthesis of QDs and provide a more in-depth outlook applicable towards the optimization of synthesis. We, in detail, investigated the role of nucleation and how the synthesis parameters such as

temperature, precursor ratio and ligand influence the final QD particle sizes. Our results show that this synthesis a growth-dominated process, which is largely independent of classical nucleation. Temperature and ligand are key players for size tuning of PbS QDs. Finally, following the guidance of proposed synthesis mechanism, the ultra-small (< 2 nm) PbS QDs were synthesized and their sizes could be controllably tuned. Synthesis of such ultra-small PbS QDs (< 2 nm) has been typically challenging [27] and size tuning in such regime has not been realized till date. The size tuning can provide additional novel application utilizing these QDs such as utilization of biological window of 700-900 nm.

4.2 Experimental

4.2.1 Materials

Lead (II) oxide (PbO, 99.99 %), hexamethyldisilathiane $(SiMe_3)_2S$, oleic acid (OA, 90 % technical grade), 1-octadecene (ODE, 99.99%), acetone, hexane and heptane were procured from Sigma- Aldrich. All chemicals were used as received.

4.2.2 Synthesis of PbS QDs

PbS QDs were synthesized based on a previously described method.[11] For the synthesis of typical PbS QDs at the precursor ratio of OA:Pb:S at 4:2:1, 178.6 mg (0.8 mmol) of PbO, 0.634 mL (1.6 mmol) oleic acid (OA) and 8 mL 1-octadecene were charged to a 100 mL schlenk flask under argon protection and heated to 150 ℃ for 1 hour to obtain a clear yellowish lead oleate solution. The obtained lead oleate solution was protected using argon and immersed into a pre-heated oil-bath set at different designated injection temperatures. In another schlenk flask, 84 µl (0.4 mmol) $(SiMe_3)_2S$ was charged to 4 ml of degassed ODE at room temperature under argon. Once the temperature of the lead oleate solution

was stabilized, the $(SiMe_3)_2S$ solution was quickly injected using argon washed syringe. The temperature of the reacting solution was monitored using a thermocouple. The reaction conditions were adjusted accordingly for various precursor ratios and temperatures. 200 µl aliquot were drawn from the reaction vessel at various time intervals to monitor particle growth profiles. The final QDs were precipitated with acetone, centrifuged (~10,000 rpm) and diluted in 3 ml hexane for further characterization.

4.2.3 Synthesis of Ultra Small PbS QDs

For the synthesis of ultra-small PbS QDs (< 2 nm), the synthesis protocol was slightly modified. The precursor ratio (OA:Pb:S) was maintained at 4:2:1 while the injection temperature was kept at 70 ^{o}C. Immediately following the injection of the sulphur precursor (~ 5 – 10 s), cold hexane or heptane at -20 ^{o}C was injected into the reaction solution and quickly placed into an ice bath maintained at ~ 5 ^{o}C. The particle growth was allowed to occur for ~ 30 min to focus QDs. The size tuning of the PbS QDs in the ultra-small regime was performed by increasing the growth temperature to different temperatures followed by size focusing for ~ 15 min.

4.2.4 Absorbance and Fluorescence Emission

The absorption measurements were performed in a Shimadzu 1601 UV-vis. spectrometer. The fluorescence measurements were carried out in Princeton Instruments spectrofluorimeter, utilising excitation from a tungsten halogen lamp and Acton 2150 spectrograph, and emission spectra analysed and detected using an Acton SP2300i spectrograph and a Princeton Instruments PIXIS 256 spectrographic CCD detector. The excitation wavelength during the fluorescence measurements was maintained as 400 nm.

4.3 Results and discussion

4.3.1 Role of Nucleation

To study the influence of nucleation, we first synthesized PbS QDs at various injection and growth temperatures (**Table S4-1**). Here, the temperature of hot lead precursor solution is referred as 'injection temperature'. After the injection of room temperature sulphur precursor, the temperature of reaction solution reduces and is typically maintained at this temperature for the duration of synthesis, which is referred as 'growth temperature'. Since the growth temperature is attained immediately after precursor injection (i.e. very short mixing period), we refer this growth temperature to represent the overall synthesis temperature unless stated otherwise. Timed aliquots were drawn from the reaction mixture to monitor particle growth, and QDs growth profiles for the synthesis were monitored using absorption spectroscopy (**Figure S4-1**). The wavelengths of the excitonic peak increase with time and gradually saturate as reaction time prolongs. **Figure S4-2** shows the photoluminescence (PL) spectra for the particles synthesized at 90 ^{o}C injection and 70 ^{o}C growth temperatures. The red-shifts in both the absorption and photoluminescence spectra indicate the increment of QDs size with reaction time. The high resolution transmission electron microscopy (HRTEM) image also shows that the as-synthesized QDs are highly crystalline (**Figure S4-3**).

During the experiment, we are not able to track the exact size of nuclei at various synthesis temperatures due to the quick nucleation process. However, distinct nuclei with absorbance from 480 to 550 nm are consistently observed for the first aliquot samples (**Figure S4-4**). The initial nuclei have rather broad distribution and the calculated size of these nuclei would be approximately 1.4 - 1.5 nm. The particle diameters and concentrations can be

calculated from the absorption spectra using the previously described method.[14, 28] Considering the bulk lattice parameter of PbS to be ~ 0.69 nm,[28] these initial nuclei would constitute only a few structural units (~ 8-10 units) per particle. Such small particle sizes as nuclei are not uncommon and are routinely qualified as nucleation products.[29, 30] A broader size distributions during the nucleation period is reasonable and is commonly observed during NC synthesis.[23] These nucleated particles eventually grow and focus to form larger particles in solution.

From **Figure 4-1(a)**, the initial nuclei concentration is much higher for the high temperature reaction indicating that high temperature accelerates the nucleation of particles. At the same time, the higher temperature also gives rise to the increase in final QDs sizes with a low final overall QDs concentration (**Figure 4-1(a) and 4-1(b)**). Theoretically, faster nucleation at high temperature should result in a large number of smaller nuclei with smaller particle size[23] (due to less monomers available to feed the nucleated particles). These results contradict with the classical hot injection synthesis indicating a different mechanism on operation.[23]

The influence of temperature on final QDs size is rather complicated due to the temperature dependence of monomer generation, nucleation and growth. The monomer generation is related to the precursor conversion kinetics and induces the supersaturation in solution. On the other hand, the nucleation and growth rates both increase with the increase in temperature and supersaturation. The nucleation rate is much sensitive to the level of supersaturation and even a small change in supersaturation drastically influences the nucleation. Recent studies report that the nucleation of insoluble salts such as PbS nanocrystals are controlled only by the precursor conversion kinetics, i.e. monomer

generation controls the nucleation.[29] The bistrimethylsilyl mediated formation of nanocrystals are generally found to be endothermic, i.e. precursor conversion rate increases with temperature.[31] During the synthesis of PbS QDs, the sulphur precursor is also a bistrimethylsilyl mediated compound i.e. bistrimethylsilylsulfide $(SiMe_3)_2S$.[11] Thus, the higher nucleation at high temperature is consistent with the higher precursor reaction at high temperatures.

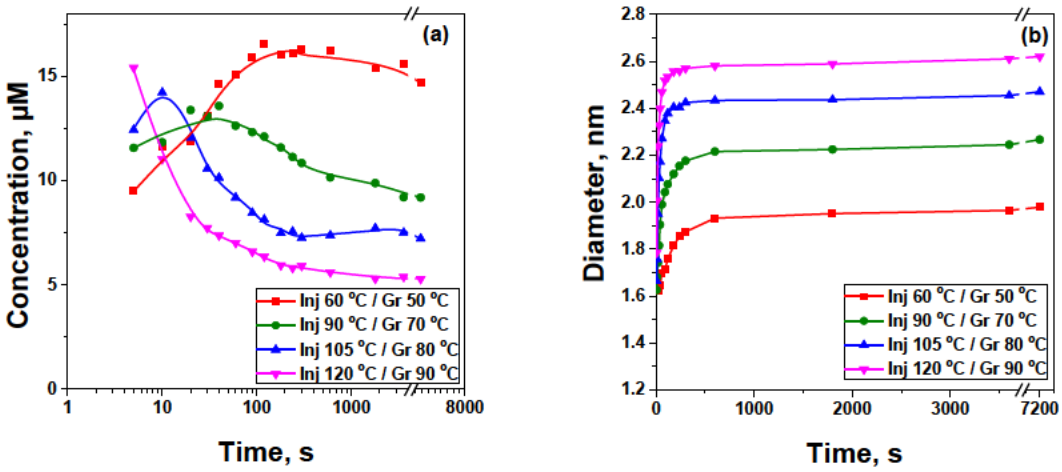

Figure 4-1. Influence of different injection and growth temperatures on the sizes and concentrations of PbS QDs. Temporal evolution of (a) concentrations of PbS QDs (b) diameters of PbS QDs.

In order to understand the influence of temperature on nucleation and final particle size, we synthesized PbS QDs at various injection temperatures while deliberately maintaining the same growth temperature. The temperature attained after injection of sulphur precursor was maintained for a certain period (~10 sec) before bringing it to same growth temperature. The injection temperatures were varied as 105 °C, 90 °C, 60 °C and 30 °C, while the growth temperature was maintained at 80 °C. The chosen reaction period of ~10 s immediately following the precursor injection allows the nucleation to occur at different

temperatures and hence monitor its effect on final particle sizes. Interestingly, the final particle sizes after saturation are similar for all these reaction conditions (**Figure 4-2 and S4-5**) i.e. varying the nucleation by changing the reaction temperature has negligible influence on the equilibrium size of particles.

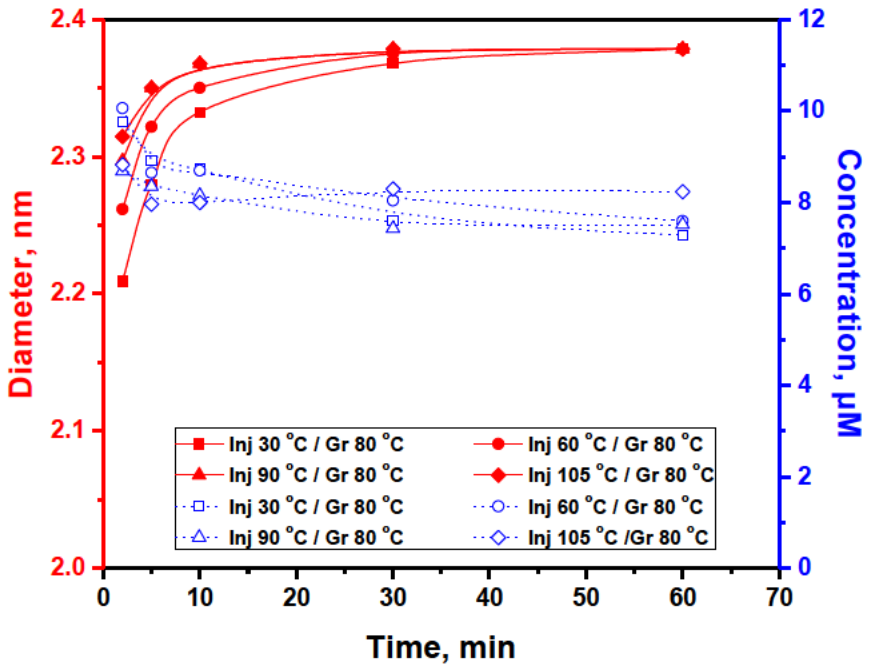

Figure 4-2. Diameter and concentration versus time plot for PbS QDs growth at various injection temperatures with the same growth temperature (80 °C). The filled symbols refer to the diameter of PbS QDs while the open symbols are the concentration of the QDs.

To further elucidate the influence of nucleation on final particle sizes, we synthesized PbS QDs at various precursor ratios while keeping the same injection and growth temperatures. Tuning the precursor reactivity by varying the feed precursor ratio can significantly alter the QDs nucleation while keeping the same injection and growth temperature eliminates the temperature influence. During the synthesis of PbS QDs, the sulphur precursor is the

limiting reactant and undergoes near completion during chemical reaction.[11] We initially fixed the concentration of sulphur precursor (limiting reactant) and varied the concentration of lead precursor to tune the reaction rates so as to generate an equivalent amount of lead sulphide while increasing only the reaction rate. The formation of PbS QDs from the precursor/monomers can be estimated from the absorbance at 400 nm, where the QDs molar extinction coefficient scales with nanocrystal volume.[28] Similar conversions of precursors to PbS QDs are observed on fixing the sulphur precursor concentration (**Figure S4-6(a) and S4-6(b)**). **Figure 4-3(a) and 4-3(b)** shows the temporal evolution of particle diameter and concentration at various feed lead precursor concentrations. QDs nucleation is much faster at the higher Pb:S ratios due to its faster reaction rate, which is similar to the temperature effect on nucleation. In addition, the final equilibrium sizes of the particles are similar and the final concentrations of the particles are also equivalent. That means varying the nucleation by changing the precursor ratios also does not significantly influence the final particle sizes.

Similarly, we also investigated the influence of sulphur precursors on nucleation and final particle size while keeping the other parameters constant. **Figure 4-3(c) and 4-3(d)** shows the temporal evolution of particle diameter and concentration at various sulphur precursor ratios while keeping other reaction parameters constant. Although more nuclei are formed, varying the sulphur precursor ratios also does not significantly alter the final particle sizes. The higher feed sulphur precursor however produces higher concentration of final particles, i.e. more QDs are formed as sulphur precursor increases. It has to be noted that the lead precursors should always be in excess amount as compared to sulphur precursors to avoid particle agglomeration. The higher particle concentration with increasing feed

sulphur precursor is due to the complete consumption of all sulphur precursors during the course of QDs synthesis. Clearly, the above observation suggests that the nucleation conditions (i.e. nucleation temperature and precursor ratios) cannot significantly influence the final size of PbS QDs.

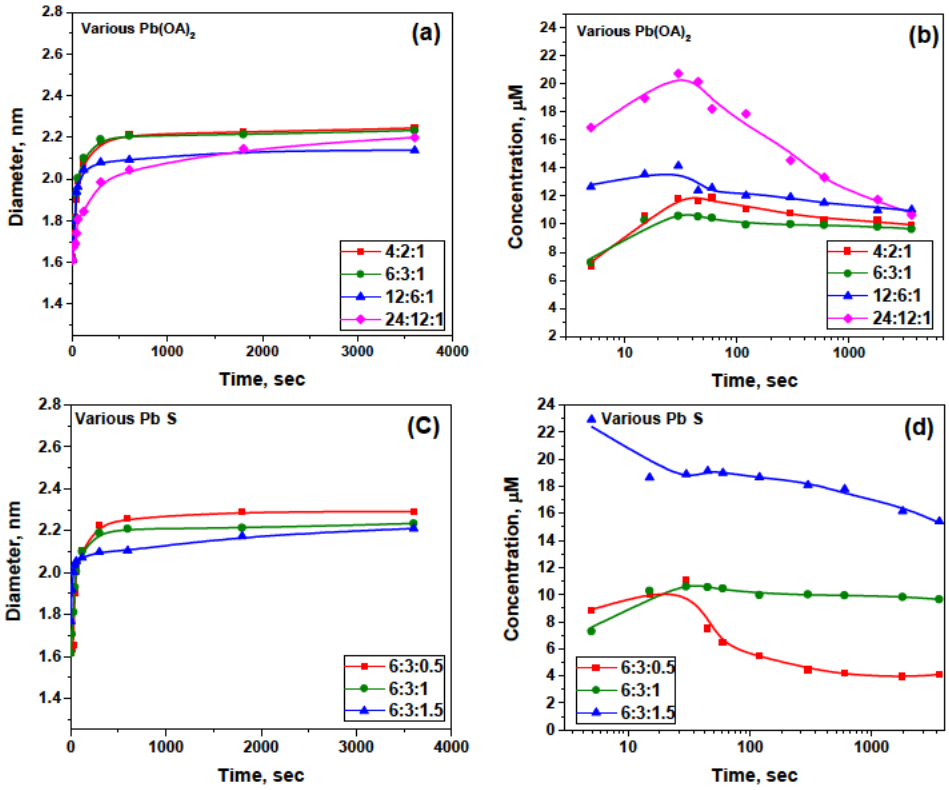

Figure 4-3. Precursor (OA:Pb:S) influence during the synthesis of PbS QDs. Lead precursor $Pb(OA)_2$ influence on (a) the diameter of PbS QDs and (b) the concentration of PbS QDs. Sulphur precursor influence on (c) the diameter of PbS QDs and (d) the concentration of PbS QDs. The injection temperature was maintained at 90 °C and growth temperature was 70 °C for all reactions.

4.3.2 Understanding the particle growth kinetics

From above, it can be concluded that the synthesis of PbS QDs does not follow the typical characteristics of hot injection synthesis where the nucleation stage plays an important role in controlling the final particle size. These observations are in contrast with the commonly applied models of nucleation and growth for the hot-injection based synthesis.[31, 32]

Interestingly, the growth profile of PbS QDs shows interesting pertinence to temperature with higher temperature producing larger sized crystals. Such growths of particles that are largely independent of classical nucleation processes are generally controlled by the non-molecular process such as Ostwald ripening or orientation attachment, which is enhanced at higher temperatures.[31]

The Ostwald ripening growth for a particle is generally described by the Lifshitz–Slyozov–Wagner (LSW) model [33, 34]

$$(d - d_o) = k(t - t_o)^{1/n} \qquad (1)$$

where d_o is the diameter of the particle at time t_o, d is the diameter at time t, k is a temperature dependent material constant appropriate to the value of the exponent 'n'. The value of the exponent 'n' can vary from 2 to 4 which depends on how the crystal growth is controlled.[33] When the exponent n = 2, the crystal growth is controlled by the diffusion of monomers at the solution particle boundary. When n = 3, the growth is controlled by the diffusion of monomers in the solution and when n = 4, the growth is controlled by dissolution of the smaller particle at the solution-particle interface.

The orientation attachment growth for a particle is expressed as[33]

$$d = \frac{d_o(\sqrt[3]{2}kt+1)}{(kt+1)} \qquad (2)$$

d_o is the diameter of the particle at time t_o, d is the diameter at time t, k is a temperature dependent material constant.

To understand how the PbS QDs crystal growth is controlled, the crystal growth kinetics was fitted to the above equations with do and k as the fitting parameters. The least square fitting of these equations to the measured particle growth curve shows that the best fit

occurred for Ostwald ripening model at a value of n = 3 **(Table S4-2 to S4-5)**, i.e. the particle growth is likely to be controlled by the diffusion of monomers in solution. Further, Arrhenius plot of various kinetic constant, k can be used to determine the activation energy for the particle growth. The activation energy of 29.6±4.4 kJ/mol can be obtained from Arrhenius equation using the rate constants 'k' obtained by fitting the growth curve to standard Ostwald ripening model. This value for activation energy matches well to our previously calculated activation energy (~27 kJ/mol) for the living growth of PbS QDs.[35]

4.3.3 Influence of ligand on controlling QDs growth

Since the synthesis of PbS QDs is largely independent of nucleation conditions, the synthesis is a growth-dominated process, and the growth of PbS QDs follows the solution diffusion controlled Ostwald ripening mechanism. It is important to understand the influence of various synthesis parameters on the Ostwald ripening of PbS QDs and the final particle size. Our previous investigation [35] along with others [36] suggests a strong influence of ligand (oleic acid) concentration on the final size of PbS QDs, where increasing the oleic acid content results in the increase of particle size on heating.

The increase in particle size with the increment of ligand concentration has been previously linked to a reduction in precursor reactivity during nucleation or a suppression of nucleation due to an increase in precursor solubility.[37, 38] The initial nuclei concentration (after ~5 s) for higher feed ratio of oleic acid (OA:Pb:S of 12:3:1) is much higher than that of lower feed ratio of oleic acid (i.e. OA:Pb:S of 6:3:1), indicating that the increase in oleic acid concentration cannot suppress nucleation. In fact, the higher nucleation with increasing oleic acid concentration possibly indicates higher precursor reactivity. Recently, rapid reduction of tris(trimethylsilyl)phoshphine ($P(SiMe_3)_3$) (similar

to $(SiMe_3)_2S$) in the presence of carboxylic acid was found as a competing reaction pathway during the synthesis of InP NCs.[39] Hence, the observed higher nucleation at increasing free oleic acid concentrations could be due to the faster precursor conversion in presence of excess oleic acid.

Figure 4-4(a) and 4-4(b) shows the timed evolution of particle diameter and concentration at various feed ratios of oleic acid. The presence of a small excess of oleic acid greatly enhances the particle growth while producing a lower concentration of final particles. Beyond certain limit of excess oleic acid, the particle size saturates to a constant value. Interesting phenomenon is observed when the OA:Pb is fixed at 12:6 (stoichiometric OA:Pb ratio as compared to 12:3), where a negligible impact on the final particle size and concentration occurs even though an equivalent amount of oleic acid is used in the synthesis. Increasing the stoichiometric OA:Pb forms a cluster of particles of various sizes before focusing to the final size (**Figure S4-7(a) to S4-7(d)**). The final particle sizes are much broader and the excitonic peaks are less distinct. However, these nucleation clusters disappears immediately for higher feed oleic acid ratio (i.e. OA:Pb > 2:1) (**Figure S4-7(e) and S4-7(f)**) and larger sized particles are formed with distinct excitonic peaks and prolonged size focusing.

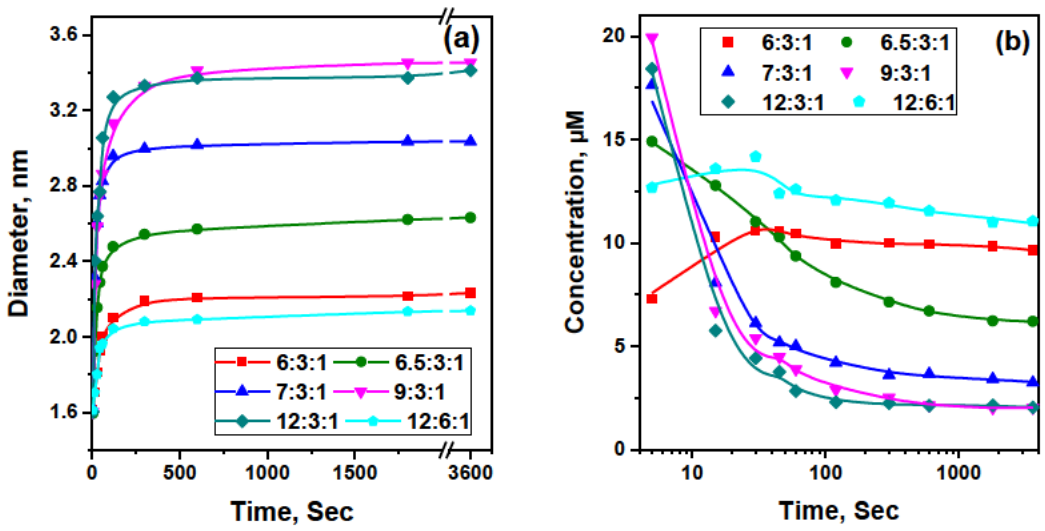

Figure 4-4. Influence of ligand (oleic acid) concentration on the (a) diameter and (b) concentration of PbS QDs. The injection temperature was maintained as 90 °C and growth temperature was 70 °C for all conditions.

We can understand the difference in growth characteristics between stoichiometric OA:Pb (2:1) and excess free oleic acid (i.e. OA:Pb > 2:1) by considering the oleic acid interaction on PbS NCs surface and its influence on NCs solubility. Previous reports indicate a strong but yet reversible binding between the oleic acid and PbS NCs surface i.e. the oleic acid interaction on nanocrystal surface occurs through adsorption and desorption process.[36, 40] The solubility of a particle of radius (r), $[M]_r$ on the other hand is related to the equilibrium monomer solubility $[M]_o$ as[38]

$$[M]_r = [M]_o \exp\left(\frac{2\gamma v_m}{rRT}\right) \qquad (3)$$

Here, γ is surface tension in QDs, v_m is molar volume of PbS QDs, r is radius of QDs at a given time, T is absolute temperature and R is gas constant. The solubility of particles increases exponentially with the decrease in size and even a small variation in equilibrium

monomer solubility has a more profound effect in smaller sized particles (**Figure S4-8**). Oleic acid can influence the NCs solubility as the equilibrium monomer solubility is altered in the presence of excess oleic acid. The equilibrium monomer solubility can be expressed in terms of monomer adsorption and desorption as [38]

$$[\boldsymbol{M}]_{\mathbf{0}} = \frac{\boldsymbol{k_d^{\infty}}}{\boldsymbol{k_g^{\infty}}} \qquad \textbf{(4)}$$

where k_d^{∞} and k_g^{∞} are monomer desorption and adsorption rate constants respectively. It has been reported that increasing the oleic acid ligand coverage beyond a certain threshold favours its desorption from QDs surface.[41] Desorption of ligand generally occurs via removal of surface Pb atoms and lead towards the disintegration (or shrinkage) of QDs in the presence of excess oleic acid.[35, 36, 42] Increasing the feed oleic acid ratio should thus promote desorption of monomers from the existing QDs and the monomer desorption rate constant increases. This increases the equilibrium monomer solubility in solution. The perturbation of equilibrium monomer solubility with increasing ligand concentration further enhances the dissolution of smaller nucleated particles, which initiates the Ostwald ripening of particles.

In the presence of excess lead precursor (i.e. stoichiometric OA:Pb), the equilibrium shifts towards less desorption of monomers is reduced leading to a decrease in equilibrium monomer solubility. This means the increase in lead precursor slows the dissolution of nucleated particles and delays the onset of Ostwald ripening. Our previous study has also confirmed that the presence of lead oleate decreases the PbS QDs dissolution.[35] In such a case, Ostwald ripening occurs much slower and thus forming a cluster of particles before focusing to a larger size.

4.3.4 Synthesis and size tuning of ultra-small PbS QDs

The detailed mechanistic understanding for the synthesis of PbS QDs allows us to extend the size tunability of these QDs in the ultra-small regime which is typically challenging till date. For the synthesis of ultra-small PbS QDs, we made some modification to the typical synthesis approach. Typically, the nucleation was allowed to occur at temperature of 70 - 90 oC for ~ 5-10 s, followed by the quick injection of cold hexane or heptane (-20 ^{o}C) to quench QD growth. The growth of QDs was then allowed to occur at a relatively low temperature (0 to 5 ^{o}C). **Figure 4-5 and S4-9** shows the typical illustration for the synthesis of ultra-small PbS QDs.

The reaction at a moderate temperature (70 -90 ^{o}C) allows the quicker precursor conversion and nucleation of particles as compared to a reaction at low temperatures (0 to 5 ^{o}C). The quick injection (~ 5 s) of cold hexane on the other hand abruptly terminates the nucleation and allows the growth to occur at lower temperatures. The dilution of reacting medium by hexane (non-coordinating solvent) further reduces the supersaturation below the nucleation threshold and partially aids in maintaining the solubility of reacting medium (considering the high freezing point of octadecene at ~15 ^{o}C). Since the QD growth is quenched immediately after the sulphur precursor injection, a portion of the precursor remains unreacted. The incomplete conversion of the sulphur precursor is evident from the presence of typical pungent smell of $(SiMe_3)_2S$. The slow conversion of remaining precursor at low temperature can also act as a source for QDs growth and allow the focusing of the nucleated particles to form ultra-small PbS QDs.

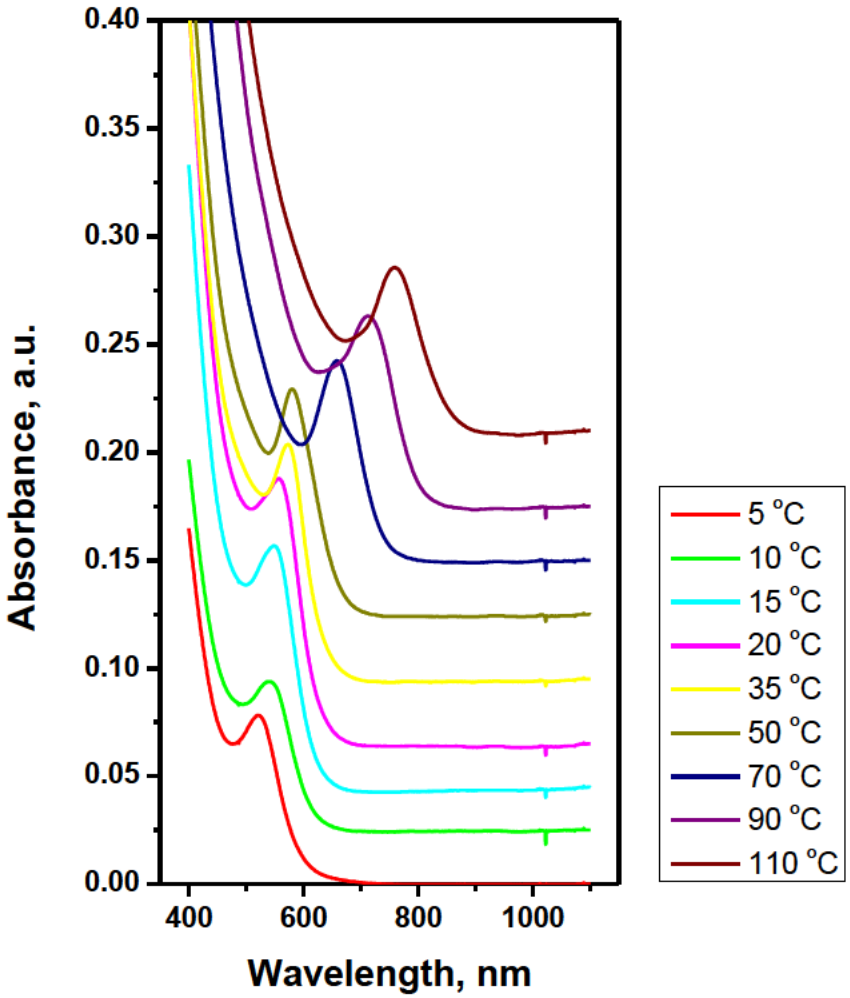

Figure 4-5. Size tuning of ultra-small PbS QDs by varying the growth temperature from 5 °C to 110 °C

The temperature dependent QDs growth further plays an instrumental role in the size tuning of these QDs in the ultra-small regime. The size of these QDs can be simply tuned by slowly increasing the growth temperature much similar to the heat-up synthesis. As the temperature increases, the precursor conversion as well as growth rate increases. The faster growth rate at higher temperature further consumes more monomers and allows the focusing of size distribution. Once all generated monomers are consumed, the growth

proceeded by the consumption of smaller particles followed a typical Ostwald ripening growth. Typically, the size of QDs obtained after heat-up synthesis are smaller than the conventional “hot-injection” synthesis. During the hot-injection synthesis, a large portion of small nucleated particles are dissolved to feed the growth of stable nuclei, while in the heat-up synthesis, only a small fraction of these particles (only below the mean particle size) dissolves away to feed the particle growth. Thus, the monomer starving condition in the heat-up synthesis resultes in smaller sized particles

4.4 Conclusions

In conclusion, we investigated the nucleation and growth mechanism of oleic acid capped PbS QDs in detail, and provided the guidance for future QDs synthesis. Although the hot-injection synthesis is typically employed for the synthesis of PbS QDs, the synthesis is found to be largely independent of classical nucleation process. The hot-injection of precursors may not be necessary for the successful synthesis of PbS QDs. The synthesis course is a growth dominated process and controlled by the Ostwald ripening of PbS QDs. Increasing the temperature enhances the QDs growth and the activation barrier for the growth of PbS QDs is calculated to be 29 kJ/mol. The Ostwald ripening can be activated in presence of free oleic acid while bound oleic acid to lead precursor inhibits the Ostwald ripening. Even a small excess of free oleic acid is enough to trigger the Ostwald ripening growth of PbS QDs. Following the mechanism influencing the size of PbS QDs, the size tuning in the ultra-small (<2 nm) regime is also achieved which provides more leverage in the application of these materials for various applications.

Acknowledgements

This work was financially supported by the Australian Research Council Discovery Projects DP110102877 and DP140104062.

References

[1] A. H. Ip, S. M. Thon, S. Hoogland, O. Voznyy, D. Zhitomirsky, R. Debnath, L. Levina, L. R. Rollny, G. H. Carey, A. Fischer, K. W. Kemp, I. J. Kramer, Z. Ning, A. J. Labelle, K. W. Chou, A. Amassian, E. H. Sargent, *Nat. Nanotechnol.* 2012, 7, 577.

[2] S. A. McDonald, G. Konstantatos, S. Zhang, P. W. Cyr, E. J. D. Klem, L. Levina, E. H. Sargent, *Nat. Mater.* 2005, 4, 138.

[3] P. O. Anikeeva, J. E. Halpert, M. G. Bawendi, V. Bulović, *Nano Lett.* 2009, 9, 2532.

[4] I. L. Medintz, A. R. Clapp, H. Mattoussi, E. R. Goldman, B. Fisher, J. M. Mauro, *Nat. Mater.* 2003, 2, 630.

[5] O. Chen, J. Zhao, V. P. Chauhan, J. Cui, C. Wong, D. K. Harris, H. Wei, H.-S. Han, D. Fukumura, R. K. Jain, M. G. Bawendi, *Nat. Mater.* 2013, 12, 445.

[6] (a) E. H. Sargent, *Adv. Mater.* 2005, 17, 515; (b) F. C. J. M. van Veggel, *Chem. Mater.* 2013, 26, 111.

[7] R. J. Ellingson, M. C. Beard, J. C. Johnson, P. Yu, O. I. Micic, A. J. Nozik, A. Shabaev, A. L. Efros, *Nano Lett.* 2005, 5, 865.

[8] J. E. Murphy, M. C. Beard, A. G. Norman, S. P. Ahrenkiel, J. C. Johnson, P. Yu, O. I. Mićić, R. J. Ellingson, A. J. Nozik, *J. Am. Chem. Soc.* 2006, 128, 3241.

[9] C.-H. M. Chuang, P. R. Brown, V. Bulović, M. G. Bawendi, *Nat. Mater.* 2014, 13, 796.

[10] J. Akhtar, M. Azad Malik, P. O'Brien, K. G. U. Wijayantha, R. Dharmadasa, S. J. O. Hardman, D. M. Graham, B. F. Spencer, S. K. Stubbs, W. R. Flavell, D. J. Binks, F. Sirotti, M. El Kazzi, M. Silly, *J. Mater. Chem.* 2010, 20, 2336.

[11] M. A. Hines, G. D. Scholes, *Adv. Mater.* 2003, 15, 1844.

[12] T.-Y. Liu, M. Li, J. Ouyang, M. B. Zaman, R. Wang, X. Wu, C.-S. Yeh, Q. Lin, B. Yang, K. Yu, *J. Phys. Chem. C* 2009, 113, 2301.

[13] L. Cademartiri, J. Bertolotti, R. Sapienza, D. S. Wiersma, G. von Freymann, G. A. Ozin, *J. Phys. Chem. B* 2005, 110, 671.

[14] J. Zhang, J. Gao, E. M. Miller, J. M. Luther, M. C. Beard, *ACS Nano* 2013, 8, 614.

[15] D. Berhanu, K. Govender, D. Smyth-Boyle, M. Archbold, D. P. Halliday, P. O'Brien, *Chem. Commun.* 2006, 4709.

[16] L. Bakueva, I. Gorelikov, S. Musikhin, X. S. Zhao, E. H. Sargent, E. Kumacheva, *Adv. Mater.* 2004, 16, 926.

[17] D. Deng, W. Zhang, X. Chen, F. Liu, J. Zhang, Y. Gu, J. Hong, *Eur. J. Inorg. Chem.* 2009, 2009, 3440.

[18] A. Stavrinadis, R. Beal, J. M. Smith, H. E. Assender, A. A. R. Watt, *Adv. Mater.*2008, 20, 3105.

[19] K. Xu, J. Heo, *J. Non-Cryst. Solids* 2014, 387, 76.

[20] J. Yang, T. Ling, W.-T. Wu, H. Liu, M.-R. Gao, C. Ling, L. Li, X.-W. Du, *Nat. Commun.* 2013, 4, 1695.

[21] (a) K. Biswas, C. N. R. Rao, Chemistry – A European Journal 2007, 13, 6123; C. Zhang, Z. Kang, E. Shen, E. Wang, L. Gao, F. Luo, C. Tian, C. Wang, Y. Lan, J. Li, X. Cao, *J. Phys. Chem. B* 2005, 110, 184; (b) T. Ding, J.-R. Zhang, S. Long, J.-J. Zhu, *Microelectron. Eng.* 2003, 66, 46.

[22] J. Baumgartner, A. Dey, P. H. H. Bomans, C. Le Coadou, P. Fratzl, N. A. J. M. Sommerdijk, D. Faivre, *Nat. Mater.* 2013, 12, 310.

[23] C. de Mello Donegá, P. Liljeroth, D. Vanmaekelbergh, *Small* 2005, 1, 1152.

[24] S. G. Kwon, T. Hyeon, *Small* 2011, 7, 2685.

[25] (a) K. A. Abel, J. Shan, J.-C. Boyer, F. Harris, F. C. J. M. van Veggel, Chem. Mater. 2008, 20, 3794; (b) A. H. Khan, U. Thupakula, A. Dalui, S. Maji, A. Debangshi, S. Acharya, *J. Phys. Chem. C* 2013, 117, 7934.

[26] D. Deng, J. Cao, J. Xia, Z. Qian, Y. Gu, Z. Gu, W. J. Akers, *Eur. J. Inorg. Chem.* 2011, 2011, 2422.

[27] A. Antanovich, A. Prudnikau, M. Artemyev, *J. Phys. Chem. C* 2014, 118, 21104.

[28] I. Moreels, K. Lambert, D. Smeets, D. De Muynck, T. Nollet, J. C. Martins, F. Vanhaecke, A. Vantomme, C. Delerue, G. Allan, Z. Hens, *ACS Nano* 2009, 3, 3023.

[29] R. Xie, Z. Li, X. Peng, *J. Am. Chem. Soc.* 2009, 131, 15457.

[30] R. Xie, X. Peng, *Angew. Chem. Int. Ed.* 2008, 47, 7677.

[31] J. Baek, P. M. Allen, M. G. Bawendi, K. F. Jensen, *Angew. Chem. Int. Ed.* 2011, 50, 627.

[32] S. Abe, R. K. Čapek, B. De Geyter, Z. Hens, *ACS Nano* 2011, 6, 42.

[33] F. Huang, H. Zhang, J. F. Banfield, *Nano Lett.* 2003, 3, 373.

[34] H. O. K. Kirchner, MT 1971, 2, 2861; A. L. Brazeau, N. D. Jones, *J. Phys. Chem. C* 2009, 113, 20246.

[35] A. Shrestha, B. Jin, T. W. Kee, S. Z. Qiao, S. Dai, *ChemNanoMat* 2016, 2, 49.

[36] Q. Dai, Y. Zhang, Y. Wang, Y. Wang, B. Zou, W. W. Yu, M. Z. Hu, *J. Phys. Chem. C* 2010, 114, 16160.

[37] (a) J. van Embden, P. Mulvaney, *Langmuir* 2005, 21, 10226; (b) E. V. Shevchenko, D. V. Talapin, H. Schnablegger, A. Kornowski, Ö. Festin, P. Svedlindh, M. Haase, H. Weller, *J. Am. Chem. Soc.* 2003, 125, 9090; (c) P. M. Allen, B. J. Walker, M. G. Bawendi, *Angew. Chem. Int. Ed.* 2010, 49, 760.

[38] S. Abe, R. K. Capek, B. De Geyter, Z. Hens, *ACS Nano* 2013, 7, 943.

[39] D. C. Gary, B. M. Cossairt, *Chem. Mater.* 2013, 25, 2463.

[40] (a) I. Moreels, B. Fritzinger, J. C. Martins, Z. Hens, *J. Am. Chem. Soc.* 2008, 130, 15081; (b) X. Ji, D. Copenhaver, C. Sichmeller, X. Peng, *J. Am. Chem. Soc.* 2008, 130, 5726; (c) C. Bullen, P. Mulvaney, *Langmuir* 2006, 22, 3007.

[41] C. R. Bealing, W. J. Baumgardner, J. J. Choi, T. Hanrath, R. G. Hennig, *ACS Nano* 2012, 6, 2118.

[42] Z. Lingley, S. Lu, A. Madhukar, *Nano Lett.* 2011, 11, 2887.

Supporting Information

Mechanistic insight into the nucleation and growth of oleic acid capped lead sulfide quantum dots

Aabhash Shrestha[1], Nigel A. Spooner[2,3], Shi Zhang Qiao[1]*, and Sheng Dai[1]*

[1]School of Chemical Engineering, The University of Adelaide, Adelaide, SA, 5005, Australia

[2]School of Physical Sciences, Physics, The University of Adelaide, Adelaide, SA, 5005, Australia

[3]DST Group, PO Box 1500, Edinburg, SA 5111, Australia

* Corresponding Authors

Email: s.dai@adelaide.edu.au , s.qiao@adelaide.edu.au

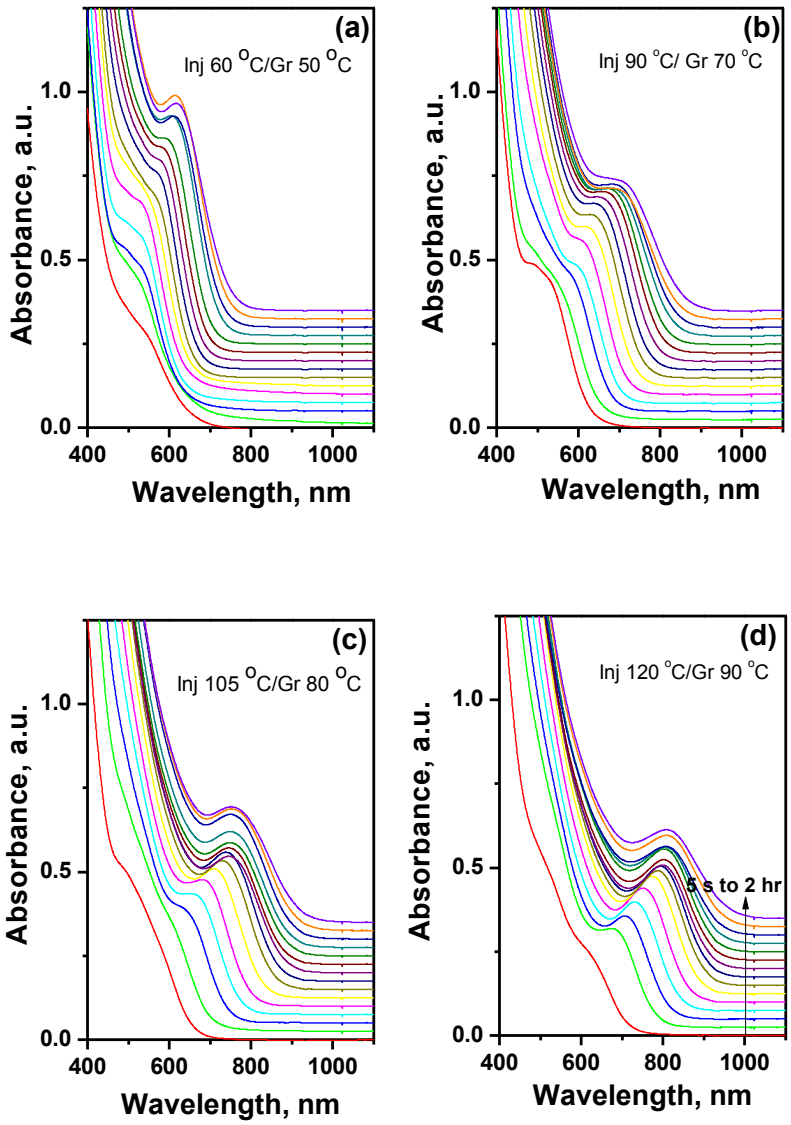

Figure S4-1. Temporal evolution of the absorption spectra of PbS QDs synthesized at various injection and growth temperatures.

(The wavelengths of the 1st exciton peak gradually increase with time indicating the increase in particle sizes. The particle sizes increase rapidly during the initial stage of the growth and gradually saturates as reaction time prolongs. The growth of the QDs ceases once the particle size reached optimal sizes)

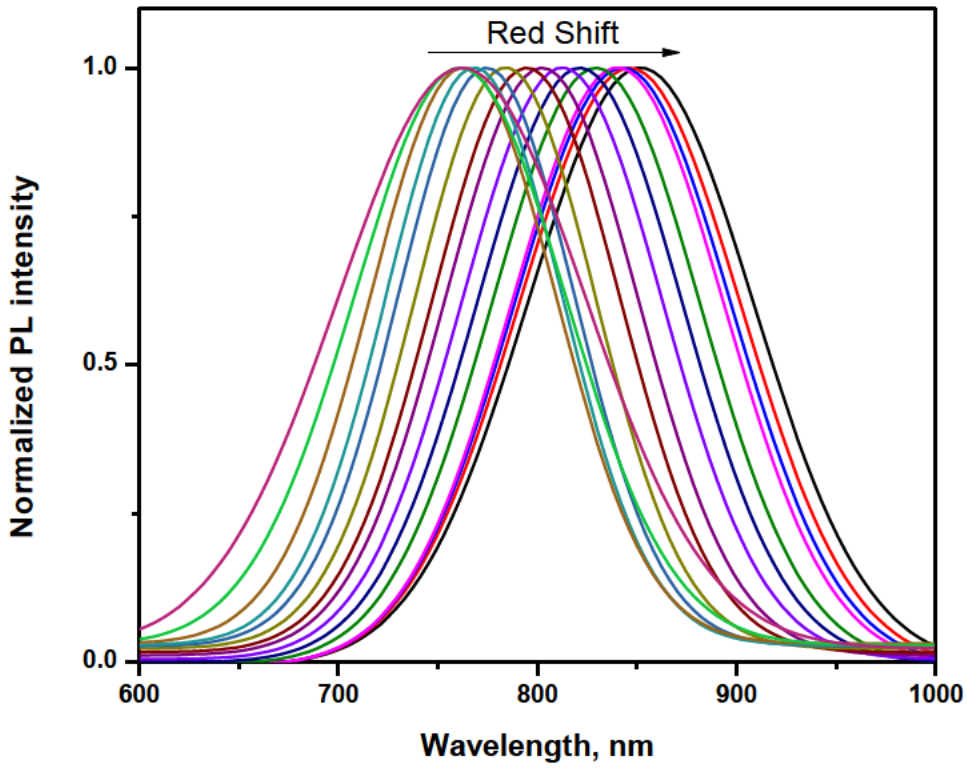

Figure S4-2. Photoluminescence (PL) spectra of PbS QDs. Synthesis condition - OA:Pb:S = 4:2:1, Injection temperature 90 °C and Growth temperature 70 °C.

(The red-shift of the PL peak indicates the increase in particle sizes).

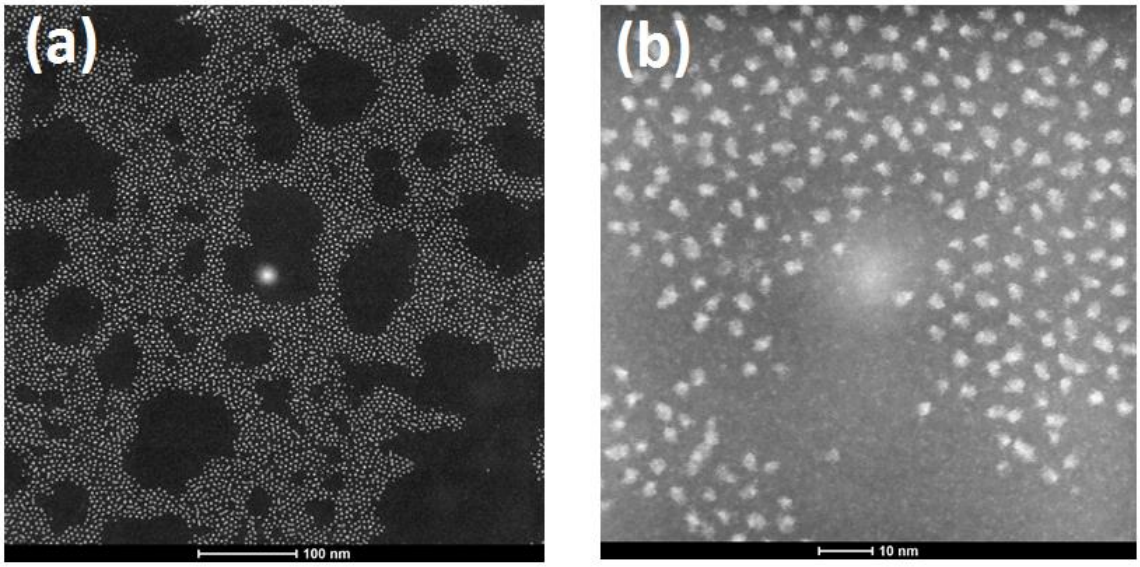

Figure S4-3. TEM image of synthesized PbS QDs (a) at low magnification (b) at high magnification

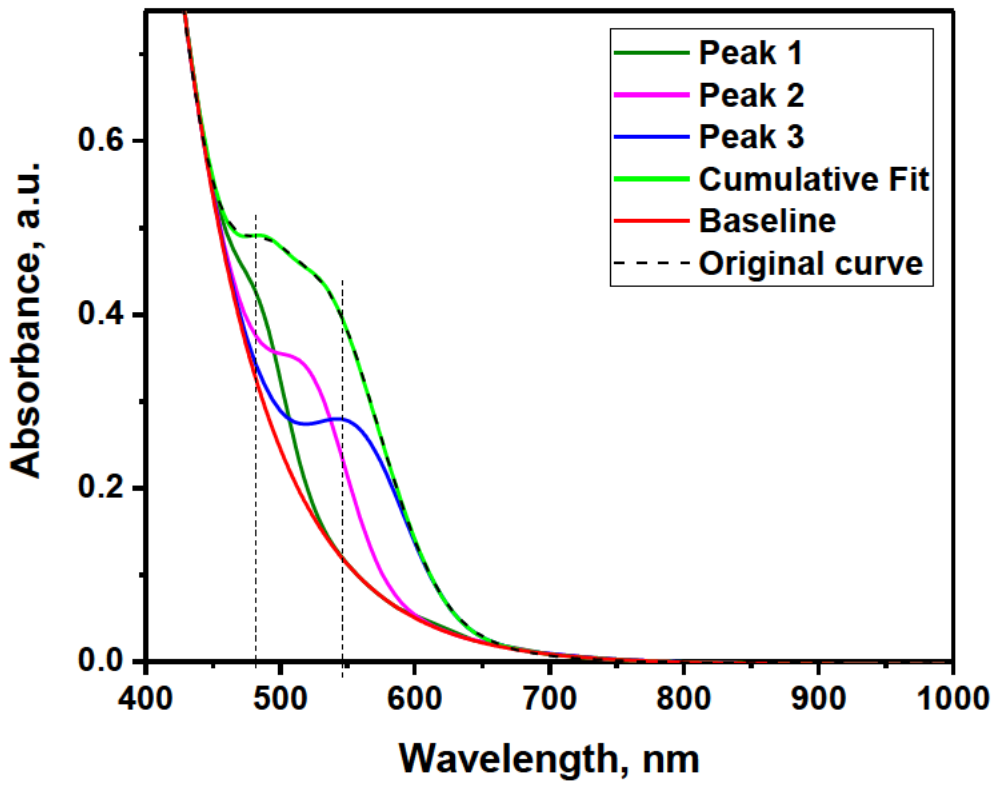

Figure S4-4. Peak fitting procedure to determine initial nuclei sizes.

(The absorbance spectra for 5 s aliquot for 90 °C injection and 70 °C growth condition was fitted to three Gaussian curves using the Origin Pro© software to determine the various nuclei sizes[1] Considering the bulk lattice parameter of PbS to be ~0.69 nm,[2] the various nuclei sizes were chosen to constitute 8-10 structural units per particle. For example, the nuclei with absorbance at ~480 nm (i.e. 1.4 nm particle diameter) would constitute 8 structural units of PbS per particle).

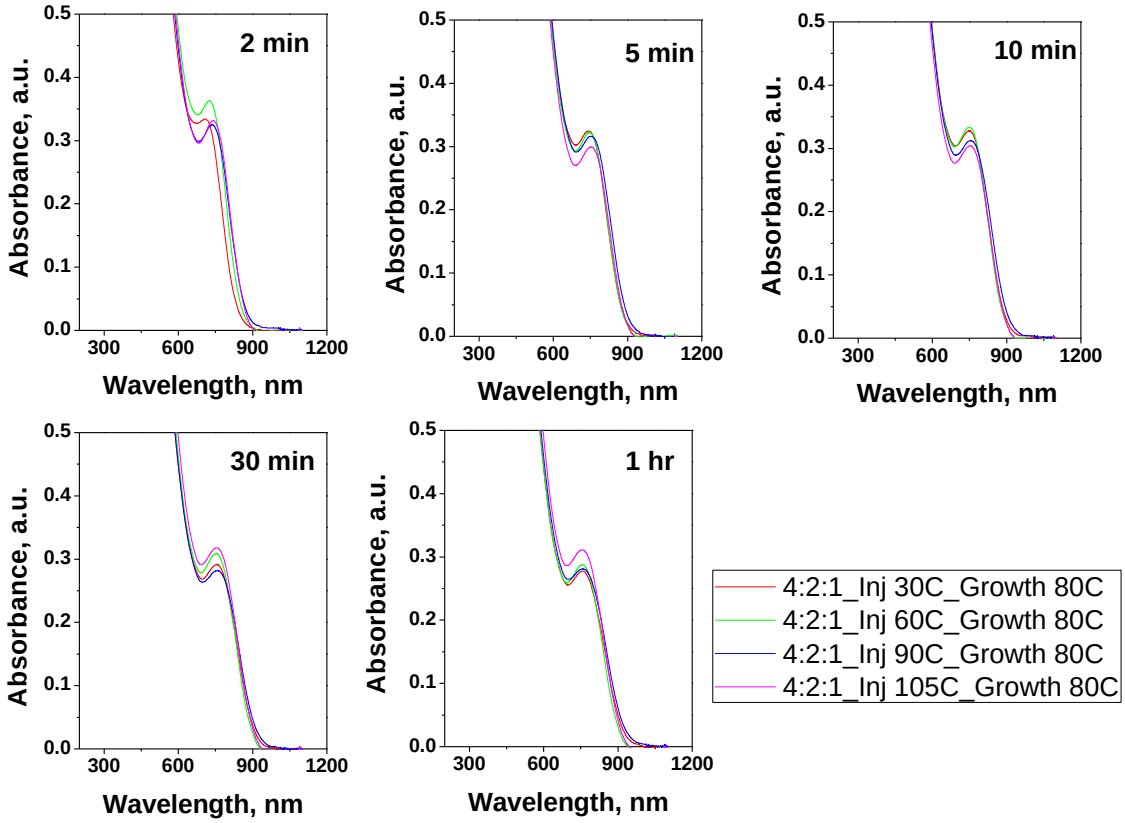

Figure S4-5. Absorption spectra for PbS QDs synthesis - different injection temperatures while maintaining the same growth temperature.

(The exciton peaks for all conditions saturate to the same position indicating the independence of nucleating temperatures on the final size of PbS QDs.)

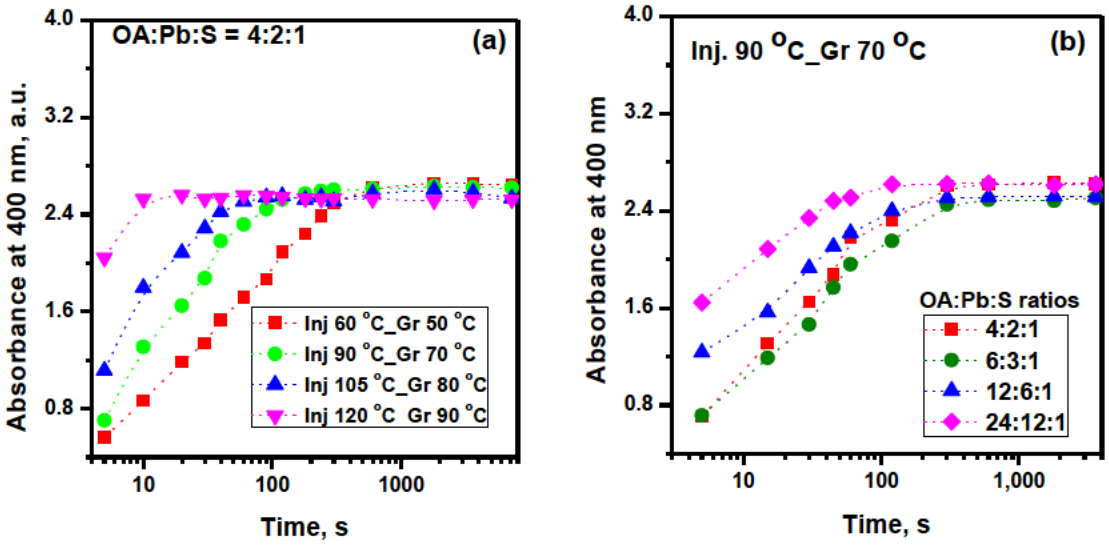

Figure S4-6. Temporal evolution of PbS QDs absorbance at 400 nm (a) at various injection and growth temperatures while the precursor ratio is maintained at OA:Pb:S=4:2:1 (b) at various ratios of lead precursor while keeping the same injection and growth temperatures (Injection temperature = 90 °C and Growth temperature = 70 °C growth). In both cases, the sulphur precursor concentration is kept the same.

(The formation of PbS QDs from precursor/monomers can be estimated from the absorbance spectra at 400 nm[2]. The molar extinction coefficient scales with nanocrystal volume at 400 nm and the precursor conversion to QDs can be estimated from the absorbance at 400 nm. We find that the higher temperature has a faster precursor conversion to QDs compared to lower temperature.)

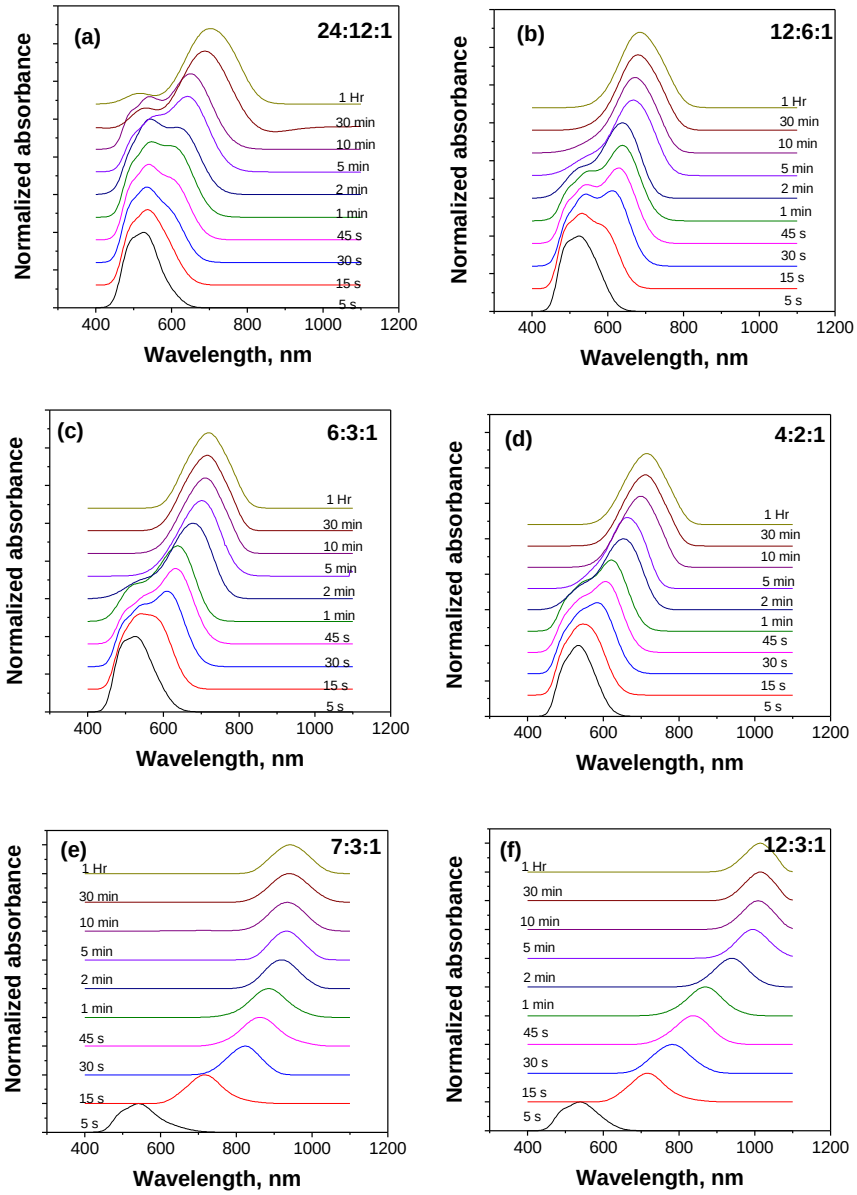

Figure S4-7. Absorption spectra fitting to a standard Gaussian distribution for various feed precursor ratios. Here, the precursor ratio are indicated as OA:Pb:S.

(The absorption spectra were fitted to the Gauss distribution using the curve fitting (spline function) in the Origin© software. It can been seen that at higher stoichiometric ratios

OA:Pb forms the cluster of various sizes before focusing while in presence of free oleic acid i.e. at higher OA:Pb ratios no such clusters are formed.)

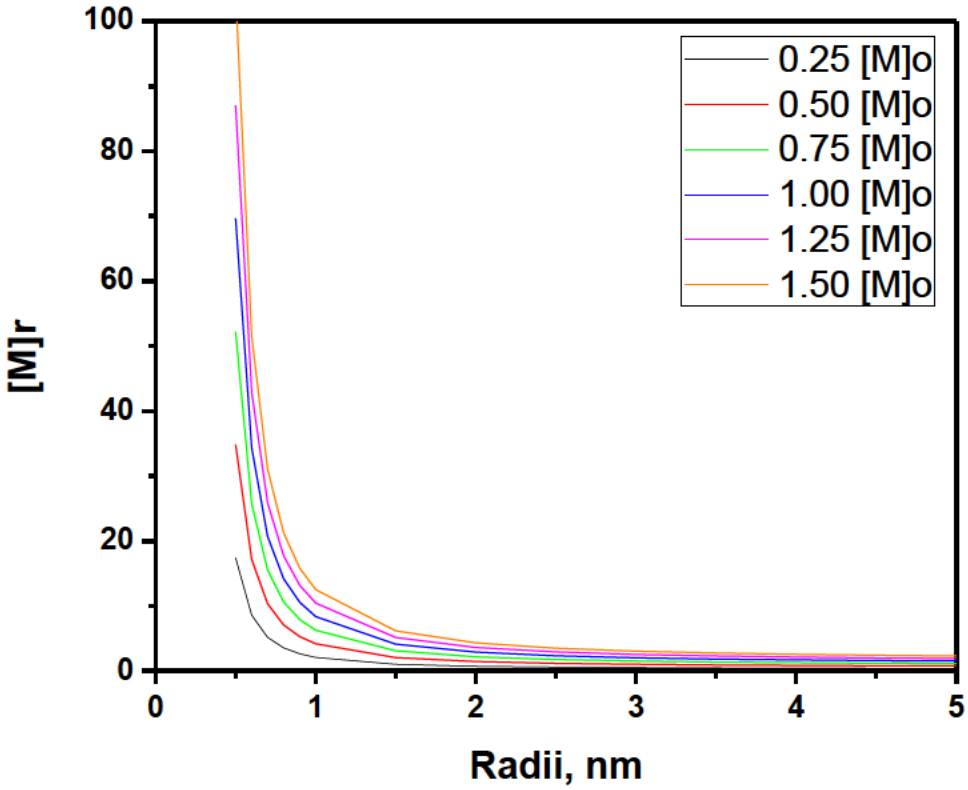

Figure S4-8. Change in solubility for various sized QDs particles with the change in equilibrium monomer solubility (**Equation 3** main text).

(The simulation parameters are V_m = 3.15x10^{-5} m^3/mol, γ = 0.125 J/m^2, and R = 8.314 J/mol.K.)

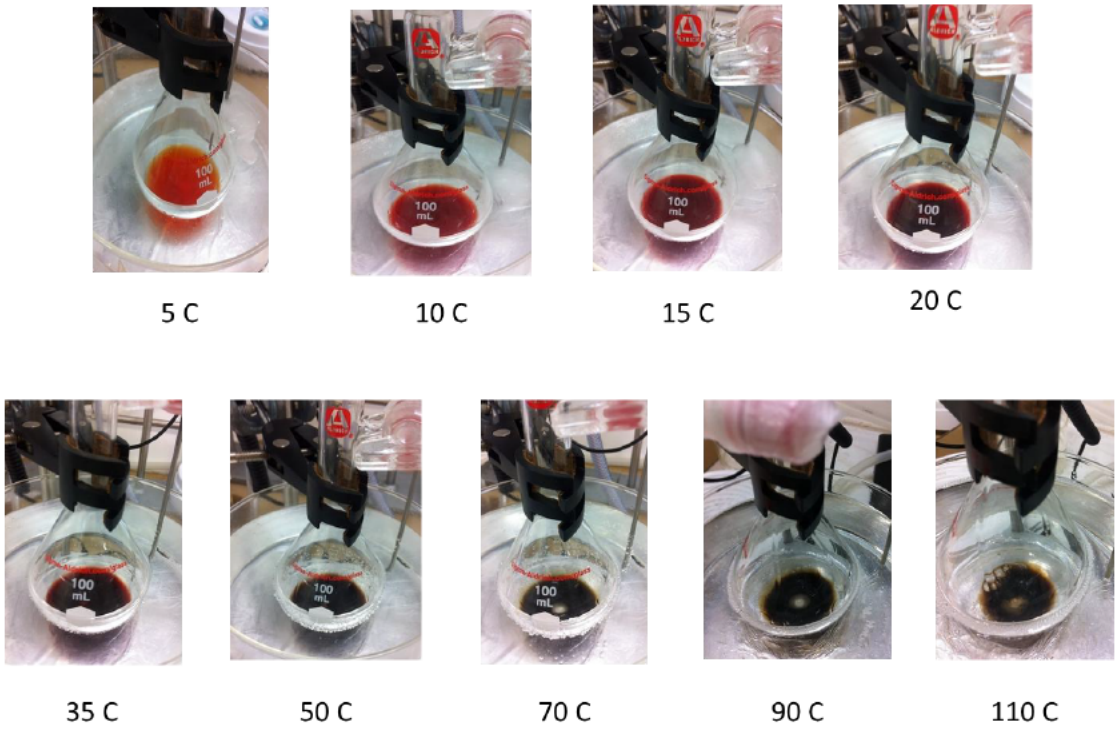

Figure S4-9. Snap shot of the synthesis of ultra-small PbS QDs at various growth temperatures

Table S4-1. Designed experiments at various synthesis parameters. Each green shade indicates the reaction parameters (i.e. temperature and reactant ratios) used at a certain condition.

	Feed ratio (OA:Pb:S)	Injection (°C)/Growth temperature (°C)						
		120 °C/90 °C	105 °C/80 °C	90 °C/70 °C	60 °C/50 °C	90 °C/80 °C	60 °C/80 °C	30 °C/80 °C
Temperature Influence	(4:2:1)							
Lead precursor Influence	(4:2:1)							
	(6:3:1)							
	(12:6:1)							
	(24:12:1)							
Oleic acid (Ligand)Influence	(6:3:1)							
	(6.5:3:1)							
	(7:3:1)							
	(9:3:1)							
	(12:3:1)							
Sulphur precursor Influence	(6:3:1)							
	(6:3:0.5)							
	(6:3:1.5)							

Table S4-2. Natural logarithmic, standard Ostwald ripening (OR) model and orientation attachment (OA) model fitting for the exciton peak at various temperature as a function of time (min) for OA:Pb:S as 4:2:1

OA:Pb:S (4:2:1)				
	OR model fitting			**OA model fitting**
Temperature, ^{o}C	***SSE, n=2***	***SSE, n=3***	***SSE, n=4***	***SSE***
50 ^{o}C	0.0062	0.0017	0.0070	0.0544
70 ^{o}C	0.0264	0.0080	0.0337	0.1781
80 ^{o}C	0.0534	0.0185	0.0767	0.2797
90 ^{o}C	0.0745	0.0286	0.1174	0.3624

Table S4-3. Natural logarithmic, standard Ostwald ripening (OR) model and orientation attachment (OA) model fitting for the exciton peak at various temperature as a function of time (min) for OA:Pb:S as 5:2:1

OA:Pb:S (5:2:1)				
	OR model fitting			**OA model fitting**
Temperature, ^{o}C	***SSE, n=2***	***SSE, n=3***	***SSE, n=4***	***SSE***
24 ^{o}C	0.0013	0.0003	0.0014	0.0131
40 ^{o}C	0.0042	0.0011	0.0046	0.0386
50 ^{o}C	0.0081	0.0022	0.0093	0.0692
60 ^{o}C	0.0128	0.0036	0.0153	0.1054
70 ^{o}C	0.0192	0.0056	0.0236	0.1416
80 ^{o}C	0.0647	0.0234	0.0966	0.2803
90 ^{o}C	0.0712	0.0264	0.1088	0.2836

Table S4-4. Natural logarithmic, standard Ostwald ripening (OR) model and orientation attachment (OA) model fitting for the exciton peak at various temperature as a function of time (min) for OA:Pb:S as 7:2:1

OA:Pb:S (7:2:1)				
	OR model fitting			**OA model fitting**
Temperature, ^oC	***SSE, n=2***	***SSE, n=3***	***SSE, n=4***	***SSE***
24 ^oC	0.0039	0.0010	0.0043	0.0360
50 ^oC	0.0266	0.0081	0.0339	0.1784
60 ^oC	0.0327	0.0103	0.0430	0.2047
70 ^oC	0.0587	0.0205	0.0851	0.2508
80 ^oC	0.0638	0.0231	0.0954	0.2939
90 ^oC	0.1030	0.0432	0.1755	0.2427

Table S4-5. Natural logarithmic, standard Ostwald ripening (OR) model and orientation attachment (OA) model fitting for the exciton peak at various temperature as a function of time (min) for OA:Pb:S as 10:2:1

OA:Pb:S (10:2:1)				
	OR model fitting			**OA model fitting**
Temperature, ^oC	***SSE, n=2***	***SSE, n=3***	***SSE, n=4***	***SSE***
24 ^oC	0.0023	0.0006	0.0025	0.0223
40 ^oC	0.0096	0.0027	0.0112	0.0825
70 ^oC	0.0656	0.0238	0.0984	0.2919

[1] C. M. Evans, A. M. Love, E. A. Weiss, *J. Am. Chem. Soc.* 2012, 134, 17298-17305.

[2] I. Moreels, K. Lambert, D. Smeets, D. De Muynck, T. Nollet, J. C. Martins, F. Vanhaecke, A. Vantomme, C. Delerue, G. Allan, Z. Hens, *ACS Nano* 2009, 3, 3023-3030.

Chapter 5

Versatile PbS quantum dot ligand exchange systems in the presence of Pb-thiolates

Aabhash Shrestha[1], Nigel A. Spooner[2,3], Shi Zhang Qiao[1]*, and Sheng Dai[1]*

[1] School of Chemical Engineering, The University of Adelaide, Adelaide, SA, 5005, Australia

[2] School of Physical Sciences, Department of Physics, The University of Adelaide, Adelaide, SA, 5005, Australia

[3]DST Group, PO Box 1500, Edinburg, SA 5111, Australia

* Corresponding Authors

Email: s.dai@adelaide.edu.au , s.qiao@adelaide.edu.au

Submitted to the Journal **Small** (Submission ID: smll.201601046)

Statement of Authorship

Title of Paper	Versatile PbS quantum dot ligand exchange systems in the presence of Pb-thiolates
Publication Status	☐ Published ☐ Accepted for Publication ☑ Submitted for Publication ☐ Unpublished and Unsubmitted work written in manuscript style
Publication Details	Aabhash Shrestha, Nigel A. Spooner, Shi Zhang Qiao*, and Sheng Dai*, **Versatile PbS quantum dot ligand exchange systems in the presence of Pb-thiolates**, ***Small*** (submission ID: smll.201601046)

Principal Author

Name of Principal Author (Candidate)	Aabhash Shrestha
Contribution to the Paper	Experimental design, performing of the experiments, analysis of the results and writing of the manuscript
Certification:	This paper reports on original research I conducted during the period of my Higher Degree by Research candidature and is not subject to any obligations or contractual agreements with a third party that would constrain its inclusion in this thesis. I am the primary author of this paper.
Signature	Date: 04/April/2016

Co-Author Contributions

By signing the Statement of Authorship, each author certifies that:

the candidate's stated contribution to the publication is accurate (as detailed above);

permission is granted for the candidate in include the publication in the thesis; and

the sum of all co-author contributions is equal to 100% less the candidate's stated contribution.

Name of Co-Author	Nigel A. Spooner
Contribution to the Paper	Assistance in fluorescence characterization and assessment.
Signature	Date: 05/04/2016.

Name of Co-Author	Shizhang Qiao
Contribution to the Paper	Assisting in the manuscript review and assessment.
Signature	Date: 08/April/2016

Name of Co-Author	Sheng Dai		
Contribution to the Paper	Supervising the development of the work, assisting in the data interpretation, manuscript review and assessment.		
Signature		Date	4/04/2016

Please cut and paste additional co-author panels here as required.

Abstract

A robust solution phase ligand exchange system for lead sulfide (PbS) quantum dots (QDs) in the presence of Pb-thiolate ligands is presented that can better preserve the excitonic absorption and emission features as compared to the conventional ligands. As a result, the photoluminescence after ligand exchange of PbS QDs with Pb-thiolate ligand is preserved up to 78% of the original oleate capped PbS QDs. Further, such a Pb-thiolate ligand exchange system is versatile for the phase transfer of PbS QDs using a number of thiol ligands and solvent systems.

Keywords: lead sulfide, quantum dots, thiols, ligand exchange

TOC Figure

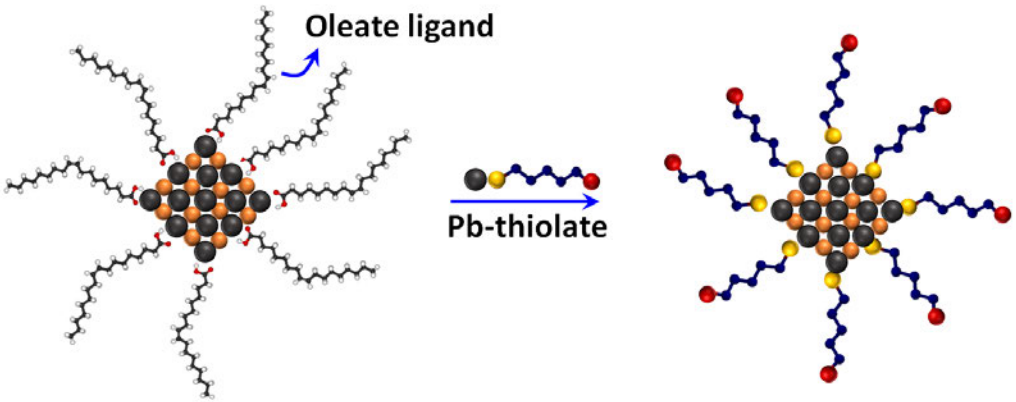

Semi-conducting QDs with its size tunable bandgaps offer potential applications in solar cells,[1-3] nanostructured electronic arrays[4] and optoelectronic devices.[5] Recently, the near-infrared (NIR) active QDs of lead chalcogenides (PbX; X=S, Se or Te) are receiving much attention due to their narrow bulk band gaps, large excitonic Bohr radii and the possibility of multiple exciton generation.[6] Utilizing these QDs in solar cells with extendable IR absorption, biolabels for deep tissue imaging and other optoelectronic applications is promising.

Various ligands are generally introduced during the synthesis of QDs and provide colloidal stabilization of QDs in solution. Ligands play an essential role for the utilization of these QDs in many practical applications such as passivating the trap state densities and provide charge balance on QD surfaces, maintaining their hydophilicity or hydrophobicity and providing functional groups for further conjugation to various substrates.[1, 7] Further, ligands can also influence the size and shape of QDs during synthesis.[8] A proper understanding of the ligand chemistry on QD surfaces can lead to optimal performance while utilizing these QDs in end-use applications. The majority of successful colloidal QDs synthesis relies on the use of long chain hydrophobic ligands with polar head groups such as carboxylate, amine, phosphonate etc.[9, 10] These bulky ligands are generally insulating and non-functional for a number of applications such as optoelectronic devices and bio-conjugation. Efficient replacement of these bulky ligands with non-insulating and functional ligands is crucial for the utilization of these QDs in diverse applications.

The solution phase ligand exchange of lead-chalcogenide QDs has been typically challenging due to the propensity of these QDs to oxidation, coalescence and aggregation upon addition of small molecules as replacing ligand.[3, 11-13] Only a handful of thiol and

inorganic based ligands have been shown to successfully exchange the native ligands while also maintaining their colloidal stability.[3, 11-14, 15] The issue is further complicated by the narrow range of exchanging conditions (such as pH and solvent) that can yield a stable colloidal solution. Although the recent developments in inorganic based ligands are promising, they are still limited by the lack of functionality for conjugation to various substrates. Herein, we explore the thiol based ligand exchange for lead sulphide (PbS) QDs. Consistent with previous reports,[3, 11-13, 15] the ligand exchange using the thiol anchoring groups is sensitive to exchanging conditions. In this communication, we show that the ligand exchange efficiency of PbS QDs can be improved by pre-complexing the thiol ligands with Pb^{2+} ions prior to the ligand exchange. We found that the photoluminescence quantum yields (PLQY) can be preserved up to 78% of the original oleate capped QDs in organic solvents by performing the ligand exchange using Pb-thiolate as the exchanging ligands. Moreover, we also show that the Pb-thiolate has a beneficial effect on preserving the stability of PbS QDs during ligand exchange and are applicable to a number of other ligand/solvent systems. Such ligand exchange strategy would provide a more facile approach for the phase transfer of oleophilic PbS QDs for different end use applications.

Oleate capped PbS QDs were synthesized on the basis of hot-injection process as reported by Hines et al.[9] **Figure 5-1(a)** shows the absorption and emission spectra of the as-synthesized oleate capped PbS QDs. The absorption spectrum shows a sharp excitonic peak at ~945 nm while a narrow emission peak is centred at ~1050 nm. As shown in **Figure 5-2(a) and 5-2(b)**, the HRTEM image of as-synthesized QDs has an average diameter of 2.9±0.1 nm which agrees well with the size calculated from the absorption

spectrum (~3 nm for 945 nm excitonic peak).[16] The high resolution transmission electron microscopy (HRTEM) image also shows that the QDs are highly crystalline (**Figure 5-2(b)**).

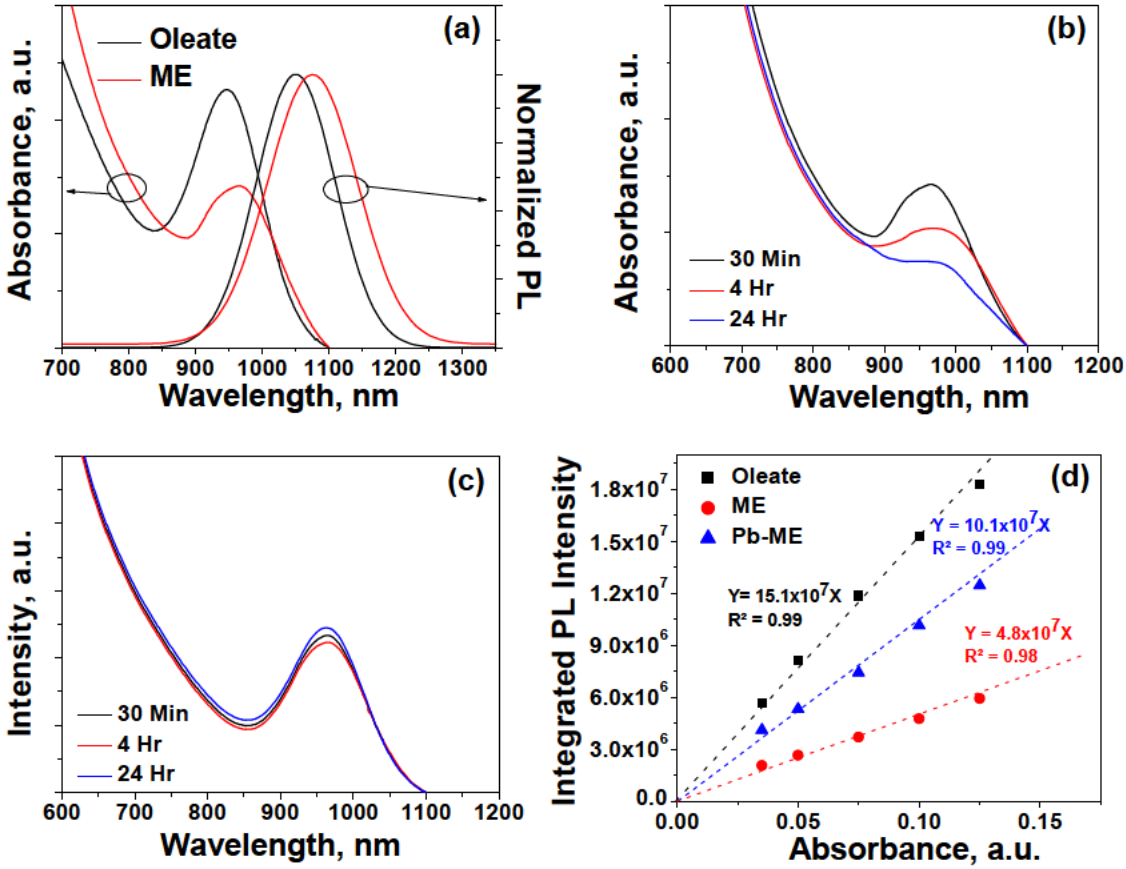

Figure 5-1. (a) Absorbance and photoluminescence (PL) spectra for oleate capped PbS QDs before ligand exchange (black) and ME capped QDs after ligand exchange (red) (b) Absorption spectra evolution for ligand exchange using ME (c) Absorption spectra evolution for ligand exchange using Pb-ME in presence of TEA (d) Integrated PL intensity versus absorbance plot for native oleate capped QDs before ligand exchange and after ligand exchange using ME and Pb-ME in presence of TEA.

To explore the ligand exchange of oleate capped PbS QDs, mercaptoethanol (ME) in dimethylsulfoxide (DMSO) is chosen as a model exchanging ligand. The choice of the exchanging ligand is based on the hard acid strong base (HASB) principle.[11, 17] The softer character of thiols has strong interaction with Pb atoms on QD surfaces while the relatively stronger basic character of –OH has weaker interaction with Pb atoms. Hence, only the thiol group of ME interacts with the Pb on QDs surfaces and their influence on ligand exchange can be effectively monitored (**Figure 5-1**).

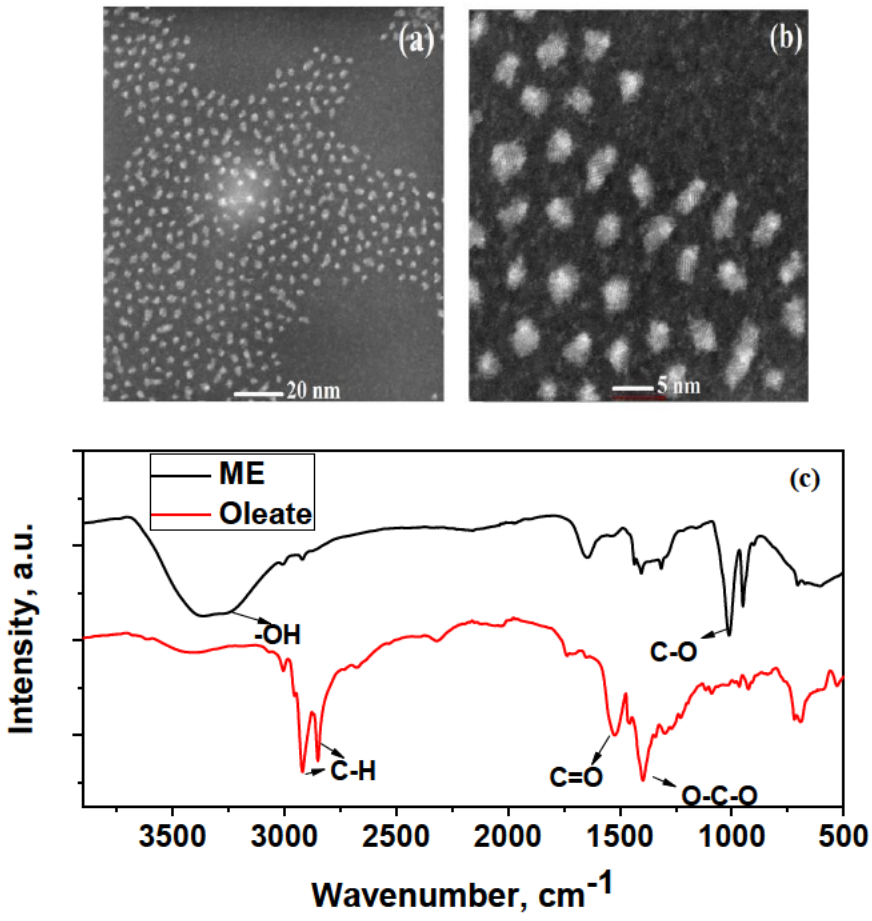

Figure 5-2. (a) and (b) HRTEM images of PbS QDs at different magnifications (c) FTIR spectra of PbS QDs capped with oleate and that after ME ligand exchange

The ligand exchange of as-synthesized QDs was performed using a simple bi-phasic transfer procedure. Upon gentle shaking, the oleate capped PbS QDs can be transferred from the non-polar hexane to polar DMSO. The oleate capped PbS QDs do not migrate to DMSO in the absence of ME indicating that DMSO does not interact with PbS QDs during this phase transfer process. To further verify the exchange of oleate with ME, FTIR spectrums were recorded before and after the ligand exchange (**Figure 5-2(c)**). The FTIR spectrum shows that the typical IR absorbance from the C-H (2850-3000 cm^{-1}), C=O (1700-1725 cm^{-1}) and symmetric O-C-O (1360-1400 cm^{-1}) vibrations of the oleate ligands disappears completely after the ligand exchange and the new IR absorbance corresponding to the –OH (3200-3600 cm^{-1}) and C-O (1050-1150 cm^{-1}) vibrations of the ME appears, which indicates the higher percentage replacement of oleate by ME.

A typical bathochromatic shift (~25 nm) of the absorption and emission spectrum are observed after the phase transfer of PbS QDs to DMSO (**Figure 5-1(a)**). Such bathochromatic shifts of absorption and emission spectrum upon thiol ligand exchange can be attributed to the contribution of S3p orbital of the thiol ligands to the higher occupied states of ligand-QD systems.[12] Both the absorption and emission peak intensities decrease upon extending the period of ligand exchange with ME and broaden over time (**Figure 5-1(b)**). Recently, Reinhart et al[15] attributed such evolution of optical spectra upon ligand exchange of PbS QDs with 3-mercaptopropionic acid (3-MPA) to the oxidative reaction of 3-MPA to form disulfides and the possible cross-linking of QDs. Although the oxidative reaction of ME with time to form disulfides is not avoidable, such nonmonotonic change in the absorbance bandwith and the optical spectra evolution during the ligand exchange is highly undesirable.

To solve these issues of optical properties degradation upon thiol ligand exchange, we pre-complex the thiol ligands with lead cations prior to ligand exchange. Typically, ME was mixed with lead nitrate, $Pb(NO_3)_2$ in the presence of triethylamine, TEA to form Pb-ME complex prior to ligand exchange. As a control, ligand exchange in the absence of either $Pb(NO_3)_2$ or TEA was also performed. As shown in **Figure 5-1(c)**, the ligand exchange of oleate capped PbS QDs with Pb-ME in the presence of TEA shows the sharp absorption excitonic peak similar to that of oleate capped QDs in hexane. Obviously, the typical bathochromatic shift of the excitonic peak (~25 nm) is also observed upon ligand exchange with Pb-ME. Moreover, the nonmonotonic change of the absorption bandwidth and the reduction of excitonic peak intensity are not observed upon ligand exchange with Pb-ME (**Figure 5-1(c)**). The excitonic peak intensities and their bandwidth remain unchanged for the duration of ligand exchange without any visible signs of QD precipitation.

To ascertain the role of $Pb(NO_3)_2$ and TEA, the ligand exchange of PbS QDs was conducted in the absence of either $Pb(NO_3)_2$ or TEA. The ligand exchange in the absence of TEA (an organic base) had no measurable difference in comparison to the ligand exchange with only ME. Notably, $Pb(NO_3)_2$ and ME in the absence of TEA shows a colourless solution in DMSO whereas a light yellowish solution is viewed upon addition of TEA indicating that Pb-ME complex may not be formed in the absence of TEA (**Figure S5-1**). Further, the QDs cannot be transferred to DMSO in the presence of only TEA or TEA and $Pb(NO_3)_2$ (i.e. no ME) showing that neither TEA nor $Pb(NO_3)_2$ directly participates in ligand exchange. The ligand exchange in presence of only ME and TEA i.e. with no $Pb(NO_3)_2$ induced the rapid aggregation of PbS QDs during the phase transfer process. The aggregation of PbS QDs during the ligand exchange in presence of only ME

and TEA can be due to the rapid displacement of surface Pb-carboxylate during the ligand exchange. The L-type ligands i.e. the electron donor nucleophiles such as thiols have shown to displace the metal-carboxylate complexes from the QDs surface during the ligand exchange.[18] The addition of TEA (i.e. a base) to a solution of ME in DMSO induces the deprotonation of thiol to thiolate. The thiolate ligands generally exhibit much stronger nucleophilic character than thiols[11] and can accelerate the removal of surface Pb atoms to induce the precipitation of QDs (**Scheme 5-1**).

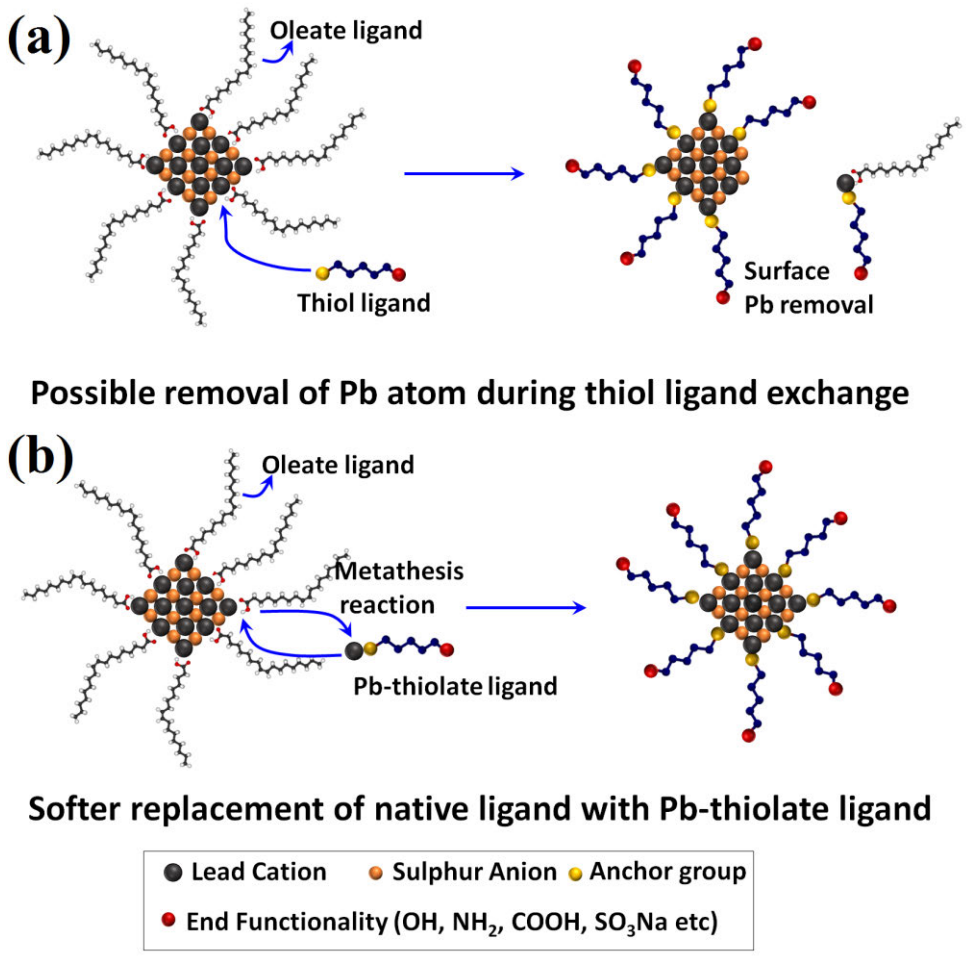

Scheme 5-1. Schematic illustration for the ligand exchange using (a) only thiol as exchanging ligand (b) Pb-thiolate as the exchanging ligand

Obviously, the formation of Pb-thiolate is important for the successful ligand exchange of PbS QDs. In the presence of $Pb(NO_3)_2$ and TEA (1:2 ratio), ME reacts with Pb^{2+} ions to form Pb-thiolate. Recently, Zn^{2+} ions were found to play an important role for the efficient ligand exchange of CdSe/ZnS core/shell QDs.[19] Although the role of Zn^{2+} ions in the exchange mechanism is not fully understood, the ligand exchange in the presence of Zn-thiolate in NaOH solution was found to enhance the exchange efficiency by preventing the etching of nanocrystals during the exchange. The metathesis reaction occurring at the QDs surface in the presence of Zn-thiolate ligand was presented as a possible mechanism for efficient ligand exchange.[19] Recent studies also reveal that the chemical reaction between the metal ions on the surface of QDs and the inorganic complex in a solution is more facile than the reaction between the free metal ion and the inorganic complex in the same solution i.e. the QDs surface presents lower barrier for the chemical reaction to occur.[20] These observations indicate that the metathesis reaction between Pb-thiolate and the Pb-carboxylate on QDs surface can occur in a more facile manner leading to the replacement of native oleate ligand (**Scheme 5-1**). The Pb^{2+} ions can have a similar effect as Zn^{2+} ions[19] on presenting milder reaction conditions for the efficient ligand exchange of PbS QDs.

The efficiency of the ligand exchange in presence of Pb-ME complex is also evident from the emission intensities of PbS QDs after ligand exchange. As shown in **Figure 5-1(d)** (also see **Figure S5-2**), the integrated photoluminescence (PL) intensities for the post ligand exchanged QDs with Pb-ME complex are much higher than that using only ME as exchanging ligand. The relative photoluminescence quantum yield (PLQY) for the post ligand exchanged QDs versus the oleate capped QDs shows that the ligand exchange with

Pb-ME preserves the PLQY up to 78 % to that of original oleate capped QDs. As a comparison, the ligand exchange with ME preserves only 37 % PLQY of the initial oleate capped QDs.

To further investigate the generality of ligand exchange using Pb-thiolate, we performed the ligand exchange experiments using a number of other thiol containing ligands such as mercaptophenol (MP), mercaptoethanesulfonate (MESNA) and L-glutathione (GSH). The ligand exchange for MP was performed in DMSO while the ligand exchange for MESNA and GSH were performed in water. The Pb-MP were formed in DMSO using the TEA as base similar to that for Pb-ME while the Pb-MESNA and Pb-GSH were formed in water by adjusting the pH to ~12 using NaOH. It has to be noted that the ligand exchange using bi-phasic hexane/water system takes much longer time for the complete transfer of PbS QDs to water phase as compared to ligand exchange using hexane/DMSO system due to the higher polarity difference between water and hexane.

Similar to the ligand exchange using Pb-ME, the ligand exchange with other Pb-thiolates also showed clear excitonic absorption peak and similar absorption bandwidth as the oleate capped QDs (**Figure 5-3(a)**). No changes in the absorption excitonic peaks are observed with time (**Figure 5-2(a)**) similar to the ligand exchange using Pb-ME. Similar to ligand exchange using Pb-ME, the PLQY of PbS QDs are better preserved using the Pb-thiolate ligands in comparison to those using only thiol groups during the ligand exchange (**Figure 5-3(b)** and **Figure S5-2**). Typically, the PLQY of 52.4 % and 60.3 % are preserved using the Pb-MESNA and Pb-GSH as the exchanging ligand. As a comparison, the ligand exchange using only MESNA at pH 5 preserves 30 % PLQY while that with GSH at pH 5 preserves 39 % PLQY of the initial oleate capped PbS QDs. However, the luminescence of

MP capped PbS QDs are completely quenched. MP are known to act as the good hole scavenging agents and have shown to promote the efficient funnelling of the photogenerated holes in PbSe QDs based solar cells.[21] Thus, the ligand exchange with MP will lead to the extraction of photogenerated holes in PbS QDs and quenching the luminescence of the QDs.

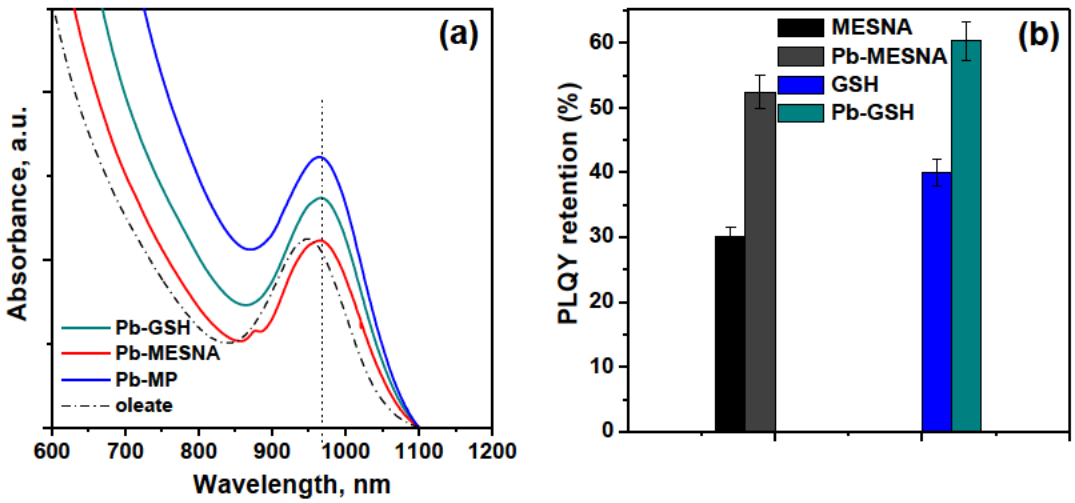

Figure 5-3. (a) Absorbance spectrum of PbS QDs using Pb-GSH, Pb-MESNA and Pb-MCP as the exchanging lignads. As a comparison, absorption spectrum of oleate capped QDs is also presented (b) PLQY retention as compared to initial oleate capped PbS QDs after ligand exchange with Pb-MESNA and Pb-GSH. As a comparison PLQY retention of MESNA and GSH at pH 5 is also presented.

In conclusion, we present an efficient ligand exchange strategy for PbS QDs by using Pb-thiolate as the exchanging ligand. The Pb-thiolate ligands can better preserve the exciton absorption features as well as the emission intensities during the ligand exchange procedure. The Pb-thiol ligand exchange approach is versatile and applicable to a number of other ligand/solvent systems. The ligand exchange using Pb-thiolates will provide a facile procedure for future ligand exchange involving lead chalcogenide based QDs.

5.1 Experimental

5.1.1 Materials

Lead (II) oxide (PbO, 99.99 %), hexamethyldisilathiane (TMS)2S, oleic acid (OA, 90 % technical grade), 1-octadecene (ODE, 99.99%), 2-Mercaptoethanol (ME, >99%), Sodium 2-mercaptoethanesulfonate (MESNA, 98%), L-Glutathione reduced (GSH, >98%), 4-Mercaptophenol (MP, 98%), dimethylsulfonic acid (DMSO), sodium hydroxide (NaOH), triethylamine (TEA, >99.5%), acetone, hexane and heptane were procured from Sigma-Aldrich. All chemicals were used as received.

5.1.2 Synthesis of PbS QDs

The PbS QDs were synthesized using a previously described method.[9] Typically, the lead precursor was prepared by heating 178.6 mg (0.8 mmol) of PbO and 0.634 mL (1.6 mmol) oleic acid (OA) in 8 mL 1-octadecene (ODE) in a 100 mL schlenk flask under argon protection at 150 ℃ for 1 hour to obtain a clear yellowish lead oleate solution. The temperature of the lead oleate solution was then reduced to 130 ^{o}C and 84 µl (0.4 mmol) of $(TMS)_2S$ in 4 ml ODA at room temperature was quickly injection into the hot lead precursor solution. The growth temperature was then maintained at 110 ^{o}C for 10 minutes. The final QDs were precipitated with acetone, centrifuged (~7,000 rpm) and diluted in 3 ml hexane for further use and characterization.

5.1.3 Ligand exchange of PbS QDs

The ligand exchange of PbS QDs was performed using a simple biphasic exchange procedure. Typically for ligand exchange with ME (or MP), 0.1 mmol of ME and 0.05 mmol of $Pb(NO_3)_2$ was dissolved in 5 ml of DMSO. 0.1 mmol of TEA was added into the

ligand solution to form Pb-ME complex. The Pb-ME complex was then added to 5 ml of PbS QD in hexane. The biphasic solution was vigorously mixed for a couple of minutes and the QDs in hexane were transferred to DMSO. Similarly, for ligand exchange using MESNA (or GSH), 0.1 mmol of MESNA and 0.05 mmol of $Pb(NO_3)_2$ was dissolved in 5 ml of water and the pH of the resulting solution was adjusted to 12 by adding NaOH solution. The Pb-MESNA complex was then added to 5 ml PbS QDs in hexane. Upon shaking, the PbS QDs were gradually transferred to water phase.

5.1.4 Materials Characterization

Absorption measurements were performed in a Shimadzu 1601 UV-vis. spectrometer. Fluorescence emission measurements were carried out in an Edinburgh Instruments, FLS-980 fluorescence spectrometer with emission detected using a Hamamatsu LN-cooled R5509-72 NIR-PMT. The excitation wavelength for fluorescence measurements was maintained as 650 nm.

The transmission electron microscopy images were collected using a FEI Titan transmission electron microscope. The FTIR spectra were acquired using the transmission module of Thermo Nicolet 6700 FTIR spectrometer at the resolution of 2 cm^{-1}.

Acknowledgements

This work was financially supported by the Australian Research Council Discovery Projects DP110102877 and DP140104062

References

[1] A. H. Ip, S. M. Thon, S. Hoogland, O. Voznyy, D. Zhitomirsky, R. Debnath, L. Levina, L. R. Rollny, G. H. Carey, A. Fischer, K. W. Kemp, I. J. Kramer, Z. Ning, A. J. Labelle, K. W. Chou, A. Amassian, E. H. Sargent, *Nat. Nanotechnol.* 2012, 7, 577.

[2] J. Tang, K. W. Kemp, S. Hoogland, K. S. Jeong, H. Liu, L. Levina, M. Furukawa, X. Wang, R. Debnath, D. Cha, K. W. Chou, A. Fischer, A. Amassian, J. B. Asbury, E. H. Sargent, *Nat. Mater.* 2011, 10, 765.

[3] A. Fischer, L. Rollny, J. Pan, G. H. Carey, S. M. Thon, S. Hoogland, O. Voznyy, D. Zhitomirsky, J. Y. Kim, O. M. Bakr, E. H. Sargent, *Adv. Mater.* 2013, 25, 5742.

[4] D. V. Talapin, J.-S. Lee, M. V. Kovalenko, E. V. Shevchenko, Chemical Reviews 2009, 110, 389; E. V. Shevchenko, D. V. Talapin, N. A. Kotov, S. O'Brien, C. B. Murray, *Nature* 2006, 439, 55.

[5] (a) S. Coe-Sullivan, Nat Photon 2009, 3, 315; J. M. Caruge, J. E. Halpert, V. Wood, V. Bulovic, M. G. Bawendi, *Nat. Photon.* 2008, 2, 247; (b) P. O. Anikeeva, J. E. Halpert, M. G. Bawendi, V. Bulović, *Nano Lett.* 2009, 9, 2532.

[6] (a) A. J. Nozik, Physica *E: Low-dimensional Systems and Nanostructures* 2002, 14, 115; (b) R. J. Ellingson, M. C. Beard, J. C. Johnson, P. Yu, O. I. Micic, A. J. Nozik, A. Shabaev, A. L. Efros, *Nano Lett.* 2005, 5, 865; (c) J. E. Murphy, M. C. Beard, A. G. Norman, S. P. Ahrenkiel, J. C. Johnson, P. Yu, O. I. Mićić, R. J. Ellingson, A. J. Nozik, *J. Am. Chem. Soc.* 2006, 128, 3241.

[7] D. Deng, J. Cao, J. Xia, Z. Qian, Y. Gu, Z. Gu, W. J. Akers, *Eur. J. Inorg. Chem.* 2011, 2011, 2422.

[8] (a) H. Li, D. Chen, L. Li, F. Tang, L. Zhang, J. Ren, *CrystEngComm* 2010, 12, 1127; (b) C. R. Bealing, W. J. Baumgardner, J. J. Choi, T. Hanrath, R. G. Hennig, *ACS Nano* 2012, 6, 2118.

[9] M. A. Hines, G. D. Scholes, *Adv. Mater.* 2003, 15, 1844.

[10] (a) J. Y. Woo, S. Lee, S. Lee, W. D. Kim, K. Lee, K. Kim, H. J. An, D. C. Lee, S. Jeong, *J. Am. Chem. Soc.* 2015; (b) L. Cademartiri, J. Bertolotti, R. Sapienza, D. S. Wiersma, G. von Freymann, G. A. Ozin, *J. Phys. Chem. B* 2005, 110, 671.

[11] C. Giansante, L. Carbone, C. Giannini, D. Altamura, Z. Ameer, G. Maruccio, A. Loiudice, M. R. Belviso, P. D. Cozzoli, A. Rizzo, G. Gigli, *J. Phys. Chem. C* 2013, 117, 13305.

[12] C. Giansante, I. Infante, E. Fabiano, R. Grisorio, G. P. Suranna, G. Gigli, *J. Am. Chem. Soc.* 2015, 137, 1875.

[13] D. Deng, J. Xia, J. Cao, L. Qu, J. Tian, Z. Qian, Y. Gu, Z. Gu, J. *Colloid and Interface Sci.* 2012, 367, 234.

[14] (a) M. V. Kovalenko, M. I. Bodnarchuk, J. Zaumseil, J. S. Lee, D. V. Talapin, *J. Am. Chem. Soc.* 2010, 132, 10085; (b) D. N. Dirin, S. Dreyfuss, M. I. Bodnarchuk, G. Nedelcu, P. Papagiorgis, G. Itskos, M. V. Kovalenko, *J. Am. Chem. Soc.* 2014, 136, 6550; (c) H. Zhang, J. Jang, W. Liu, D. V. Talapin, *ACS Nano* 2014, 8, 7359.

[15] C. C. Reinhart, E. Johansson, *Chem. Mater.* 2015, 27, 7313.

[16] I. Moreels, K. Lambert, D. Smeets, D. De Muynck, T. Nollet, J. C. Martins, F. Vanhaecke, A. Vantomme, C. Delerue, G. Allan, Z. Hens, *ACS Nano* 2009, 3, 3023.

[17] R. G. Pearson, *J. Am. Chem. Soc.* 1963, 85, 3533.

[18] N. C. Anderson, M. P. Hendricks, J. J. Choi, J. S. Owen, *J. Am. Chem. Soc.* 2013, 135, 18536.

[19] D. Liu, P. T. Snee, *ACS Nano* 2011, 5, 546.

[20] S. Roy, S. Bhandari, A. Chattopadhyay, *J. Phys. Chem. C* 2015, 119, 21191.

[21] N. Guijarro, T. Lana-Villarreal, T. Lutz, S. A. Haque, R. Gómez, *J. Phys. Chem. Lett.* 2012, 3, 3367.

Supporting Information

Versatile PbS quantum dot ligand exchange systems in the presence of Pb-thiolates

Aabhash Shrestha[1], Nigel A. Spooner[2,3], Shi Zhang Qiao[1]*, and Sheng Dai[1]*

[1]School of Chemical Engineering, The University of Adelaide, Adelaide, SA, 5005, Australia

[2]School of Physical Sciences, Department of Physics, The University of Adelaide, Adelaide, SA, 5005, Australia

[3]DST Group, PO Box 1500, Edinburg, SA 5111, Australia

* Corresponding Authors

Email: s.dai@adelaide.edu.au , s.qiao@adelaide.edu.au

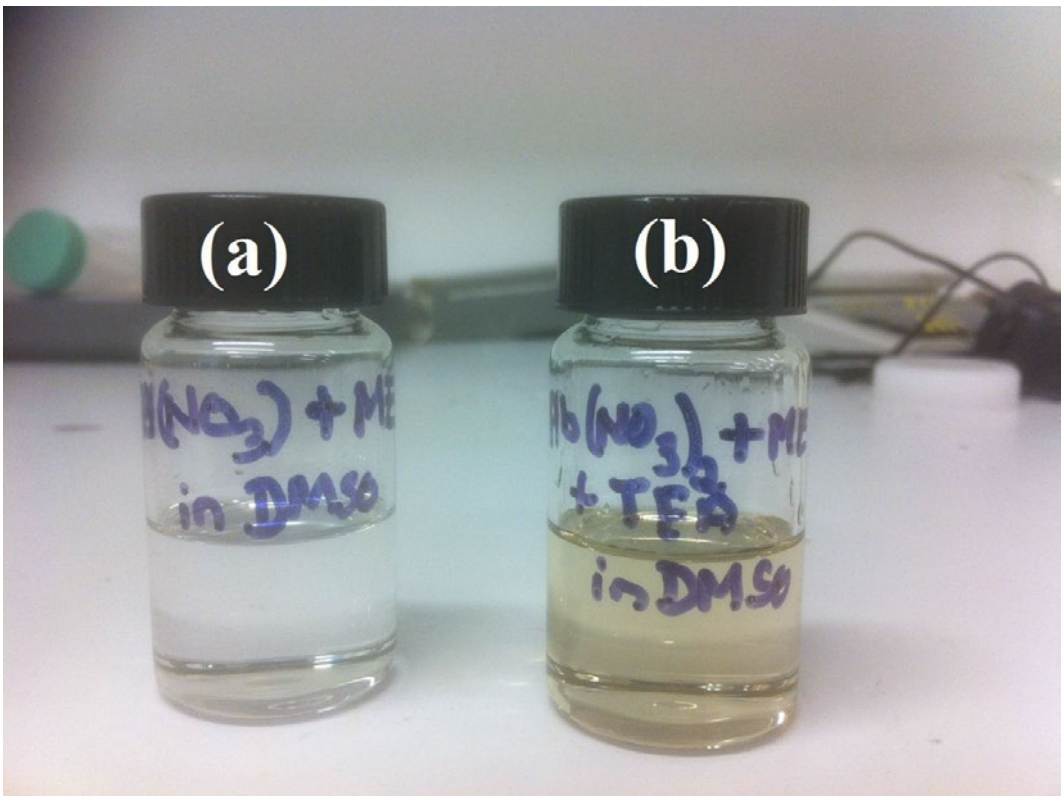

Figure S5-1. Photographs of solutions of (a) $Pb(NO_3)_2$ and ME in DMSO (b) $Pb(NO_3)_2$, ME and TEA in DMSO. The light yellow coloured solution in presence of $Pb(NO_3)_2$, ME and TEA in DMSO indicate the Pb-thiolate formation in solution.

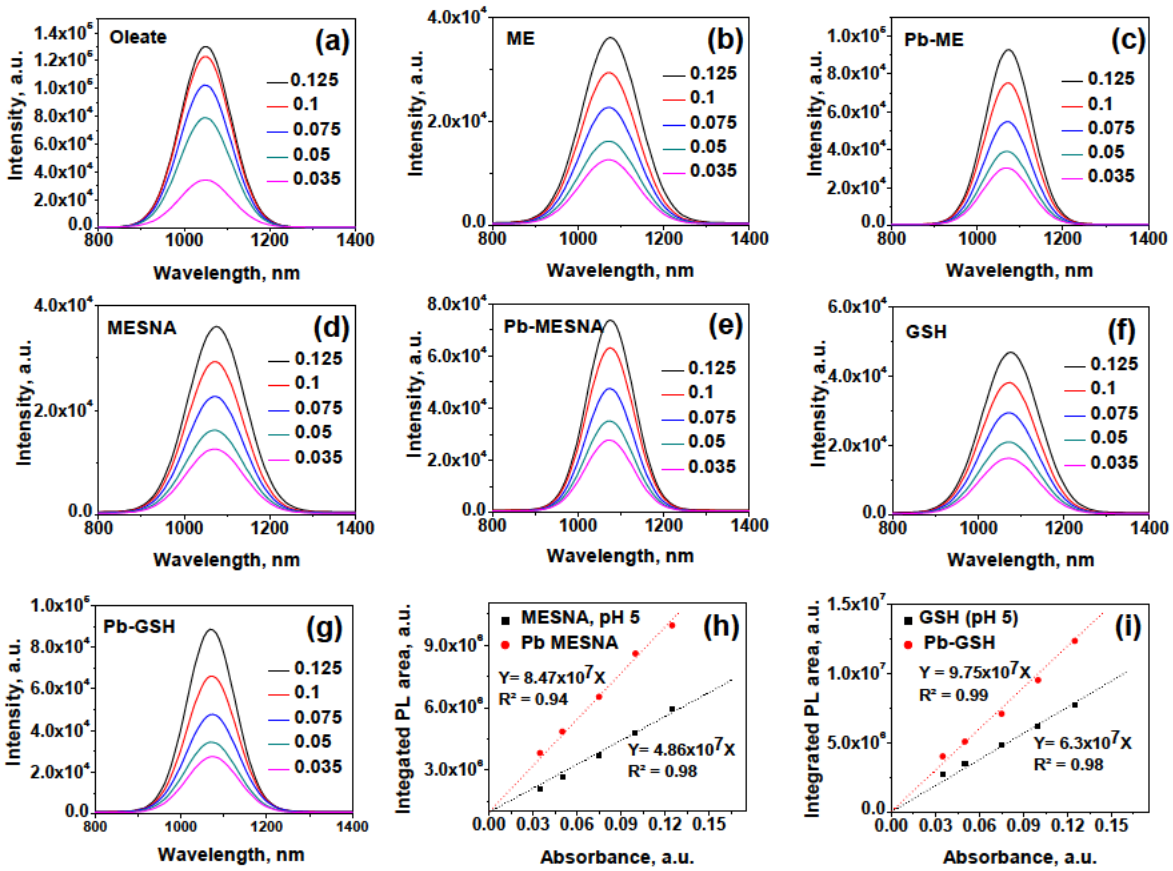

Figure S5-2. PL plots for different concentrations of QDs (the Figures indicate the absorbance of excitonic peak) (a) oleate capped PbS QDs before ligand exchange (b)ME ligand exchange (c) Pb-ME ligand exchange (d) MESNA ligand exchange at pH 5 (e) Pb-MESNA ligand exchange (f) GSH ligand exchange at pH 5 (g) Pb-GSH ligand exchange. Integrated PL area plots at various QDs concentrations for (h) MESNA and Pb-MESNA ligand exchange (i) GSH and Pb-GSH ligand exchange

Chapter 6

Enhancing the stability of pre-synthesized PbS quantum dot sensitized solar cells in polysulfide electrolyte by treating with cadmium salts

Aabhash Shrestha[1], Munkhbayar Batmunkh[1,2], Joe Shapter[2], Shizhang Qiao[1]*, Sheng Dai[1]*

[1]School of Chemical Engineering, The University of Adelaide, Adelaide, SA, 5005, Australia

[2]School of Chemical and Physical Sciences, Flinders University, Bedford Park, Adelaide, SA 5042, Australia

* Corresponding Authors

Email: s.dai@adelaide.edu.au , s.qiao@adelaide.edu.au

To be submitted

Statement of Authorship

Title of Paper	Enhancing the stability of pre-synthesized PbS quantum dot sensitized solar cells in polysulfide electrolyte by treating with cadmium salts
Publication Status	☐ Published ☐ Accepted for Publication ☐ Submitted for Publication ☑ Unpublished and Unsubmitted w ork w ritten in manuscript style
Publication Details	Aabhash Shrestha, Munkhbayar Batmunkh, Joseph G. Shapter*, Shizhang Qiao*, Sheng Dai*, **Enhancing the stability of pre-synthesized PbS quantum dot sensitized solar cells in polysulfide electrolyte by treating with cadmium salts**

Principal Author

Name of Principal Author (Candidate)	Aabhash Shrestha
Contribution to the Paper	Experimental design, performing of the experiments, analysis of the results and writing of the manuscript
Certification:	This paper reports on original research I conducted during the period of my Higher Degree by Research candidature and is not subject to any obligations or contractual agreements with a third party that would constrain its inclusion in this thesis. I am the primary author of this paper.
Signature	Date 04/April/2016

Co-Author Contributions

By signing the Statement of Authorship, each author certifies that:

the candidate's stated contribution to the publication is accurate (as detailed above);

permission is granted for the candidate in include the publication in the thesis; and

the sum of all co-author contributions is equal to 100% less the candidate's stated contribution.

Name of Co-Author	Munkhbayar Batmunkh
Contribution to the Paper	Assisted in performing the solar cell experiments and writing of the manuscript
Signature	Date 08/04/2016

Name of Co-Author	Joseph G. Shapter
Contribution to the Paper	Supervising the development of solar cell work, assisting in the manuscript review and assessment.
Signature	Date 8/4/16

Name of Co-Author	Shizhang Qiao		
Contribution to the Paper	Assisting in the manuscript review and assessment.		
Signature		Date	08/April/2016

Name of Co-Author	Sheng Dai		
Contribution to the Paper	Supervising the development of the work, assisting in the data interpretation, manuscript review and assessment.		
Signature		Date	4/04/2016

Please cut and paste additional co-author panels here as required.

Abstract

Quantum dots (QDs) of lead sulfide (PbS) are promising materials for quantum dot sensitized solar cells (QDSSCs). The efficiency of PbS QDSSCs are comparatively lower as compared to cadmium based QDSSCs. The stability of PbS QDs in various electrolytes limits the usage of pre-synthesized PbS QDs in QDSSCs. We show that the treatment of PbS QD photoelectrode with cadmium chloride enhances PbS QD stability in polysulfide based electrolytes. Treatment with cadmium chloride forms a protection layer of cadmium on PbS QDs surface by forming a protective shell which prevents PbS QDs exposure to polysulfide electrolytes. Further, the PbS QDSSCs is also optimized by varying the number of cycles of CdS and ZnS treatment. As a result, a maximum photoconversion efficiency of 1.77 % can be achieved for the optimized solar cells.

Keywords: PbS QDs, CdSe QDs, CdS, quantum dot sensitized solar cells, polysulfide electrolytes

TOC Figure:

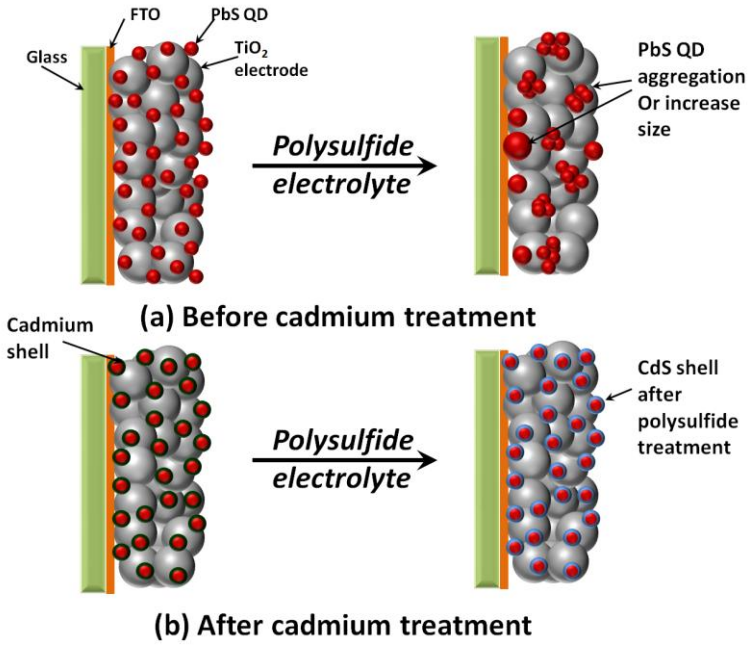

6.1 Introduction

Energy crisis and the associated climate change present major challenge for sustainable future. The third generation solar cells utilizing organic dyes,[1] polymers,[2] quantum dot (QDs)[3, 4] and perovskites[5] can potentially address the current energy related issues owing to their low manufacturing cost, ease of fabrication as well as good performance. Amongst the third generation solar cells, QDs based solar cells are emerging with promising photovoltaic efficiencies.[4, 6] QDs in solar cells offer several advantages such as size tunable band gaps across a wide range of energy levels, high extinction coefficients and enhanced stability.[7]

The QDs of lead sulfide (PbS) are interesting due to their narrow bulk bandgap, large exciton Bohr radii and the possibility of multiple exciton generation.[8] Utilizing these QDs in solar cells with extendable IR absorption is promising. Although quantum dot sensitized solar cells (QDSSCs) with efficiencies ~9 % have been reported for tertinary CdSeTe QDs,[6] the progress for lead chalcogenide QDSSCs has been slow. The highest reported efficiency for lead chalcogenide QDSSCs is ~5.73 % based on in-situ growth of PbS QDs using successive ionic layer adsorption reaction (SILAR).[9] SILAR based QD deposition usually leads into polydispersed QD size distribution and the control over light harvesting is difficult to achieve. In contrast, pre-synthesized QDs allow better control over the light harvesting and are more desirable approach for QD sensitization. However, the maximum efficiency achieved by utilizing pre-synthesized PbS QDs is ~2.67 %.[10] In addition, the photoconversion efficiency (PCE) of the pre-synthesized PbS QDs utilizing bi-functional linker assisted attachment is just 1.1 %.[11] One of the reasons for relatively low efficiencies for pre-synthesized lead chalcogenide QDSSCs is their instability in liquid electrolytes used for making solar cells.[12] Although efforts have been reported on using

solid state hole transport layers (HTL) such as spiro-MeOTAD (N2,N2,N2′,N2′,N7,N7,N7′,N7′-octakis(4-methoxyphenyl)-9,9′-spirobi[9H-fluorene]-2,2′,7,7′-tetramine), they have resulted in an efficiency of 1.5 %.[13] The electron-hole recombination at anode-QDs-HTL interface is identified as the reason for low efficiencies using solid hole transport layers in QDSSCs.[14] Thus, a viable method to enhance the stability of pre-synthesized PbS QD for use in liquid based electrolytes is essential. In this work, we explore the use of bifunctional linker assisted sensitization of pre-synthesized PbS QDs in QDSSCs. We show that the formation of protective cadmium sulfide (CdS) layer after the treatments with cadmium chloride enhances the stability of pre-synthesize QDs in commonly used polysulfide based electrolytes. Furthermore, we optimized the number of cycles of CdS and zinc sulfide (ZnS) treatments to achieve maximum photoconversion efficiency (PCE) of 1.77 %.

6.2 Experimental

6.2.1 Materials

Lead (II) oxide (PbO, 99.99 %), cadmium oxide (CdO, >99.99 %), selenium dioxide (SeO_2, 98 %), hexamethyldisilathiane $(TMS)_2S$, oleic acid (OA, 90 % technical grade), 1-octadecene (ODE, 99.99 %), 3-mercaptopropionic acid (3-MPA, >99 %), L-glutathione reduced (GSH, >98 %), zinc chloride ($ZnCl_2$, >98 %), cadmium chloride ($CdCl_2$, >98 %), cadmium acetate dihydrate ($Cd(CH_3CO)_2.2H_2O$, >98 %), cadmium nitrate ($Cd(NO_3)_2$, 98 %) sodium sulfide nonahydrate (Na_2S, >98 %), sulphur (S, 99.99 %), tetraethyl orthosilicate (TEOS, 98 %), ethylcellulose, potassium chloride (KCl), sodium hydroxide (NaOH), copper sulfate pentahydrate, terpeniol, acetone, ethanol, hexane and heptane were procured from Sigma- Aldrich. All chemicals were used as received.

6.2.2 Synthesis of PbS QDs

PbS QDs were synthesized using a previously described method.[15] Typically, the lead precursor was prepared by heating 178.6 mg (0.8 mmol) of PbO and 0.634 mL (1.6 mmol) oleic acid (OA) in 8 mL 1-octadecene (ODE) in a 100 mL schlenk flask under argon protection at 150 ℃ for 1 hour to obtain a clear yellowish lead oleate solution. The temperature of the lead oleate solution was then reduced to 130 ^{o}C and 84 µl (0.4 mmol) of $(TMS)_2S$ in 4 ml ODA at room temperature was quickly injection into the hot lead precursor solution. The growth temperature was then maintained at ~110 ^{o}C for 10 minutes. The final QDs were precipitated with acetone, centrifuged (~7,000 rpm) and diluted in 15 ml hexane for further use and characterization.

6.2.3 Ligand exchange of PbS QDs

The ligand exchange of PbS QDs was performed using a simple biphasic exchange procedure. 2 mmol of GSH and 1 mmol of $Pb(NO_3)_2$ was dissolved in 5 ml of water and the pH of the resulting solution was adjusted to 12 by adding NaOH. The Pb-GSH complex was then added to 5 ml PbS QDs in hexane. Upon shaking, the PbS QDs were gradually transferred to water phase. The QDs in water phase were precipitated with acetone and re-dispersed in 10 ml of 0.2 M GSH solution at pH 5.

6.2.4 Fabrication of photoelectodes

FTO coated substrates (purchased from Solaronix™) were cleaned by a detergent followed by washing with Milli-Q water, acetone and ethanol under ultrasonication for 10 min each. The cleaned and dried FTO/glass substrates were immersed in a 40 mM $TiCl_4$ aqueous solution for 30 min at 70 ^{o}C. Then nanocrystalline TiO_2 films were prepared from a commercial TiO_2 paste by doctor blading technique using two layer adhesive tape

(Magic™ Tape, 3M), followed by heating under an air flow at 125 ^{o}C for 5 min, 325 ^{o}C for 5 min, at 375 ^{o}C for 5 min and at 450 ^{o}C for 30 min. After cooling to ~50 ^{o}C, TiO_2 coated films were soaked in 40 mM $TiCl_4$ solution at 70 ^{o}C for 30 min and then again sintered at 450 ^{o}C for 30 min. After cooling to room temperature, the prepared TiO_2 photoelectrode films were immersed into the PbS QDs solution for 24 hours.

The PbS QDs sensitized photoelectrodes were immersed in 0.1 M cadmium chloride ($CdCl_2$) solution for 40 min. The photoelectrodes were then rinsed with water and ethanol and dried with compressed air. To form the CdS layer on photoelectrodes, the cadmium treated photoelectrodes were immersed in 0.1 M Na_2S solution for 1 min. Additional cycles of CdS treatment were performed by sequentially dipping the photoelectrodes in 0.1M $CdCl_2$ solution for 1 min and then followed by dipping in 0.1M Na_2S solution for 1 min. The CdS treated photoelectrodes were then coated with ZnS electron blocking layer by sequentially soaking in 0.1 M $ZnCl_2$ solution and 0.1 M Na_2S solution for 2-8 cycles.

6.2.5 Preparation of counter electrodes

For the synthesis of Cu_xS paste, Cu_xS was synthesized by mixing 10 mmol of Na_2S solution with 20 mmol of $CuSO_4$ solution. The resulting blackish precipitate was washed with milli-Q (MQ) water and ethanol for three times each and freeze dried for 24 hrs. 1g of Cu_xS solids were mixed with 10 % ethylcellulose in terpeniol to make a viscous paste of Cu_xS. The prepared catalyst pastes were coated onto the cleaned FTO electrodes via a doctor blade technique, followed by drying in an oven at 90 ^{o}C for 5-10 min. After drying the films, these CEs were further annealed at 420 ^{o}C for 30 min. Pt-CEs were prepared by coating Pt precursor onto FTO substrates using a brush-painting method.

6.2.6 Assembly of QDs based solar cells

The QDs-adsorbed TiO_2 photoelectrodes and counter electrodes were assembled into a sealed sandwich-type cell, with a 60 μm thick hot-melt sealing Surlyn between each layer. The electrolyte solution, Iodolyte Z-50 (Solaronix™) or polysulfide electrolyte was injected into the cell via a vacuum-filling method through an injection hole on the counter electrode side. The polysulfide electrolyte was composed of 2M Na_2S, 2M S and 0.2 M KCl solution in water. For the preparation of polysulfide electrolyte, 2M Na_2S, 2M S and 0.2 M were stirred in water for 24 hrs before use. Finally, the hole at the counter electrode was sealed by tape to prevent possible leakage of electrolyte.

6.2.7 Solar cell characterization

The J–V characteristics were studied using a Keithley 2400 SMU instrument and recorded using a custom LabView Virtual Instrument program. A standard silicon test cell with NIST-traceable certification was used to calibrate the power density as 100 mW cm^{-2} at the sample plane of the collimated xenon-arc light source, which was passed through an AM 1.5 G filter. The active area of each device was 0.28 cm^2.

6.3 Results and discussions

6.3.1 Sensitization of TiO_2 photoelectrodes with pre-synthesized PbS QDs

Oleate capped PbS QDs were synthesized according to the method described by Hines et al.[15] **Figure 6-1(a)** shows the absorption and emission spectra for as-synthesized PbS QDs. The absorption spectra show a sharp excitonic peak at ~940 nm while a narrow emission peak is centered at ~1065 nm. The high resolution transmission electron microscopy (HRTEM) image of as-synthesized QDs displays an average diameter of

2.9±0.1 nm which agrees well with the size calculated using the absorption spectrum (~3nm for absorption peak at 940 nm) (**Figure 6-1(b)**). The ligand exchange of the as-synthesized QDs was performed using a simple bi-phasic transfer procedure and L-glutathione (GSH) as the exchanging ligand. Upon vigorous shaking, the oleate capped PbS QDs are transferred from the non-polar hexane to water phase. A typical bathochromic shift (~25 nm) of the absorption and emission spectrum is observed upon the phase transfer of PbS QDs to water due to the contribution of S^{3p} orbital of the thiol ligands to the higher occupied states of ligand-QD systems.[16] (**Figure 6-1(a)**). FTIR spectra of PbS QDs before and after the ligand exchange shows that the typical IR absorbance from the C-H (2850-3000 cm^{-1}) vibrations of the oleate ligands disappears completely after the ligand exchange and the new IR absorbance corresponding to the N-H stretch (3500-3300 cm^{-1}), N-H bend (1560-1640 cm^{-1}) and C-N stretch (1000-1350 cm^{-1}) appears indicating the successful exchange of oleate with GSH (**Figure 6-1(c)**).

TiO_2 photoelectrodes were sensitized with PbS QDs by immersing the photoelectrodes into the GSH capped PbS QDs solution at pH 5 for 24 hrs. GSH has multiple chelating groups and are strongly bound to the surface Pb atoms of PbS QDs via thiolate-metal bond. The carboxylate group of GSH interacts with TiO_2 surface for adsorption of PbS QDs onto photoelectrodes. Upon sensitization with PbS QDs, the color of TiO_2 photoelectrodes changes from semi-transparent to deep brown indicating the adsorption of PbS QDs onto TiO_2 (**Figure 6-1(d)**). Furthermore, the absorption spectrum of PbS QDs sensitized photoelectrode shows a sharp excitonic peak at 960 nm similar to that of the GSH capped PbS QDs in water indicating the successful sensitization of PbS QDs. Similarly, the TiO_2 photoelectrodes were also sensitized with the reference CdSe QDs capped with

mercaptopropionic acic (MPA) using the procedure described in **Section S6-2**.(**Figure S6-1**)[17]

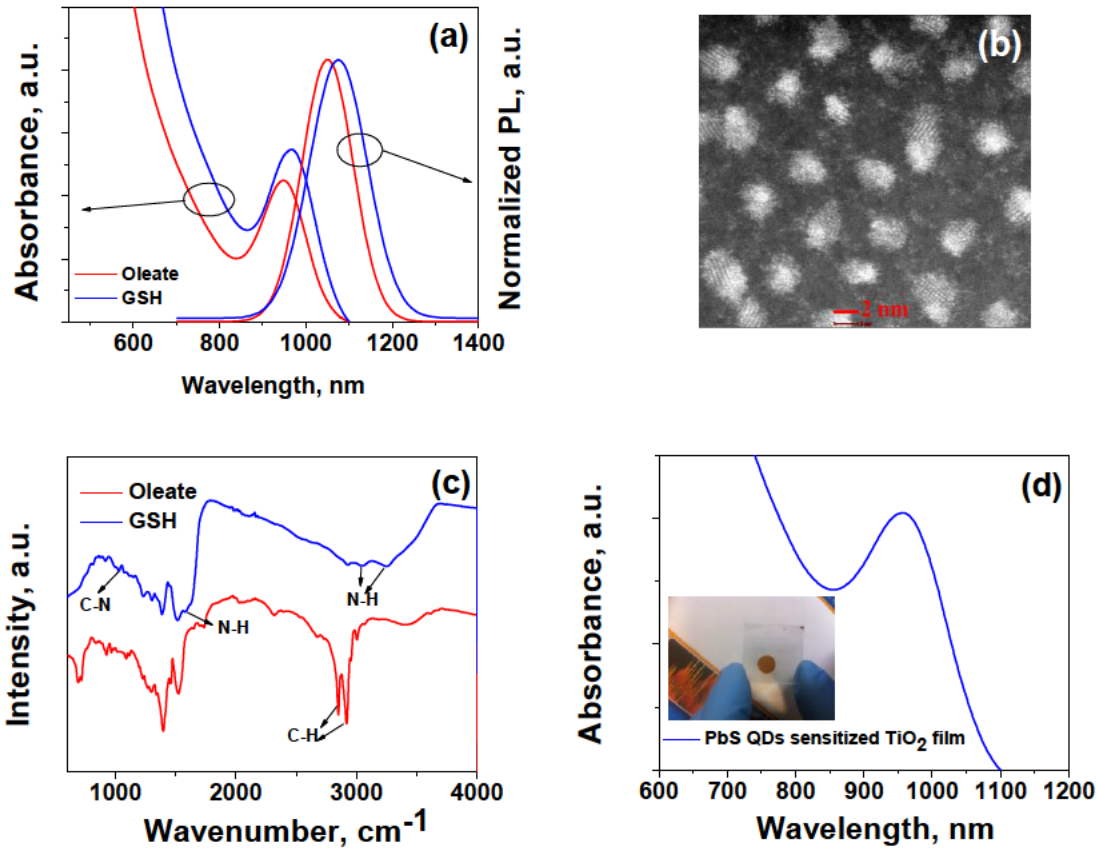

Figure 6-1. (a) Absorption and emission spectra for PbS QDs before and after ligand exchange using GSH (b) HRTEM image of oleate capped PbS QDs (c) FTIR spectra for oleate and GSH exchanged PbS QDs (d) absorption spectrum for PbS QDs sensitized TiO_2 photoelectrode. Figure in the inset shows the photograph of PbS QDs sensitized TiO_2 photoelectrode

6.3.2 Electrolytes for QDs based solar cells

Two different electrolytes were chosen for PbS QDs sensitized solar cells- (i) a tri-iodide electrolyte typically employed in DSSCs and (ii) an aqueous polysulfide electrolyte. The tri-iodide electrolyte employed platinum (Pt) on FTO as the counter electrode while the polysulfide electrolyte employed copper sulfide (Cu_xS) film on FTO as the counter

electrode. **Figure S6-2(a)** shows the current density-voltage (J-V) curve for PbS QDSSCs utilizing the tri-iodide based electrolytes. Although the open circuit voltage (V_{oc} ~ 0.65) and the fill factor (FF ~ 0.8) for PbS QDSSCs employing tri-iodide electrolytes are reasonable, current density (J_{sc}) for the cells are very low. The color of PbS QDs sensitized photoelectrode changed from dark brown to the original semi-transparent upon exposure to tri-iodide electrolyte (**Figure S6-2(b)**) indicating that the PbS QDs could either detach from the TiO_2 substrate or dissolve upon exposure to tri-iodide electrolytes. To further understand the influence of tri-iodide treatment on PbS QDs sensitized TiO_2 photoelectrodes, PbS QDs were in-situ deposited using the SILAR approach. Upon exposure of SILAR generated PbS-SILAR QDs sensitized TiO_2 photoelectrodes to tri-iodide electrolytes, similar phenomenon of color change from dark brown to colorless is observed. Since the SILAR generated PbS-SILAR QDs are adsorbed onto TiO_2 photoelectrodes without any molecular linkers, the exposure of tri-iodide electrolytes cannot induce desorption of QDs from TiO_2 substrates. The tri-iodide electrolytes are known to be corrosive to cadmium chalcogenide based QDs and has shown to induce the etching of these QDs.[12, 18] Thus, it is plausible that the exposure of PbS QDs to tri-iodide electrolyte can cause severe etching of PbS QDs and induce the dissolution of QDs.[12] The exposure tri-iodide treated PbS QD photoelectrodes to sodium sulfide again changed the color of photoelectrodes to deep brown indicating that the tri-iodide dissolves the PbS QDs to its corresponding salts. These observations indicate that the tri-iodide electrolytes are not a suitable electrolyte for the PbS QDSSCs.

On the other hand, aqueous polysulfide electrolytes have shown good performance for in-situ SILAR grown PbS and cadmium based QDSSCs. [9, 17] **Figure S6-3** shows the J-V curve for our pre-synthesized PbS QDSSCs utilizing polysulfide based electrolytes. The

photo conversion efficiency (PCE) for our pre-synthesized PbS QDSSCs shows poor efficiency as compared to the reference CdSe QDSSCs. Both the J_{sc} and V_{oc} for the cells are much lower. To understand the reason for low performance of such cells, PbS QDs sensitized photoelectrodes were exposed to polysulfide electrolytes and their absorption spectra were measured. **Figure S6-4** shows the absorption spectra for PbS QDs photoelectrode before and after exposure to polysulfide electrolyte. The excitonic absorption features for PbS QDs completely disappears and the color of PbS QDs sensitized photoelectrodes becomes darker upon exposure to the polysulfide electrolyte. The polysulfide electrolytes are composed of chalcogenide anions (Na_2S) and elemental sulfur. Recently, the metal chalcogenide complex (MCC) and the metal free chalcogenides anions have been seen as good inorganic ligands for PbS QDs.[19] Additionally, treating the thin films of lead chalcogenide (PbS and PbSe) QDs with chalcogenides such as Na_2S fused the QDs into ordered thin film solids.[20] The exposure of PbS QDs sensitized photoelectrode to polysulfide electrolytes can thus potentially replace GSH leading to QD agglomeration. The absence of any distinct excitonic features and darkening of QDs film upon exposure to polysulfide electrolytes also indicate that the polysulfide electrolytes induced agglomeration of QDs and increase QD size.[20] Previous studies have shown that the electron injection from PbS QDs to TiO_2 becomes unfavorable as the QDs size becomes larger than 4 nm.[21] The increase in PbS QDs size upon exposure to polysulfide electrolytes can thus lead to the inefficient electron injection to TiO_2 photoelectrode and lower the performance. Even the addition of ZnS protection layer by sequentially dipping the photolectrodes into the Zn^{2+} and S^{2-} ion solution does not preserve the excitonic features of PbS QDs. Exposure of the reference CdSe QDs photoelectrodes to polysulfide electrolytes does not show any distinct change in their excitonic spectral features (**Figure**

S6-1(b)) and the PCE of 3.02 % can be achieved for CdSe QDSSCs (**Figure S6-3**). These observations show that the cadmium cations are more stable to polysulfide electrolytes than lead cations and the protection of PbS QDs with cadmium shell can potentially improve the performance of PbS QDSSCs.

6.3.3 Treatment with cadmium sulfide to improve the stability

To improve the stability of pre-synthesized PbS QDs upon exposure to polysulfide electrolytes, PbS QDs sensitized photoelectrodes were treated with cadmium chloride ($CdCl_2$) solution. **Figure 6-2(a)** shows the absorption spectra of PbS QDs sensitized photoelectrode upon exposure to $CdCl_2$ solution. The treatment of PbS QDs photoelectrode with $CdCl_2$ solution induces the progressive blue shift in the excitonic absorption features. The blue shift of the excitonic peak saturates at longer exposure times (>30 mins) and does not change significantly thereafter.

The $CdCl_2$ solution is composed of cadmium cations and chloride anions. The cadmium cations are known to replace the surface lead cations to form PbS/CdS core-shell structures.[22] On the other hand, the chloride anions are also known to act as inorganic ligands for PbS QDs.[23] In order to isolate the influence of cadmium cations from its anion counterparts, three types of cadmium salts viz. cadmium chloride, cadmium acetate and cadmium nitrate were chosen as a cadmium source. The interaction of the various cadmium anions with PbS QDs follows the order chloride>acetate>nitrate.[23] As shown in **Figure S6-5**, the type of anion species do not have significant influence on the evolution of excitonic absorption features of PbS QDs and a similar blue shift in absorption spectra can be observed for all cadmium salts. These results show that the cadmium cations replace the

surface lead atoms and can form a layer of cadmium on the surface of PbS QD photoelectrodes.

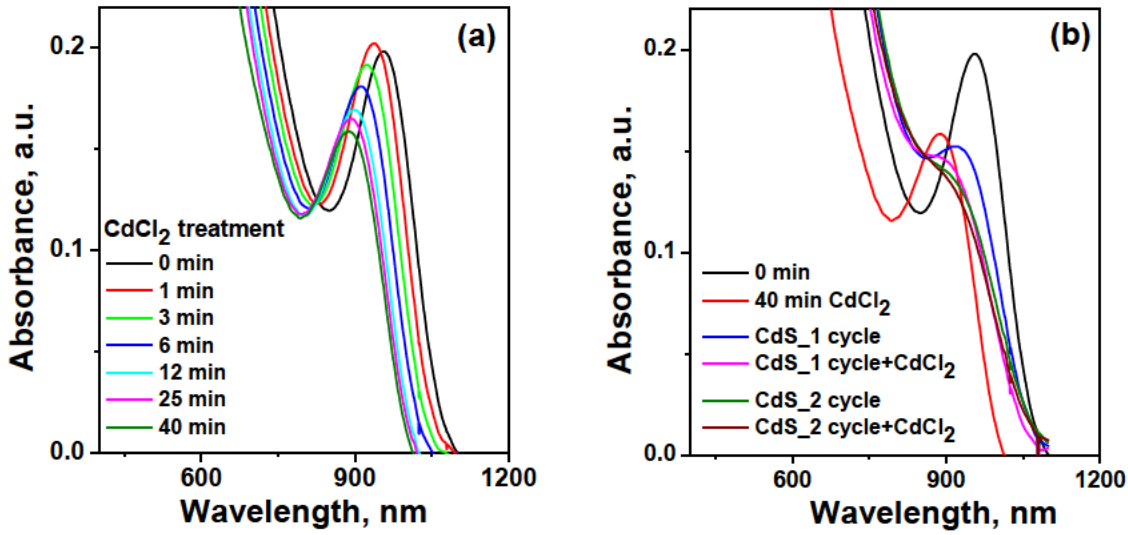

Figure 6-2. (a) Temporal evolution of absorption spectra for PbS QDs sensitized photoelectrode upon treatment with $CdCl_2$ (b) absorption spectra of PbS QDs sensitized photoelectrode upon various cycles of cadmium and sulfide treatments.

Upon exposure of cadmium treated PbS QDs photoelectrode to sulfide anions (i.e. Na_2S solution), the excitonic absorption peak red shifts again due to the formation of CdS layer on the surface. Although the excitonic absorption features of cadmium treated PbS QDs diminishes after sulfide treatment, the excitonic peak of PbS QDs after sulfide treatment can be distinctly resolved. Upon subsequent treatment of additional CdS layers, the excitonic peak of PbS QDs are still well-preserved indicating that the initial treatment with cadmium salt is essential for preserving the excitonic features of PbS QD photoelectrodes.

6.3.4 Photovoltaic characteristics of cadmium sulfide (CdS) treated PbS QDSSCs

To study the PV characteristics of cadmium treated PbS QDSSCs, different cells with and without CdS treatment was prepared. **Figure 6-3(a)** shows the J-V curve for the various cycles of CdS treated PbS QDSSCs with the aqueous polysulfide solution as the electrolyte and the Cu_xS as the counter electrode. For a comparison, PbS QDSSCs without cadmium treated cells (only ZnS treatment) is also presented. The PCE of the CdS treated PbS QDSSCs is enhanced up to 1.77 % (8 cycles of CdS) as compared to 0.14 % for the cells without cadmium treatment. The enhancement in both the J_{sc} and V_{oc} can be observed for CdS treated cells. The reference PbS QDSSCs without any surface treatment (i.e. no CdS and ZnS) showed the PCE of 0.02 %.

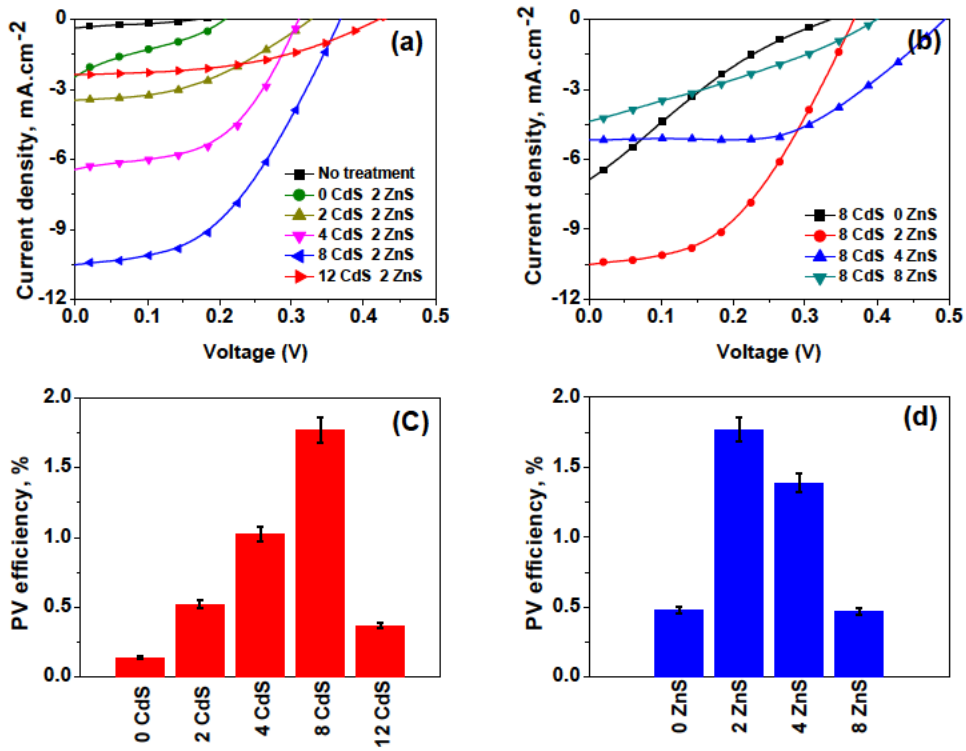

Figure 6-3. (a) J-V curve for PbS QDSSCs for various cycles of CdS treatments (b) J-V curve for various cycles of ZnS treatments (c) PCE plot for various cycles of CdS treatments (d) PCE plot for various cycles of ZnS treatments

The number of cycles of CdS and ZnS treatment also influences the PCE of PbS QDSSCs. As the number of cycles for CdS treatment is increased, the coverage of CdS layers on PbS QDs are increased. To study the influence of CdS treatment on PCE, four different cells with different cycles of CdS treatments (2, 4, 8 and 12 cycles) are compared and their PCE is plotted in **Figure 6-3(b)**. The corresponding photovoltaic parameters are listed in **Table 6-1**.The number of ZnS treatment is kept constant in all these cells (i.e. 2 cycles of ZnS). Increasing the cycle of CdS treatment increased the PCE of cells. The enhancement in PCE with increasing CdS treatment is due to the protection of PbS QDs from polysulfide electrolytes. However, the PCE of cells decrease rapidly once the CdS treatment exceeds 8 cycles. As shown in **Scheme 6-1**, CdS forms Type II core/shell structure with PbS QDs. When the thickness of CdS shell is relatively low, the electron injection from the PbS QDs to TiO_2 is not hindered. As the thickness of CdS layer grows, it can potentially block the efficient injection of electrons to TiO_2 photoelectrode and thus lowering the performance of the cells. In addition to decrease in electron injection, higher thickness of CdS can also potentially block the hole transfer process. As a result, we see that the J_{sc} of the cells starts to suffer upon increasing the CdS treatment beyond 8 cycles.

Table 6-1. Summary of PV parameters for various cycles of CdS and ZnS treatments

Treatments	J_{sc}, mA.cm^{-2}	V_{oc}, V	FF	PCE (%)
0 CdS + 0 ZnS	0.352	0.166	0.30	0.02
0 CdS + 2 ZnS	2.423	0.208	0.27	0.14
2 CdS + 2 ZnS	3.454	0.327	0.42	0.48
4 CdS + 2 ZnS	6.415	0.312	0.51	1.02
8 CdS + 2 ZnS	10.528	0.368	0.46	1.77
12 CdS +2 ZnS	2.351	0.420	0.46	0.46
8 CdS + 0 ZnS	6.892	0.335	0.21	0.47
8 CdS + 4 ZnS	5.159	0.494	0.54	1.39
8 CdS + 8 ZnS	4.367	0.402	0.30	0.52

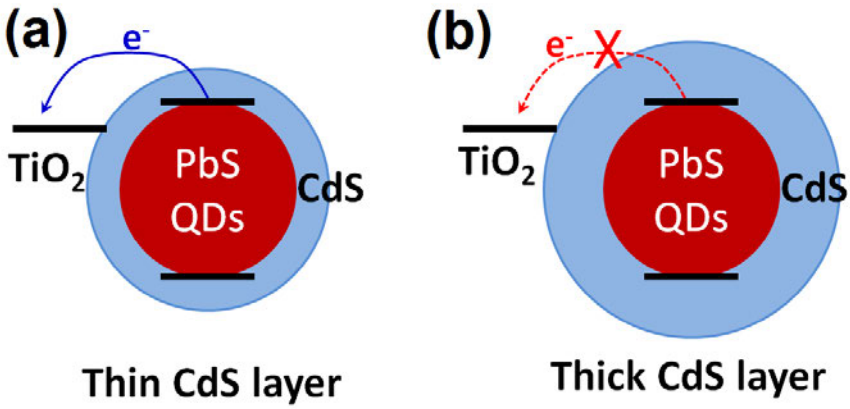

Scheme 6-1. Influence of CdS treatment (a) Less barrier for electron injection from PbS QDs to TiO_2 at low cycles of CdS treatment (b) at higher cycles of CdS treatment, electron injection is hindered.

Zinc sulfide (ZnS) electron blocking layer is normally employed in QDSSCs to block the back transfer of electrons from the TiO_2 to electrolyte.[24] The thickness of ZnS blocking layer also influences the PCE of PbS QDSSCs. Four different cycles of ZnS treatment (0, 2, 4 and 8 cycles) are compared to optimize the solar cells (**Figure 6-3(c) and 6-3(d)**). The number of CdS treatment is kept constant to evaluate the influence of ZnS treatments (i.e. 8 cycles of CdS treatment). As compared to cells without ZnS blocking layer, the cells with ZnS layer significantly enhanced the PCE of PbS QDSSCs. As shown in **Figure 6-3(d)**, the cells without ZnS treatment show the PCE of 0.48 % while the cells with 2 cycles of ZnS treatment show the maximum PCE of 1.77 %. Upon further increasing the number of ZnS cycles, the PCE again starts to decrease. As shown in **Scheme 6-2**, the conduction band of ZnS is above the conduction band of the PbS QDs and can efficiently act to block the recombination of electron with the electrolytes. However, the valence band of ZnS also lies below the valence band of PbS QDs and a higher thickness of ZnS can create a barrier for regeneration of QDs, thus lowering the performance.[24]

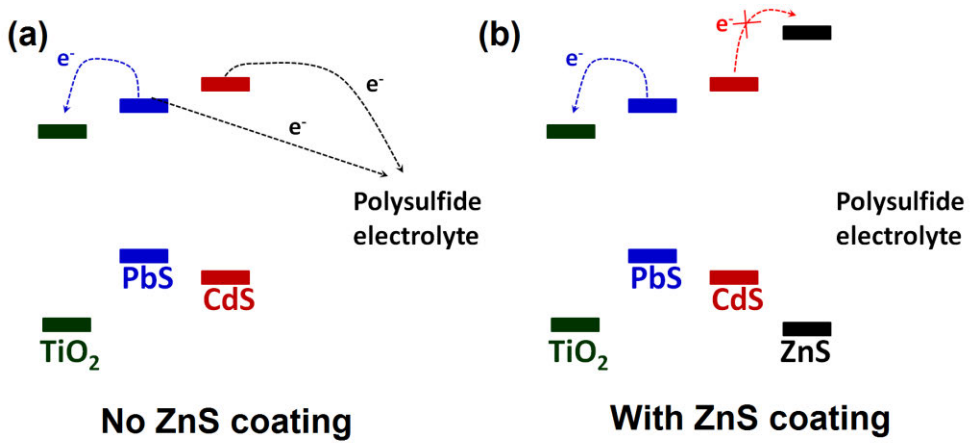

Scheme 6-2. Influence of ZnS treatment (a) with no treatment back transfer of electrons to electrolyte (b) with ZnS treatment, back transfer of electrons is hindered

6.4 Conclusion

In conclusion, PbS QDs without surface treatment is unstable in most commonly used electrolytes such as tri-iodide and polysulfide electrolytes. The stability of PbS QDs in polysulfide electrolytes can be improved by treating the sensitized photoelectrodes with cadmium salts. Treatment with cadmium salts forms a protection layer of cadmium on PbS QDs surface which prevents the PbS QDs from exposure to polysulfide electrolytes. Further, the numbers of cycles of CdS and ZnS treatments are optimized for PbS QDSSCs, and a maximum PCE of 1.77 % can be achieved for optimized solar cells.

Acknowledgements

This work was financially supported by the Australian Research Council Discovery Projects DP110102877, DP140104062 and DP160104632

References

[1] (a) X. Dang, H. Yi, M.-H. Ham, J. Qi, D. S. Yun, R. Ladewski, M. S. Strano, P. T. Hammond, A. M. Belcher, *Nat. Nanotechnol.* 2011, 6, 377; (b) B. E. Hardin, H. J. Snaith, M. D. McGehee, *Nat. Photon*. 2012, 6, 162; (c) S. Mathew, A. Yella, P. Gao, R. Humphry-Baker, F. E. CurchodBasile, N. Ashari-Astani, I. Tavernelli, U. Rothlisberger, K. NazeeruddinMd, M. Grätzel, *Nat. Chem.* 2014, 6, 242.

[2] (a) L. Lu, L. Yu, *Adv. Mater.* 2014, 26, 4413; (b) Z. He, C. Zhong, S. Su, M. Xu, H. Wu, Y. Cao, *Nat. Photon.* 2012, 6, 591.

[3] (a) A. H. Ip, S. M. Thon, S. Hoogland, O. Voznyy, D. Zhitomirsky, R. Debnath, L. Levina, L. R. Rollny, G. H. Carey, A. Fischer, K. W. Kemp, I. J. Kramer, Z. Ning, A. J. Labelle, K. W. Chou, A. Amassian, E. H. Sargent, *Nat. Nanotechnol.* 2012, 7, 577; (b) G. H. Carey, L. Levina, R. Comin, O. Voznyy, E. H. Sargent, *Adv. Mater.* 2015, 27, 3325.

[4] G.-H. Kim, F. P. García de Arquer, Y. J. Yoon, X. Lan, M. Liu, O. Voznyy, Z. Yang, F. Fan, A. H. Ip, P. Kanjanaboos, S. Hoogland, J. Y. Kim, E. H. Sargent, *Nano Lett.* 2015, 15, 7691.

[5] M. A. Green, A. Ho-Baillie, H. J. Snaith, *Nat. Photon*. 2014, 8, 506.

[6] J. Yang, J. Wang, K. Zhao, T. Izuishi, Y. Li, Q. Shen, X. Zhong, *J. Phys. Chem. C* 2015, 119, 28800.

[7] E. H. Sargent, *Nat. Photon*. 2012, 6, 133.

[8] (a) R. J. Ellingson, M. C. Beard, J. C. Johnson, P. Yu, O. I. Micic, A. J. Nozik, A. Shabaev, A. L. Efros, *Nano Lett*. 2005, 5, 865; (b) A. J. Nozik, M. C. Beard, J. M. Luther, M. Law, R. J. Ellingson, J. C. Johnson, *Chem. Rev*. 2010, 110, 6873.

[9] S. D. Sung, I. Lim, P. Kang, C. Lee, W. I. Lee, *Chem. Commun*. 2013, 49, 6054.

[10] X. Li, W. Lu, Y. Wang, Y. Fang, L. Wang, Q. Ai, X. Zhou, Y. Lin, *Electrochimica Acta* 2014, 144, 71.

[11] A. N. Jumabekov, F. Deschler, D. Böhm, L. M. Peter, J. Feldmann, T. Bein, *J. Phys. Chem. C* 2014, 118, 5142.

[12] G. Niu, L. Wang, R. Gao, B. Ma, H. Dong, Y. Qiu, *J. Mater. Chem.* 2012, 22, 16914.

[13] H. Lee, H. C. Leventis, S.-J. Moon, P. Chen, S. Ito, S. A. Haque, T. Torres, F. Nüesch, T. Geiger, S. M. Zakeeruddin, M. Grätzel, M. K. Nazeeruddin, *Adv. Func. Mater*. 2009, 19, 2735.

[14] K. E. Roelofs, S. M. Herron, S. F. Bent, *ACS Nano* 2015, 9, 8321.

[15] M. A. Hines, G. D. Scholes, *Adv. Mater.* 2003, 15, 1844.

[16] C. Giansante, I. Infante, E. Fabiano, R. Grisorio, G. P. Suranna, G. Gigli, *J. Am. Chem. Soc.* 2015, 137, 1875.

[17] H. Zhang, K. Cheng, Y. M. Hou, Z. Fang, Z. X. Pan, W. J. Wu, J. L. Hua, X. H. Zhong, *Chem. Commun*. 2012, 48, 11235.

[18] Y.-L. Lee, C.-H. Chang, *J. Power Sources* 2008, 185, 584.

[19] M. V. Kovalenko, M. Scheele, D. V. Talapin, Science 2009, 324, 1417; M. V. Kovalenko, M. I. Bodnarchuk, J. Zaumseil, J. S. Lee, D. V. Talapin, *J. Am. Chem. Soc.* 2010, 132, 10085.

[20] S. J. Oh, N. E. Berry, J.-H. Choi, E. A. Gaulding, H. Lin, T. Paik, B. T. Diroll, S. Muramoto, C. B. Murray, C. R. Kagan, *Nano Lett*. 2014, 14, 1559.

[21] B.-R. Hyun, Y.-W. Zhong, A. C. Bartnik, L. Sun, H. D. Abruña, F. W. Wise, J. D. Goodreau, J. R. Matthews, T. M. Leslie, N. F. Borrelli, *ACS Nano* 2008, 2, 2206.

[22] J. M. Pietryga, D. J. Werder, D. J. Williams, J. L. Casson, R. D. Schaller, V. I. Klimov, J. A. Hollingsworth, *J. Am. Chem. Soc.* 2008, 130, 4879.

[23] D. N. Dirin, S. Dreyfuss, M. I. Bodnarchuk, G. Nedelcu, P. Papagiorgis, G. Itskos, M. V. Kovalenko, *J. Am. Chem. Soc.* 2014, 136, 6550.

[24] C. Shen, D. Fichou, Q. Wang, *Chem. Asian J.* 2016.

Supporting Information

Enhancing the stability of pre-synthesized PbS quantum dot sensitized solar cells in polysulfide electrolyte by treating with cadmium salts

Aabhash Shrestha[1], Munkhbayar Batmunkh[1,2], Joe Shapter[2], Shizhang Qiao[1]*, Sheng Dai[1]*

[1]School of Chemical Engineering, The University of Adelaide, Adelaide, SA, 5005, Australia

[2]School of Chemical and Physical Sciences, Flinders University, Bedford Park, Adelaide, SA 5042, Australia

* Corresponding Authors

Email: s.dai@adelaide.edu.au , s.qiao@adelaide.edu.au

Section S6-1. Synthesis of CdSe QDs

CdSe QDs were synthesized using a modification to previously described method. Briefly, 0.6 mmol of CdO was heated with 1.5 mmol of OA in 40 ml ODE at 200 ^{o}C for 30 mins to form cadmium oleate, $Cd(OA)_2$ solution. Then, 0.6 mmol of SeO_2 was added to the $Cd(OA)_2$ solution and degassed at room temperature using a vacuum pump of 30 mins and re-filled with argon. The resulting solution was heated from the room temperature to 240 ^{o}C in a sand bath and the growth temperature was maintained at 240 ^{o}C for 15 min. The resulting QDs were cooled to room temperature, precipitated with acetone, centrifuged at 8000 rpm and re-dispered in 10 ml hexane. The washing cycle was repeated for three times.

Section S6-2. Ligand exchange and sensitization of CdSe QDs

The ligand exchange of CdSe QDs was performed using 3-mercaptopropionic acid (MPA) as the exchanging ligand. Briefly, the QDs solution in hexane was diluted with 10 fold volume of chloroform and 1 mmol of 3-MPA solution (pH adjusted to 11) was added to the QDs solution. The resulting solution was stirred at room temperature for 30 min and 10 ml of water was added to the solution. Upon gentle shaking, QDs were transferred to water phase. The MPA capped QDs were precipitated with acetone and centrifuged at 8000 rpm for 5 mins. Finally, the MPA capped QDs were re-dispersed in 10 ml of 0.2 M MPA solution at pH 10.

For the sensitization of TiO_2 photoelectrodes, the photoelectrode films were immersed into the CdSe QD solution for 24 hours. The QDs sensitized TiO_2 photoelectrodes were further coated with ZnS electron blocking layer by sequentially soaking in 0.1 M $ZnCl_2$ solution and 0.1 M Na_2S solution for 2 cycles.

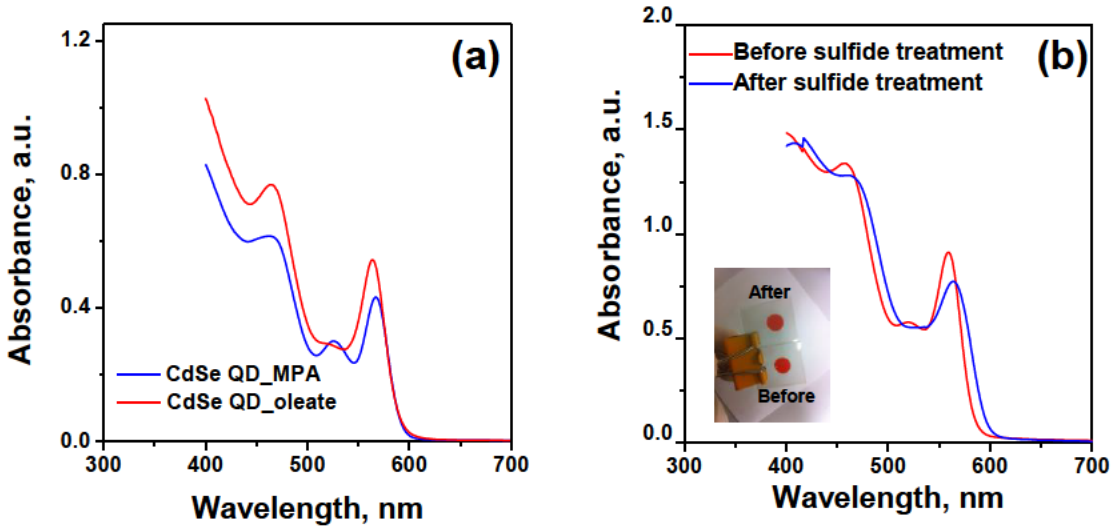

Figure S6-1. Absorption spectra of (a)CdSe QDs before and after ligand exchange using MPA (b) CdSe QD sensitized photoelectrodes before and after treatment with polysulfide electrolytes. Inset shows the photographs before and treatment with polysulfide electrolytes.

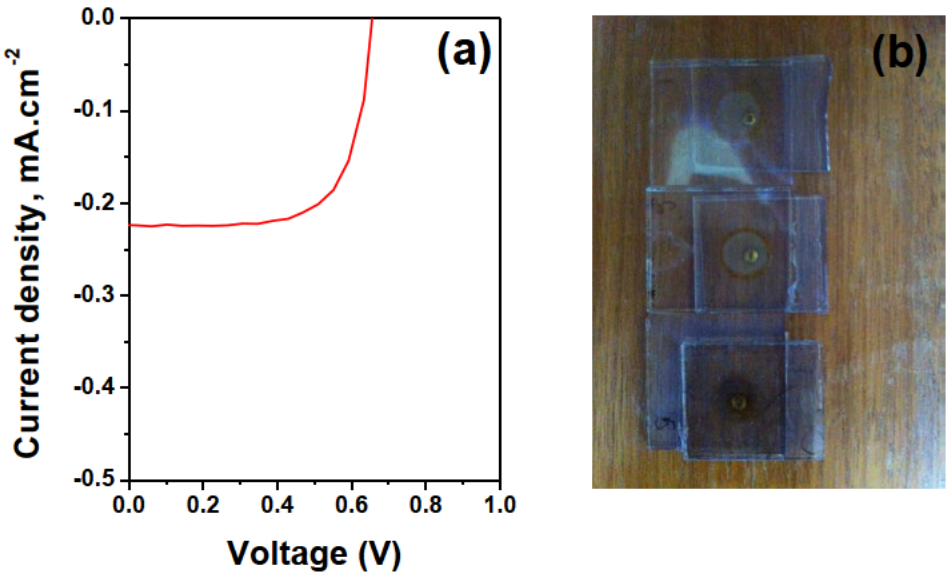

Figure S6-2. (a) J-V curve for PbS QDSSCs with tri-iodide electrolyte (b) Photographs of PbS QDSSCs with tri-iodide electrolytes. Tri-iodide electrolytes dissolve the PbS QDs.

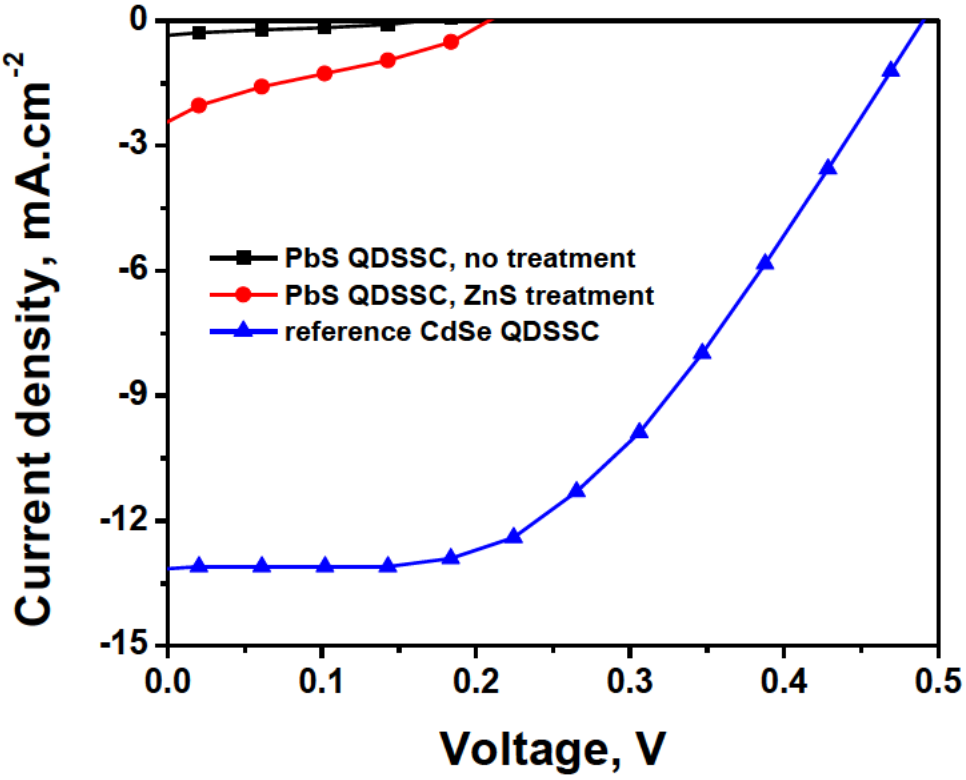

Figure S6-3. J-V curve for PbS and CdSe QDSSCs using polysulfide electrolytes

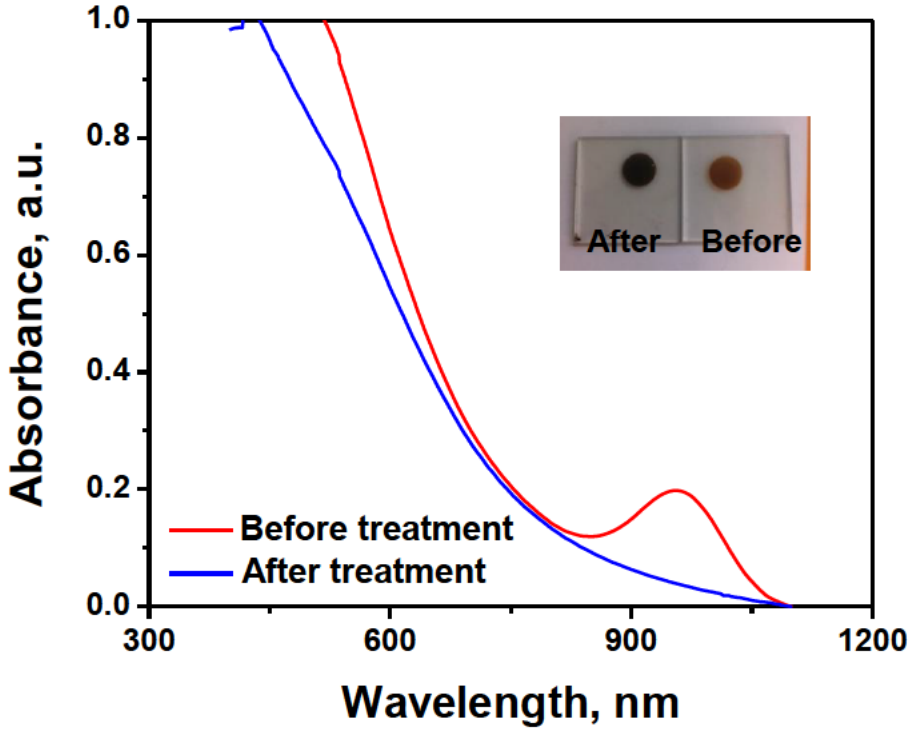

Figure S6-4. Absorption spectra of PbS QDs sensitized photoelectrodes before and after treatment with polysulfide electrolytes

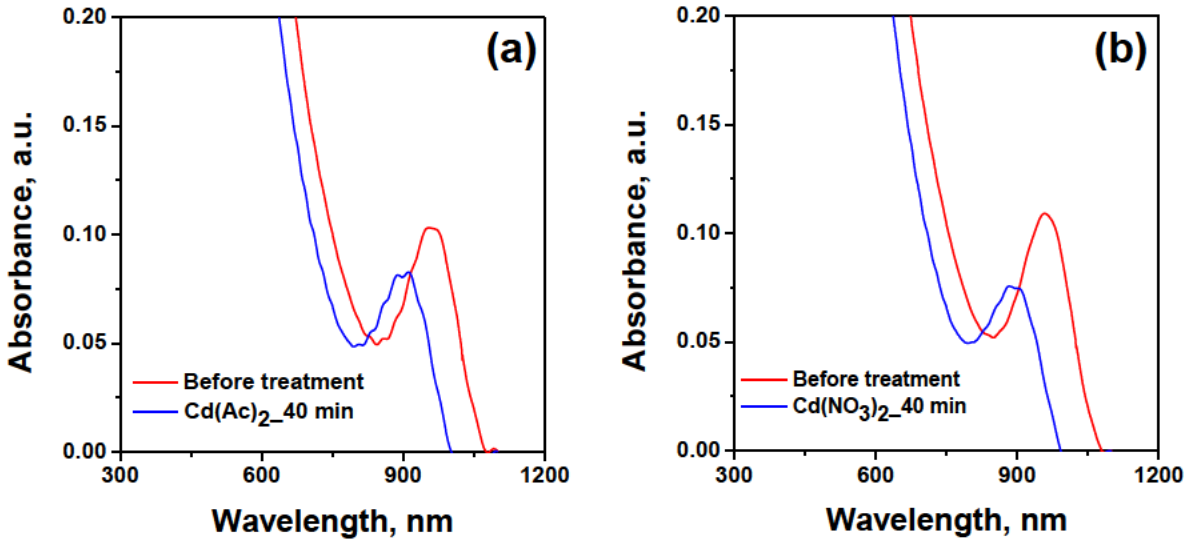

Figure S6-5. Absorption spectra of PbS QDs sensitized photoelectrodes before and after 40 min treatment with (a) $Cd(Ac)_2$ (b) $Cd(NO_3)_2$

Chapter 7

Nitrogen-doped CN_x/CNTs hetero-electrocatalysts for highly efficient dye sensitized solar cells

Aabhash Shrestha[1], Munkhbayar Batmunkh[1,2], Cameron J. Shearer[2], Yanting Yu[2], Gunther Andersson[2], Joseph G. Shapter[2]*, Shizhang Qiao[1]*, Sheng Dai[1]*

[1] School of Chemical Engineering, The University of Adelaide, Adelaide, SA, 5005, Australia

[2] School of Chemical and Physical Sciences, Flinders University, Bedford Park, Adelaide, SA 5042, Australia

* Corresponding Authors

Email: s.dai@adelaide.edu.au , s.qiao@adelaide.edu.au , joe.shapter@flinders.edu.au

To be submitted to Journal Advanced Energy Materials

Statement of Authorship

Title of Paper	Nitrogen-doped CN_x/CNTs hybrid electrocatalysts for highly efficient dye sensitized solar cells
Publication Status	☐ Published ☐ Accepted for Publication ☐ Submitted for Publication ☑ Unpublished and Unsubmitted w ork w ritten in manuscript style
Publication Details	Aabhash Shrestha, Munkhbayar Batmunkh, Cameron J. Shearer, Yanting Yu, Gunther Andersson, Joseph G. Shapter*, Shizhang Qiao*, Sheng Dai*, **Nitrogen-doped CN_x/CNTs hybrid electrocatalysts for highly efficient dye sensitized solar cells**

Principal Author

Name of Principal Author (Candidate)	Aabhash Shrestha
Contribution to the Paper	Experimental design, performing of the experiments, analysis of the results and writing of the manuscript
Certification:	This paper reports on original research I conducted during the period of my Higher Degree by Research candidature and is not subject to any obligations or contractual agreements with a third party that would constrain its inclusion in this thesis. I am the primary author of this paper.
Signature	Date: 04/April/2016

Co-Author Contributions

By signing the Statement of Authorship, each author certifies that:

the candidate's stated contribution to the publication is accurate (as detailed above);

permission is granted for the candidate in include the publication in the thesis; and

the sum of all co-author contributions is equal to 100% less the candidate's stated contribution.

Name of Co-Author	Munkhbayar Batmunkh
Contribution to the Paper	Assisted in performing the solar cell experiments and writing of the manuscript
Signature	Date: 08/04/2016

Name of Co-Author	Cameron J. Shearer
Contribution to the Paper	Assistance in electrochemical impedance spectroscopy and assessment.
Signature	Date: 11/4/16

Name of Co-Author	Yanting Yu
Contribution to the Paper	Assistance in X-ray photoelectron spectroscopy and assessment.
Signature	Date 08/04/2016

Name of Co-Author	Gunther Andersson
Contribution to the Paper	Assistance in X-ray photoelectron spectroscopy and assessment.
Signature	Date 08/04/2016

Name of Co-Author	Joseph G. Shapter
Contribution to the Paper	Supervising the development of solar cell work, assisting in the manuscript review and assessment.
Signature	Date 8/4/16

Name of Co-Author	Shizhang Qiao
Contribution to the Paper	Assisting in the manuscript review and assessment.
Signature	Date 09/April/2016

Name of Co-Author	Sheng Dai
Contribution to the Paper	Supervising the development of the work, assisting in the data interpretation, manuscript review and assessment.
Signature	Date 4/04/2016

Please cut and paste additional co-author panels here as required.

Abstract

The use of polydopamine (PDA) as a nitrogen containing precursor to generate catalytically active N-doped carbon (CN_x) materials on carbon nanotubes (CNTs) is reported. These N-doped CN_x/CNT materials display excellent electrocatalytic activity towards the reduction of tri-iodide electrolyte in dye-sensitized solar cells (DSSCs). Further, the influence of various synthesis parameters on the catalytic performance of CN_x/CNTs is also investigated in detail. The best performing device fabricated with the CN_x/CNTs material delivers power conversion efficiency (PCE) of 7.3 %, which is comparable or slightly higher than that of Pt (7.1 %) counter electrode (CE) based DSSC. The PCE obtained using these CN_x/CNTs are comparable to the best efficiencies obtained for literature reported CE materials till date. These CN_x/CNTs materials show great potential to substitute expensive and rare Pt electrocatalyst for high efficiency DSSC devices.

Keywords: dye sensitized solar cells (DSSCs), nitrogen doping, electrocatalyst, carbon nanotubes, polydopamine

TOC Figure

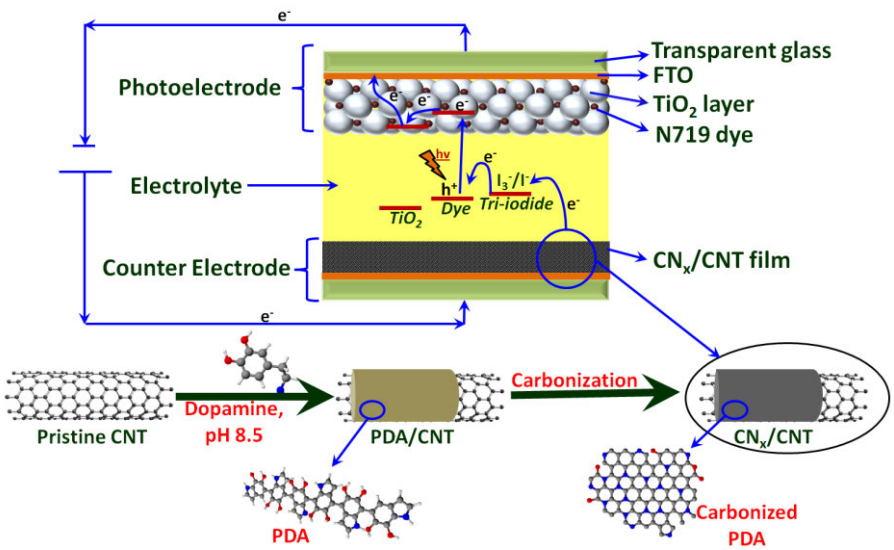

7.1 Introduction

Dye sensitized solar cells (DSSCs) are interesting next generation solar cells due to their easy fabrication and the potential for high efficiency photovoltaic (PV) devices.[1-3] Therefore, excellent progresses have been made over the years to enhance the performance of the cells and to lower their production cost.[2-4] A typical DSSC relies significantly on platinum (Pt) based electrocatalyst as the counter electrode (CE) to reduce tri-iodide to iodide. However, the development of low-cost DSSCs is hindered due to the use of expensive and easily corroded Pt CEs.[3, 5] With this in mind, alternative materials to replace Pt electrocatalyst for DSSC counter electrodes are highly desirable.

Ideally, CEs materials should have a combination of excellent catalytic activity, high electrical conductivity and superior electrochemical stability.[5, 6] Till date, various new materials such as transition metal compounds (TMCs), conductive polymers, carbon materials and their hybrids have been explored as an alternative to Pt.[5] Among them, carbon based catalysts are seen as a promising alternative for Pt due to their high conductivity, low cost and high electrochemical stability. The pristine carbon materials are however catalytically inactive. The carbon based catalysts are engineered by chemical doping with heteroatoms into the defective sites of carbon materials or by hybridizing together with other catalysts to utilize the high conductivity of carbon materials. Chemical doping of carbon materials such as graphene and carbon nanotubes (CNTs) with nitrogen,[7-10] sulphur,[11] phosphorous,[12] oxygen[13, 14] or boron[15] have shown promising performance for the reduction of tri-iodide in DSSCs.[7, 8, 10, 15, 16] Among these doped carbon materials, nitrogen doped (N-doped) carbon structures are extensively studied and have shown distinguished performances comparable to Pt CEs. Dual doped carbon materials such as nitrogen and sulphur co-doped graphene have also shown good

performance in DSSCs.[11] Others have attempted to enhance the catalytic activity by increasing the catalytic surface areas with structures such as N-doped graphene foams,[9] N-doped graphene nano-platelets,[7] N-doped graphene nano-ribbons[16] or brick-like N-doped graphene/CNT 3D structures.[17] The electroactive surface areas of carbon materials are closely related to their defective sites,[6, 18, 19] but the presence of excessive defects within carbon materials can lead to the drop in electrical conductivity and possibly lowering cell performance.[13, 18] The precise control over defective sites in carbon materials is difficult to achieve. Further, the batch to batch variability cannot be ignored. Hence, new methods to create doped carbon structures with good control over the hetroatom doping process while also maintaining the high electrical conductivity is essential.

Polydopamine (PDA) and their derivatives are exciting biomaterials that show great potential for different applications including energy, environment and biomedical fields.[20-22] The structure of PDA is unique in that it consists of multiple functional groups which allows it to be deposited spontaneously on any substrate, regardless of their chemical nature.[21] It is also non-toxic, easy to synthesize and has good solubility in a range of solvents. Furthermore, carbonization of PDA yields nitrogen-doped (N-doped) carbon structures which can be advantageous for many catalytic reactions.[23, 24] The use of PDA as a precursor for the formation of catalytically active materials has rarely been reported.[23, 24, 25]

In this work, we use PDA as an excellent source for generating catalytically active N-doped carbon (CN_x) materials on CNTs and explore these materials as alternatives to Pt counter electrode in DSSCs. The excellent adhesive properties of PDA are beneficial to deposit a thin PDA layer on CNTs. Upon carbonization of the resulting PDA/CNTs

composites, highly catalytic and conductive N-doped CN_x/CNTs are obtained, which can be employed as an efficient electrocatalyst for DSSCs. The advantage of creating such structures is two folds- a) forming a controllable layer of uniform and high catalytically active CN_x materials by carbonization of PDA and b) utilizing highly conductive structural support provided by CNTs for these materials. This work is the first effort on the use of such structures in DSSC counter electrode. The DSSC devices fabricated with CN_x/CNTs materials exhibit high power conversion efficiency (PCE) of 7.3 % which is comparable or higher than that of conventional Pt counter electrode based cells.

7.2 Results and Discussion

7.2.1 Materials synthesis and characterization

As illustrated schematically in **Scheme 7-1**, PDA/CNTs were first synthesized by mixing a given amount of dopamine (DA) with CNTs in 10 mM Tris buffer solution (pH 8.5) at ambient atmosphere. Under such condition, DA can be adsorbed onto CNT surface and the alkaline solution induces a self-oxidative polymerization of DA to form uniform PDA coating on CNTs surface.[20] Transmission electron microscopy (TEM) images in **Figure 7-1(a) and 7-1(b)** show the morphologies of pristine CNTs and PDA/CNTs. As shown in **Figure 7-1(b)**, a visible layer of PDA is deposited uniformly on the surface of CNTs, indicating the formation of PDA/CNTs. The formation of PDA on CNTs can be further confirmed by the Fourier transform infrared spectroscopy (FTIR) (**Figure 7-1(d)**). The absorption bands at 1100 cm^{-1} and 1280 cm^{-1} can be assigned to the C-N stretching vibration and C-O-H asymmetric bending vibration, respectively. A broad peak between 3200–3600 cm^{-1} results from the aromatic O-H stretching vibrations of PDA. The peaks at

1502 and 1616 cm^{-1} are also consistent with the characteristics of stretching vibrations of indole or indoline structures,[24] indicating that the formation of PDA on CNTs is successful. Moreover, the loading of PDA on CNT surface is increased with increasing the mixing ratios of PDA:CNTs (**Figure S7-1**, Supporting information). Three different loadings of PDA on CNTs were prepared by varying the mixing ratio between PDA and CNTs in this study. The prepared PDA/CNTs samples were washed throughly with water and freeze-dried in vacuum.

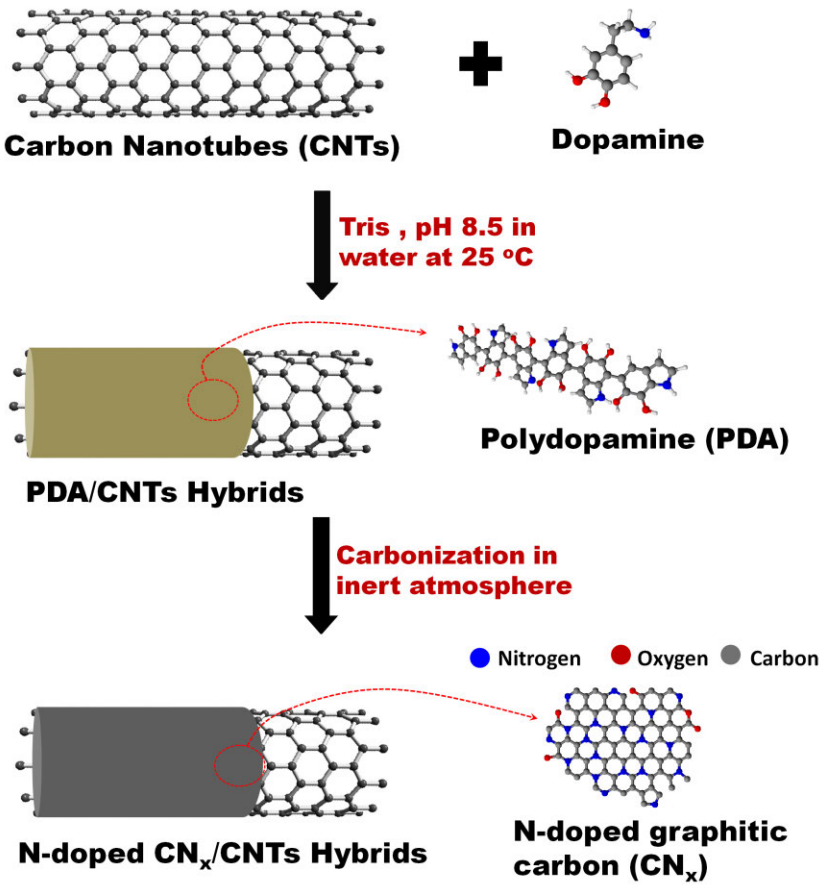

Scheme 7-1. Schematic illustration of the synthesis procedure for CNx/CNTs hybrids

The carbonization of as-prepared PDA/CNTs was carried out in an inert (nitrogen) atmosphere at various temperatures (700 ^{o}C, 800 ^{o}C, 900 ^{o}C and 1000 ^{o}C) to form N-doped CN_x/CNTs. The resulting products (CN_x/CNTs) are termed as "CN_x/CNTs (R:1)–T" where "R:1" indicates the mixing ratio of PDA:CNTs and "T" represents the carbonization temperature.

The morphological structures of CN_x/CNTs were investigated using TEM, X-ray diffaction (XRD) and Raman spectroscopy. **Figure 7-1(c)** shows the morphological structure for the representative CN_x/CNTs (2:1)-800 samples. The typical tubular morphology and the layered graphitic structures corresponding to the inner walls of CNTs are well preserved during carbonization, and the adsorbed PDA layer transforms to form a uniform carbon material (CN_x) on CNTs surface. Furthermore, as shown in **Figure 7-1(e)**, XRD pattern of the PDA/CNTs (2:1) exhibits a small sharp peak at $2\theta = 26^{o}$, which corresponds to a highly ordered and crystalline graphitic structures of CNTs[26] combined with broad and weak peak of amorphous PDA. The intensity of peak at $2\theta = 26^{o}$ is diminished due to the presence of PDA polymer on CNT. The broad and weak peak of the PDA become sharp and strong after carbonization and the intensity of crystalline graphitic peak at $2\theta = 26^{o}$ was also increased. The increase of XRD peak at $2\theta = 26^{o}$ indicates the graphitization of PDA on carbonization. Notably, Yu et al[27] previously reported that the carbonization of PDA particles showed the mixed structural features of amorphous carbon and nanosized crystalline graphite. Thus, the carbonization of PDA/CNTs can form a semi-crystalline graphitic carbon structure on CNTs. The Raman spectrum of CN_x/CNTs (2:1)-800 structure reveals a typical "D" band at 1350 cm^{-1} resulting from the defects/disordered structures and the "G" band at 1580 cm^{-1} is assigned to the sp^2 hybridized graphitic carbon structures. The intensity ratio of D-peak to G-peak (I_D/I_G) is conveniently used to estimate

the defect/disordered structures of carbon materials.[16, 24] The higher I_D/I_G ratio of the CN_x/CNTs structure as compared to the pristine CNTs suggests that the presence of more defective sites in CN_x/CNTs hyrbids (**Figure 7-1(f)**) is favourable to act as the catalytic sites for electrolyte reduction. Similar I_D/I_G ratios were also observed for other CN_x/CNT samples.

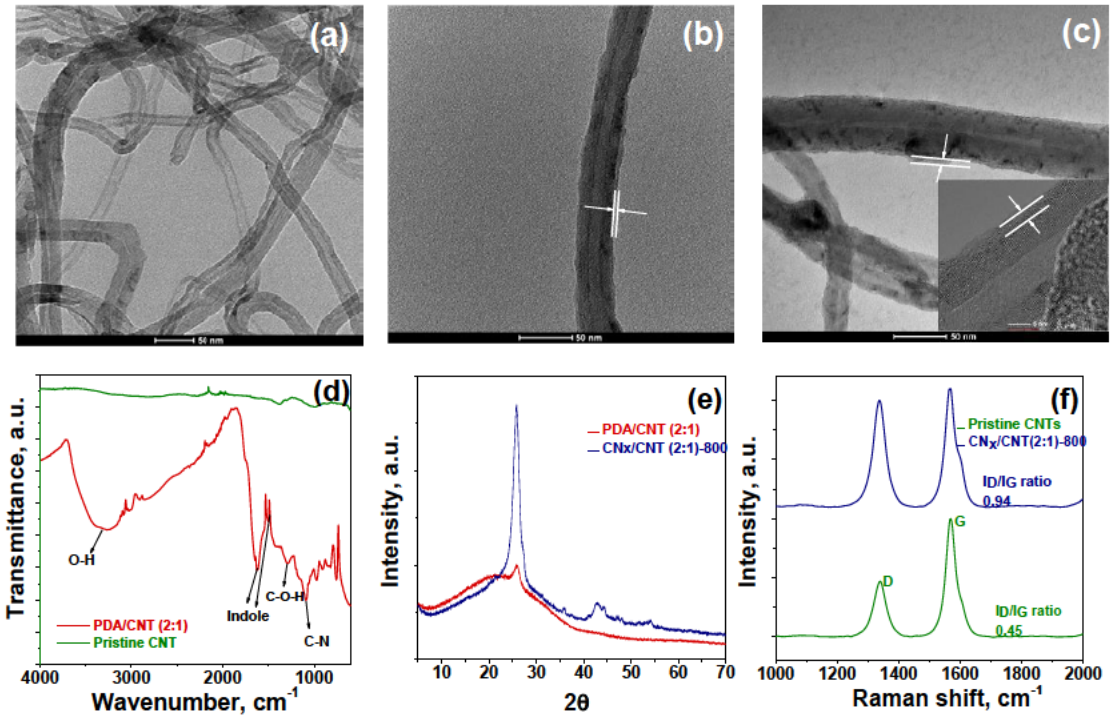

Figure 7-1. TEM image of (a) pristine CNTs, (b) PDA:CNT (2:1) and (c) CN_x/CNTs (2:1)-800. Inset shows the HR-TEM of the CN_x/CNTs (2:1)-800 (d) FTIR spectra of the pristine CNT and PDA:CNT (2:1) (e) XRD patterns of the PDA:CNT (2:1) and CN_x/CNTs (2:1)-800 and (f) Raman spectra of pristine CNTs and CN_x/CNTs (2:1)-800.

Moreover, the chemical composition of the as-prepared CN_x/CNTs was investigated using an X-ray photoelectron spectrscopy (XPS). As shown in **Figure 7-2(a)** (also **Figure S7-2 & S7-3**, supporting information), the XPS survey spectra of CN_x/CNTs reveals that

carbon, oxygen and nitrogen elements are present on surface. The appearance of nitrogen species in the CN_x/CNTs is due to the formation of N-doped carbon structures during the carbonization of PDA/CNTs. High resolution XPS scans were further used to quantify the nature of these species in CN_x/CNTs. The deconvolution of high resolution C^{1s} spectra of CN_x/CNT, as shown in **Figure 7-2(b)** (also **Figure S7-2 & S7-3**, Supporting Information), demonstrate a relatively dominant C=C peak at 284.6 eV along with C-N/C-H (285.4 eV), C-O (286.4 eV) and C=O (287.3 eV) configurations. For O^{1s} spectra (**Figure 7-2(c)**), the main peaks are deconvoluted to H-O-C=O (530.7 eV), C=O (532.1 eV) and C-OH (533.2 eV) (also **Figure S7-2 & S7-3**, Supporting Information). Similarly, high resolution N^{1s} spectra (**Figure 7-2(d)**) are deconvoluted into four major peaks located at 398.2 eV, 399.3 eV, 400.8 eV and 403.2 eV corresponding to pyridinic N, pyrrolic N, graphitic N and oxides of nitrogen species, respectively (also **Figure S7-2 & S7-3**, Supporting Information). It can be seen from **Figure S7-4** (Supporting Information) that the total nitrogen content in the CN_x/CNTs increases with increasing the PDA loading, while it decreases when the carbonization temperature is increased. Moreover, high resolution N^{1s} spectra reveal that the CN_x/CNTs consist of various nitrogen species. At 700 ^oC, the CN_x/CNTs have more graphitic and pyridinic nitrogens together with a small amount of pyrrolic nitrogen (**Figure S7-4(b)**, Supporting Information). N-doped graphene prepared by mixing graphene oxide with cyanamide and carbonized at 700 ^oC shows the predominace of pyrrolic nitrogen species and a smaller amount of pyridinic and graphitic nitrogen species.[8] The carbonization temperature has shown significant influence on the nitrogen species of carbon materials as the less stable nitrogen species such as pyrrolic nitrogen can be transformed to more stable graphitic nitrogen at higher temperatures according to the "ring expansion" model.[8, 16, 24, 28] This means CN_x/CNTs shows quicker

transformation of pyrrolic nitrogen species of PDA[24] to more catalytically active graphitic and pyridinic nitrogen at relatively lower temperatures. As the carbonization temperature increases to 800 ^{o}C, the percentage of graphitic nitrogen increases from 1.51 % to 2.32 %, while the pyrrolic nitrogen species completely disappears. The percentage of the pyridinic nitrogen also decreases from 2.00 % to 1.52 %. It is well known that both the pyridinic and pyrrolic nitrogens are less stable at high temperature and can be converted to more stable graphitic nitrogen upon heating.[8, 24] Apart from the transformation of nitrogen species, some of the nitrogen species can be completely removed from the carbon structures upon annealing at high temperatures.[8] The total nitrogen content in CN_x/CNTs decreases from 4.40 % to 3.84 % upon increasing the carbonization temperature from 700 ^{o}C to 800 ^{o}C. On increasing the carbonization temperature to 900 ^{o}C and 1000 ^{o}C, the total nitrogen contents further decrease, which is due to the removal of more nitrogen species upon annealing at high temperatures.

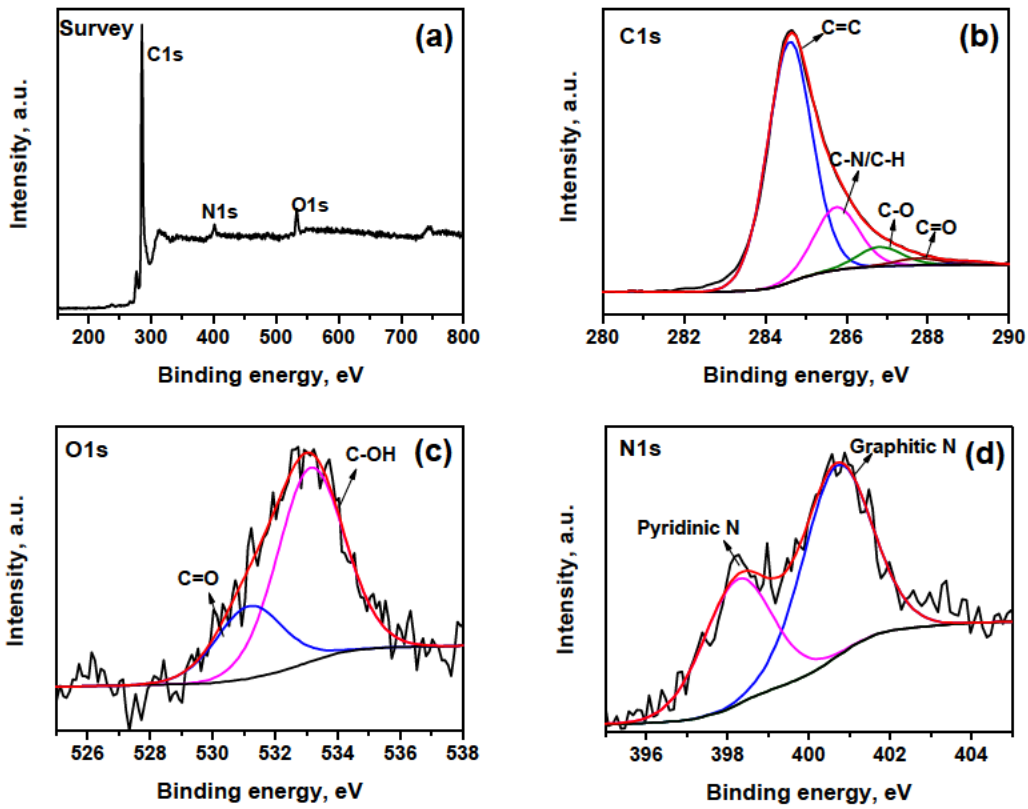

Figure 7-2. (a) XPS survey scan and the high resolution (b) C^{1s} spectra (c) O^{1s} spectra and (d) N^{1s} spectra for CN_x:CNTs (2:1)-800 sample.

The electronic structures of the CN_x/CNTs were also evaluated using a ultra-violet photoelectron spectroscopy (UPS). **Figure S7-5** (Supporting Information), shows the UPS scan for CN_x/CNTs (2:1)-800 and the reference pristine CNTs. UPS analysis provides important information on the work function of carbon-based materials,[29] and the calculated work functions of pristine CNTs and CN_x/CNTs (2:1)-800 are ~ -4.4 eV and ~ -4.0 eV, respectively. The work functions for other CN_x/CNTs are similar to that of CNx/CNTs (2:1)-800. Such n-type transformation of carbon materials is commonly observed after nitrogen doping and will enhance the electron transfer rates from electrode to electrolyte.[29, 30]

7.2.2 CN_x/CNT as efficient catalyst for tri-iodide reduction

To evaluate electrocatalytic activity of the CN_x/CNTs as the CEs materials for DSSCs, cyclic voltammetry (CV) analysis was carried out with key results being plotted in **Figure 7-3(a)** (also **Figure S7-6**, Supporting Information). The CV measurements for the Pt and pristine CNTs at same scan rate of 100 mV s^{-1} were investigated as the references. Two typical peaks corresponding to the oxidation and reduction of tri-iodide electrolytes are observed for all samples. The left pair (A) in the low potential of the CV is attributed to the oxidation and reduction of I^-/I_3^-, while the right pair (B) in the high potential corresponds to the oxidation and reduction of I_3^-/I_2. The higher intensity of characteristic peaks (A) and the low peak to peak separation (E_p) indicates higher catalytic activity of the materials for the reduction of I_3^- to I^-.[31] It is found that both the loading of PDA on CNT surfaces and the carbonization temperature have significant influence on the catalytic activity of the resulting CN_x/CNTs. The CV based on CN_x/CNTs (2:1)-800 shows the smallest peak to peak separation and relatively high peak current densities as compared to other CN_x/CNTs materials. Moreover, the E_p values for the CN_x/CNTs (2:1)-800 is smaller than that of Pt, and its peak current density is also greater than that of Pt, indicating that the CN_x/CNTs (2:1)-800 possesses higher catalytic activity for the reduction of I_3^- to I^-. On the basis of CV analysis, the PV performance of the DSSCs fabricated with CN_x/CNTs (2:1)-800 based counter electrodes is expected to be high.

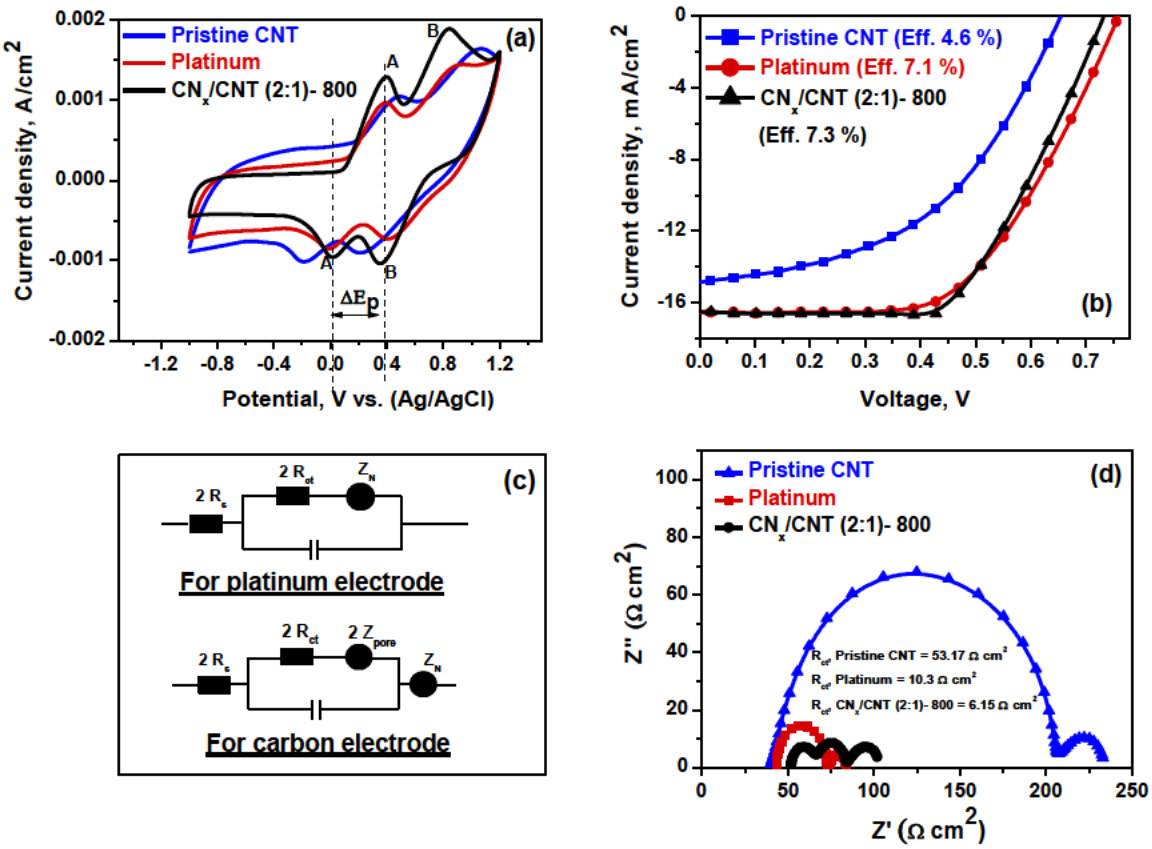

Figure 7-3. (a) Cyclic voltammograms of pristine CNT, Pt and CN_x/CNT (2:1)-800 on a FTO glass substrate cycled in the I^-/I_3^- electrolyte at a scan rate of 100 mV s^{-1}. (b) J–V curves of DSSCs fabricated with pristine CNTs, Pt and CN_x/CNT (2:1)-800 based counter electrode. (c) Equivalent circuit diagrams for Pt and carbon electrodes for EIS analysis. (d) Nyquist plots of dummy cells with a symmetric sandwich-like structure fabricated for different CE materials.

To explore the suitability of these materials (CN_x/CNTs (R:1)-T) as the counter electrodes in DSSCs, PV devices were assembled with a conventional 20-30 nm TiO_2 semiconductor and different CN_x/CNTs (R:1)-T based counter electrodes. The PV characteristics were evaluated using simulated AM1.5 sunlight with an output power of 100 mW cm^{-2}. Pristine

CNTs and Pt CEs based DSSCs were also fabricated with their performances for comparison purpose. The photocurrent density–voltage (J–V) characteristics of the cells fabricated with the CN_x/CNTs (2:1)-800 based CE and control CEs (pristine CNTs and Pt) are illustrated in **Figure 7-3(b)**. The control Pt-CE based device exhibits a short-circuit current (J_{sc}) of 16.54 mA cm^{-2}, open-circuit voltage (V_{oc}) of 0.76V and fill factor (*FF*) of 0.57; and yielding a PCE of 7.1 % while the CN_x/CNTs (2:1)-800 CE based device shows a PCE of 7.3 % (with a J_{sc}=16.51 mA cm^{-2}, V_{oc}=0.73 V and *FF*=0.6). The pristine CNTs CE based device shows a PCE of 4.5 % (with a J_{sc}=14.87 mA cm^{-2}, V_{oc}=0.65 V and *FF*=0.47) due to the lower electrolyte reduction capability of pristine CNTs. **Figure S7-7** (supporting Information) shows the J-V curves for the other CN_x/CNT CEs. The obtained PV parameters of J_{sc}, V_{oc}, *FF* and PCE of all fabricated devices are summarized in **Table 7-1**.

Table 7-1. Summary of PV parameters for various CEs based DSSCs.

Counter electrode	J_{sc} (mA cm^{-2})	V_{oc} (mV)	*FF*(%)	Efficiency (%)
Pt	16.54±0.12	762.5±2.2	57.1±1.1	7.13±0.10
Pristine CNT	14.82±0.06	648.0±2.8	46.5±0.7	4.48±0.17
CN_X/CNT(1:1)-800	16.19±0.10	720.5±2.1	61.5±0.7	6.98±0.12
CN_X/CNT(2:1)-700	15.12±0.20	733.5±2.2	60.5±0.6	6.65±0.14
CN_X/CNT(2:1)-800	16.30±0.20	734.2±1.6	61.5±2.2	7.38±0.12
CN_X/CNT(2:1)-900	15.48±0.16	733.5±2.1	61.4±0.8	6.96±0.14
CN_X/CNT(2:1)-1000	14.26±0.10	744.1±2.0	53.0±1.2	5.60±0.12
CN_X/CNT(4:1)-800	15.6±0.30	734.0±1.4	48.5±2.1	5.58±0.15

The PDA loading and the carbonization temperature show considerable influence on the PCE of DSSCs fabricated with CN_x/CNTs (R:1)-T CEs, as similar trend being observed from the CV analysis. It can be seen from **Figure 7-4(a)** that the PCE increases from CN_x/CNTs (0:1) to CN_x/CNTs (2:1) (increasing PDA loading) and decreases sharply at higher loadings of PDA i.e. CN_x/CNTs (4:1). The increase of PCE with increasing PDA loading is due to the increase in active nitrogen species while the decrease in PCE after introducing more PDA on CNTs may be due to the fact that large amount of PDA reduces the conductivity of CN_x/CNTs. On the other hand, the PCE increases with carbonization temperature up to 800 ^oC and then starts to decrease at the carbonization temperature beyond 900 ^oC (**Figure 7-4(b)**). The increase in PCE with carbonization temperature from 700 ^oC to 800 ^oC is due to the increased N-hybridization in CN_x/CNTs. Decreased PCEs of the cells fabricated with high temperatures (900 ^oC and 1000 ^oC) processed CEs can be attributed to the reduced active nitrogen species in CN_x/CNTs. Therefore, it is clear that there is an optimal condition for the best PCE, and the highest PCE of 7.3 % can be achieved for the DSSC fabricated with CN_x/CNTs (2:1)-800 based CE. This PCE of our N-doped CN_x/CNTs counter electrode based cell is comparable or slightly higher than that of the control Pt CE based device. Although the PCE as high as Pt has been previously reported for various N-doped graphene structures such as N-doped graphene foams (PCE 0.95 of Pt) and nano-ribbons (PCE 1.09 of Pt), other heteroatom doped graphene such as B-graphene (PCE 1.06 of Pt) and dual element doped graphene such as N,S doped graphene (PCE 0.98 of Pt), our CN_x/CNT (PCE 1.03 of Pt) presents a simple, environmentally benign and more controllable N-doped structures. This result further indicates that the CN_x/CNTs based CEs can potentially replace the expensive Pt for DSSC application.

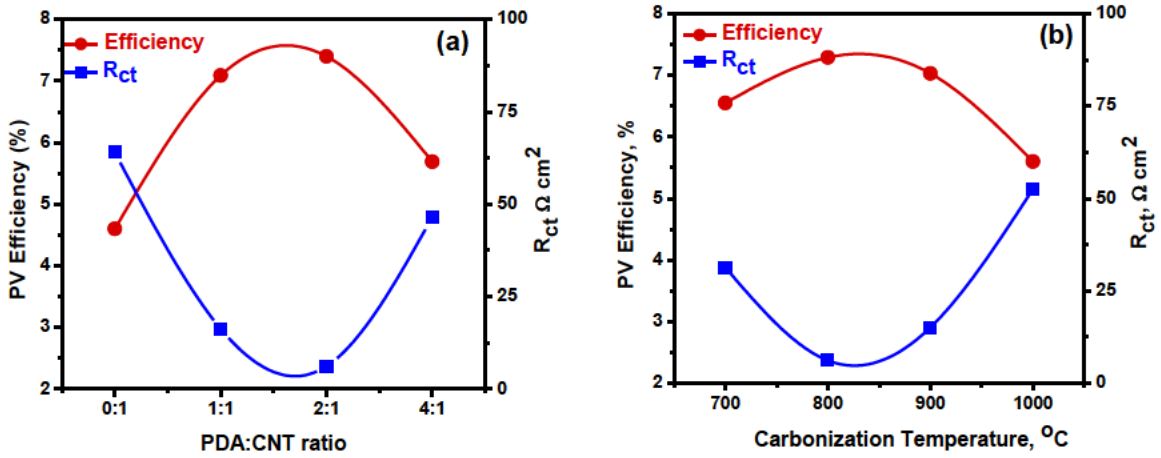

Figure 7-4. Influence of (a) PDA:CNT ratios and (b) carbonization temperatures on the DSSC efficiency and R_{ct} of the electrode. Here, PDA:CNT as 0:1 signifies pristine CNTs.

To further understand the possible reasons behind the high PCE of the CN_x/CNTs (2:1)–800 CEs, the electrochemical impedance spectroscopy (EIS) were conducted at 0 V using a symmetrical dummy cell configuration. **Figure 7-3(c)** shows the modeled equivalent circuit diagrams typically used for Pt and carbon based CEs. The Nyquist plots shown in **Figure 7-3(d)** (also **Figure S7-8**, Supporting Information) are obtained by fitting the resulting EIS data to a modeled equivalent circuit diagram. A typical Nyquist plot for Pt CEs consists of two semi-circles. The one at low frequency range is associated with the Nernst diffusion impedance (Z_w) corresponding to diffusion in electrolytes, and the other at the high frequency range is related to charge transfer resistance (R_{ct}) originating from the interface between CEs and electrolyte.[16] Unlike Pt CE, carbon based materials usually exhibit an additional semi-circle originating from the secondary Nernst diffusion impedance which results from the diffusion through pores (Z_{pore}).[13, 16] The high frequency intercept of the Nyquist plot on the real axis (Z') gives the series resistance (R_s) of the cells. For high efficiency DSSCs, the catalytic performance at CEs is inversely correlated

to the Rct at the interface of CE and electrolyte.[6] The Rct values in DSSCs generally exhibit significant influence on the Jsc and FF parameteres. As shown in **Figure 7-3(d)**, the CN_x/CNT (2:1)-800 based CE exhibits lowest Rct of 6.15 Ω cm^2 among others, where Pt based CE shows a Rct of 10.30 Ω cm^2 and the pristine CNTs-CE exhibits a much higher Rct of 53.17 Ω cm^2. The lower Rct value for CN_x/CNT (2:1)-800 is consistent with the distinguished catalytic performance towards I_3^- reduction and higher PCE as compared to the control CEs.

To gain further insight on the influence of PDA loading and carbonization temperature on PCE, the EIS analysis were conducted at 0 V bias for all CN_x/CNTs. The corresponding Rct values obtained from EIS are plotted in **Figure 7-4(a) & 7-4(b)**. The R_{ct} value initially drops with increasing the PDA loading and then increases at higher PDA loadings due to the influence of overall nitrogen contents in CN_x/CNTs. It is plausible that the increase in the active nitrogen species enhances the catalytic reduction of I_3^- at the CEs and thus lowers the R_{ct} values. However, the excessive loadings of PDA create a barrier for the efficient electron transfer from the electrodes and thus increase the R_{ct} values. The variation in the R_{ct} values with PDA loading has been reflected from the corresponding PCE values.

Similar to PDA thickness, the R_{ct} values are also influenced by the carbonization temperature. The R_{ct} value decreases up to 800 ^oC and then increases as the carbonization temperature is further increased. The carbonization temperature can influence the formation of different types of nitrogen species in carbon structures and can consequently affect the catalytic behavior for various catalytic reactions. Recently Meng et al[16] showed using density functional theory DFT that the ionization energy, E_i, of iodide at the

electrolyte-electrode interface is a rate limiting step for the reduction of I_3^-. It was found that the graphitic nitrogen species possess the lowest ionization energy for I_3^- reduction.[16] The ionization energies for different nitrogen species have been reported to follow the order of "graphitic N < pyrrolic N < pyridinic N".[16] Higher concentration of the graphitic nitrogen species can enhance the electron transfer from the external circuit to the I_3^- and consequently reduce the R_{ct}. As shown in **Figure S7-4** (Supplementary Information), the carbonization temperature at 800 ^oC yields the highest percentage of graphitic nitrogen, the lowest value of R_{ct} and exhibits the best performance of DSSC in the present work.

7.3 Conclusion

In this work, we demonstrate the use of PDA as a nitrogen containing precursor to prepare functional N-doped CN_x/CNT. These N-doped CN_x/CNTs are utilized as highly efficient electrocatayst materials for DSSC applications. The influence of PDA loadings and carbonization temperatures on the catalytic performance of CN_x/CNTs is investigated in detail. The best performing device fabricated with the CN_x/CNTs (2:1)-800 exhibits a PCE of 7.3 %, which is slightly higher than that of Pt CE (7.1 %) based DSSC. The CN_x/CNTs materials show great potential to substitute the expensive and rare Pt electrocatalyst for the highly efficiency DSSC devices.

7.4 Experimental Section

7.4.1 Materials

Dopamine hydrochloride (DA), Tris(hydroxymethyl)aminomethane (Tris base), terpeniol, carboxymethyl cellulose, ethyl cellulose, lithium iodide (LiI), lithium perchlorate ($LiClO_4$) and iodine (I_2) were purchased from Sigma-Aldrich. MWCNTs (purity >98%) were

purchased from Zhongke Leiming (Beijing) Science and Technology Co. Ltd. The as-received CNTs were washed with hydrochloric acid/water and dried prior to use for removing impurities. TiO_2 paste (Ti-Nanoxide T/SP), Ruthenizer 535-bisTBA (N719 dye), iodide/tri-iodide electrolyte (Iodolyte Z-50), DuPont Surlyn® (Meltonix 1170-60) and Platinum catalyst (Platisol T) were purchased from Solaronix, Switzerland.

7.4.2 Preparation of PDA/CNT hybrid

In a typical experiment, PDA/CNTs (2:1) was prepared by mixing 80 mg CNTs in 80 ml of 10 mM Tris base at pH 8.5. The resulting mixture was sonicated for 2 min. After adding 160 mg DA, the mixture was again sonicated for another 20 min, followed by stirring for 24 h at room temperature. The PDA/CNTs were recovered by filtration and washed for three times with de-ionized (DI) water, and then freeze dried. The thickness of PDA/CNTs was controlled by changing the feed amount of DA in reaction solutions. For example, 80 mg and 320 mg DA were used to produce PDA/CNTs (1:1) and PDA/CNTs (4:1), respectively.

7.4.3 Preparation of CN_x/CNT hybrid

CN_x/CNTs were prepared by the carbonization of as-prepared PDA/CNTs in a programmable tube furnace under N_2 atmosphere. Typically, the as-prepared PDA/CNT were placed in a crucible and heated at 400 ^oC for 2 h with a heating rate of 1 ^oC/min. The crucible was further heated to 800 ^oC (or 700, 900 or 1000 ^oC) at a heating rate of 5 ^oC/min. After reaching the desired temperature, thermal treatment was carried out for 3 h. Finally the samples were cooled to room temperature.

7.4.4 Fabrication of DSSCs

FTO coated substrates (purchased from Solaronix™) were cleaned by a detergent followed by washing with Milli-Q water, acetone and ethanol under ultrasonication for 10 min each. The cleaned and dried FTO/glass substrates were immersed in a 40 mM $TiCl_4$ aqueous solution for 30 min at 70 ^oC. Then nanocrystalline TiO_2 films were prepared from a commercial TiO_2 paste by doctor blading technique using two layer adhesive tape (Magic™ Tape, 3M), followed by heating under an air flow at 125 ^oC for 5 min, 325 ^oC for 5 min, at 375 ^oC for 5 min and at 450 ^oC for 30 min. After cooling to ~50 ^oC, TiO_2 coated films were then soaked in 40 mM $TiCl_4$ solution at 70 ^oC for 30 min, then again sintered at 450 ^oC for 30 min. After cooling to room temperature, the prepared TiO_2 photoanode films were immersed into 0.5 mM N719 dye in an ethanol solution for ~36 h at 40 ^oC.

In the meantime, viscous carbon pastes were prepared from the CN_x/CNTs (R:1)-T samples according to the established procedures described in the literature.[14] The prepared carbon pastes were coated onto the cleaned FTO electrodes via a doctor blade technique, followed by drying in an oven at 90 ^oC for 5-10 min. After drying the films, these CEs were further annealed at 420 ^oC for 30 min under the protection of Ar gas. For comparison, Pt-CEs were prepared by coating Pt precursor onto FTO substrates using a brush-painting method. The dye-adsorbed TiO2 photoanodes and counter electrodes were assembled into a sealed sandwich-type cell, with a 60 μm thick hot-melt sealing Surlyn between each layer. The electrolyte solution, Iodolyte Z-50 (Solaronix™), was injected into the cell via a vacuum-filling method through an injection hole on the counter electrode side. Finally, the hole at the counter electrode was sealed to prevent the possible leakage of electrolyte.

7.4.5 Materials Characterization

FTIR spectra were acquired using the transmission module of Thermo Nicolet 6700 FTIR spectrometer at the resolution of 2 cm^{-1}. The low resolution TEM images were obtained using FEI Technai G2 spirit TEM while the high resolution TEM images were obtained using a FEI Titan TEM. XRD diffraction patterns were obtained using Philips 1130 X-ray diffractometer (40 kV, 25 mA and Cu kα X-rays) at ambient condition. The Raman spectra were acquired using a 532 nm laser as an excitation source on the HORBIA scientific iHR550 instrument. XPS spectra were acquired using an ultrahigh vacuum apparatus (e-10) built by SPECS (Berlin, Germany). A 12kV-200 W nonmonochromatic X-ray source was used for measurements with Mg anode. The XPS spectra were referenced to the carbon^{1s} peak at 284.6 eV. The UPS spectra were also acquired using the same instrument.

The cyclic voltammetry (CV) data were recorded using an electrochemical analysis work station (CHI 760D CH Instruments USA). Typically for CV measurements, 2 mg of CN_x/CNT samples were dispersed in 1 ml of 0.1% carboxymethyl cellulose (CMC) solution in DI water to prepare a homogeneous catalyst ink. 50 µl of as-prepared ink was dropped on the mirror polished glassy carbon electrode. The glassy carbon electrode with catalysts was then introduced into a three cell electrode set up containing 200 ml of 0.1 M $LiClO_4$, 10 mM lithium iodide (LiI), and 1 mM iodine (I_2) electrolyte in acetonitrile. Platinum wire was used the counter electrode while Ag/AgCl/KCl (4 M) was used as the reference electrode. The scan rate for CV was maintained as 100 mV s^{-1}.

EIS was also measured using the electrochemical analysis workstation (Autolab Nova Potentiostat). Typically for EIS, a symmetrical dummy cell configuration was fabricated. Briefly, the CN_x/CNT catalyst paste was applied on to FTO using doctor blade coating technique, which was followed by sintering at 420 ^oC for 30 mins to prepare two identical

CEs. A 50 μm DuPontTM Surlyn® spacer was sandwiched between the two identical CEs to prepare the symmetrical dummy cells. The electrolyte was then introduced into the cells by vacuum back filling technique.

The J–V characteristics were studied using a Keithley 2400 SMU instrument and recorded using a custom LabView Virtual Instrument program. A standard silicon test cell with NIST-traceable certification was used to calibrate the power density as 100 mW cm^{-2} at the sample plane of the collimated xenon-arc light source, which was passed through an AM 1.5G filter. The active area of each device was 0.25 cm^2.

Acknowledgements

This work was financially supported by the Australian Research Council Discovery Projects DP110102877, DP140104062 and DP160104632

References

[1] B. O'Regan, M. Gratzel, *Nature* 1991, 353, 737.

[2] A. Yella, H.-W. Lee, H. N. Tsao, C. Yi, A. K. Chandiran, M. K. Nazeeruddin, E. W.-G. Diau, C.-Y. Yeh, S. M. Zakeeruddin, M. Grätzel, *Science* 2011, 334, 629.

[3] B. E. Hardin, H. J. Snaith, M. D. McGehee, *Nat. Photon*. 2012, 6, 162.

[4] (a) T. Daeneke, T.-H. Kwon, A. B. Holmes, N. W. Duffy, U. Bach, L. Spiccia, *Nat. Chem.* 2011, 3, 211; (b) J. Burschka, A. Dualeh, F. Kessler, E. Baranoff, N.-L. Cevey-Ha, C. Yi, M. K. Nazeeruddin, M. Grätzel, *J. Am. Chem. Soc.* 2011, 133, 18042; (c) L. Kavan, J.-H. Yum, M. K. Nazeeruddin, M. Grätzel, *ACS Nano* 2011, 5, 9171.

[5] S. Yun, A. Hagfeldt, T. Ma, *Adv. Mater.* 2014, 26, 6210.

[6] J. E. Trancik, S. C. Barton, J. Hone, *Nano Lett.* 2008, 8, 982.

[7] M. J. Ju, J. C. Kim, H.-J. Choi, I. T. Choi, S. G. Kim, K. Lim, J. Ko, J.-J. Lee, I.-Y. Jeon, J.-B. Baek, H. K. Kim, *ACS Nano* 2013, 7, 5243.

[8] S. Hou, X. Cai, H. Wu, X. Yu, M. Peng, K. Yan, D. Zou, *Energy Environ. Sci.* 2013, 6, 3356.

[9] Y. Xue, J. Liu, H. Chen, R. Wang, D. Li, J. Qu, L. Dai, *Angew. Chem. Int. Ed.* 2012, 51, 12124.

[10] K. S. Lee, W. J. Lee, N.-G. Park, S. O. Kim, J. H. Park, *Chem. Commun.* 2011, 47, 4264.

[11] A. G. Kannan, J. Zhao, S. G. Jo, Y. S. Kang, D.-W. Kim, *J. Mater. Chem. A* 2014, 2, 12232.

[12] Z. Wang, P. Li, Y. Chen, J. He, J. Liu, W. Zhang, Y. Li, *J. Power Sources* 2014, 263, 246.

[13] J. D. Roy-Mayhew, D. J. Bozym, C. Punckt, I. A. Aksay, *ACS Nano* 2010, 4, 6203.

[14] J. D. Roy-Mayhew, G. Boschloo, A. Hagfeldt, I. A. Aksay, *ACS Appl. Mater. Interfaces* 2012, 4, 2794.

[15] H. Fang, C. Yu, T. Ma, J. Qiu, *Chem. Commun.* 2014, 50, 3328.

[16] X. Meng, C. Yu, X. Song, Y. Liu, S. Liang, Z. Liu, C. Hao, J. Qiu, *Adv. Energy Mater*. 2015, 5.

[17] J. Ma, C. Li, F. Yu, J. Chen, *J. Power Sources* 2015, 273, 1048.

[18] M. Batmunkh, M. J. Biggs, J. G. Shapter, *Small* 2015, 11, 2963.

[19] S. Hwang, M. Batmunkh, M. J. Nine, H. Chung, H. Jeong, *ChemPhysChem* 2015, 16, 53.

[20] Y. Liu, K. Ai, L. Lu, *Chem. Rev.* 2014, 114, 5057.

[21] H. Lee, S. M. Dellatore, W. M. Miller, P. B. Messersmith, *Science* 2007, 318, 426.

[22] (a) F. He, G. Chen, Y. Yu, Y. Zhou, Y. Zheng, S. Hao, *Chem. Commun.* 2015, 51, 6824; (b) Y. Liu, K. Ai, J. Liu, M. Deng, Y. He, L. Lu, *Adv. Mater.* 2013, 25, 1353.

[23] (a) K. Ai, Y. Liu, C. Ruan, L. Lu, G. Lu, *Adv. Mater*. 2013, 25, 998; (b) K. Qu, Y. Zheng, S. Dai, S. Z. Qiao, *Nano Energy* 2016, 19, 373.

[24] K. Qu, Y. Zheng, S. Dai, S. Z. Qiao, *Nanoscale* 2015, 7, 12598.

[25] D. Zhou, L. Yang, L. Yu, J. Kong, X. Yao, W. Liu, Z. Xu, X. Lu, *Nanoscale* 2015, 7, 1501.

[26] C. Liang, L. Ding, C. Li, M. Pang, D. Su, W. Li, Y. Wang, *Energy Environ. Sci.* 2010, 3, 1121.

[27] X. Yu, H. Fan, Y. Liu, Z. Shi, Z. Jin, *Langmuir* 2014, 30, 5497.

[28] J. Liang, Y. Jiao, M. Jaroniec, S. Z. Qiao, *Angew. Chem. Int. Ed.* 2012, 51, 11496.

[29] S. Das, P. Sudhagar, V. Verma, D. Song, E. Ito, S. Y. Lee, Y. S. Kang, W. Choi, *Adv. Func. Mater.* 2011, 21, 3729.

[30] S. Ni, Z. Li, J. Yang, *Nanoscale* 2012, 4, 1184.

[31] C.-L. Wang, J.-Y. Liao, S.-H. Chung, A. Manthiram, *Adv. Energy Mater.* 2015, 5.

Supporting Information

Nitrogen-doped CN_x/CNTs hetero-electrocatalysts for highly efficient dye sensitized solar cells

Aabhash Shrestha[1], Munkhbayar Batmunkh[1,2], Cameron J. Shearer[2], Yanting Yu[2], Gunther Andersson[2], Joseph G. Shapter[2]*, Shizhang Qiao[1]*, Sheng Dai[1]*

[1] School of Chemical Engineering, The University of Adelaide, Adelaide, SA, 5005, Australia

[2] School of Chemical and Physical Sciences, Flinders University, Bedford Park, Adelaide, SA 5042, Australia

* Corresponding Authors

Email: s.dai@adelaide.edu.au , s.qiao@adelaide.edu.au , joe.shapter@flinders.edu.au

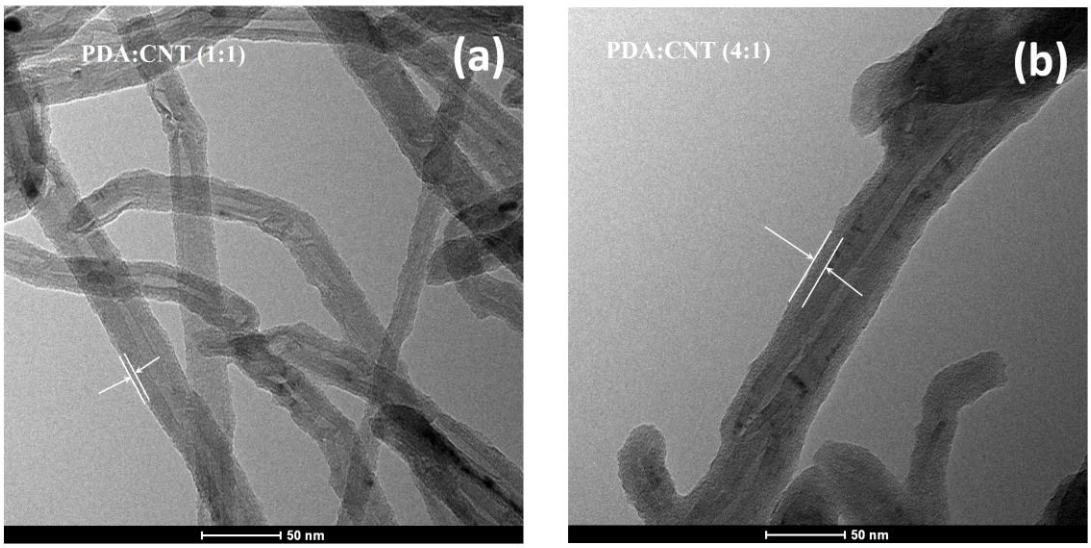

Figure S7-1. TEM image of (a) PDA:CNT (1:1) and (b) PDA:CNT (4:1)

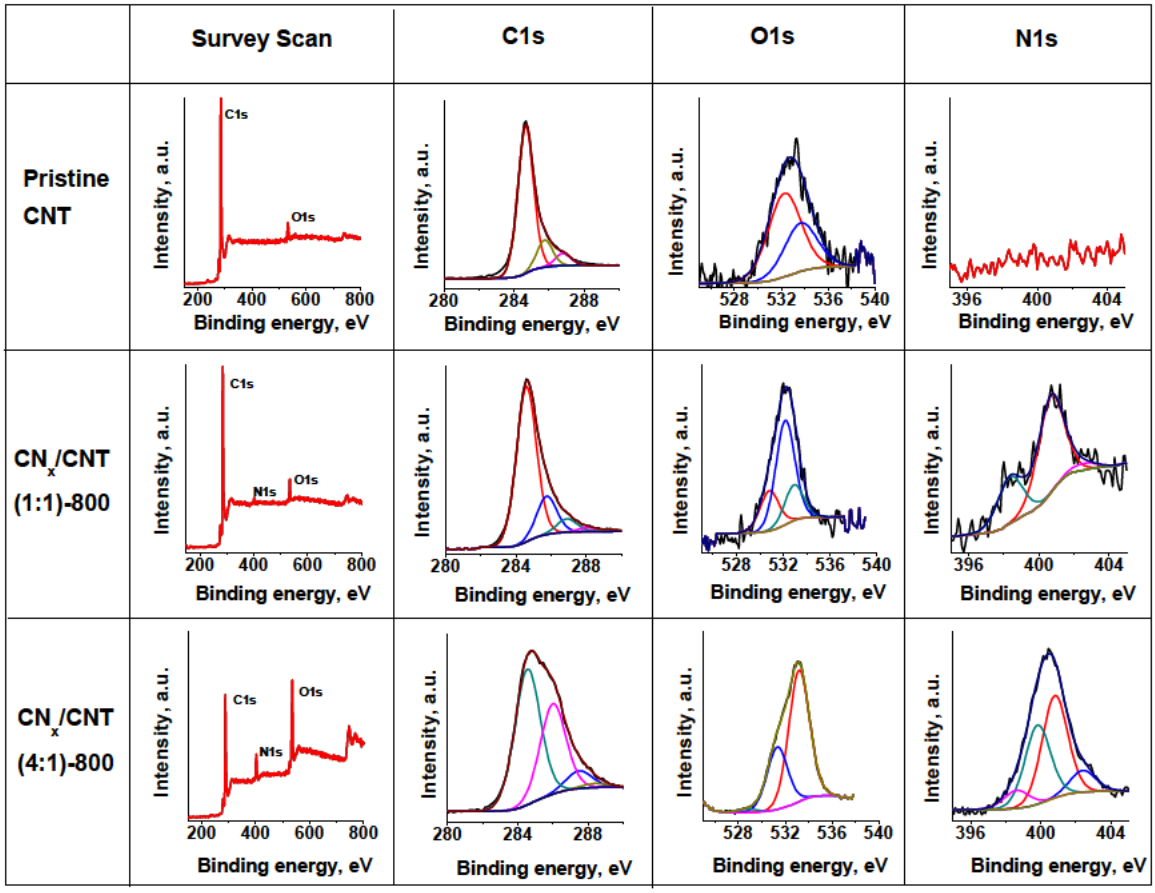

Figure S7-2. XPS survey scan and the high resolution C^{1s}, O^{1s} and N^{1s} spectra for (a) pristine CNTs (b) CN_x:CNT (1:1)-800 and (c) CN_x:CNT (4:1)-800 samples.

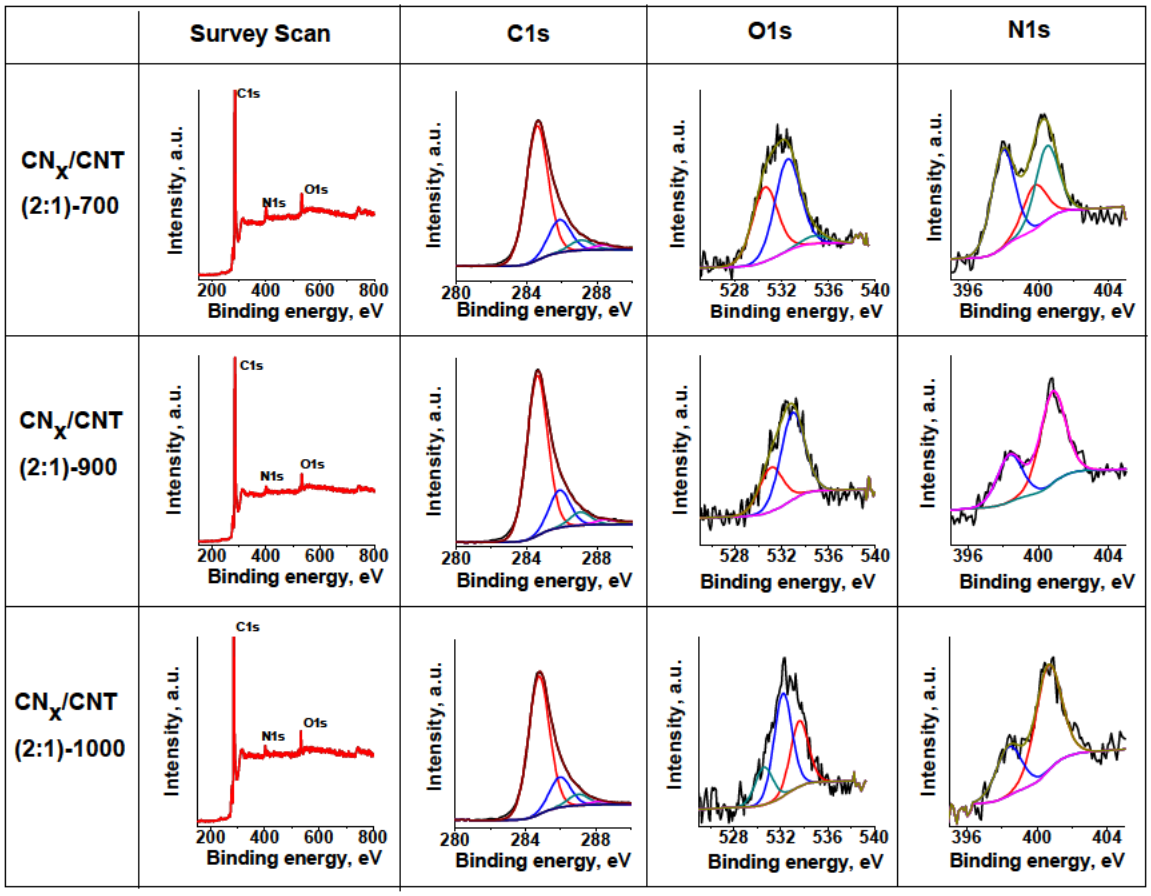

Figure S7-3. XPS survey scan and the high resolution C^{1s}, O^{1s} and N^{1s} spectra for (a) CN_x:CNT (2:1)-700 (b) CN_x:CNT (2:1)-900 and (c) CN_x:CNT (2:1)-1000 samples

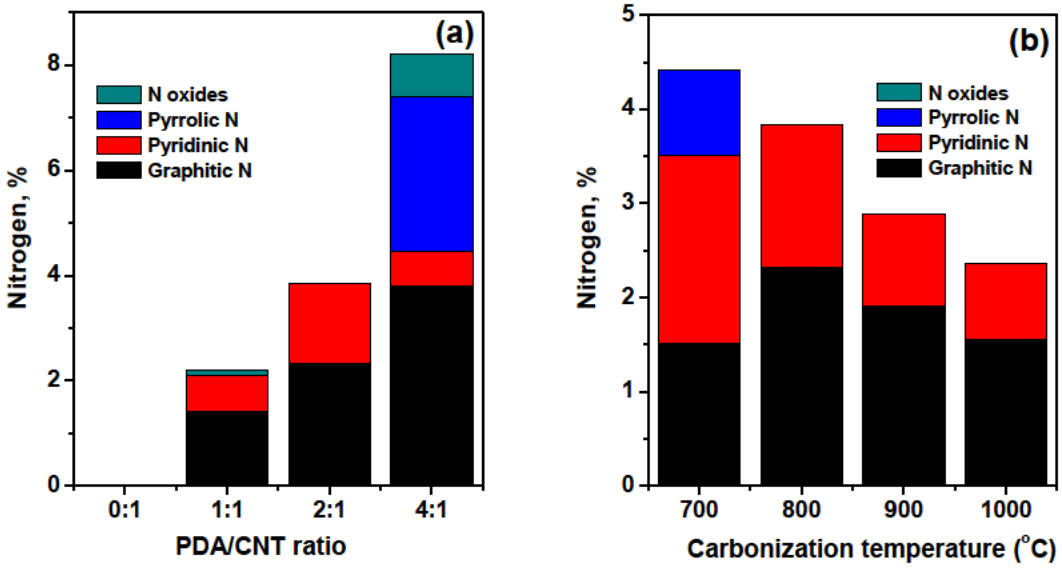

Figure S7-4. Percentage of various nitrogen species with (a) change in PDA:CNTs ratios at carbonization temperature of 800 °C and (b) different carbonization temperature and PDA:CNT ratio as 2:1

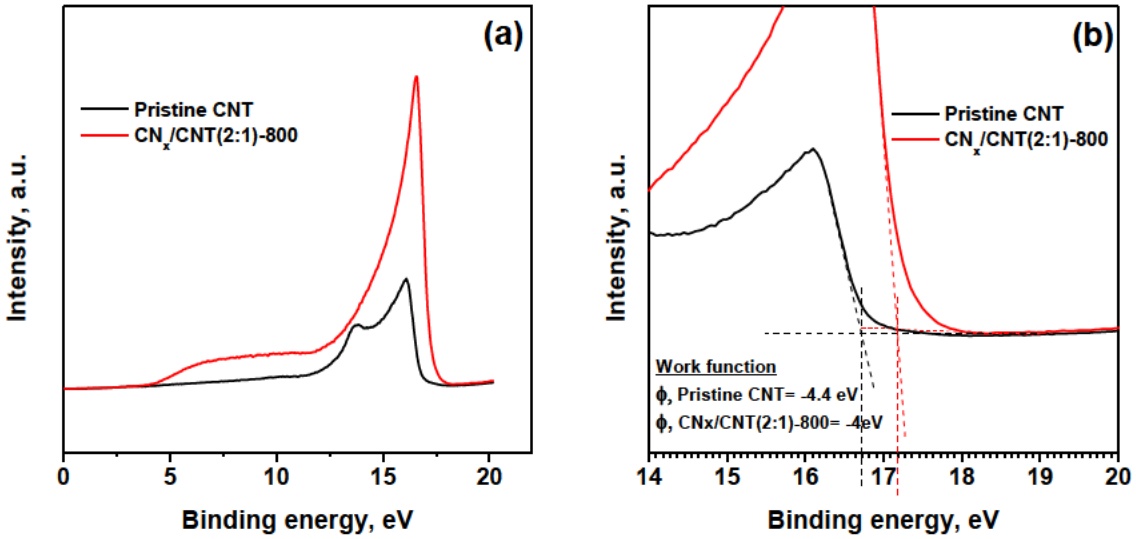

Figure S7-5. (a) UPS-MIES spectrum of pristine CNT and CN_x/CNT (2:1)-800 hybrid (b) Calculation of work function for pristine CNT and CN_x/CNT (2:1)-800 hybrid using UPS data. Work function of the carbon materials were calculated as: ϕ= -(21.2-intercept value) eV. For pristine CNT, the intercept is found at 16.8 eV in x-axis. Thus, the calculated work function for pristine CNT is -4.4 eV. Similarly, work function for CN_x/CNT (2:1)-800 hybrid is -4 eV.

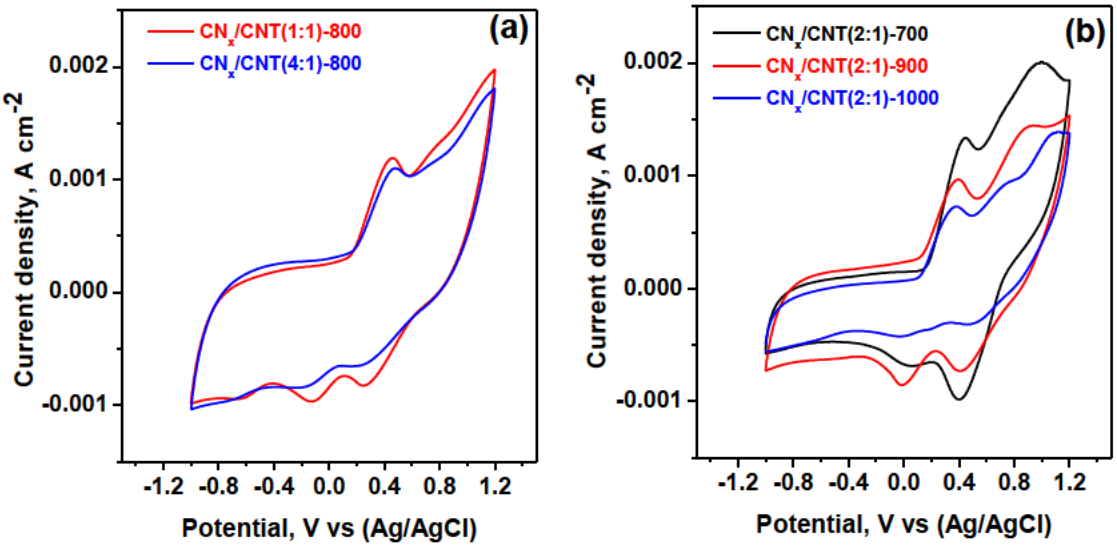

Figure S7-6. CV curves for (a) CN_x/CNT (1:1)-800 and CN_x/CNT (4:1)-800 °C and (b) CN_x/CNT (2:1)-700, CN_x/CNT (2:1)-900 and CN_x/CNT (2:1)-1000

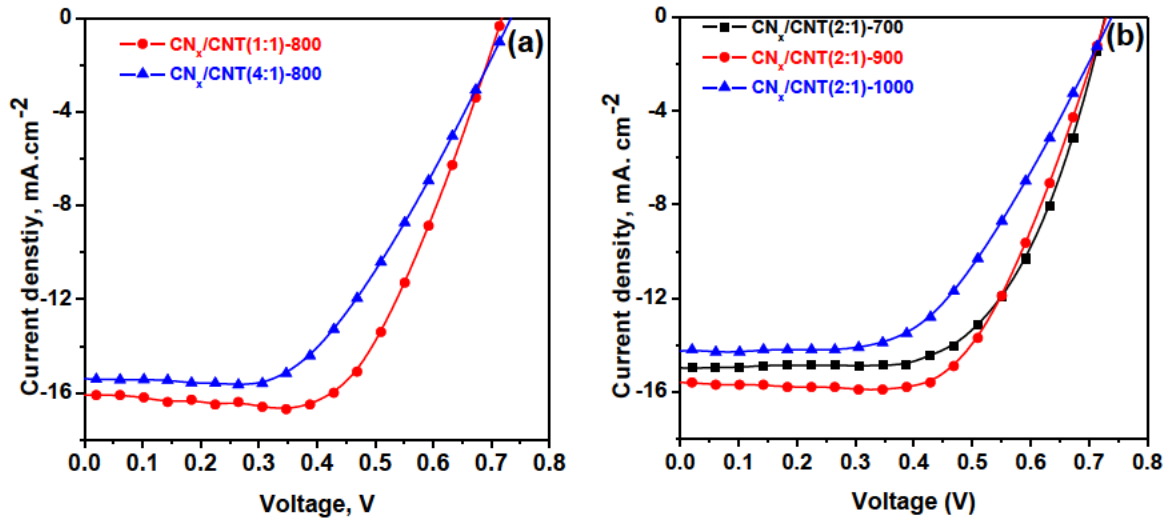

Figure S7-7. JV curves for (a) CN_x/CNT (1:1)-800 and CN_x/CNT (4:1)-800 °C and (b) CN_x/CNT (2:1)-700, CN_x/CNT (2:1)-900 and CN_x/CNT (2:1)-1000

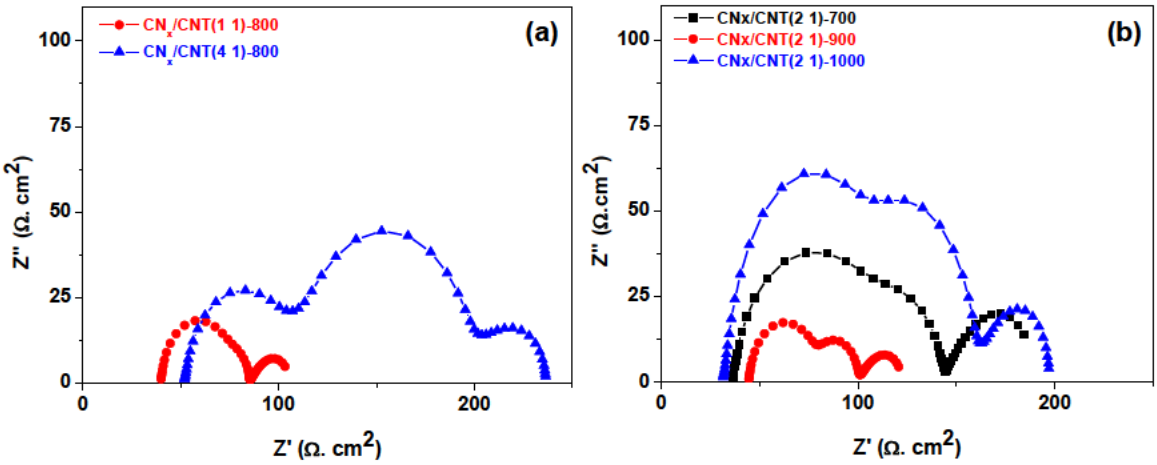

Figure S7-8. EIS curves for (a) CN_x/CNT (1:1)-800 and CN_x/CNT (4:1)-800 °C and (b) CN_x/CNT (2:1)-700, CN_x/CNT (2:1)-900 and CN_x/CNT (2:1)-1000

Chapter 8

Conclusion

8.1 Conclusions

This PhD thesis was focused on the utilization of PbS QDs in quantum dot sensitized solar cells. The progress of PbS QDSSCs is lacking due to the limited understanding of their synthesis and surface chemistry. The development of QDSSCs is also hindered due to the lack of proper counter electrode materials for reduction of electrolytes. As such, the main objectives were to investigate the PbS QD synthesis, surface ligand exchange of PbS QDs, and the development of new counter electrode materials. In this PhD thesis, the nucleation and growth mechanism of PbS QDs and the various synthesis conditions that influence the QD synthesis was investigated. A robust method to synthesize differently sized PbS QDs by simple heating of pre-synthesized PbS QDs was also developed. Next, the surface ligand exchange of PbS QDs was investigated and a versatile ligand exchange strategy using Pb-thiolates as the exchanging ligands was developed. Then, a new N-doped hybrid CN_x/CNT catalyst material was developed and utilized as a counter electrode materials in DSSCs. Finally, the ligand exchanged PbS QDs was employed in QDSSCs. The main conclusions drawn from the experimental results presented in chapters 3-7 are summarized below:

Chapter 3 reported a novel strategy for "living" growth of PbS QDs. A series of differently sized PbS QDs were synthesized by heating preformed QDs in the presence of excess oleic acid. The detailed growth mechanism for such "living" growth of PbS QDs was also elucidated. The QD growth mechanism followed the "living" growth by addition of monomers in early stages and followed by Ostwald ripening in the later stages.

Chapter 4 investigated the nucleation and growth mechanism of oleic acid capped PbS QDs in detail. The synthesis was found to be independent of classical nucleation process

and the hot-injection of precursors may not be necessary for successful synthesis of PbS QDs. The PbS QDs synthesis was a growth dominated process and controlled by the Ostwald ripening of QDs. Temperature and oleic acid concentration influenced the growh of PbS QDs. Increasing the temperature enhanced the QDs growth and the activation barrier for the growth of PbS QDs was calculated to be 29 kJ/mol. The Ostwald ripening of QDs was activated in presence of free oleic acid while bound oleic acid to lead precursor inhibited the Ostwald ripening. Even a small excess of free oleic acid was enough to trigger the Ostwald ripening growth of PbS QDs. Using the guidance of the synthesis mechanism, the synthesis of ultra-small (<2 nm) PbS QDs was also achieved. The results in this study can provide guidance for future QDs synthesis.

Chapter 5 presented versatile ligand exchange strategy for PbS QDs by using Pb-thiolate as the exchanging ligand. The Pb-thiolate ligands better preserved the exciton absorption features as well as the emission intensities during the ligand exchange procedure. The Pb-thiol ligand exchange approach was versatile and applicable to a number of other ligand/solvent systems. The ligand exchange using Pb-thiolates provided a facile procedure for future ligand exchange involving lead chalcogenide based QDs.

Chapter 6 showed that the PbS QDs without any treatment is unstable in commonly used electrolytes such as tri-iodide and polysulfide electrolytes. The stability of PbS QDs in polysulfide electrolytes was improved by treating the sensitized photoelectrodes with cadmium salt solution. Treatment with cadmium salt solution formed a protection layer of cadmium on PbS QDs surface which prevented the PbS QDs from exposure to polysulfide electrolytes. Further, the number of CdS and ZnS treatment cycles was also optimized for

PbS QDSSCs. As a result, a maximum PCE of 1.77 % was achieved for optimized solar cells.

Chapter 7 demonstrated the use of PDA as a nitrogen containing precursor to form N-doped CN_x/CNT hybrids. These N-doped CN_x/CNT hybrids were utilized as a highly efficient electrocatayst material for DSSC applications. The influence of various PDA loadings and the different carbonization temperatures on the catalytic performance of CN_x/CNTs was also investigated. The best performing device fabricated with the CN_x/CNTs hybrid material exhibited a PCE of 7.3 %, which was even higher than that (7.1%) of Pt CE based DSSC.

8.2 Recommendations

For the future development and advancement of QD based solar cell technology, the following recommendations in terms of scientific research and development are made based on the results generated from this PhD thesis:

a) One of the major problems encountered during the integration of PbS QDs in QDSSCs is their instability in various electrolyte systems. Thus, a future recommendation would be to investigate various electrolyte systems that can maintain the stability of PbS QDs.

b) Although our new PDA based CN_x/CNT hybrid materials showed higher catalytic properties than Pt counter electrodes for reduction of tri-iodide electrolytes in DSSCs, these materials were not effective for the reduction of polysulfide based electrolytes. The future research could be directed towards understanding the reduction behaviour of various electrolytes and the materials properties that significantly influences the electrolyte reduction. As such the new catalytic

materials with the desired properties can be synthesized for the specified electrolytes.

c) Another avenue of research could be the expansion of ligand exchange of PbS QDs using the semiconducting polymers, as such a proper depleted heterojunction systems can be created for all solid state solar cells.

d) Investigation of QD nucleation and growth mechanism for other lead chalcogenide based QDs as well as that of other non-toxic NIR emitting QDs can also be performed that can yield other better performing materials for solar cell applications.

Appendix A

Shrestha, A., Jin, B., Kee, T., Qiao, S. & Dai, S. (2016). A Robust Strategy for Living Growth of Lead Sulphide Quantum Dots.
ChemNanoMat, 2(1), 49-53.